

Dear Dr. Hamilton,

please find attached our response letters and marked-up files, along with the revised manuscript. Upon reflecting on the title, we believe it should finally read: "Gas phase composition and secondary organic aerosol formation from standard and particle filter-retrofitted gasoline direct injection vehicles investigated in a batch and flow reactor", to best cover the revised content of the paper.

We had suggested "Gas phase composition and secondary organic aerosol formation from gasoline direct injection vehicles with prototype particle filters investigated in a batch and flow reactor" in our response letters, which, however, would not be fully correct as the bigger part of our data set is in "standard configuration", not with GPFs.

Further, upon preparing the revised manuscript, we have found further ways to make our language more concise and clarify the manuscript to avoid confusions as suggested by the referees, as you will see in the marked-up version.

During the update of the manuscript, we noted that on Figure 5 which we suggested in the author response, we should replace the SC experiment given (which was initially B1), with a more typical and well understood experiment. We have therefore, replaced B1 with experiment A2. This is now in line with our updates in response to the referee questions on the yield-discussion: We added in the discussion that A1, B1 and B2 are unexpectedly high and potentially impacted by an unaccounted for interference, hence, we think it is more consistent to show one of the well-understood experiments (A2, A3 and B3) in Figure 5 as a typical example. Additionally, we have indicated which data points correspond to A1-3 and B1-3 in Figure 6 and 7 (by adding identifiers compared to the versions given in the response letter and initial manuscript), and have slightly modified colors in Figure 6a and b, to help guide the reader through our discussions in the text. We apologize for inconvenience caused by this late modification, but believe that while they do not alter our conclusions or arguments in the response letter are bringing big improvements and facilitations to the reader. We attach the further improved figures (including the identifiers) here once more.

We hope you find our work significantly improved and are looking forward to your feedback.

Thanks and best regards,  
Simone Pieber, and co-authors.

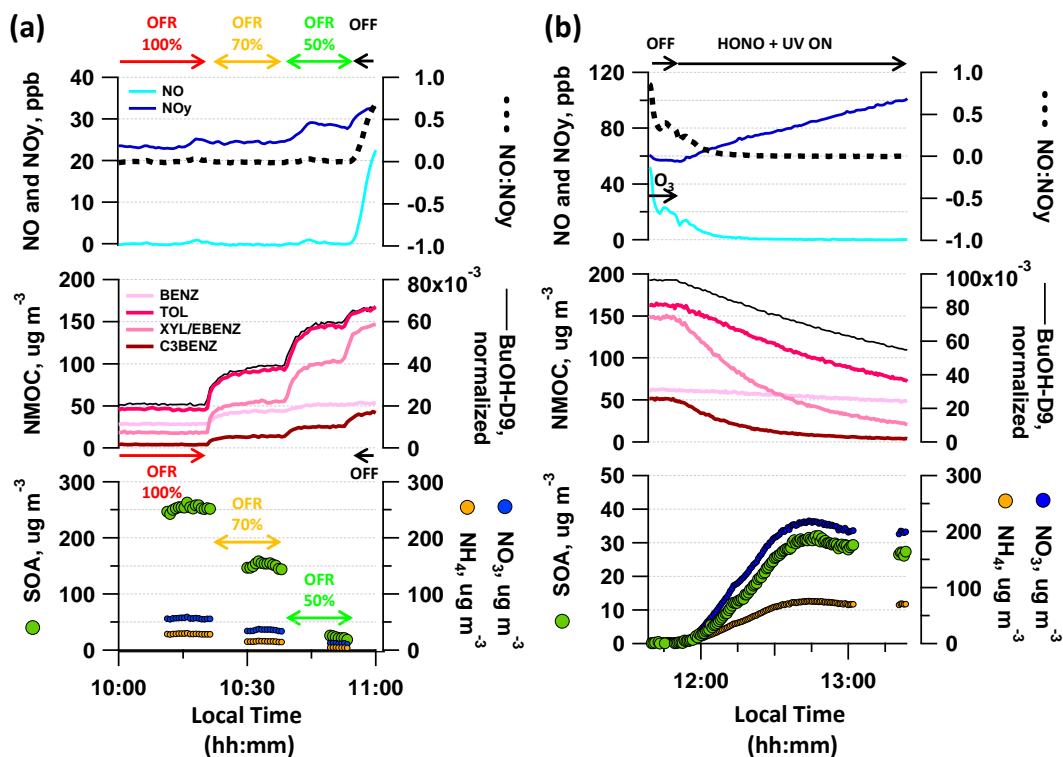


Figure 1. Typical OFR-from-SC and SC photochemistry experiment. Decay of dominant SOA precursors (benzene (BENZ), toluene (TOL), *o*-/*m*-/*p*-xylene (XYL) or ethylbenzene (EBENZ), C3-benzenes (C3BENZ)) upon photochemistry and associated SOA formation in (a) OFR (sampling from SC batch at different UV intensities, displayed is expt D3) and (b) SC (displayed is expt A2). (a-b) UV status, O<sub>3</sub> and HONO injection are indicated along with the NO:NO<sub>y</sub> ratio and the OH tracer BuOH-D9. Reacted ArHC fractions are provided in Figure S5 per experiment. Local time is given in intervals of 15 min.

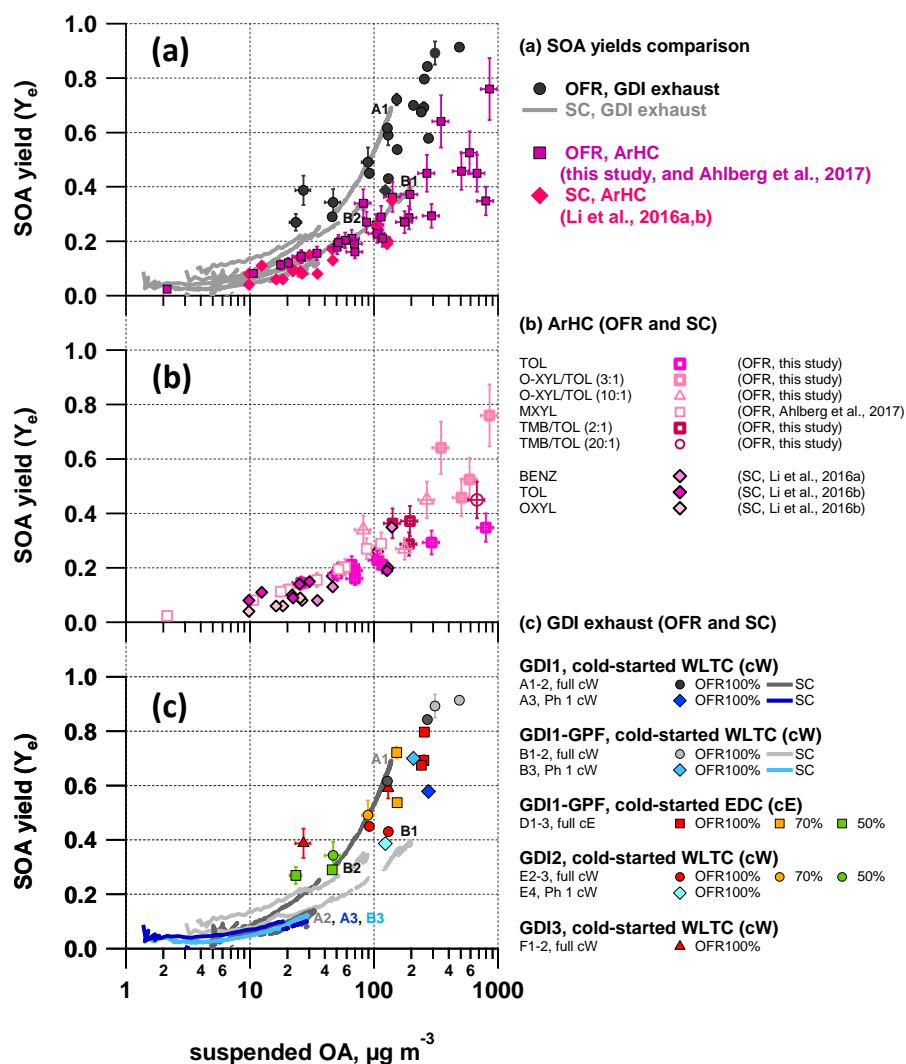


Figure 2. Effective SOA yields. Vehicle exhaust from GDI1-3 (full cW, full cE, Ph1 (cW)) photo-chemically aged in the SC and OFR-from-SC compared to effective SOA yields from selected ArHC (toluene, *o*-xylene, 1,2,4-TMB) photo-chemically aged in our OFR (this study, w/o NO; *m*-xylene data from Ahlberg et al., 2017) and in a SC (benzene, toluene, *o*-xylene from Li et al., 2016a and Li et al., 2016b, w/o NO). (a) all data combined, (b) OFR (average $\pm$ 15% measurement variability) and SC yields of single ArHC or mixtures, (c) vehicle exhaust photo-chemically aged in SC and OFR-from-SC (average $\pm$ 1SD of AMS OA measurement during stable conditions). Error bars on data from OFR represent the variability of the measurement. SC yield curves per experiment are presented in Figure S13 and potential factors enhancing yields in experiments A1, B1, B2 (Table S4) are discussed in Section 3.6.1. (a-c) OH data are given in Figure 3 and summarized here: OH exposures up to  $1.4 \times 10^{11}$  molec  $\text{cm}^{-3}$  s, after  $\sim 2$  hours of SC photochemistry (average  $[\text{OH}] = 2 \times 10^7$  molec  $\text{cm}^{-3}$ ). OFR100%:  $[\text{OH}] = (2.7\text{--}5.2) \times 10^9$  molec  $\text{cm}^{-3}$ ;  $[\text{OH}]_{\text{exp}} = (3.0\text{--}5.8) \times 10^{11}$  molec  $\text{cm}^{-3}$  s (at  $\sim 8$  ppm  $\text{O}_3$ ). OFR70%:  $[\text{OH}] = (1.4\text{--}2.2) \times 10^9$  molec  $\text{cm}^{-3}$ ;  $[\text{OH}]_{\text{exp}} = (1.6\text{--}2.5) \times 10^{11}$  molec  $\text{cm}^{-3}$  s (at  $\sim 3$  ppm  $\text{O}_3$ ). OFR50%:  $[\text{OH}] = (0.28\text{--}0.44) \times 10^9$  molec  $\text{cm}^{-3}$ ;  $[\text{OH}]_{\text{exp}} = (0.31\text{--}0.49) \times 10^{11}$  molec  $\text{cm}^{-3}$  s (at  $\sim 0.7$  ppm  $\text{O}_3$ ). The max. OH exposure in the SC corresponds to the range of green to orange colored OFR data points in panel (c), see Figure 3.

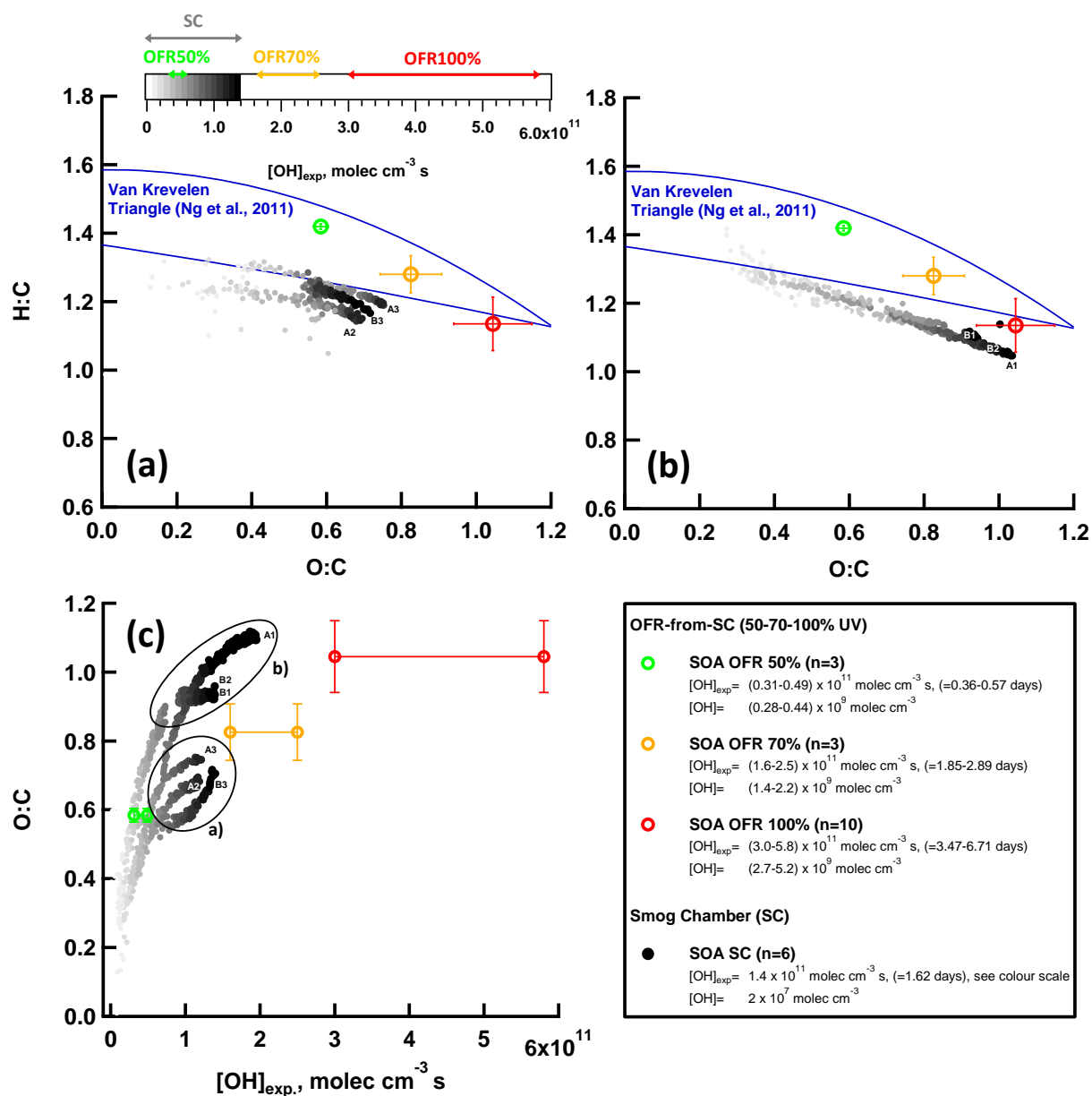


Figure 3. Bulk OA composition of SC and OFR SOA. a-b) Van-Krevelen plot (O:C vs. H:C) for SOA formed during SC expts (n=6, GDI1 standard and w/GPF, cW and Ph 1 (cW)) and OFR-from-SC data points (n=10, GDI1 standard and w/GPF, full cW, full cE, Ph 1 (cW)) at different OFR UV settings (100%, 70%, 50%). a) shows SC Expt (A2, A3, B3; Table S4) and b) SC Expt (A1, B1, B2; Table S4), experiments with  $\text{NH}_4\text{NO}_3$  levels outside our  $\text{CO}_2^+$ -AMS interference calibration range (Pieber et al., 2016). The POA contribution was subtracted from the total OA bulk composition; SOA/POA ratios were  $> 10$ . The Aiken parameterization (Aiken et al., 2007; Aiken et al., 2008) has been applied to HR fitted data. Lines indicate the Van-Krevelen (VK) space typical for ambient AMS measurements (Ng et al., 2011). Error bars represent one standard deviation of measurement variability. (c) O:C of a) and b) as a function of  $[OH]_{exp}$  exposure.  $[OH]_{exp}$  in days refers to an assumed average ambient  $[OH]$  of  $10^6 \text{ molec cm}^{-3}$ .

## Referee Comments #1 (acp-2017-942-RC1-supplement) and author response.

Simone M. Pieber et al.

We thank the editor and referees for their comments. To guide the review process we have copied the referee comments in black text. Our responses are in regular blue font. We have responded to all the referee comments and made alterations to our paper (*in italic text*) and removed redundancies for clarification. Along with the revision we suggest a slightly changed title: “*Gas phase composition and secondary organic aerosol formation from gasoline direct injection vehicles with prototype particle filters investigated in a batch and flow reactor*”

### General:

---

**RC1:** Interactive comment on “Gas phase composition and secondary organic aerosol formation from gasoline direct injection vehicles investigated in a batch and flow reactor: effects of prototype gasoline particle filters.” By Simone M. Pieber et al

This paper evaluates the gas phase composition and secondary organic formation from gasoline vehicles in a batch and flow reactor. Excusive results about primary emission factors, gas vapor composition and SOA formation are shown. This paper is well written and organized. The paper describes a large amount of data, but critical evaluation and analysis is missing, that is needed to have confidence on the quantification of results. Therefore I recommend that the paper may be published in ACP after addressing the major revisions below.

**Author Response:** We agree with referee 1 that our manuscript describes an extensive data set on GDI vehicles with novel after-treatment systems, including a comprehensive analysis of the gas- and particle phase, as well as the SOA formation. We are confident, that our manuscript at its initial stage includes an extended discussion of experimental uncertainties in the main text and provides additional critical evaluation in detail in main text and supporting information. We provide answers to RC1 and modifications to our manuscript to the best of our abilities.

### Major revisions:

---

**RC1-1:** 1) The analysis of vapor losses to walls is inadequate. Enormous progress has been made on this area recently, and there is no excuse to ignore those corrections in current studies. Comparability with past studies that were performed when vapor wall losses were not understood is not an excuse to ignore this major issue. Comparability with future studies, for which all the good ones will include analysis of this effect, should be the relevant criterion. It will benefit the citation of this paper for showing both results. This is an essential correction which could introduce large bias (a factor of 3-4 in Zhang et al. 2014) and is related to multiple key calculation including SOA yield, NMHC composition etc. Taken vapor loss corrections into account, comparison results can be more accurately assessed, especially crucial for some main focuses of this paper: SOA yield between SC and OFR, SOA yield of vehicle exhaust vs single precursors. As the authors stated in page 21 line 27-29 “we expect both SC and OFR yields to be underestimated, by factors of approximately 1.5-2 (SC) and 1.25 (OFR) ((Platt et al., 2017);(Zhang et al., 2014);(Palm et al., 2016)) due to vapor wall losses. Corrections would reduce the discrepancy between the two systems.” Thus a gas vapor wall loss correction is needed for this study. The model of Krechmer et al. (2016) can be used for the SC, and has been recently shown ((Ye et al., 2016); also at AAAR 2017) to be consistent among all Teflon chambers. The model of Palm et al. (2016) should be applied to the OFR.

**Author Response:** We agree with the need to address vapor wall losses in smog chamber (SC) and oxidation flow reactor (OFR) studies. For this reason, we have provided estimates for vapor wall losses for both systems in the initial version of the manuscript, as the referee mentions in the second part of this comment. We believe that our transparent approach to provide the data along with the expected correction factor which we have determined for this specific smog chamber, using gasoline vehicle emissions in our related publication (please refer to Platt et al., 2017), is a valid option, as dedicated experiments to study the exact losses during the presented experiments have been missing. It would be misleading to apply correction factors from literature. We would like to note, that the correction factor determined in Platt et al., 2017 (1.5-2) is in line with reports by others (e.g. Zhang et al., 2014, reports a factor of 1.1-4.2 underestimation, La et al., 2016, found a factor of 1.1.-6). Generally, we disagree that gas/vapor loss corrections are transferrable from one chamber to the next

without specific characterization experiments, and don't see this as a conclusion in previous literature reports either (see Krechmer et al., 2016).

Regarding the OFR, the model from Palm et al., 2016, has been applied in the initial version of our manuscript and the corresponding correction factor is already stated in the manuscript.

Loss corrections on our primary NMOC composition are not needed: The compounds of interest for SOA formation which we were able to identify by PTR-ToF-MS in our emissions mix are mainly BTEX, C3-Benzenes and Naphthalene. Based on their saturation mass concentration, these compounds are classified as VOCs or correspond to the upper end of the IVOC range, and are therefore not expected to be impacted significantly by losses to SC walls on a time-scale relevant to our SOA study. We performed measurements with emissions containing these substances to test their loss to chamber walls without oxidation chemistry initiated, and have monitored the aromatic composition and absolute concentrations of our identified species over the course of several hours: it did not change significantly enough to impact our findings, i.e. during experiments lasting between 2 and 6-8 hours the stability of relative gas phase composition (determined as the change in the ratio of relevant SOA-precursors to benzene) changed only by 3% (after 2 hours, which is a typical time-scale for the presented experiments) to 7-12% (at 6-8 hours).

**Text modifications:** We have modified the section (2.2.5) to include also additional references to newer literature and report the possible spread for SOA yield underestimations better. The new text reads as follows:

- “a robust strategy for their determination and correction remains challenging (Krechmer et al., 2016). In our previous work, we estimated that vapor wall losses may cause SOA yields to be underestimated for the SC used herein (assessed based on gasoline vehicle exhaust SOA, see Platt et al., 2017, by a factor 1.5-2 for our experimental conditions), comparable to suggestions by others, e.g. a factor of 1.1-4.2 by (Zhang et al., 2014) and 1.1-6 (La et al., 2016). Data correction would increase SOA yields on average by a factor 1.5-2.”
- “Given the high SOA concentration and hence particle surface  $((1-5) \times 10^9 \text{ nm}^2 \text{ cm}^{-3})$  based on the SMPS size distribution of SOA, at least 80% of the formed LVOC was calculated to partition to the pre-existing OA mass based on the model by Palm et al., 2016. Data correction would increase SOA yields by a factor of 1.25 on average.”

**RC1-2:** 2) The comparison on SOA formation between OFR and SC should also consider gas vapor loss in the tubing (Pagonis et al., 2017). The different tubing lengths and materials can also result in a SOA yield difference between SC and OFR. A vapor loss calculator can be found in Pagonis et al. (2017). Please clarify the tubing material and length as well. Page 16 line 17-18: In addition to the residence time of OFR, this SOA delay was also possibly caused by the delayed gas vapor in the tube, as suggested in Pagonis et al. (2017).

**Author Response:** We agree that this should be specified.

**Tubing material and length:** Tubing to sample direct emissions from the vehicle tailpipe for a) injection into the SC or online-OFR, or b) direct gas-phase measurements are made of SilcoTek®-coated steel (12 mm diameter), temperature controlled at 140°C, operated under high flows (30 L min<sup>-1</sup>), and of roughly 8 m length. Ejector dilutor 1 is placed in a temperature controlled housing (200°C), and ejector dilutor 1 is operated at 80°C. Instruments sampling either a) from the SC or b) behind the OFR, or c) directly, are connected via separated tubing for gas-phase and particle phase. Particle-phase tubing is exclusively made of stainless steel, no copper tubing is used. Sampling lines are of 6 mm diameter, and up to 2 m length. Support pumps are used at the instrument inlets, to minimize sampling residence time by increasing the flow rate. Similar approach is used for gas-phase sampling (total tubing length to reach all of the instrument inlets, which are also equipped with support pumps is up to 2 m). Tubing for gas-phase sampling is made of either SilcoTek®-coated steel or Teflon, temperature controlled at 60°C where necessary (i.e. for PTR-ToF-MS measurements and FID), to avoid losses of the VOC and IVOC species relevant to our SOA-study and PTR-ToF-MS analysis (including essentially BTEX, C3-Benzenes, Naphthalenes, and eventually phenolic compounds, benzaldehyde). SilcoTek®-coating and Teflon are also suitable for the sampling of species known to be easily retained on surfaces, such as formaldehyde, acetic acid, acetaldehyde, for which, in addition to the uncertainties of PTR-ToF-MS analysis, also tubing losses may induce a slight shift in our gas-composition analysis.

We are confident that the differences in SOA yields obtained in the SC and OFR are not caused by losses on sampling lines between the SC and OFR. This sampling system was made of a combination of SilcoTec® coated steel with carbon-coated Teflon (i.e. electrically conductive Teflon suitable for simultaneous gas- and particle phase sampling), and the total length between SC and OFR inlet was roughly 35 cm (6 mm diameter, ca. 8 L min<sup>-1</sup> flow). Additionally, all measurements from the dark smog chamber (which is the basis for gas-phase composition data), were performed for at least 10-15 minutes, to reach a stable signal. We experimentally determined potential losses in the sampling from dark smog chamber and sampling through dark OFR and observed a reduced mass of species by less than 5% and no change in the composition of the SOA precursors, which, in our case, is the determining factor.

**Page 16, Line 17-18:** Our statement is in line with findings of other researcher (Zhao et al., 2018), who state “After the vehicle was turned off at the end of bags 2 and 3 it took approximately 3 min for the OA signal at the PAM reactor outlet to return to background levels. This delay reflects the time it takes for the exhaust to pass through the PAM reactor.”, in analogy to our interpretation. However, we do generally agree that delays due to retention on sampling lines can cause a shift in the signal, and hence add this also specifically to our manuscript.

**Text modifications:** Tubing material, length, temperature and flow rates are specified in the SI as follows:

- *Tubing to sample direct emissions from the vehicle tailpipe for injection into the SC or online-OFR, or direct gas-phase measurements are made of SilcoTek®-coated steel (12 mm diameter), temperature controlled at 140°C and operated under high flows (30 L min<sup>-1</sup>) to avoid substantial losses over the sampling length of roughly 8 m. Ejector dilutor 1 is placed in a temperature controlled housing (200°C), and ejector dilutor 1 is operated at 80°C.*
- *Instruments sampling either from the SC, behind the OFR, or directly from the dilution system are connected via specific tubing for gas-phase and particle phase. Particle-phase tubing is made of stainless steel (6 mm diameter), and up to 2 m length. Support pumps are used at the instrument inlets, to minimize sampling residence time by increasing the flow rate. Total tubing length to reach all of the gas-phase instrument inlets, which are likewise equipped with support pumps is up to 2 m. Tubing is made of Teflon or SilcoTek®-coated steel. The sampling line of the PTR-ToF-MS instrument and FID is temperature controlled at 60°C.*
- *SilcoTek®-coating and Teflon are also suitable for the sampling of species known to be easily retained on surfaces, such as formaldehyde, acetic acid, acetaldehyde, for which, in addition to the uncertainties of PTR-ToF-MS analysis, also tubing losses may induce a slight shift in our gas-composition analysis.*
- *The sampling system between the SC and OFR (for OFR-from-SC experiments) was made of a combination of SilcoTec® coated steel and conductive Teflon tubing, suitable for simultaneous gas- and particle phase sampling. The total length between SC and OFR inlet was roughly 35 cm (6 mm diameter, ca. 8 L min<sup>-1</sup> flow). Additionally, all measurements from the dark SC batch sample were performed for at least 10 minutes, to reach a stable signal.”*

Signal delay was addressed as follows:

*“The latter is related to a delay of the OFR signal by the residence time in the reactor, as also observed by others (Zhao et al., 2018), and might potentially also be caused by a delay of SOA forming species which are retained on surfaces (Pagonis et al., 2017).”*

**RC1-3:** 3) The particle losses due to heating in the sampling line and the hotter temperature in SC when UV light is on should be addressed. The aerosol loss due to tubing (under no heating condition) needs to be estimated as well. The model for aerosol loss calculation in the tubing can be found in (von der Weiden et al., 2009). The particle loss due to heating can be experimentally determined.

**Author Response:** Particle losses in the SC are assessed with our data as presented in our initial manuscript, which takes all factors leading to particle losses, including temperature effects into account.

**Text modifications:** “The main losses of particles are due to (1) diffusion, (2) electrostatic deposition and (3) gravitational settling, *which are in turn affected by temperature changes due to the UV lights.* Wall losses of particles in the SC were accounted for using the method described in (Weitkamp et al.,

2007) and (Hildebrandt et al., 2009), which accounts for all these loss processes simultaneously, including the aforementioned temperature effects.”

**RC1-4:** 4) Page 10 line 20-30: The SOA photolysis in OFR should be considered as well. For example in OFR with full UV light setting (100%), half of the SOA from toluene SOA (OH chemistry) or naphthalene SOA (OH chemistry) can be photolyzed under 254 UV light with a low quantum yield of 0.1, as shown in Fig. 8b in (Peng et al., 2016). This photolysis effect on SOA formation and SOA yield calculation under 50% and 100% UV light setting should be considered.

**Author Response:** Non-OH losses of SOA precursors via photolysis within the OFR was assessed for all our experimental conditions (OFR-from-SC, online-OFR 2014 and online-OFR 2015) as described in the discussion manuscript (section 2.2.5 and the corresponding information in the SI).

We summarize our findings and implications here: Given that non-OH losses strictly only imply a non-OH induced reaction of the compounds, but do not rule out any SOA formation from the obtained reaction/photolysis products, no corrections for any non-OH reaction can be made in our view (as already stated in our manuscript) regarding the formation of SOA. However, we agree to note specifically that the observed SOA may not only be related to OH-induced aging but also to UV-induced reactions that produce SOA, (in addition to potential O<sub>3</sub>-induced SOA, as well as NO<sub>3</sub>-induced SOA). Our discussion paper contains this information already in the SI (page 3, line 5) as follows “*This only refers to the reactive interaction of OH vs. the excitation by UV, and does not allow conclusions on the formation of SOA. Also chemistry initiated by UV185 or UV254 may lead to the formation of SOA. Additionally, it does not suggest any conclusions about the interaction of O<sub>3</sub> with double bonds made available by first ring-opening reactions.*” (...) “*Potential effects of O<sub>3</sub> on first generation products are not taken into account. Under those diluted conditions (initial NO < 100 ppb), we regard the experiments in OFR as low NO conditions (Peng and Jimenez, 2017). The dominant SOA precursors found in the exhaust are not reactive towards NO<sub>3</sub> radicals that can be formed in the OFR; potential effects on first generation products are not taken into account.*”

In this specific comment (RC1-4), the referee addresses in addition the destruction of previously formed SOA by photolysis, which we have not previously addressed in our manuscript. We address this here: Our OFR photon-flux is (1.2-2.3) $\times 10^{15}$  photons cm<sup>-2</sup> at 185 nm and (1.7-2.9) $\times 10^{17}$  photons cm<sup>-2</sup> at 254 nm (100% UV setting, which is the maximum and hence inducing maximum photolysis impact). Those photon-fluxes can be considered “medium” if comparing to Peng et al., 2016, Figure 8. The estimated SOA-photolysis is <1% for naphthalene at a quantum yield of 0.1 and <5% at a quantum yield of 1, for 185 nm. For 254 nm, the estimated SOA-photolysis is around 20% at a quantum yield of 0.1, but reaches 60-80% if a quantum yield of 1 is assumed, according to Figure 8 in Peng et al., 2016. Significant uncertainties are associated with this assessment: 1) we do not have any precise information about photon fluxes of our OFR, 2) dependent on the assumption of the quantum yield, we obtain a result which ranges from insignificant to significant, 3) as a full description of the chemical composition of the SOA is missing, it is not clear which effects photon-interactions will induce and whether photolytic destruction of molecules will lead to a loss of SOA mass and to which extent; hence, this assessment is at the current point in time of speculative nature only. Future work should address this in further detail before any corrections can be applied. Our conclusion is in line with Peng et al., 2016, who state: “Thus, to our current knowledge, lack of solid information on quantum yields of SOA components with multiple carbonyls and hydroxyls at 254nm prevents a clear assessment of SOA photolysis in OFRs at the medium and high UV.

**Text modifications:** “... Also chemistry initiated by UV185 or UV254 may lead to the formation of SOA, and likewise photons may also lead to the destruction of OH-formed SOA; both processes deserve attention in future research.” was added to the corresponding SI section, and “The results and implications of photon-induced effects on SOA formation or destruction are discussed in the SI.” was added to the main text.

**RC1-5:** 5) Page 14 line 1-2. How did the mass quantification between AMS and SMPS compare? It is essential to document this comparison in the form of scatterplots and regressions. Collection efficiency (CE) vary with chemical composition and aerosol phase (Middlebrook et al., 2012). CE for AMS quantification should vary in this study since relative OA and NO<sub>3</sub> fraction in total aerosol changed a lot. Why do the authors choose a CE ~1 here. I would expect a slight variation on RIE

since there were POA dominated periods during the studies, for which RIE may be higher (Jimenez et al., 2016; Murphy, 2016). Attention needs to be paid for the size cut differences between AMS and SMPS as well, when nucleation was happened.

**Author Response:** CE: Typical assumptions for ambient aerosols assume CE=0.5, which is related to large extents to the fact that ambient aerosol contains ammonium sulfate and solid or glassy organics, which lead to significant bounce on the AMS vaporizer. Ammonium-Nitrate and Organic Aerosol mixtures are not expected to bounce significantly, and hence we have used a CE=1. Middlebrook et al., 2012, observed a CE close to 1 (0.8) for ambient aerosol containing ammonium nitrate, but no ammonium sulfate.

RIE: In principle, the RIEs of organic material may vary with the molecular weight of the parent molecule. However, most compounds undergo extensive thermal decomposition in the AMS and ionize as much smaller molecules, which have similar ionization cross-sections and thus similar RIEs. In the current study, the observed POA is dominated by aliphatic hydrocarbons, which have been shown in other studies to have RIEs of approximately 1.4, the same as SOA (Jimenez et al., 2016). For example, there is no significant difference in the decane, diesel fuel, and lubricating oil despite a factor of 2 differences in molecular weight. Therefore we do not expect significant differences between POA and SOA RIEs in this study. Further, even if the POA and SOA RIEs were different, the very low POA/SOA ratios observed in this study would prevent a significant bias in the results, even if the POA RIE was as high as that suggested by Murphy et al., 2016 (~4 assuming the molecular weight of lubricating oil), which we note again would be in conflict with experimental evidence (Jimenez et al., 2016), our conclusions won't be affected. An RIE of 1.4 for SOA remains reasonable, and hence, any conclusions on SOA yields are neither effected by applying the standard assumption of RIE=1.4 to our data set.

Lens-cut-off/Nucleation: AMS pToF size distributions are described in the SI. As provided in the main text, no lens-transmission analysis was performed.

**Text modifications:** The new text reads as follows:

*"We used a collection efficiency of 1, as upon photochemistry, significant amounts of  $NH_4NO_3$  were formed, and under those  $(NH_4)_2SO_4$  -free conditions, our aerosol mixture is not expected to bounce significantly. No corrections for lens transmission were performed, pTOF distributions are provided in Figure S10."*

**RC1-6:** 6) Schematic of the sampling strategy is confusing. I did not get the timing for the sampling strategy. Was the UV light setting is constant during vehicle testing cycle? Then the background of aerosol and gases under UV light is off in SC and OFR was obtained by repeating the testing cycle of the cars? Sufficient detail needs to be provided, that would enable someone else to repeat the experiments, as it is standard in scientific publications.

**Author Response:** We have provided a lengthy (9 pages) description of our experimental set-up, strategy and conditions on Page 5-14 of the discussion paper (section 2 "Experimental"), which we believe allows for a full repeat of our experiments, specifically, this is true for our detailed description in section 2.2.1. Additionally, we refer to Platt et al., 2013 and 2017, in which we have published our experimental set-up earlier in further detail. Further, our photochemistry sampling scheme is discussed in section 3.5, along with representation of a typical experiment in Figure 5. We provide further information on background levels in our answer to RC2 and RC1-9 below, and have added additional information on control experiments to the text (see RC1-9). We have clarified this lengthy description to avoid confusions.

In the following our specific explanations:

- SC sampling: Background measurements were conducted prior each experiment and emissions were injected thereafter during a full cold-started test cycle or selected phases thereof. During this injection phase, emissions in the SC were only monitored with a limited set of experiments. The mass spectrometers for gas- and particle phase characterization were monitoring the direct emissions sampling (online) and online-OFR instead. When the cold-started emissions test was completed, mass spectrometers were set to characterize the emissions sample collected in the SC for about 15 minutes; thereafter, the hot-started vehicle test was conducted for which instruments were again disconnected from the SC, to monitor

the online OFR and direct emissions instead. Meanwhile, no photochemistry was initiated in the SC.

- **OFR-from-SC** (also “batch-OFR”) OFR-from-SC experiments refers to experiment that included aging a sample of emissions in the OFR reactor at fixed conditions, with UV lamps set to either 50, 70 or 100% intensity and with UV off (dark). Emissions which were pre-collected in the dark SC used as a buffer/storage volume were sampled via a short sampling system described in detail within answer to RC1-2 from the SC into the OFR. Sampling was conducted until the SOA formation in the OFR reached a stable signal, and conditions were kept stable for several minutes from this point onwards. Prior and after UV on conditions, fresh emissions (OFR UV off as well as directly in the SC) were characterized to allow for estimating the POA contribution to the OA mass measured under UV on conditions, as well as to allow for calculating the reacted SOA precursor mass. OFR cleaning with clean air under UV on conditions was performed prior to the measurements to minimize any background contamination.
- **Direct emissions sampling (online)**: PTR-ToF-MS data were collected at the inlet of the OFR. These data were used for selected experiments (e.g. data on GDI4 in 2015, labelled “online”). For all other vehicles and experiments we present the average composition and emissions factors from samples that were collected in the SC (w/o photochemical aging). Essentially, integrating the direct emissions sampling (online) vs. the composition determined in the SC yielded comparable results (Figure 4, GDI4, SC vs. online).
- **Online-OFR**: yes, here we have tested vehicles up to 4 times with cold-started and 4 times with hot-started experiments (as stated in Table 1). Only one cold-started vehicle test could be conducted each day, hence, typically 3 cold-started vehicle tests were performed on 3 consecutive days with UV lights switched on in the OFR, and 3 hot-started vehicle tests with UV lights switched on. One a 4<sup>th</sup> experiment day, we conducted the same set of experiment with OFR- UV lights switched off, to determine primary OA emissions and calculate the SOA. Essentially, much less POA was found then SOA (please see our online-OFR experiments, one of which is provided in the main text (Figure 3), as well as the corresponding figures in the SI). Note, however, that only for selected experiments (GDI4 in 2015), these online-OFR data were used in a quantitative way. For all other vehicles and experiments, we rely on SC and OFR-from-SC data (regarding SOA), as well as batch sampled experiments for primary NMOC composition. Essentially, integrating the online OFR-SOA for GDI 4 yielded comparable results to the SC (Figure 2b, GDI-4 SC vs. online).

**Text modifications:** We have made small modifications to shorten and clarified this section which has become more logic to facilitate experiment repeats now; information on backgrounds and control experiments was added as described in answer to RC1-9.

#### **Other revisions:**

**RC1-7:** Page 5 Line 8: EDC was defined as “older” low-road European Driving cycle (EDC), which is inconsistent with the definition of “New” EDC in the abbreviation/definition list.

**Author Response:** We have made the modifications to the abbreviations list, the modified text is provided in the following. The so-called “New European Driving Cycle”, is by now the “older” cycle and overtaken by the recent “WLTC”, which is, why nowadays, the NEDC is referred to as EDC, although the strict definition is “NEDC”.

**Text modifications:** “EDC =European Driving Cycle (previously known as the “New European Driving Cycle”)”

**RC1-8:** Page 7 line 26-27: Please specify the dilution factor for smog chamber (SC) and oxidation flow reactor (OFR).

**Author Response:** Dilution factors are provided in main text (Figure 1) and SI for our experimental set-up in the initial version of the manuscript. The final dilution value for the SC is determined by the volume sampled during a driving cycle. The decisive characteristic of a SC experiment are the concentration levels, rather than the dilution ratio, which are provided in Table S4-S7 of the initial SI.

**Text modifications:** Adjustments were made in section 2.2.2 and 2.2.3 to add the specific values for SC and OFR. *“Concentration-levels of our SC experiments were representative for urban ambient conditions, as reported in Table S4-S7.”* and *“...the diluted exhaust (either 1 or 2 ejector dilutors, each at a dilution ratio of 1:8)...”*

**RC1-9:** Page 8 line 14-15: What is the aerosol background level in SC and OFR experiments with clean air when the UV light is on? If it is high, this background needs to be subtracted in the calculation of formed SOA mass concentration.

**Author Response:** The background was generally low (with UV off, as well as UV on, and the SOA background was insignificant compared to our typical experiments ( $<1$  and  $<2 \text{ ug m}^{-3}$  for SC and OFR respectively, during SC and OFR-from-SC experiments;  $< 10 \text{ ug m}^{-3}$  during online OFR experiments (compared to  $100 - 2000 \text{ ug m}^{-3}$  SOA formed during these experiments, this is not significant). See also our response to RC-2. As we noted in the text, however, Ph2-4 experiments in the SC were close to the background measurements with the PTR-ToF-MS and hence we have noted this specifically in the discussion paper (figure caption of figure 4 *“Note that the total NMOC levels for Ph 2-4 (cW) are about 1/10 of full cW and Ph 1 (cW) concentrations only and measurements are close to the background measurements (signal not significantly different from 3 standard deviations of the background measurement)”*).

**Text modifications:**

- *Background measurements of the clean chamber were conducted prior to each experiment, and was insignificant compared to our measurements except for Ph2-4 or GDI4 experiments as stated in the results. Photochemistry control experiments were conducted regularly to estimate the contribution of the SC background to SOA formation; these experiments were conducted after the standard cleaning procedure. Instead of vehicle exhaust, pure air was used as a sample and ammonium sulfate ( $50 \text{ ug m}^{-3}$ ) injected as seed. Other experimental procedures were in line with the typical vehicle experiments. We found a SOA background of  $< 1 \text{ ug m}^{-3}$ , which is below the SOA concentrations formed during vehicle exhaust aging. Concentration-levels of our SC experiments were representative for urban ambient conditions, as reported in Table S4-S7.”*
- *“Background levels were  $<2 \text{ ug m}^{-3}$  SOA before OFR-from-SC experiments (when sampling from cleaned SC) and  $<10 \text{ ug m}^{-3}$  when sampling diluted (1:8) test bench room air prior online-experiments.”*

**RC1-10:** Page 8 line 26-29: Figure S1 shows the aerosol and gas-phase species are sampled through the same tube in the center of OFR. If it is true, there will be large loss either on VOCs species (if stainless or copper tube is used) or on aerosols (if Teflon tube is used)

**Author Response:** We described our sampling system and tubing materials, length and flows in our response to RC1-major revisions, and have discussed implications for losses of the species of interest within our study in this response. We kindly ask the referee and editor to refer to this section.

**Text modifications:** As provided in “RC1-major revisions”, we have added a description in the SI.

**RC1-11:** Page 9 line 26-27: The particle loss can be determined by measuring the aerosol concentration before and after OFR when the UV-light is off. The aerosol concentration before the OFR can also be roughly determined with aerosols in the SC chamber if the dilution factors and volatility of OA are known in OFR and SC. There have also been some reports from FIREX (Jesse Kroll’s group) that particles containing BC can be charged by the UV lights and be lost much faster, also see (Federer et al., 1983). Was this effect evaluated?

**Author Response:** The referee refers to a sentence where we state that particle losses in the OFR were evaluated by comparing eBC concentrations before and after the OFR during experiments. We find this test to provide a more realistic evaluation of the OFR performance than the lights-off tests suggested by the referee due to differences in temperature and potential losses due to charging of BC particles by UV light, as suggested by the referee. As noted in the original manuscript, observed eBC losses were negligible, consistent with previous characterization of this OFR for similarly-sized particles (Lambe et al., 2011).

Although we have not specifically investigated the effects of UV charging, the fact that

overall BC losses are negligible across the OFR suggests that this loss process is also negligible for our experimental set-up.

**Text modifications:** No major adjustments were needed, we have modified wording to highlight that we are using an experimentally determined transmission under actual operating conditions (“in-situ”). The section reads now as follows: “A comparison of eBC mass before and after the OFR indicated no significant losses during UV on or UV off periods (experimentally determined transmission was equal to 1). Consequently no further correction was applied. Particle wall losses in the OFR have been quantified previously by Lambe et al., 2011, who reported at least 80% transmission efficiency through the OFR for particles of mobility diameter ( $d_m$ ) > 150 nm (Lambe et al., 2011). The particles measured behind the OFR in our study had a median vacuum aerodynamic diameter ( $d_{va}$ ) between 200-400 nm based on HR-ToF-AMS measurements (size distributions are provided in Figure S9), which correspond to  $d_m$  > 150 nm when assuming spherical particles and an OA density of 1.2 g cm<sup>-3</sup> (Turpin et al., 2001) supporting our experimentally determined transmission efficiency. “

**RC1-12:** Page 10 line 16: “1000-5000 nm<sup>2</sup> cm<sup>-3</sup>” Is this unit true? These values indicate the particle surface areas in this study are very small, which is inconsistent with mass values reported in Fig. 3. It is ~10<sup>6</sup> times less than those in the typical chamber studies, e.g. (Zhang et al., 2014).

**Author Response:** We thank the referee for spotting this typo. The values should indeed read (1-5)x10<sup>9</sup> nm<sup>2</sup> cm<sup>-3</sup>. The particle surface area noted here corresponds to the OFR-from-SC aging experiments (i.e. an average SOA mass value of 100 μg m<sup>-3</sup>), and no primary eBC seed (b/c of GPF installation) was present. We have revised the corresponding section to clarify this point further.

**Text modifications:** We have corrected the stated values to read (1-5)x10<sup>9</sup>.

**RC1-13:** Page 11 line 19-24: Does the OH exposure estimated from BuOH-D9 agree with the OH exposure calculated based on Peng et al. (2015)? A plot showing the comparison of these two methods will be beneficial for readers to understand how accurate of the OH exposure used here.

**Author Response:** The comparison requested by RC1 can be found in the SI of the current version of the discussion manuscript, as also highlighted in the main text. We copy-paste the information here:

“Based on these input parameters, the model (Peng et al., 2016) predicted an  $[OH]_{exposure}$  (OH concentration integrated over time, see discussion in main text “OH exposure estimation”, in molec cm<sup>-3</sup> s) in the OFR of

$$UV100\%: [OH]_{exposure} = (10-13) \times 10^{11}$$

$$UV70\%: [OH]_{exposure} = (2.4-3.1) \times 10^{11}$$

$$UV50\%: [OH]_{exposure} = (0.35-0.48) \times 10^{11}$$

The estimated  $[OH]_{exposure}$  (in molec cm<sup>-3</sup> s) and OH concentration (in molec cm<sup>-3</sup>),  $[OH]$ , based on the experimental measurements of the decay of BuOH-D9 correspond instead to

$$UV100\%: [OH]_{exposure} = (3.0-5.8) \times 10^{11}, \text{ i.e. } [OH] = (2.7-5.2) \times 10^9$$

$$UV70\%: [OH]_{exposure} = (1.6-2.5) \times 10^{11}, \text{ i.e. } [OH] = (1.4-2.2) \times 10^9$$

$$UV50\%: [OH]_{exposure} = (0.31-0.49) \times 10^{11}, \text{ i.e. } [OH] = (0.28-0.44) \times 10^9$$

It appears that the model is able to re-produce our experimental measurements correctly at lower UV-intensity of the OFR reactor (i.e. the same order of magnitude is achieved), but fails to predict the OH exposure correctly at the higher UV intensity, where it over predicts the OH exposure). We believe the experimentally determined tracer-based method (d9-BuOH here) is more accurate because it is specific to the current system whereas the model is a generalized parametrization that here uses only the O<sub>3</sub>-concentration as an input to determine the photon flux of the UV lamps. Therefore the tracer-based method is used throughout the manuscript and we strongly encourage other users of the OFR reactors to supply a proper tracer (such as BuOH-D9, see Barmet et al., 2012) for the experimental in-situ determination of the OH exposure whenever possible.

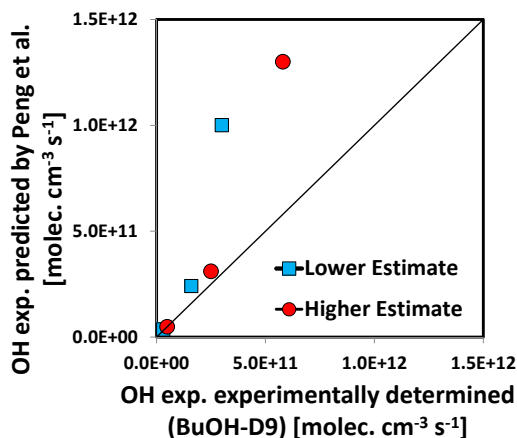


**Figure R1-1.** OH exposure predicted by the Peng-model vs. our experimentally determined OH exposure (data as stated in the SI). This plot was not added to the SI, as the data are compared in the text.

**Text modifications:** In the main text we have added the following: “*The tracer-based OH exposure calculations are generally in good agreement with exposures predicted by the model, except at the highest OH exposures where the tracer method is approximately a factor of 2 higher. Tracer-based OH exposures are used throughout this analysis, as these measurements are specific to the current OFR system.*”

**RC1-14:** Page 12 line 2: Please specify the dilution factor.

**Author Response:** The dilution ratio in the CVS-dilution tunnel is variable and was controlled by means of the CO<sub>2</sub>-analysis, and is at a range of 8 during high engines loads to 30-40 at idle conditions.

**Text modifications:** We added the information as described above.

**RC1-15:** Page 12 line 5-7: Why heat the sample before CPC? Why 300 oC.

**Author Response:** These settings are based on the PMP- Particle Measurement Program of the ECE GRPE Group; thermo-conditioning is a pre-requisite in order to measure only non-volatile particles.

**Text modifications:** We noted that we are not presenting any data from the CPC instrument in our manuscript and have therefore removed this statement from the main text, however.

**RC1-16:** Page 14 line 19-24: These descriptions cannot be found in the Fig. 1 e.g. No graph compares “Ph 1 of cW and hW vs. Ph 2-4 of cW and hW” in line 20.

**Author Response:** We are unable to follow the referee’s argument. As we noted in the text, these comparison discuss the data presented in Figure 2, panel a and c. Specifically, the NMHC comparison for Ph 1 of cW and hW vs. Ph 2,3 and 4 of cW and hW are derived by looking at the data presented in Figure 2 panel c, and are discussed in the text.

**Text modifications:** No modifications were made specific to this request. However, we have revised Figure 2 along with suggestions by Referee 2 and have hence modified parts of section 3.1, which the Referee 1 refers to here; please refer to our response to RC-2.

**RC1-17:** Page 15 line 2-3: It is hard to draw such a conclusion based on Fig. 2b. A scatter plot between POA+BC vs PM is needed or at least please give the value POA+BC.

**Author Response:** We agree with the referee’s argument, and have added a comparison plot in the SI to support our statement “*PM measured in the batch samples (sum of eBC and POA, Figure 2b) compares generally well with the gravimetric PM analysis of filters sampled from the CVS (Figure 2a).*”

**Text modifications:** As noted above, we have added an additional Figure to the SI and refer to it in the main text. “*PM measured in the batch samples (sum of eBC and POA) are compared with gravimetric PM analysis of filters sampled from the CVS in Figure S16.*”

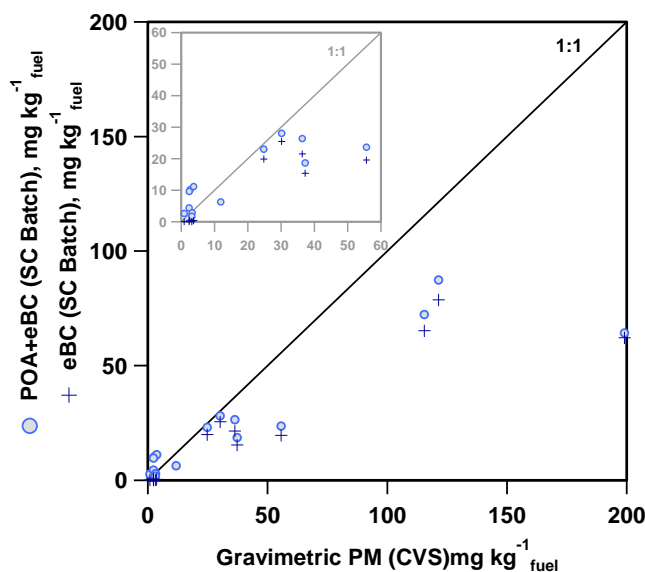


**Figure R1-2:** Comparison of POA+eBC from batch SC sampling to gravimetric PM measurements from filter samples taken from the CVS, added to the SI; the figure caption reads: “POA and eBC measurements in the SC batch sample compared to gravimetric PM measurements from the CVS.”

**RC1-18:** Page 15 line 9: Please give the value ranges for “previous finding”.

**Author Response:** This information is provided in the current version of the discussion paper few lines further down (“median 60, range ~10-400 mg kg<sup>-1</sup> fuel”), i.e. on Page 15, line 12.

**Text modifications:** We have revised this paragraph to remove redundancies and make the range of previous findings easier to grasp for the reader, along with suggestion by RC-2.

**RC1-19:** Page 15 line 16-19: A smaller vapor loss in the OFR is also a possible explanation.

**Author Response:** We agree with the referee (as also indicated by our provided vapor correction factors 1.25 for the OFR and 1.5-2 for the SC) and have revised the statement.

**Text modifications:** As described above, we have put a reference to the subsections which discuss those issues at other locations within the manuscript.

**RC1-20:** Page 18 line 5: publishing year is required for “Jordan et al”

**Author Response:** Thanks for the hint; the reference was corrected.

**Text modifications:** “Jordan et al.” was revised to “Jordan et al., 2011”.

**RC1-21:** Page 20 line 1: How to define the “high NO condition”.

**Author Response:** The answer to the definitions is provided in the publication (Peng and Jimenez, 2017) which is cited along with above statement. We have clarified this now in our manuscript.

**Text modifications:** The statement ““high NO” conditions may be reached in the OFR ((Peng and Jimenez, 2017)).“ was modified to read now ““high NO” conditions may be reached in the OFR as defined by (Peng and Jimenez, 2017).“

**RC1-22:** Page 20 line 21: No OH exposure is shown in Fig. 6.

**Author Response:** We refer to the OH exposure data which are noted in the caption to Figure 6. We have clarified this statement.

**Text modifications:** The statement “...OH exposure data at the end point of SC experiments and for the OFR are provided in Figure 6 and Figure 7).“ was revised and reads now “OH exposure data at the end point of SC experiments and for the OFR are provided in caption to Figure 6, and Figure 7).“

**RC1-23:** Page 21 line 5: Please clarify “Limited experimental statistics”

**Author Response:** We conducted 2 experiments with Ph2-4 emissions aged in the SC (1 with GDI1 with standard configuration and 1 with GDI1 equipped with a GPF). Additionally, Ph2-4 SOA-precursor emissions collected in the SC were close to background concentrations (as already discussed within this answer to referees as well as noted in caption to Figure 4). Therefore, the available data are not sufficient to allow a reliable SOA yield analysis for Ph2-4 analysis. Others (Zhao et al., 2018) have recently published a SOA yield comparison from an OFR data set on cold- and hot-engine emissions, and also discuss the potential background effects in their publication.

**Text modifications:** We have re-adjusted the main text, to read as follows: “Data are presented as a function of suspended OA for all experimental conditions of cold-started GDI1-3 (i.e. for full cW, cE; and Ph 1 (cW)), while GDI4 or hot engine conditions, i.e. Ph 2-4 (cW) are not included in our the analysis, as this data set includes only two experiments with concentrations levels close to our background measurements; a discussion of SOA yields from cold- and hot-engine emissions has recently been published by Zhao et al., 2018 for an OFR data set).”

**RC1-24:** Page 21 line 30-32: The fragmentation effect on aerosol phase under high OH exposure in OFR should also be considered.

**Author Response:** We are unable to follow the referee’s argument. Page 21 line 30-32 discusses discrepancies among SC experiments, not OFR. Page 21 line 21 onwards discusses discrepancies between OFR and SC experiments, which, noting that they were conducted at somewhat different OA loadings, let us conclude that OFR-yields tend to be higher than SC yields, especially at higher OH exposures. Fragmentation (over functionalization) would tend to a) yield lower OFR SOA yields and b) as discussed in our previous publication (Bruns et al., 2015) and by Lambe et al., 2012, would yield higher O:C. We do not find any of these effects in our data set, hence, while we may be looking at compensating effects, we don’t see results that seem to be driven into any direction by fragmentation only.

**Text modifications:** No modifications are required.

**RC1-25:** Page 22 line 12: “This generally indicates that we are able to identify the most relevant SOA precursors in the vehicle exhaust.” This statement is not true. The SOA yield in SC and OFR was calculated based on a larger group of ArHC than merely OXYL/TOL. The author should calculate the SOA formation based on OXYL/TOL consumption in the SC (and OFR) and yield from OXYL/TOL experiment. Then compare the calculated SOA to the SOA formed in the SC.

**Author Response:** We agree with the referee’s observation. We have used two different ways to approach the mass closure in our manuscript: 1) with a forward closure as presented in the initial Figure 5 as an example for 1 experiment (i.e. the reacted aromatic SOA precursor mass was weighted by a fixed SOA yield from the literature, which is the procedure suggested by the Referee 1 on RC1-25), and 2) via an indirect approach normalizing the formed SOA to the reacted ArHC mass (i.e. deriving an “effective yield” combining all reacted species), which allows to present the result as a function of OA loading. Because it appears confusing to have two different methods to address this, we decided to remove the SOA-closure from initial Figure 5 (bottom panels), and instead present data as “effective yield closure” (Figure 6) only.

**Text modifications:** We have revised all text sections to allow this modification; instead of a mass closure we discuss the results now in terms of a yield-closure in the original section 3.6. We have removed the statements on the mass closure from the text.

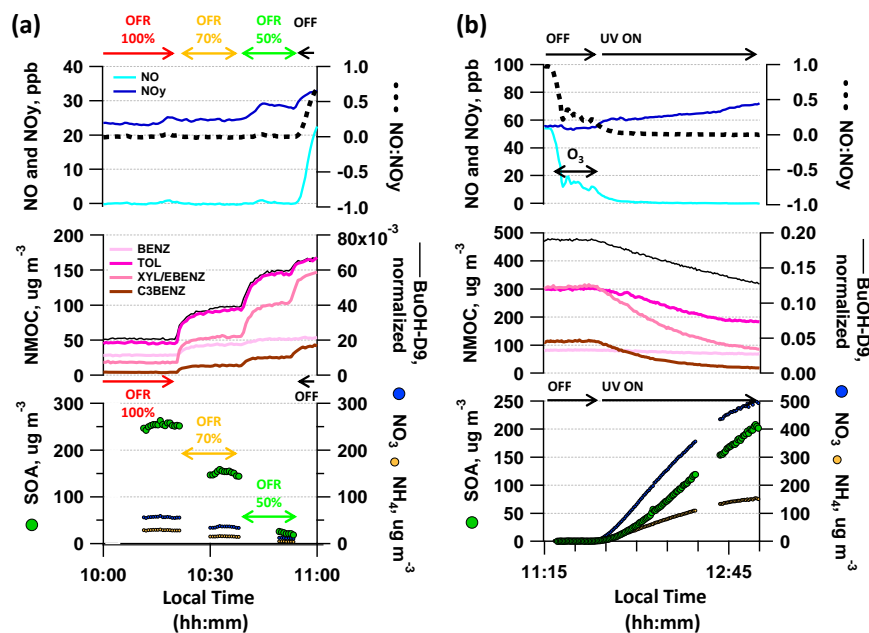


**Figure R1-3:** New Figure 5 with modified lower panels; the new figure caption reads as follows: *“Typical OFR-from-SC and SC photochemistry experiment. Decay of dominant SOA precursors (benzene (BENZ), toluene (TOL), o-/m-/p-xylene (XYL) or ethylbenzene (EBENZ), C3-benzenes (C3BENZ)) upon photochemistry and associated SOA formation in (a) OFR (sampling from SC batch at different UV intensities, displayed is expt D3) and (b) SC (displayed is expt B1). (a-b) UV status and O<sub>3</sub> are indicated along with the NO:NO<sub>y</sub> ratio and the OH tracer BuOH-D9. Reacted ArHC fractions are provided in the SI per experiment, see Figure S4. Local time is given in intervals of (a) 30 min and (b) 15 min.”*

**RC1-26:** Page 24 line 13-14: To conclude this, it is better to plot a graph showing O:C comparison as a function of OH exposure between SC and OFR. The SC shows similar O:C ratios with OH exposure of  $1.2 \times 10^{11}$  molec cm<sup>-3</sup> s to the those in OFR under 4.5 molec cm<sup>-3</sup> s, which seems not agreeable. The different vapor losses between the SC and OFR might also a reason.

**Author Response:** Our OH exposures are provided as color code; hence the data requested by the referee are already presented in the main text Figure 7 and initial SI Figure S16ab. However, while all our 6 SC experiments yield a similar end-point OH exposure as the 70% UV intensity setting in the OFR (marked in orange), there are 3 SC experiments which appear to have been conducted under conditions yielding higher NO<sub>3</sub>/OA ratios and we believe that these experiments have reached exceptionally high O/C ratios compared to the other 3 SC experiments, despite no difference in their OH exposure. To facilitate the understanding of this plot, we have prepared an additional plot of O/C ratio vs. OH exposure as suggested by the referee.

**Text modifications:** We have replaced our initial Figure 7 and adjusted the corresponding text.

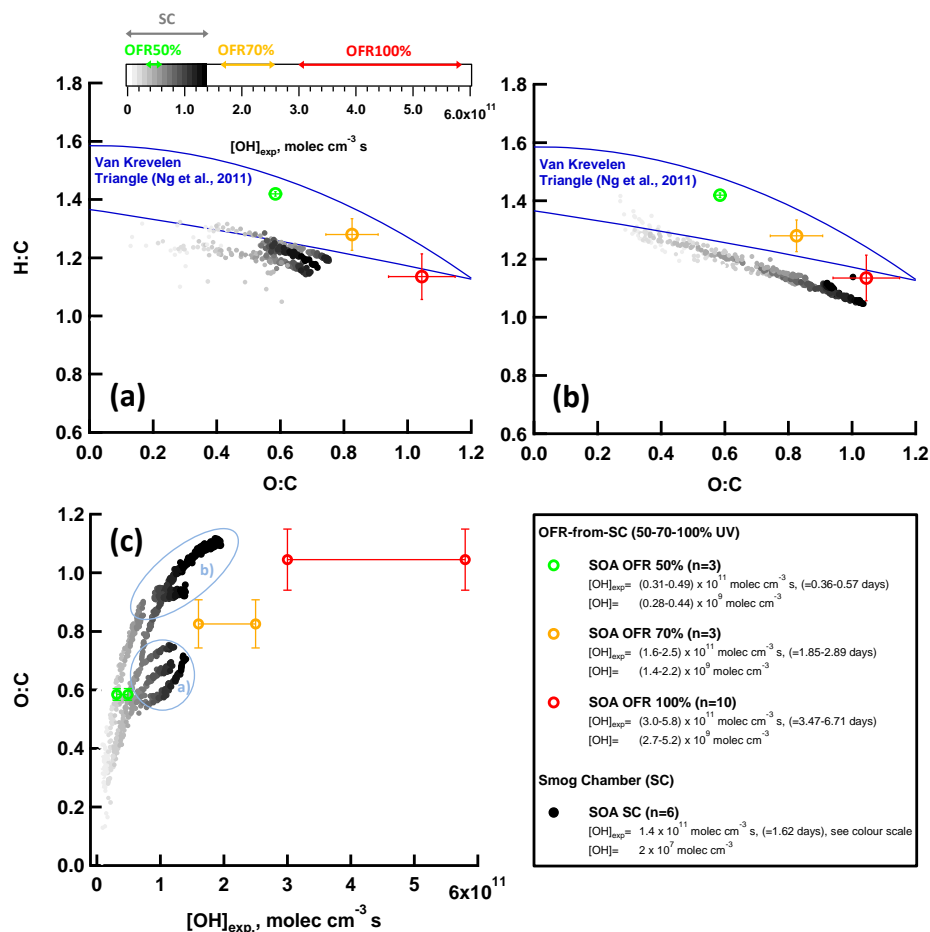


**Figure R1-4:** New version of Figure 7, splitting the experiments into a) and b) by their NO<sub>3</sub>/OA ratio, as previously addressed in Figure S16 and in addition panel c) showing the plot requested by the referee (O:C vs. OH exposure); the new figure caption reads as follows:

*“Bulk OA composition of SC and OFR SOA. a-b) Van-Krevelen plot (O:C vs. H:C) for SOA formed during SC expts (n=6, GDI1 standard and w/GPF, cW and Ph 1 (cW)) and OFR-from-SC data points (n=10, GDI1 standard and w/GPF, full cW, full cE, Ph 1 (cW)) at different OFR UV settings (100%, 70%, 50%). a) shows SC Expt (A2, A3, B3; Table S4) and b) SC Expt (A1, B1, B2; Table S4), experiments which are characterized by a NH<sub>4</sub>NO<sub>3</sub> is outside our CO<sub>2</sub><sup>+</sup>-AMS interference calibration range (Pieber et al., 2016). The POA contribution was subtracted from the total OA bulk composition; SOA/POA ratios are >> 10. The Aiken parameterization (Aiken et al., 2007; Aiken et al., 2008) has been applied to HR fitted data. Lines indicate the Van-Krevelen (VK) space typical for ambient AMS measurements (Ng et al., 2011). Error bars represent one standard deviation of measurement variability. (c) O:C of a) and b) as a function of [OH] exposure. [OH]<sub>exp</sub> in days refers to an assumed average ambient [OH] of 10<sup>6</sup> molec cm<sup>-3</sup>.”*

**RC1-27:** Fig. 2(b) POA point is missing for GDI4-catGPF (CW)

**Author Response:** The data point is now visible Figure 2.

**Text modifications:** The revised version of Figure 2 is provided in the answer to RC-2.

**RC1-28:** Fig. 5 Better to show the OH exposure range as well.

**Author Response:** Figure 5 presents one example experiment, and the OH-exposure information is provided in the figure caption to our earlier Figure 6 and Figure 7, as already described in the initial manuscript.

**Text modifications:** As described in our response above, no further modifications were made.

## References by RC1

See acp-2017-942-RC1 for references mentioned by Referee 1.

### References to Author's Response:

- Aiken, A. C., DeCarlo, P. F., and Jimenez, J. L.: Elemental analysis of organic species with electron ionization high-resolution mass spectrometry, *Anal. Chem.*, 79, 8350-8358, 10.1021/ac071150w, 2007.
- Aiken, A. C., Decarlo, P. F., Kroll, J. H., Worsnop, D. R., Huffman, J. A., Docherty, K. S., Ulbrich, I. M., Mohr, C., Kimmel, J. R., Sueper, D., Sun, Y., Zhang, Q., Trimborn, A., Northway, M., Ziemann, P. J., Canagaratna, M. R., Onasch, T. B., Alfarra, M. R., Prevot, A. S. H., Dommen, J., Duplissy, J., Metzger, A., Baltensperger, U., and Jimenez, J. L.: O/C and OM/OC ratios of primary, secondary, and ambient organic aerosols with high-resolution time-of-flight aerosol mass spectrometry, *Environ. Sci. Technol.*, 42, 4478-4485, 10.1021/es703009q, 2008.
- Barnet, P., Dommen, J., DeCarlo, P. F., Tritscher, T., Praplan, A. P., Platt, S. M., Prévôt, A. S. H., Donahue, N. M., and Baltensperger, U.: OH clock determination by proton transfer reaction mass spectrometry at an environmental chamber, *Atmos. Meas. Tech.*, 5, 647-656, 10.5194/amt-5-647-2012, 2012.
- Bruns, E. A., El Haddad, I., Keller, A., Klein, F., Kumar, N. K., Pieber, S. M., Corbin, J. C., Slowik, J. G., Brune, W. H., Baltensperger, U., and Prévôt, A. S. H.: Inter-comparison of laboratory smog chamber and flow reactor systems on organic aerosol yield and composition, *Atmos. Meas. Tech.*, 8, 2315-2332, 10.5194/amt-8-2315-2015, 2015.
- Hildebrandt, L., Donahue, N. M., and Pandis, S. N.: High formation of secondary organic aerosol from the photo-oxidation of toluene, *Atmos. Chem. Phys.*, 9, 2973-2986, 10.5194/acp-9-2973-2009, 2009.
- Jimenez, J. L., Canagaratna, M. R., Drewnick, F., Allan, J. D., Alfarra, M. R., Middlebrook, A. M., Slowik, J. G., Zhang, Q., Coe, H., Jayne, J. T., and Worsnop, D. R. (2016). Comment on "The effects of molecular weight and thermal decomposition on the sensitivity of a thermal desorption aerosol mass spectrometer", *Aerosol Sci Tech.* 50, i-xv, 10.1080/02786826.2016.1205728
- Jordan, A., Jaksch, S., Jürschik, S., Edtbauer, A., Agarwal, B., Hanel, G., Hartungen, E., Seehauser, H., Märk, L., Sulzer, P., and Märk, T. D.:  $\text{H}_3\text{O}^+$ ,  $\text{NO}^+$  and  $\text{O}_2^+$  as precursor ions in PTR-MS: isomeric VOC compounds and reactions with different chemical groups, 5th International Conference on Proton Transfer Reaction Mass Spectrometry and its Applications, 2011.
- Krechmer, J. E., Pagonis, D., Ziemann, P. J., and Jimenez, J. L. (2016). Quantification of Gas-Wall Partitioning in Teflon Environmental Chambers Using Rapid Bursts of Low-Volatility Oxidized Species Generated in Situ, *Environ Sci Technol.* 50, 5757-5765, 10.1021/acs.est.6b00606
- La, Y. S.; Camredon, M.; Ziemann, P. J.; Valorso, R.; Matsunaga, A.; Lannuque, V.; Lee-Taylor, J.; Hodzic, A.; Madronich, S.; Aumont, B. Impact of chamber wall loss of gaseous organic compounds on secondary organic aerosol formation: explicit modeling of SOA formation from alkane and alkene oxidation. *Atmos. Chem. Phys.* 2016, 16, 1417-1431.
- Lambe, A. T., Ahern, A. T., Williams, L. R., Slowik, J. G., Wong, J. P. S., Abbatt, J. P. D., Brune, W. H., Ng, N. L., Wright, J. P., Croasdale, D. R., Worsnop, D. R., Davidovits, P., and Onasch, T. B.: Characterization of aerosol photooxidation flow reactors: heterogeneous oxidation, secondary organic aerosol formation and cloud condensation nuclei activity measurements, *Atmos. Meas. Tech.*, 4, 445-461, 10.5194/amt-4-445-2011, 2011.
- Middlebrook, A. M., Bahreini, R., Jimenez, J. L., and Canagaratna, M. R. (2012). Evaluation of Composition-Dependent Collection Efficiencies for the Aerodyne Aerosol Mass Spectrometer using Field Data, *Aerosol Sci Tech.* 46, 258-271, 10.1080/02786826.2011.620041
- Murphy, D. M. (2016). The effects of molecular weight and thermal decomposition on the sensitivity of a thermal desorption aerosol mass spectrometer, *Aerosol Sci Tech.* 50, 118-125, 10.1080/02786826.2015.1136403
- Ng, N. L., Canagaratna, M. R., Jimenez, J. L., Chhabra, P. S., Seinfeld, J. H., and Worsnop, D. R.: Changes in organic aerosol composition with aging inferred from aerosol mass spectra, *Atmos. Chem. Phys.*, 11, 6465-6474, 10.5194/acp-11-6465-2011, 2011.
- Pagonis, D., Krechmer, J. E., de Gouw, J., Jimenez, J. L., and Ziemann, P. J. (2017). Effects of gas-wall partitioning in Teflon tubing and instrumentation on time-resolved measurements of gas-phase organic compounds, *Atmos. Meas. Tech.* 10, 4687-4696, 10.5194/amt-10-4687-2017
- Palm, B. B., Campuzano-Jost, P., Ortega, A. M., Day, D. A., Kaser, L., Jud, W., Karl, T., Hansel, A., Hunter, J. F., Cross, E. S., Kroll, J. H., Peng, Z., Brune, W. H., and Jimenez, J. L. (2016). In situ secondary organic aerosol formation from ambient pine forest air using an oxidation flow reactor, *Atmos. Chem. Phys.* 16, 2943-2970, 10.5194/acp-16-2943-2016
- Peng, Z., Day, D. A., Ortega, A. M., Palm, B. B., Hu, W., Stark, H., Li, R., Tsigaridis, K., Brune, W. H., and Jimenez, J. L. (2016). Non-OH chemistry in oxidation flow reactors for the study of atmospheric chemistry systematically examined by modeling, *Atmos. Chem. Phys.* 16, 4283-4305, 10.5194/acp-16-4283-2016
- Peng, Z., Day, D. A., Stark, H., Li, R., Lee-Taylor, J., Palm, B. B., Brune, W. H., and Jimenez, J. L. (2015). HOx radical chemistry in oxidation flow reactors with low-pressure mercury lamps systematically examined by modeling, *Atmos. Meas. Tech.* 8, 4863-4890, 10.5194/amt-8-4863-2015
- Pieber, S. M., El Haddad, I., Slowik, J. G., Canagaratna, M. R., Jayne, J. T., Platt, S. M., Bozzetti, C., Daellenbach, K. R., Frohlich, R., Vlachou, A., Klein, F., Dommen, J., Miljevic, B., Jimenez, J. L., Worsnop, D. R., Baltensperger, U., and Prévôt, A. S. H.: Inorganic Salt Interference on  $\text{CO}_2^+$  in Aerodyne AMS and ACSM Organic Aerosol Composition Studies, *Environ Sci Technol.* 50, 10494-10503, 10.1021/acs.est.6b01035, 2016.
- Platt, S. M., El Haddad, I., Pieber, S. M., Zardini, A. A., Suarez-Bertoa, R., Clairrotte, M., Daellenbach, K. R., Huang, R. J., Slowik, J. G., Hellebust, S., Temime-Roussel, B., Marchand, N., de Gouw, J., Jimenez, J. L., Hayes, P. L., Robinson, A. L., Baltensperger, U., Astorga, C., and Prévôt, A. S. H.: Gasoline cars produce more carbonaceous particulate matter than modern filter-equipped diesel cars, *Sci Rep.* 7, 4926, 10.1038/s41598-017-03714-9, 2017.

- Turpin, B. J., and Lim, H.-J.: Species Contributions to PM<sub>2.5</sub> Mass Concentrations: Revisiting Common Assumptions for Estimating Organic Mass, *Aerosol Sci. Technol.*, 35, 602-610, 10.1080/02786820119445, 2001.
- Weitkamp, E. A., Sage, A. M., Pierce, J. R., Donahue, N. M., and Robinson, A. L.: Organic aerosol formation from photochemical oxidation of diesel exhaust in a smog chamber, *Environ. Sci. Technol.*, 41, 6969-6975, 10.1021/es070193r, 2007.
- Zhang, X., Cappa, C. D., Jathar, S. H., McVay, R. C., Ensberg, J. J., Kleeman, M. J., and Seinfeld, J. H. (2014). Influence of vapor wall loss in laboratory chambers on yields of secondary organic aerosol, *Proceedings of the National Academy of Sciences*, 10.1073/pnas.1404727111
- Zhao, Y., Lambe, A. T., Saleh, R., Saliba, G., and Robinson, A. L.: Secondary Organic Aerosol Production from Gasoline Vehicle Exhaust: Effects of Engine Technology, Cold Start, and Emission Certification Standard, *Environ Sci Technol*, 52, 1253-1261, 10.1021/acs.est.7b05045, 2018.

## Referee Comments #2 (acp-2017-942-RC2-supplement) and author response.

Simone M. Pieber et al.

We thank the editor and referees for their comments. To guide the review process we have copied the referee comments in black text. Our responses are in regular blue font. We have responded to all the referee comments and made alterations to our paper (*in italic text*) and removed redundancies for clarification. Along with the revision we suggest a slightly changed title: “*Gas phase composition and secondary organic aerosol formation from gasoline direct injection vehicles with prototype particle filters investigated in a batch and flow reactor*”

### General:

**RC2-1:** This paper describes measurements of primary emissions and secondary organic aerosol from four modern gasoline direct injection (GDI) engine equipped vehicles. The market share of GDI vehicles is rapidly increasing in the US and other countries, displacing the more traditional port fuel injection engine equipped vehicles. This paper represents probably most systematic study of SOA formation from GDI vehicles to date. The paper also investigates the impact of adding a retrofitted gasoline particulate filter (GPF) to two of the vehicles. While others have investigated the effect of this technology on primary emissions, I am not aware of previous studies that have investigated its impact on SOA formation. The paper also uses an oxidation flow reactor (OFR) and a smog chamber to investigate SOA formation, comparing the results between the two systems and with measurements made with individual compounds. The paper shows SOA formation dominates primary PM emissions (consistent with previous studies, though the SOA/POA ratio seem much larger than previous studies). The paper demonstrates that the majority of SOA formation is formed from cold-start emissions, which is not surprising but I have not seen it demonstrated before. The paper shows that somewhat more than half of the SOA formation appears due to 8 single-ring aromatics. Finally the paper shows GPF reduces primary PM emissions but does not reduce the SOA formation (or non-methane organic compound emissions). Overall the paper is well written and very comprehensive. The experiments appear to have been carefully conducted (though I agree with the other reviewer’s concerns on treatment of wall loss), with results from repeated experiments shown (it would be nice to describe the precision a bit more). I think this paper makes a nice contribution and recommend that it be published in ACP after addressing the following comments.

**Author Response:** We thank the referee for the positive feedback and address the specific comments in the following. We provide answers to RC2 and modifications to our manuscript to the best of our abilities and have condensed and clarified the text where possible.

### Specific comments

**RC2-2:** Abstract and a few other places “a large fraction (>0.5)” These statements refer to the mass closure of the SOA production based on measured precursors. 1 is greater than 0.5. The authors need to be more quantitative; e.g. give a range (or some other metric such as median and interquartile range).

**Author Response:** We agree with the referee’s comment and have reformulated the statement in the abstract. As the assessment of the contribution is complex and condition-dependent, we prefer to remove the quantitative information in the abstract and rather keep the discussion of this issue in the results and discussion section 3.6 where we can address the details of this closure.

**Text modifications:** Abstract: “*A significant fraction of the SOA production was explained by those compounds, based on investigation of reacted NMOC mass and comparison of effective SOA yield curves with those of toluene, o-xylene and 1,2,4-trimethylbenzene determined in our OFR within this study and others from literature. Remaining discrepancies may result from diverse reasons including apart from unaccounted precursors also aging conditions, uncertainties of SOA yields for the aromatic hydrocarbons with different degrees of substitution, as well as experimental uncertainties in the assessment of particle and vapor wall losses.*”

**RC2-3:** Figure 6 suggests that this ratio likely varies with OA concentrations. Figure 5 suggests poor closure for 100% and 70% OFR conditions, but good closure for 50% OFR. SC has better closure at short timescales. The authors need to be more quantitative about the mass closure.

**Author Response:** We agree with the referee's observation. We have used two different ways to approach the closure in our manuscript: 1) with a forward mass closure as presented in initial Figure 5 as an example for 1 experiment (i.e. the reacted aromatic SOA precursor mass was weighted by a fixed SOA yield from the literature), and 2) via an indirect approach normalizing the formed SOA to the reacted ArHC mass (i.e. deriving an "effective yield" combining all reacted species), which allows to present the result as a function of OA loading, takes partitioning into account and is interpreted by comparing to the yields of classes of compounds (such as ArHC). As also Referee 1 noted that this is confusing, we have decided to remove the SOA-mass closure from initial Figure 5 (bottom panels), and instead present all our data only as a "yield closure" (method 2, Figure 6).

**Text modifications:** We have revised all text sections to allow this modification; instead of a mass closure we discuss the results now in terms of the yield-closure presented in section 3.6.

**RC2-4:** Retrofitted GPF – How was this done? How representative is it of how a true OEM designed and installed GPF-system would operate? It is hard to simply add a control system to a vehicle for which it was not designed (I have seen tests with a retrofit GPF hanging off the back of a car!), therefore I am always concerned about how representative the performance of researcher retrofitted system versus what might be done by a vehicle manufacturer. This is not to say that they are not seeing some effect of the GPF but it may be (much) less than the performance of bottom up engineered system. For example, I was surprised that the catalyzed GPF did not further reduce the NMOC emissions – what was the operating temperature of the GPF? Anyways I think the GPF results are interesting, but a bit more detail on how the retrofit was done, specifically limitations of researcher retrofitted systems should be acknowledged. Unless they can document that the retrofitted is representative of OEM designed and installed systems the conclusion section (line 10 on page 25) is too strong.

**Author Response:** We agree that validity of the experiments to transfer our results to bottom up engineered systems is a crucial point. We have highlighted that our GPF system was a "retrofit" in our discussion paper, and have described the system in section 2.1.1 (page 6, line 5 onwards). It is indeed difficult to judge how such systems will be implemented by manufacturers and there will be also variability between different vehicles. For our experiments, which we designed with experts from the industry, we replaced the "muffler" which was located ca. 60 cm downstream of the three-way-catalyst (TWC) with the GPF. Pictures are provided in Figure R2-1 which has been added to the SI of our revised manuscript. The GPF was not externally heated, and its temperature dependent on the exhaust conditions, in the same way the temperature of the TWC is dependent on this.

We believe our retrofit is installed in a location that is representative for real-world retrofitting of GDI vehicles which are on the market currently, and that our experiments represent also the typical temperature conditions that can be found in such retrofits. An evaluation of this system on primary particle number emissions was published previously by a sub-set of our collaboration team (Czerwinski et al., 2017). The PCFEs of this investigation yielded  $\geq 98\%$  for GPF1 on either GDI1 or GDI4, and  $\geq 86\%$  for catGPF on GDI4, and indicate somewhat lower performance of the catGPF on primary PN reductions. This does not seem to be dependent on the location of installation in a vehicle, given that GPF1 on GDI4 showed good performance.

We don't believe that the generally somewhat lower performance of catGPF on primary PN is caused the limited effect on NMOCs and associated SOA. Instead, we believe that given that the vehicle is already equipped with a TWC, it is unlikely to see additional effects on NMOC reductions by a 2<sup>nd</sup> catalytic system during cold-starts. This is, because under cold-start conditions the NMOCs that pass the TWC will also pass the catGPF, which, at this point will likewise not have reached light-off temperatures to efficiently remove NMOCs.

We agree, that differently engineered systems (especially catGPFs that will be meant to replace the TWC), should be investigated in the future to see whether further NMOC reduction can be achieved.



**Figure R2-1:** “Pictures of **a)** original “muffler” and GPF in comparison, **b)** retrofitted GPF, installed underfloor in replacement to “muffler”.”

**Text modifications:** We have modified above mentioned text sections to specify the distance between TWC and GPF (replacing muffler), which was roughly 60 cm. Along with modifications within the manuscript:

- “GDI1 was studied *i)* in standard configuration, and *ii)* equipped with a prototype gasoline particle filter (GPF (cordierite, porosity 50%, pore size 19  $\mu\text{m}$ , 2000 cells per square inch)), installed at the muffler (“underfloor”), which was located 60 cm downstream of the TWC. It’s filtration quality at this configuration is equivalent to the best available technology for DPFs (personal communication by the manufacturer; particle number reductions by the application of the GPF are further assessed in Czerwinski et al., 2017, and yield PCFE  $\geq 98\%$ ).”
- “GDI4 was retrofitted with *i)* the previously tested GPF (as above: cordierite, porosity 50%, and pore size 19  $\mu\text{m}$ , 2000 cells per square inch, PCFE  $\geq 98\%$ ), as well as *ii)* a Pd/Rh catalytically coated GPF (catGPF) (installed at the muffler, underfloor, while keeping the original TWC in the original position; the PCFE was  $\geq 86\%$ ).”

For the catGPF, additionally we had already the following statement provided in the initial version of the experimental section, which we kept in its original format:

- “For the retrofitted catGPF, the primary purpose of the catalytically active coating is the constant self-cleaning of deposited carbonaceous material on the particle filter (personal communication with manufacturer). In future applications, such catalytic coating on a GPF might replace the existing TWC in GDI vehicles, or specifically, the TWC can be replaced with a GPF carrying the TWC coating.”

Along with this, however, we have modified the conclusions section to state more explicit, that GPFs carrying the TWC coating meant to replace the initial TWC will possibly lead to better NMOC removals than the current TWCs, and that research addressing this should be conducted:

- “GPF application efficiently removes eBC, which is the dominant component of primary PM, and also shows small effects on the minor POA fraction. The volatile POA fraction passes through the filter in the vapor phase and later condenses when the exhaust is emitted and cooled; hence POA emission factors are not as significantly reduced as refractory PM. NMOC emissions and SOA formation are unaffected by the tested GPFs. This is particularly true when the GPF is catalytically inactive, and at cold-started driving cycles for catalytically active GPFs (i.e. when emissions pass through the TWC and the catGPF before light-off temperatures are reached.. This means that retrofitting GDI vehicles with GPFs will likely result in an important reduction of the total primary PM emitted (removal of refractory material), but will (under conditions similar to our experiments only to a small extent reduce NMHC (or NMOC) emissions including ArHC, and thereby not directly lead to a reduction of SOA. Future work on so-called “4-way catalysts”, i.e. a TWC catalyst directly applied onto a GPF and installed at the location of the current TWC for simultaneous filtration of particulates and catalytic conversion of NMHC (or NMOC) should be conducted, to understand whether reductions of SOA precursors, SOA production, and semi-volatile primary PM can be achieved with further optimized systems.”

**RC2-5:** The dramatically higher NMOC emissions and SOA production from cold start is important. Can the authors quantify how much more important it is than hot start (e.g. using an analysis similar to that Saliba et al. EST 2017 10.1021/acs.est.6b06509 to compare hot and cold start emissions).

**Author Response:** We have provided a comparison of cold-started and hot-started cycles in Figure 2 (discussion paper), but had not given a comparison of the values previously, this is a highly interesting point. We now provide ratios of Ph1-SOA emission factors over Ph2-4-SOA emission factors in the manuscript, which is similar to Saliba et al., 2017-approach, and indicates that the cold-start is 20-50 times more important. However, it needs to be noted that this information should only carefully be transferred to the ambient air, additional parameters (e.g. how long/far will a vehicle be driven for during a real journey and what's the ambient temperature, i.e. "how cold" is the vehicle) need to be considered (see also Platt et al., 2017). In addition to our own ratio, we also provide a reference to a recent publication by Zhao et al., 2018, who also compare SOA from cold- and hot engine conditions.

**Text modifications:** *"Data are presented as a function of suspended OA for all experimental conditions of cold-started GDII-3 (i.e. for full cW, cE; and Ph 1 (cW)), while GDI4 or hot engine conditions, i.e. Ph 2-4 (cW) are not included in our the analysis, as this data set includes only two experiments with concentrations levels close to our background measurements; a discussion of SOA yields from cold- and hot-engine emissions has recently been published by Zhao et al., 2018 for an OFR data set)."*

We have also added the following and updated the conclusions.

- *"Hot-engine emissions (Ph 2-4 sampling from cold-started WLTC, as presented in Figure 2d) also resulted in SOA formation, which was, however, 20-50 times lower in terms of EFs than SOA formed from Ph 1 sampling of a cold-started WLTC. This is in line with the trends indicated by the phase-dependent NMHC emissions (Figure 2c).*
- *"Future work should investigate the quantitative use of online OFR data in further detail for additional quantification of cold- and hot-start contribution of SOA to the total SOA burden; a discussion of the associated technical issues (i.e. changes in OH-exposure and condensational sink as well as the equilibration time inside the OFR reactor) has been recently published by Zhao et al., 2018."*

**RC2-6:** The conclusion section largely repeats conclusion from earlier in the paper. The paper would be improved if they put the results in context with the growing literature in this area. In particular I was interested if the results are consistent with the existing body of knowledge on SOA formation for PFI vehicle exhaust. My sense is that it is. You tested the vehicles using two different cycles? Were there any cycle dependencies or was cold start just dominant?

**Author Response:** We have modified and shortened the manuscript and provided additional comparison with literature. Figure 2a/b includes indeed data from WLTC and EDC cycle, comparing the cold/hot cycles. We don't observe any significant cycle-dependent differences which are larger than vehicle-by-vehicle or test-by-test variability, especially during cold-started cycles. As the EDC cycle was tested only as the full cycle and not split into separate phases, no explicit analysis of the SOA contribution to the total cycle can be made in comparison to the WLTC. This information has already been provided in the discussion paper and is now also stated more clearly in the conclusions section. Further points are discussed along the referee comments below specifically to Figure 2.

**Text modifications:**

- *"While no drastic cycle-dependencies (WLTC vs. EDC) were observable from our tests (especially during cold-started cycles), EFs of primary NMHC and THC were reduced by a factor of 90 under hot-started conditions."*
- *"Emissions of all cold-started vehicles, technologies and driving tests showed significant SOA formation upon photochemical oxidation (Figure 2b), in line with other studies on GDI as well as PFI systems (Platt et al., 2017; Gordon et al., 2014; Saliba et al., 2017; Zhao et al., 2018).*
- *"Overall, the SOA potential (in terms of an emission factor) of the tested vehicles agreed with recent literature reports from both, GDI and port fuel injection systems (PFI)."*

**RC2-7:** Figure 2 – The y-axes are five orders of magnitude. This illustrates large changes, but changes of a factor of 2 or 3 can also be interesting. For most tests it does appear that the GPF is reducing the POA emissions, but not as dramatically as the EC. I did not get that impression reading the text but it does appear in the figure. More attention needs to be paid to these trends.

**Author Response:** We agree that Figure 2 is packed with details, and we have revised it (see below). Further, we refer to our related publication (Munoz et al., 2018), which discusses the difference between cold- and hot-started cycle emissions in detail for GDIs in standard configuration, regarding CO, NO<sub>x</sub>, particle number and genotoxic PAHs. We agree on the observation of POA removal with the GPF and have adjusted our statements:

**Text modifications:** *“Retrofitted GPFs (including catGPF behind the standard TWC) appeared also to reduce the POA fraction.”*, is added in the results and have also updated the abstract (*“GPF retrofitting was found to greatly decrease primary particulate matter (PM) through removal of eBC, showed partial removal of the minor POA fraction, ...”*) and conclusions (*“GPF application efficiently removes eBC, which is the dominant component of primary PM, and also shows small effects on the minor POA fraction.”*).

We also added the following: *“A detailed discussion on emissions of CO, NO<sub>x</sub>, particle number and genotoxic PAHs from cold- vs. hot-started cycle driven GDI vehicles in standard configuration can be found in our related publication by Munoz et al., 2018.*

**RC2-8:** Figure 2 – The SOA production seems surprisingly high. For GDII the total NMHC (most of which are not SOA precursors) is around 1000 mg/kg (Figure 2a). The SOA production is between 200 and 600 mg/kg (Figure 2a) – the SOA production from the GPF equipped experiments with GDII seem incredibly high. This suggests an effective of SOA of 20-60% of the total NMHC emissions of which less than half is aromatics (Figure 4b is misleading because the NMOC measured by PTR is only 65% of NMHC measured by FID). The SOA production seems higher than previous studies of modern vehicles (they are more similar to 25 year old vehicles). I guess Figure 6 suggest SOA yields are “reasonable”, but I was confused looking at Figure 2 (maybe it is just the log scale with 5 orders of magnitude). Are there background issues?

**Author Response:** We agree with the very high SOA production of especially GDII-3, but specifically GDII. For the corresponding SOA emission factors in relation to previous publications, there are two additional things to consider. 1) the OA mass at which these SOA-emission factors are determined, and 2) that most previous literature is using exclusively data from SC and not OFRs (data points at the upper end of the SOA emission factors in our experiments are derived from OFR experiments). Additionally, previous SC experiments which the referee refers to were conducted typically at lower OH exposures than our experiments, and at different ratio of NO/NO<sub>2</sub> or total NO<sub>x</sub>/VOC, points which are discussed later in the manuscript in the section “SOA yield analysis“ and in Zhao et al. 2017, which we have added to our reference list

Regarding background issues, we have provided additional information in our answer to RC1 as well as within other answers herein. Experiments were conducted with high purity air after extensive cleaning (described in the main text). Background was insignificant compared to our vehicle testing data, except for Ph2-4 experiments which were close to background levels in terms of the NMOCs (noted in Figure caption to Figure 4).

**Text modifications:** Figure 2 was modified for clarity (see below).

**RC2-9:** Figure 2c – There is a lot of vehicle to vehicle variability (2+ orders of magnitude). Are the reductions between cold and hot start consistent across vehicles? Plotting ratios may be more informative. What is up with the experiments with an NMHC emission rate of 0.1 mg/kg? Are those valid data?

**Author Response:** Vehicle by vehicle differences between cold- and hot-started cycles can be seen from Figure 2a and we have already provided ratios in our discussion in section “3.1 Pollutants as function of vehicle technology and driving cycle”; We provide median and interquartile ranges for data presented in Figure 2c now; 0.1 mg/kg is the detection limit of our NMHC measurements, and data were below this limit in some cases.

**Text modifications:** Figure 2 was modified for clarity (see below).

**RC2-10:** Figure 2 is very busy (especially panel d). It is basically impossible to sort out the trends. Pick the key points you want to make and plot just that data. The SOA production appears surprisingly close to the NMHC emissions (it even exceeds it for some vehicles).

**Author Response:** Indeed, (OFR-from-SC)-SOA is very close to the FID-based NMHC emission factors determined in the SC. SOA emission factors never exceed the emission factors of aromatic hydrocarbons (which is the relevant information for SOA in our case). Hence, the information provided is fully consistent. We have revised the figure for clarity.

**Text modifications:** The figure was revised, see below, and have clarified section 3.1.

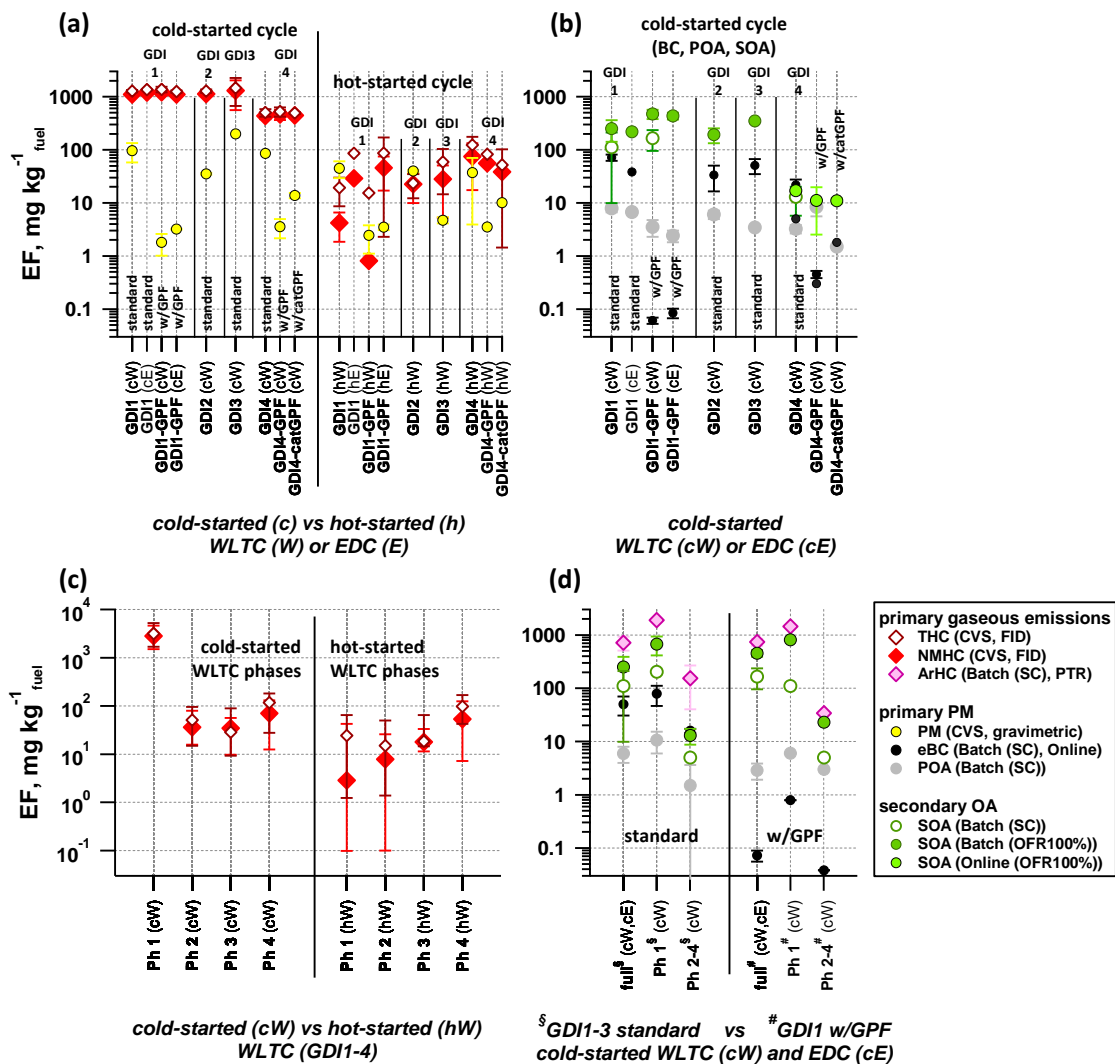


**Figure RC2-1:** new version of Figure 2; new figure caption reads as follows:

*“Emission factors (EF) of pollutants from cold-started (“c”) and hot-started (“h”) test cycles (WLTC (“W”) and EDC (“E”)). Individual cW and hW phases are indicated as “Ph” 1-4. (a) Total and non-methane hydrocarbons (THC, NMHC) and primary gravimetric particulate matter (PM) from CVS measurements over entire test cycles for different vehicle configuration and test conditions (average±1SD), (b) primary PM (equivalent black carbon (eBC) and primary organic aerosol (POA)), and secondary organic aerosol (SOA) from SC and OFR-from-SC experiments, and from online OFR operation at 100% UV per vehicle configuration for cold-started test cycles (average±1SD), (c) THC/NMHC of cW and hW experiments from (a) separated into individual cycle phases (median, and P25-P75 range are shown). (d) POA, eBC, aromatic hydrocarbons (ArHC) and SOA over the full cW and cE, compared to individual phases of cW from SC batch experiments and OFR-from-SC (average±1SD). (a-d) EF calculation is detailed in the SI. The time-resolved SOA*

*profile from online OFR measurements conducted on GDI4 in 2015 (standard and catGPF) is provided in Figure S14.”*

**RC2-11:** Additional ArHC (page 23). The analysis in Zhao et al. (EST 50(8): 4554-4563 2016) suggests some of the IVOCs are alkylated single ring aromatics larger than those included in the analysis here. How does including IVOC component measured by Zhao et al. change the analysis? His analysis suggests that IVOCs contribute somewhat less than half of the SOA in gasoline vehicle exhaust.

**Author Response:** We agree with the referee that those compounds could give additional SOA mass in our experiments. However, due to the different analytical techniques applied (we use a PTR-ToF-MS vs. the TD-GC-MS technique by Zhao et al., 2016), the data cannot be simply combined, as at the current moment, we are uncertain of which fraction of the IVOC (which makes up ca. 50% of the SOA in Zhao et al., 2016) overlaps with a fraction accounted for in our experiments, as we might be able to see fragments of e.g. alkyl-substituted aromatics that would fall into the IVOC category in Zhao et al., 2016 in our understanding. Ignoring a potential double count here, would likely allow us to conclude that those compounds make up a big fraction of the 50% of the missing mass seen by the FID but not PTR-ToF-MS, and would also bring our yield analysis in closer agreement with the yields determined for the vehicle exhaust (taking these additional compounds into account) would agree with that of single aromatic compounds.

**Text modifications:** We have added small adjustments to make this point more explicit in our manuscript.

**RC2-12:** Page 3 “diesel PM emissions have been greatly reduced.” – This is true for new diesel particulate filter (DPF) equipped vehicles but there are a lot of old diesels on the road, especially in Europe so human exposure to diesel particles has probably not yet been greatly reduced. Eventually it will be when the fleet is completely turned over. May want to refine this statement.

**Author Response:** We agree with the comment and have refined our statement to specify we are referring to test bench measurements and emission factors of the recent vehicle fleet, which isn't fully compliant with the fleet on the road.

**Text modifications:** *“Due to the regulatory attention and the improved after-treatment systems, diesel PM emissions from new generation vehicles have been greatly reduced, and fleet modernization will help to reduce their burden in the ambient air.”*

**RC2-13:** Page 4 “modern diesel vehicles” Modern is too generic. You should be more precise catalyzed-DPF equipped diesel vehicles. I don't necessarily think modern = DPF.

**Author Response:** We agree with the comment and have specified our terms.

**Text modifications:** *“modern”* was replaced with *“catalyzed-DPF equipped”*

**RC2-14:** Page 8 “experiment. Control experiments were conducted regularly in the SC to estimate the contribution of the SC background to SOA formation.” Please provide another sentence or two here that describes results from control experiments. How much SOA was formed in controls and how does it compare to what is measured in an experiment with vehicle exhaust. Did you run control experiments with the OFR – what were the background levels in that system?

**Author Response:** Thanks for the comment. In brief: control experiments were SOA experiments conducted with the SC and OFR after the standard cleaning procedures, and in both cases, SOA formed during control experiments was insignificant compared to SOA formed during vehicle testing, except for Ph2-4 which are close to background levels in the SC as stated in caption to Figure 4, and eventually GDI4 experiments which formed less SOA. SOA-control experiments with ammonium sulfate as seed in the SC yielded a SOA background  $< 1 \mu\text{g m}^{-3}$  after 2 hours of aging (i.e. comparable to the typical vehicle SC SOA experiments). Control experiments with UV on where also conducted in the OFR. When sampling test bench room air through our 1:8 dilution system (prior to online tests during cWLTC and hWLTC), background levels were  $< 10 \mu\text{g m}^{-3}$  (which is far below the online vehicle SOA measurements of 100-2000  $\mu\text{g m}^{-3}$ ). When sampling pure air from the cleaned SC before OFR-from-SC experiments, background levels were  $< 2 \mu\text{g m}^{-3}$ .

**Text modifications:** We have added the following:

- “Background measurements of the clean chamber were conducted prior to each experiment, and was insignificant compared to our measurements except for Ph2-4 or GDI4 experiments as stated in the results. Photochemistry control experiments were conducted regularly to estimate the contribution of the SC background to SOA formation; these experiments were conducted after the standard cleaning procedure. Instead of vehicle exhaust, pure air was used as a sample and ammonium sulfate ( $50 \mu\text{g m}^{-3}$ ) injected as seed. Other experimental procedures were in line with the typical vehicle experiments. We found a SOA background of  $< 1 \mu\text{g m}^{-3}$ , which is below the SOA concentrations formed during vehicle exhaust aging. Concentration-levels of our SC experiments were representative for urban ambient conditions, as reported in Table S4-S7.”
- “Background levels were  $< 2 \mu\text{g m}^{-3}$  SOA before OFR-from-SC experiments (when sampling from cleaned SC) and  $< 10 \mu\text{g m}^{-3}$  when sampling diluted (1:8) test bench room air prior online-experiments.”

**RC2-15:** Section 2.2.6 – I am pretty sure that you are calculated yields using the reacted aromatic mass in the denominator however this statement is confusing “the ratio of the SOA mass to the reacted SOA-forming mass,  $\Delta_{\text{NMOCreacted}}$ ” My understanding is that  $\Delta_{\text{NMOCreacted}}$  is not the same as the reacted aromatic mass. This needs to be cleaned up to avoid confusion. May also want to state this in the caption for Figure 6 to reminder reader of how yields are calculated.

**Author Response:** We calculated yields by normalizing the formed SOA mass to the reacted delta of the 8 selected aromatic hydrocarbons which dominated the identified NMOC fraction. We have revised this statement and clarified this also in the discussion to Figure 6.

**Text modifications:** According above description, the new text reads: “SOA yields analysis is based on SC and OFR-from-SC experiments with GDII-3. An effective SOA yield ( $Y_e$ ), was calculated as the ratio of the SOA mass to the reacted SOA-forming species  $i$  (in  $\Delta\mu\text{g m}^{-3}$ , Eq. (2)). We take into account all our identified SOA precursors (which refers to the 8 dominant aromatic hydrocarbons presented in Figure 4d), neglecting non-reactive and non-SOA forming precursors and assuming that all relevant SOA precursors are measured.

$$Y_e = \frac{\Delta_{\text{SOA}}}{\sum_i \Delta_{\text{SOA\_precursor}_i, \text{reacted}}} \quad (2)$$

**RC2-16:** Using “NMOC” to describe the sum of the PTR measurements is confusing as it is measuring less than 2/3rds of the organic gas emissions as measured with FID. This limitation needs to be stated more clearly (it is in the intro but the reader will likely forget – e.g. adding to caption of Figure 4 would be good and in other places in the main text when you discuss NMOC).

**Author Response:** We agree and have added the information throughout the manuscript and in the caption of Figure 4; further we have shortened section 3.4 and moved detailed discussion of  $\text{O}_2^+$  charge processes and fragmentation of alkyl-substituted aromatics to the SI to make this section more concise on the point of SOA-precursor identification.

**Text modifications:** As described in our response. The revised figure caption reads as follows: “(b) Relative composition of the PTR-ToF-MS derived NMOC fraction (which makes up  $65\pm 15\%$  of the FID-based NMHC signal on a carbon-basis for  $cW/cE/Ph\ 1(cW)$ ), (c) total ArHC EFs (which make up  $49\pm 8\%$  of the FID-based NMHC signal on a carbon-basis for  $cW/cE/Ph\ 1(cW)$ ), and (d) relative contribution of the 8 dominant ArHC (correspond to  $96.7\pm 3.3\%$  of the total ArHC signal for  $cW/cE/Ph\ 1(cW)$ ).”.

**RC2-17:**

Emissions data from tests in mg/kg-fuel needs to be provided in tables in supplemental.

**Author Response:** Emissions data presented in Figure 2 (in mg/kg fuel) can be made available to others upon request. Median values are stated in section 3.1.

**Text modifications:** No modifications were made to the text.

## References to Author's Response:

- Czerwinski, J., Comte, P., Heeb, N., Mayer, A., and Hensel, V.: Nanoparticle Emissions of DI Gasoline Cars with/without GPF, SAE Technical Paper 2017-01-1004, 10.1021/acs.est.7b05045, 2017.
- Gordon, T. D., Presto, A. A., May, A. A., Nguyen, N. T., Lipsky, E. M., Donahue, N. M., Gutierrez, A., Zhang, M., Maddox, C., Rieger, P., Chattopadhyay, S., Maldonado, H., Maricq, M. M., and Robinson, A. L.: Secondary organic aerosol formation exceeds primary particulate matter emissions for light-duty gasoline vehicles, *Atmos. Chem. Phys.*, 14, 4661-4678, 10.5194/acp-14-4661-2014, 2014.
- Jathar, S. H., Gordona, T. D., Hennigan, C. J., Pye, H. O. T., Pouliot, G., Adams, P. J., Donahue, N. M., and Robinson, A. L.: Unspeciated organic emissions from combustion sources and their influence on the secondary organic aerosol budget in the United States, *Proc. Natl. Acad. Sci. U. S. A.*, 111, 10473-10478, 10.1073/pnas.1323740111, 2014.
- Muñoz, M., Haag, R., Honegger, P., Zeyer, K., Mohn, J., Comte, P., Czerwinski, J., and Heeb, N. V.: Co-formation and co-release of genotoxic PAHs, alkyl-PAHs and soot nanoparticles from gasoline direct injection vehicles, *Atmos. Environ.*, 178, 242-254, 10.1016/j.atmosenv.2018.01.050, 2018.
- Nordin, E. Z., Eriksson, A. C., Roldin, P., Nilsson, P. T., Carlsson, J. E., Kajos, M. K., Hellén, H., Wittbom, C., Rissler, J., Löndahl, J., Swietlicki, E., Svenningsson, B., Bohgard, M., Kulmala, M., Hallquist, M., and Pagels, J. H.: Secondary organic aerosol formation from idling gasoline passenger vehicle emissions investigated in a smog chamber, *Atmos. Chem. Phys.*, 13, 6101-6116, 10.5194/acp-13-6101-2013, 2013.
- Platt, S. M., El Haddad, I., Pieber, S. M., Zardini, A. A., Suarez-Bertoa, R., Clairotte, M., Daellenbach, K. R., Huang, R. J., Slowik, J. G., Hellebust, S., Temime-Roussel, B., Marchand, N., de Gouw, J., Jimenez, J. L., Hayes, P. L., Robinson, A. L., Baltensperger, U., Astorga, C., and Prévôt, A. S. H.: Gasoline cars produce more carbonaceous particulate matter than modern filter-equipped diesel cars, *Sci Rep*, 7, 4926, 10.1038/s41598-017-03714-9, 2017.
- Saliba, G., Saleh, R., Zhao, Y., Presto, A. A., Lambe, A. T., Frodin, B., Sardar, S., Maldonado, H., Maddox, C., May, A. A., Drozd, G. T., Goldstein, A. H., Russell, L. M., Hagen, F. P., and Robinson, A. L.: A comparison of gasoline direct injection (GDI) and port fuel injection (PFI) vehicle emissions: emission certification standards, cold start, secondary organic aerosol formation potential, and potential climate impacts, *Environ Sci Technol*, 10.1021/acs.est.6b06509, 2017.
- Zhao, Y., Lambe, A. T., Saleh, R., Saliba, G., and Robinson, A. L.: Secondary Organic Aerosol Production from Gasoline Vehicle Exhaust: Effects of Engine Technology, Cold Start, and Emission Certification Standard, *Environ Sci Technol*, 52, 1253-1261, 10.1021/acs.est.7b05045, 2018.
- Zhao, Y., Nguyen, N. T., Presto, A. A., Hennigan, C. J., May, A. A., and Robinson, A. L.: Intermediate Volatility Organic Compound Emissions from On-Road Gasoline Vehicles and Small Off-Road Gasoline Engines, *Environ Sci Technol*, 50, 4554-4563, 10.1021/acs.est.5b06247, 2016.
- Zhao, Y., Saleh, R., Saliba, G., Presto, A. A., Gordon, T. D., Drozd, G. T., Goldstein, A. H., Donahue, N. M., and Robinson, A. L.: Reducing secondary organic aerosol formation from gasoline vehicle exhaust, *Proc Natl Acad Sci U S A*, 114, 6984-6989, 10.1073/pnas.1620911114, 2017.

# Gas phase composition and secondary organic aerosol formation from standard and particle filter-retrofitted gasoline direct injection vehicles—investigated in a batch and flow reactor: ~~effects of prototype gasoline particle filters.~~

5 Simone M. Pieber<sup>1,\*</sup>, Nivedita K. Kumar<sup>1</sup>, Felix Klein<sup>1</sup>, Pierre Comte<sup>2</sup>, Deepika Bhattu<sup>1</sup>, Josef Dommen<sup>1</sup>, Emily A. Bruns<sup>1</sup>, Dogushan Kilic<sup>1,†</sup>, Imad El Haddad<sup>1</sup>, Alejandro Keller<sup>3</sup>, Jan Czerwinski<sup>2</sup>, Norbert Heeb<sup>4</sup>, Urs Baltensperger<sup>1</sup>, Jay G. Slowik<sup>1</sup> and André S. H. Prévôt<sup>1,\*</sup>

<sup>1</sup>Paul Scherrer Institute, ~~Laboratory of Atmospheric Chemistry~~, CH-5232 Villigen, Switzerland

<sup>2</sup>Bern University of Applied Sciences, CH-2560 Nidau, Switzerland

<sup>3</sup>University of Applied Sciences Northwestern Switzerland; CH-5210 Windisch, Switzerland

<sup>4</sup>Empa Material Science and Technology; CH-8600 Dübendorf, Switzerland

<sup>†</sup>Now at Istanbul Technical University, Eurasian Institute of Earth Sciences, 34467 Sariyer, Turkey

\*Correspondence to: [simone.pieber@psi.ch](mailto:simone.pieber@psi.ch), [andre.prevot@psi.ch](mailto:andre.prevot@psi.ch)

15 **Abstract.** Gasoline direct injection (GDI) vehicles have recently been identified as a significant source of carbonaceous aerosol, of both primary and secondary origin. Here we investigated primary emissions and secondary organic aerosol (SOA) ~~formation from four GDI vehicles, two of which were also retrofitted with a prototype gasoline particle filter (GPF). We studied two exhaust for multiple vehicles and~~ driving test cycles, ~~and novel GDI after treatment systems under cold- and hot-engine conditions.~~ Emissions were characterized by proton transfer reaction time-of-flight mass spectrometry (gaseous non-methane organic compounds, NMOCs), aerosol mass spectrometry (sub-micron non-refractory particles), and light attenuation measurements (equivalent black carbon (eBC) determination using Aethalometer ~~measurements~~) together with supporting instrumentation. ~~We evaluated the effect of retrofitted prototype gasoline particle filters (GPFs) on primary eBC, organic aerosol (OA), NMOCs, as well as SOA formation. Two regulatory driving test cycles were investigated, and the importance of distinct phases within these cycles (e.g. cold engine start, hot engine start, high speed driving) to primary emissions and secondary products was evaluated.~~ Atmospheric processing was simulated using ~~both~~ the PSI mobile smog chamber (SC) and the potential aerosol mass oxidation flow reactor (OFR). ~~GPF retrofitting was found to greatly decrease primary particulate matter (PM) through removal of eBC, but showed limited partial removal of the minor POA fraction, and had no detectable effect on either NMOC emissions (absolute emission factors or relative composition) or SOA production. In all tests, overall, primary and secondary particulate matter (PM) and NMOC emissions were dominated by the engine cold start, i.e. before thermal activation of the catalytic after-treatment system. Differences were found in the bulk compositional properties of SOA produced by the OFR and the SC (O:C for OFR and SC (O:C were related to different OH exposures, but divergences in the and H:C remained unexplained ratios), while the SOA yields~~

Formatted: German (Switzerland)

Formatted: Superscript

Field Code Changed

Field Code Changed

5 agreed within experimental variability ~~our uncertainties between the two systems~~, with a tendency for lower SOA yields in SC ~~higher values in the OFR experiments than in the SC (or, vice versa, lower values in the SC)~~. A few aromatic compounds ~~are dominated~~ ~~found to dominate~~ the NMOC emissions ~~(, primarily benzene, toluene, xylene isomers/ethylbenzene and C3-benzenes)~~. A large fraction ( $\sim 0.5$ ) ~~A significant fraction~~ of the SOA production was explained by those compounds, based on ~~investigation of reacted NMOC mass and comparison with comparison of effective~~ SOA yield curves ~~of with those of~~ toluene, *o*-xylene and 1,2,4-trimethylbenzene determined in our OFR ~~within this study, and others from literature~~. Remaining ~~differences in the obtained SOA yields may~~ discrepancies (which were lower in the SC, but up to a factor of 2 for the OFR) ~~may have resulted~~ from diverse reasons including ~~apart from unaccounted precursors, also aging conditions, matrix effects, unaccounted-for precursors and differences in SOA yields of aromatic hydrocarbons with different degrees of substitution, as well as experimental uncertainties in the assessment of particle and vapor wall losses~~. GPF-retrofitting significantly reduced primary PM through removal of refractory eBC and partially removed the minor POA fraction. At cold-started conditions it did not affect hydrocarbon emission factors, relative chemical composition of NMOCs, or SOA formation, and likewise did SOA yields and bulk composition remain unaffected. Hence, GPF-induced effects at hot-engine conditions deserve attention in further studies.

Formatted: Not Highlight

Formatted: Not Highlight

Formatted: Font color: Auto

Formatted: Not Highlight

Formatted: Page break before

#### List of selected abbreviations/definitions

	AMS =	Aerosol mass spectrometer
	ArHC =	Aromatic hydrocarbons (including functionalized aromatic hydrocarbons)
	catGPF =	Catalytically active gasoline particle filter
5	cE =	Cold-started EDC vehicle test
	cW =	Cold-started WLTC vehicle test
	eBC =	Equivalent black carbon, as determined by Aethalometer measurements
	EDC =	<del>(New)</del> -European Driving Cycle <u>(previously known as the “New European Driving Cycle”)</u>
	FID =	Flame ionization detector
10	GDI =	Gasoline direct injection vehicle
	GPF =	Gasoline particle filter
	hE =	Hot-started EDC vehicle test
	hW =	Hot-started WLTC vehicle test
	NMHC =	Non-methane hydrocarbons, i.e. gaseous organic compounds (hydrocarbons) as measured by FID
15	NMOC =	Non-methane organic compounds, i.e. gaseous organic compounds as measured by PTR-ToF-MS
	OFR =	Oxidation flow reactor (a potential aerosol mass, PAM, reactor)
	OFR-from-SC =	Also referred to as “batch OFR”, OFR continuously sampling from a batch sample previously collected in the SC
	Online OFR =	OFR deployed online during a driving cycle, connected directly to diluted exhaust
20	<u>PCFE =</u>	<u>Particle count filtration efficiency</u>
	Ph 1 =	First phase of WLTC, Ph 1 (cW) refers to first phase of cold-started WLTC
	Ph 2-4 =	Second to fourth phase of WLTC, Ph 2-4 (cW) refers to the 2 <sup>nd</sup> to 4 <sup>th</sup> phase of cold-started WLTC, these are <del>quasi-quasi</del> -hot engine conditions
	POA =	Primary organic aerosol
25	PTR-ToF-MS =	Proton transfer reaction time-of-flight mass spectrometer
	SC =	Smog chamber
	SOA =	Secondary organic aerosol
	WLTC =	World-wide light duty test cycle

Formatted: Indent: Left: 0 cm, Hanging: 1.27 cm

## 1 Introduction

Vehicular emissions are a significant source of air pollution in many urban areas (~~(Platt et al., 2014);(Zotter et al., 2014);(Bahreini et al., 2012);(Borbon et al., 2013);(May et al., 2014);(Worton et al., 2014);(Gentner et al., 2017)~~). Depending on vehicle fleet technology, emissions may include fine particulate matter (PM), ~~which consists~~ consisting mainly of sub-micron primary organic aerosol (POA) and black carbon (BC), ~~as well as~~ and reactive gases such as nitrogen oxides (NO<sub>x</sub>), and organic ~~vapors~~ compounds. (Note that we refer to organic gas phase compounds as non-methane organic compounds, NMOCs. Measurements by proton transfer reaction mass spectrometry are also referred to as NMOCs herein.

Instead, when referring to measurements by flame-ionization technique, we ~~refer to organic gas phase compounds as use the term~~ non-methane hydrocarbons (NMHCs), instead.

~~The NMOCs react in the atmosphere and can form secondary organic aerosol (SOA) (Hallquist et al., 2009).~~ Human health is known to be impacted by NO<sub>x</sub> emissions, the associated ozone (O<sub>3</sub>) formation, and ~~especially~~ by fine PM emitted from combustion processes. Fine PM penetrates deep into the human body and can damage lung tissue (~~(Kunzi et al., 2015)~~), and ~~even damage~~ likewise the brain (~~(Calderon-Garciduenas and Villarreal-Rios, 2017)~~). Therefore, numerous strategies have been developed to decrease PM and NO<sub>x</sub> emissions from on-road vehicles, including optimization of engine settings and implementation of after-treatment systems. Examples of such systems ~~include~~ are oxidation catalysts that oxidize gas phase ~~products of incomplete combustion~~ pollutants (CO, NMOC) ~~to CO<sub>2</sub>~~, three-way-catalysts (TWC) (~~for gasoline on-road vehicles~~) and selective catalytic reduction (SCR) systems (~~for heavy duty diesel engines and large diesel passenger cars~~), ~~which to~~ convert NO<sub>x</sub> emissions to N<sub>2</sub> and O<sub>2</sub>, ~~and (catalyzed) diesel particle filters (DPFs) to reduce primary PM emissions from diesel vehicles.~~

Historically, diesel-fueled vehicles have been recognized as a significant source of ~~primary PM, especially~~ BC (Bond et al., 2004). Accordingly, the use of older-generation diesel vehicles may be restricted in cities and ~~catalyzed-DPF equipped diesel vehicles~~ modern are subject to stringent primary PM limits. To achieve ~~these limits~~ those, they are equipped with both diesel oxidation catalysts (DOCs) and diesel particle filters (DPFs), which have trapping efficiencies for refractory material of up to 99% (Gordon et al., 2013a). Due to the regulatory attention and the improved after-treatment systems, diesel PM emissions from new generation vehicles have been greatly reduced, and fleet modernization can reduce their burden in the ambient air further. However, NO<sub>x</sub> emissions from diesel vehicles have not been addressed as successfully and remain a topic of debate (e.g. ~~(Barrett et al., 2015);(Wang et al., 2016);(di Rattalma and Perotti, 2017)~~).

In contrast, ~~modern gasoline light-duty vehicles~~ have recently been engineered towards better fuel economy and reduced carbon dioxide (CO<sub>2</sub>) emissions to satisfy regulations aimed at mitigating climate change (Karjalainen et al., 2014).

However, recent research indicates that some of the methods used to attain these emission goals (~~including smaller engines, leaner combustion, and gasoline direct injection (GDI) systems mimicking the lower fuel consumption and decreased CO<sub>2</sub> emission factors of diesel vehicles~~), lead to an increase in the primary carbonaceous emissions (especially BC), among

Field Code Changed

Formatted: Indent: First line: 1.27 cm

Field Code Changed

Formatted: Italian (Italy)

Formatted: Italian (Italy)

Field Code Changed

Formatted: Italian (Italy)

Formatted: Italian (Italy)

Field Code Changed

Formatted: Italian (Italy)

Formatted: Italian (Italy)

Formatted: Font color: Red

Field Code Changed

gasoline systems (Karjalainen et al., 2014; Zhu et al., 2016; Platt et al., 2017; Saliba et al., 2017; Zimmerman et al., 2016b). ~~Consequently, Modern~~ modern gasoline light-duty vehicles have higher mass-based emission factors of these pollutants than ~~de-catalyzed-DPF equipped~~ diesel vehicles (Platt et al., 2017), ~~and a~~ Additionally, they have been reported to emit ammonia (NH<sub>3</sub>) (Heeb et al., 2006; Suarez-Bertoa et al., 2014) ~~from the formed on the~~ gasoline TWC. These emissions are released predominantly at engine start-up, when catalytic after-treatment systems are still cold, ~~as well as and~~ during acceleration and deceleration (Platt et al., 2017; Gentner et al., 2017).

Regarding PM abatement ~~In the light of increasingly stringent legislations for gasoline vehicles,~~ automobile manufacturers have recently considered equipping gasoline light-duty vehicles with gasoline particulate filters (GPFs) ~~in the light of increasingly stringent legislations, to reduce primary PM emissions, and f~~ First results are promising (Chan et al., 2014; Demuyne, 2017; Czerwinski et al., 2017). Although GPFs are likely to be similarly effective as DPFs in reducing primary ~~emissions-PM such as~~ (POA and BC), recent research indicates that the dominant fraction of the total PM from modern gasoline vehicles is secondary (Platt et al., 2017; Platt et al., 2013; Nordin et al., 2013; Gordon et al., 2014; Gordon et al., 2013b; Gentner et al., 2017). ~~NMOCs react in the atmosphere and can form secondary organic aerosol (SOA) (Hallquist et al., 2009).~~ Dominant secondary species include ~~secondary organic aerosol (SOA) (Hallquist et al., 2009)~~ SOA and ammonium nitrate (NH<sub>4</sub>NO<sub>3</sub>), which are formed by the reaction of emitted ~~organic gases-non-methane organic compounds (NMOCs)~~ and NO<sub>x</sub> (in the presence of NH<sub>3</sub>), respectively, with atmospheric oxidants such as hydroxyl (~~OH~~) radicals (OH). The gaseous precursors leading to secondary aerosol are unlikely to be removed by GPF systems alone. Laboratory results of the GPF effect on NMOC emissions and the associated SOA formation are, however, missing ~~so far~~.

Detailed investigations of SOA formation are typically performed in smog chambers (SC), where the emitted gases are oxidized in batch-style experiments lasting several hours under close-to-tropospheric conditions. The poor time resolution of such experiments prevents efficient study of SOA formation as a function of driving conditions (e.g., engine load or catalyst temperature), which as noted above is a critical consideration for gasoline vehicles. In contrast, oxidation flow reactors (OFR) (Kang et al., 2007; Li et al., 2015) are based on flow-through systems, allowing for investigation of SOA formation from time-varying emissions. They utilize higher-than-ambient oxidant concentrations to simulate hours to days of atmospheric aging in only a few minutes of experimental time. ~~However, few~~ Several studies have attempted the ~~quantitative application of OFR systems to complex combustion emissions - (Zhao et al., 2018; Karjalainen et al., 2015; Bruns et al., 2015; Tkacik et al., 2014; Ortega et al., 2013)~~ quantitative application of OFR systems to complex combustion emissions. An in-depth analysis of SC and OFR application to GDI exhaust, however, remains missing, and the ~~differences between~~ OFR and atmospheric oxidation conditions (e.g. high oxidant concentrations, short-wavelength light spectrum, and high wall surface-to-volume ratios) require further investigation (Lambe et al., 2011; Lambe et al., 2015; Peng et al., 2015; Peng et al., 2016; Li et al., 2015; Lambe et al., 2017; Palm et al., 2016).

Despite ~~numerous~~ recent ~~investigations~~ studies of SOA formation from gasoline vehicle exhaust (Platt et al., 2013; Gordon et al., 2013b; Gordon et al., 2014; Nordin et al., 2013; Platt et al., 2017; Zhao et al., 2017; Zhao et al., 2018), the SOA formation processes, ~~and the the~~ role of relevant precursors and their SOA yields in simulated aging

- Field Code Changed ... [1]
- Formatted ... [2]
- Field Code Changed ... [3]
- Field Code Changed ... [4]
- Formatted ... [5]
- Field Code Changed
- Formatted ... [6]
- Field Code Changed ... [7]
- Field Code Changed ... [8]
- Formatted: Not Highlight
- Field Code Changed ... [9]
- Formatted ... [10]
- Field Code Changed
- Formatted ... [11]
- Formatted ... [12]
- Field Code Changed
- Formatted ... [13]
- Field Code Changed
- Formatted ... [14]
- Field Code Changed
- Formatted ... [15]
- Formatted ... [16]
- Field Code Changed
- Formatted ... [17]
- Field Code Changed
- Formatted: English (U.S.)
- Field Code Changed ... [18]
- Formatted ... [19]

~~experiments~~ remain a subject of debate, ~~and SOA data from the European GDI fleet are scarce~~. A wide range of ratios of secondary-to-primary OA (SOA/POA), and SOA yields (mass of SOA formed per organic vapors reacted) has been reported ~~despite while using~~ standardized and repeatable testing procedures (~~(Jathar et al., 2014); (Gentner et al., 2017)~~). This is in part due to the high uncertainty related to experimental considerations, including NMOC levels, NO concentrations, OH exposure, particle and vapor wall losses and emissions sampling. ~~Further, due to limitations of~~ Moreover, the previously applied techniques ~~to study complex combustion emissions~~ (such as offline ~~gas chromatography~~ GC-MS and ~~GC-FID~~ analysis of the total hydrocarbons (THC), or quadrupole proton transfer reaction mass spectrometry (Q-PTR-MS) (~~(de Gouw et al., 2003); (Lindinger and Jordan, 1998)~~) ~~allowing which allowed~~ only for online monitoring of selected compounds having no significant interferences at the same integer  $m/z$ ). ~~show limitations when studying complex combustion emissions~~. Recently, ~~(Zhao et al., 2016)~~ suggested that the precursors are dominantly volatile organic compounds ~~(VOCs)~~ with a saturation ~~mass~~ concentration,  $C^*$ , above  $10^6 \mu\text{g m}^{-3}$ ), ~~and This~~ should ~~hence~~ allow for investigation with modern online instrumentation, such as the high resolution time-of-flight PTR-MS (PTR-ToF-MS).

Here, we investigated primary NMOC, POA, eBC emissions and SOA formation from Euro 4 and Euro 5 ~~direct injection gasoline~~ (GDI) vehicle exhaust, including vehicles retrofitted with prototype ~~gasoline particle filter~~ (GPFs). Vehicles were tested on a chassis dynamometer during a modern regulatory driving cycle (world-wide light duty test cycle, WLTC class-3) and an older low-load European driving cycle (EDC); ~~both~~ under cold- and hot-~~started~~ engine conditions. ~~We studied~~ SOA formation ~~was investigated through batch-style aging of collected emissions in (1) the PSI mobile smog chamber (SC) (Platt et al., 2013); and (2) the potential aerosol mass (PAM) oxidation flow reactor (OFR.) (Bruns et al., 2015; Lambe et al., 2011; Lambe et al., 2015) both, applying the latter for batch-style as well as time-resolved analysis, used to study oxidation of batch emissions and single precursors. Further, time-resolved analysis of aged emissions during a driving cycle using the OFR for cold and hot started emissions was performed.~~ Relevant SOA precursors were characterized using a PTR-ToF-MS, ~~and their consumption photochemical processing of both individual and total NMOC was related to SOA formation, where The SOA mass and its bulk chemical composition was were characterized derived from by~~ HR-ToF-AMS measurements.

## 25 2 Experimental

Two ~~sets of experiments to study vehicle emission~~ experimental sets were conducted (~~experiment~~ set I in 2014, ~~experiment~~ set II in 2015). In addition, selected SOA precursors NMOCs (toluene, *o*-xylene, and 1,2,4-trimethylbenzene (TMB)) were separately injected into the OFR ~~at different concentrations~~ for comparison with the vehicle ~~exhaust aging experiments~~ data (experiments conducted in 2016). In the following we describe vehicle testing (Section 2.1), ~~non-regulatory and~~ photochemistry experiments (~~including SC and OFR description and data correction~~) (Section 2.2), and mass spectrometric instrumentation (~~including data processing~~) (Section 2.3).

Field Code Changed

## 2.1 Vehicle testing

Vehicles were operated on a chassis dynamometer ~~with standard testing equipment~~ at the “Laboratories for IC-Engines and Exhaust Emission Control of the Berne University of Applied Sciences in Biel (Switzerland)”, which includes a roller dynamometer (Schenck 500 GS60), a driver conductor system (Tornado, version 3.3), a CVS dilution system (Horiba CVS-9500T with Roots blower), and an automatic air conditioning in the hall; (intake- and dilution air), which was maintained to maintain a temperature of 20–30°C and an absolute humidity of 5.5-12.2 g kg<sup>-1</sup>. The driving resistances of the test bench and the braking resistances were set according to legal prescriptions without elevation change. This equipment ~~fulfills fulfilled~~ the requirements of the Swiss and European exhaust gas legislation. The dilution ratio in the CVS-dilution tunnel ~~is~~ was variable and assessed ~~by measurement of the CO<sub>2</sub>-analysis~~ by means of the CO<sub>2</sub>-analysis; the range was from 8, during high engines loads, to 30-40, at idle conditions. ~~In addition, an FTIR instrument sampled undiluted exhaust at the tailpipe of the vehicles. Gaseous components were monitored with an exhaust gas measuring system Horiba MEXA-9400H, including measurements of CO and CO<sub>2</sub> by infrared analyzers (IR), hydrocarbons by flame ionization detector (FID) for total hydrocarbon (THC) and non-methane hydrocarbon (NMHC) measurements. Further instrumentation is listed in SI Section S2.~~

### 2.1.1 Vehicles, GPFs and fuels

~~The vehicles tested are listed in Table 1 and Table S1 list the tested vehicles (Supporting Information). In 2014, we tested two vehicles were tested: a modern GDI Opel Insignia (denoted GDI1), as well as a and a Volvo V60 (denoted GDI4). GDI1 was investigated studied i) in standard configuration, and ii) also equipped retrofitted with a prototype gasoline particle filter (GPF, cordierite, porosity 50%, pore size 19 µm, 2000 cells per square inch). The GPF was installed at the muffler (“underfloor”), ca. 60 cm downstream of the original TWC, and replaced the muffler (Figure S1). The GPF filtration quality at this configuration was equivalent to the best available technology for DPFs (personal communication by with the manufacturer; particle number reductions were further assessed in (Czerwinski et al., 2017) and yielded a PCFE >98%). In 2015, we tested two additional GDI vehicles (denoted GDI2, and GDI3) in standard configuration. We also repeated were tested (no retrofitted after treatment system). Tests with GDI4 (Volvo V60) in standard configuration were repeated in 2015; further, GDI4 and was retrofitted with two GPFs: a) the with i) the previously tested GPF (as above: cordierite, porosity 50%, and pore size 19 µm, 2000 cells per square inch), as well as ii) and b) a Pd/Rh catalytically coated GPF (denoted catGPF). Retrofitting was again performed in form of an (installed at the muffler, underfloor modification replacing the muffler ca. 60 cm downstream the, while keeping the original TWC in the original position. The PCFE was >86%). For the retrofitted catGPF, the primary purpose of the catalytically active coating is was the constant GPF self-cleaning of deposited carbonaceous material on the particle filter according to (personal communication with the manufacturer). In future applications, such catalytic coatings on a GPF might replace the existing TWC in GDI vehicles, or~~

Field Code Changed

Formatted: Not Highlight

Field Code Changed

Formatted: Not Highlight

Formatted: Not Highlight

5 ~~more specifically~~, the TWC ~~could~~ be ~~replaced with a GPF carrying the TWC coating~~ ~~combined with a GPF in one system~~. All vehicles were fueled with gasoline from the Swiss market, RON 95, according to SN EN228. It contains ~~sed~~ 35% ~~of~~ aromatic hydrocarbons, ~~below~~ 1% alkenes, 5% methyl-tert-butyl-ether (MTBE) (in 2014, ~8% in 2015) added as anti-knocking agent, ~~and~~ ~~and~~ <0.5% ethanol, all on a volumetric basis.

### 2.1.2 Test cycles

10 We used dynamic driving cycles: the world-wide light duty test cycle (WLTC-class 3), and ~~for reference~~ the common, but ~~nowadays considered~~ less representative, EDC (European driving cycle) ~~(speed profiles in Figure 1 and Figure S2 provide the speed profiles)~~. While the EDC is characterized by two phases ~~(urban and extra-urban phase of highly repetitive characteristics)~~, and lasts 20 min, the WLTC ~~is characterized by~~ has four phases at different speed levels ~~(referred to as Phase (Ph) 1-4, i.e. low, medium, high, extra-high speed)~~, ~~and~~ ~~it~~ contains patterns of disruptive acceleration and deceleration, ~~and~~ it lasts 30 min. Engines were started either after a soaking time of at least 6 hours at ~~the test bench~~ temperature (typically between 20-25°C, referred to as “cold-started”), or after warming up ~~the~~ the engine and after-treatment system by driving for 3 min at a steady-state speed of (80 km h<sup>-1</sup>, “hot-started”). ~~Cycles are classified~~ Tests are referred to as cold-started WLTC (~~denoted~~ cW), ~~and~~ hot-started WLTC (hW), cold-started EDC (cE), and hot-started EDC (hE) throughout the manuscript.

### 2.2 Non-regulatory measurements and photochemistry experiments

20 In parallel to ~~the regulatory~~ CVS sampling and tailpipe FTIR measurements, emissions were sampled ~~from the tailpipe~~ using either 1 or 2 Dekati ejector dilutors in series for characterization by non-regulatory equipment and photochemistry experiments. ~~Figure 1~~ ~~Figure 1~~ gives a scheme of the set-up, ~~including our non-regulatory equipment, the SC and OFR~~. Sampling was performed ~~similar to the description in as reported earlier in (Platt et al., 2017) and (Platt et al., 2013); It which demonstrated good agreement between of batch-sampled emissions with and (online measurements of gaseous emission pollutants at the tailpipe (Platt et al., 2013) and also gravimetric PM samples from the CVS (Platt et al., 2017). A likewise comparison of our PM measurements is provided in Figure S16. Tubing material, length, temperature and flow rates are specified in the SI Section S3. Clean air to operate the non-CVS sampling and dilution system, as well as the SC and OFR, was provided by a compressor (Atlas Copco SF 1 oil-free scroll compressor with 270 L container, Atlas Copco AG, Switzerland) combined with an air purifier (AADCO 250 series, AADCO Instruments, Inc., USA). Clean air specifications can be found in Platt et al., 2013. Along with a suite of basic gas phase monitors for measurements of CO<sub>2</sub>, CO and CH<sub>4</sub> (CRDS, Picarro), THC, CH<sub>4</sub> and NMHC (FID, Horiba), NO, NO<sub>2</sub>, O<sub>3</sub> and particle-phase instruments (CPC and SMPS for particle number and size measurements, and 7-wavelength aethalometers for eBC determination (Drinovec et al., 2015) (Aerosol d.o.o)) we deployed high resolution time-of-flight mass spectrometers were applied to investigate the chemical~~

Field Code Changed

~~composition of the fresh and aged exhaust (instruments are listed Table S2-S3, Supporting Information). Mass spectrometric instrumentation is described in Section 2.3, all instruments are listed in Tables S2-S3.~~

## 5 2.2.1 Experimental procedure

Experiments were conducted in three configurations:-

- ~~1)~~ time-resolved measurements of primary emissions and time-resolved aging in the OFR during dynamic driving cycles, denoted “OFR online”;
- ~~2)~~ OFR photochemical aging from SC batch samples which were collected over a driving cycle or phases there, denoted “OFR-from-SC”;
- ~~3)~~ SC photochemical aging of the before-mentioned SC batch sample.

~~Experiments were conducted as follows. At the start of each experiment the cleaned SC was filled to approximately two thirds full with humidified air, with the remaining volume available for sample injection. First, diluted emissions from the cold started vehicle tests were sampled online during the test bench driving cycle and characterized in real time, either fresh (“primary”), or photo-chemically aged in the OFR (“secondary”). In parallel, the Diluted emissions from the cold-started driving cycle were then sampled into the SC for a later photochemical batch experiment. The batch sampling was conducted either over the full cycle (cW and cE), the first (Ph 1, cW) or the aggregated second through fourth phases (Ph 2-4, cW). After sample injection, the chamber volume was filled up to its maximum with clean pure air, and the relative humidity (RH) was adjusted to 50%. To quantify OH exposure during the later photochemical experiments, 1 µL of 9-times deuterated BuOH (BuOH-D9, purchased from Cambridge Isotope Laboratories) was added to the sample (Barnet et al., 2012).~~

~~In parallel to SC sampling, diluted emissions from the cold-started tests were sampled online during the test bench driving cycle and characterized in real-time, either fresh (“primary”), or OFR photo-chemically aged (“secondary”). Once the first driving test was completed and the primary emissions were characterized in the SC batch, Thereafter, a second hot-started vehicle test was performed. For this purpose, for which the vehicle was warmed up for operated for 3 min at 80 km h<sup>-1</sup> steady state driving prior to the test. Emissions of the hot-started cycle test were emissions were sampled and characterized in real-time fresh, or OFR aged (“OFR online”). No sampling of hot-started driving cycle emissions of hot-started cycle emissions into the SC was performed.~~

~~When Once both driving tests were completed, the emissions previously sampled cold-started emissions collected in the SC were characterized, and when the monitored parameters and BuOH-D9 signal stabilized and indicated a well-mixed chamber, primary emissions were sampled from the SC into the OFR for photochemical aging and photochemically aged in the OFR by sampling the batch collection from the SC (“OFR-from-SC” sampling experiments, also referred to as “batch OFR” herein). Then, photochemical aging was performed in the SC. In addition to the vehicle tests (online OFR and OFR-~~

Formatted: List Paragraph, Bulleted +  
Level: 1 + Aligned at: 0.63 cm +  
Indent at: 1.27 cm

Field Code Changed

Formatted: Indent: First line: 1.27  
cm

~~from SC experiments explained above), single NMOC (toluene, o-xylene, 1,2,4-TMB) species from a liquid injection system were aged in the OFR as reference measurements.~~

At the start of each experiment the SC was filled to approximately two thirds full with humidified air, with the remaining volume available for sample injection. After sample injection, the chamber volume was filled up to its maximum with pure air, and the relative humidity (RH) was adjusted to 50%. To quantify OH exposure during the experiments, 1  $\mu$ L of 9-times deuterated BuOH (BuOH-D9, purchased from Cambridge Isotope Laboratories) was added (Barnet et al., 2012). Once the monitored emissions parameters and the BuOH-D9 signal stabilized and indicated a well-mixed chamber, primary emissions were characterized and sampled into the OFR for photochemical aging. The OFR was operated at different varied OH exposures determined by UV lamp intensity (denoted 100%, 70% and 50%, %). Finally, UV on measurements were followed by a UV off (OFR dark) period. Once OFR-from-SC sampling was completed, O<sub>3</sub> was injected into the SC to titrate NO to NO<sub>2</sub>. Nitrous acid (HONO), used as an OH precursor in the SC, was injected continuously for the remainder of the experiment and photochemistry was initiated by illuminating the SC with the UV lights for a period of 2 hours. The temperature around the SC was kept initially approximately at 25.23 $\pm$ 2 $^{\circ}$ C, but and reached up to 30.26 $\pm$ 2 $^{\circ}$ C with UV lights switched on. The OFR likely also has exhibited slightly higher than ambient temperatures close to the UV sources, due to heating from the lamps. Background measurements were conducted before every experiment in SC and OFR, see Section 2.2.2 and 2.2.3.

~~In addition to GDI exhaust experiments the vehicle tests (online OFR and OFR from SC experiments explained above), single NMOC (toluene, o-xylene and 1,2,4-TMB) species provided via from a liquid injection system were aged in the OFR as reference measurements in separate experiments.~~

## 2.2.2 PSI mobile smog chamber (SC)

The PSI mobile SC described by (Platt et al., 2013) is an approximately 12 m<sup>3</sup>, 125  $\mu$ m thick collapsible Teflon bag (DuPont Teflon fluorocarbon film (FEP), type 500A, Foiltec GmbH, Germany) suspended from a mobile aluminum frame (2.3 $\times$ 2 $\times$ 2.5 m, L $\times$ W $\times$ H) with a battery of 40 $\times$ 100W UV lights (Cleo Performance solarium lamps, Philips). It is equipped with an injection system for purified air, water vapor, and gases (~~O<sub>3</sub>, NO, NO<sub>2</sub>, SO<sub>2</sub>, propene (C<sub>3</sub>H<sub>6</sub>)~~). OH radicals used as the primary oxidant are generated by photolysis of HONO injected continuously into the chamber and generated as described in (Platt et al., 2013); (Taira and Kanda, 1990). During photochemistry, in-situ formation of O<sub>3</sub> resulted in an average OH/O<sub>3</sub> ratio of 5 $\times$ 10<sup>-6</sup>; OH concentration and exposure are provided in the results section. The SC was cleaned prior to each experiment by filling with humidified air and O<sub>3</sub> and irradiating with UV light for at least 1 hour, followed by flushing with dry, pure air for at least 10 h. Background measurements of the clean chamber-SC were conducted prior to each experiment with UV lights off. Background was insignificant compared to our measurements, except when stated otherwise. Photochemistry C<sub>2</sub> control experiments were conducted regularly in the SC to estimate the contribution of the SC background

Field Code Changed

Formatted: Not Highlight

Formatted: Not Highlight

Field Code Changed

Formatted: Subscript, Not Highlight

Formatted: Not Highlight

Field Code Changed

Field Code Changed

Formatted: Not Highlight

Formatted: Not Highlight

to SOA formation: ~~these experiments were conducted after the standard cleaning procedure. Instead of vehicle exhaust, pure air was used as a sample and ammonium sulfate (50  $\mu\text{g m}^{-3}$ ) injected as seed. Other photochemistry experimental procedures were in line with the typical vehicle experiments. We found a SOA background  $<1 \mu\text{g m}^{-3}$ . This was below the SOA concentrations formed during vehicle exhaust aging, see concentration-levels as reported in Tables S4-S7. Concentration levels in the SC, which were a result of our sampling and dilution strategy, were representative for urban ambient conditions.~~

Formatted: Font color: Auto

Formatted: Font color: Auto, Not Highlight

### 2.2.3 Oxidation flow reactor (OFR)

Experiments herein utilize the potential aerosol mass (PAM) OFR, of which several different configurations currently exist (~~(Bruns et al., 2015); (Lambe et al., 2011); (Kang et al., 2007); (Lambe et al., 2015); (Lambe and Jimenez)~~). Our OFR was previously described by ~~(Bruns et al., 2015)~~ and consists of a 0.015  $\text{m}^3$ , cylindrical glass chamber (0.46 m length, 0.22 m diameter) containing two low pressure mercury UV-lamps, each with discrete emission lines at 185 and 254 nm (BHK Inc.) (~~(Li et al., 2015); (Peng et al., 2015); (Peng et al., 2016)~~). The lamps ~~are-were~~ cooled by a constant flow of air. The incoming reactant flow ~~is-was~~ mixed radially dispersed by a perforated mesh screen at the inlet flange. In our experiments, the flow through the OFR was regulated by the flow pulled by instruments and pumps behind the reactor, and was set to  $\sim 8\text{-}9 \text{ L min}^{-1}$ ; ~~. This corresponding corresponds~~ to a plug flow residence time of 90-100 s. A ~~small~~ fraction of the total flow ( $0.5\text{-}1 \text{ L min}^{-1}$ ) was sampled behind a second perforated mesh, ~~(often termed "ring-flow")~~ and discarded ~~to limit wall effects~~. The OFR was equipped with an injection system for water vapor (a Nafion humidifier) and organic compounds (BuOH-D9 as an OH tracer, and toluene, *o*-xylene and 1,2,4-TMB purchased from Sigma-Aldrich (p.a.) for single-precursor tests) (~~Figure S1, Supporting Information~~). ~~Figure S3 provides a scheme. OH radicals in the OFR were produced by photolysis of water vapor at 185 nm, and by production of atomic oxygen in excited state  $\text{O}(^1\text{D})$  from photolysis of ozone ( $\text{O}_3$ ) at 254 nm, which can react with  $\text{H}_2\text{O}$  to form OH.  $\text{O}_3$  itself was produced by reaction of atomic oxygen in ground state,  $\text{O}(^3\text{P})$ , with  $\text{O}_2$ .  $\text{O}(^3\text{P})$  in turn was formed by photolysis of  $\text{O}_2$  at 185 nm. Lamp power can be regulated between 0 and 100%, with lower intensities lowering both,  $\text{O}_3$  and OH production. The ratio of  $\text{OH}/\text{O}_3$  remained relatively constant at our test points:  $(1.4\text{-}2.6)\times 10^{-5}$  at 100%,  $(1.9\text{-}3.0)\times 10^{-5}$  at 70%, and  $(1.7\text{-}2.6)\times 10^{-5}$  at 50%. OH concentration and exposure are provided in the results section.~~

Formatted: German (Switzerland)

Field Code Changed

During "online" (time-resolved) operation ~~of the OFR~~, the diluted exhaust (~~either~~ 1 or 2 ejector dilutors, ~~each at a dilution ratio of 1:8~~) was mixed with humidified air up to ~~50% of the total volume~~ ~~50% of the total~~ flow through the reactor, ~~leading to an additional dilution of up to a factor 2. When sampling from the SC (For OFR-from-SC experiments)~~ instead, no separate addition of water vapor or BuOH-D9 was required. ~~OH radicals in the OFR are produced by photolysis of water vapor ( $\text{H}_2\text{O}$ ) at 185 nm, or by production of atomic oxygen in excited state  $\text{O}(^1\text{D})$  from photolysis of ozone ( $\text{O}_3$ ) at 254 nm, which can react with  $\text{H}_2\text{O}$  to form OH.  $\text{O}_3$  itself is produced by reaction of atomic oxygen in ground state,  $\text{O}(^3\text{P})$ , with  $\text{O}_2$ .  $\text{O}(^3\text{P})$  itself is formed by photolysis of  $\text{O}_2$  at 185 nm. Lamp power can be regulated between 0 and 100%, with lower intensities lowering both,  $\text{O}_3$  and OH production. The ratio of  $\text{OH}/\text{O}_3$  remained relatively constant at our test points ( $(1.4\text{-}2.6)\times 10^{-5}$  at 100%,  $(1.9\text{-}3.0)\times 10^{-5}$  at 70%, and  $(1.7\text{-}2.6)\times 10^{-5}$  at 50%).~~ The OFR was cleaned prior to each experiment by

Formatted: Not Highlight

flushing it with humidified, pure air, while keeping the UV lights on for at least 10 min. Background levels were  $<2 \mu\text{g m}^{-3}$  SOA before OFR-from-SC experiments (when sampling from cleaned SC) and  $<10 \mu\text{g m}^{-3}$  when sampling diluted (1:8) test bench room air prior online-experiments.

Formatted: Superscript

## 2.2.4 Particle losses in SC and OFR

Loss of particulate (and gaseous) material to reactor walls are one of the largest causing significant uncertainties in simulations of atmospheric aging and are variable between systems (Zhang et al., 2014; Lambe et al., 2011; McMurry and Grosjean, 1985). Minimizing the surface area to volume ratios (i.e. building bigger chambers), using inert wall materials (such as Teflon), and attempting to isolate the sampled flow from the walls (as in our OFR), help to reduce losses. The main losses of particles are due to (1) diffusion, (2) electrostatic deposition and (3) gravitational settling, which are in turn affected by temperature changes due to the UV lights.

Field Code Changed  
Field Code Changed  
Field Code Changed

Wall losses of particles in the SC Those losses were accounted for in our SC experiments using the method described in (Weitkamp et al., 2007) and (Hildebrandt et al., 2009). This addresses all effects, including the aforementioned temperature effects, simultaneously. The suspended OA concentration,  $C_{\text{OA,suspended}}$ , was consequently corrected to yield  $C_{\text{OA,wlc}}$  according to following Eq. (1) from (Hildebrandt et al., 2009), for vapor losses see discussion in section 2.2.5). Particulate wall-loss rates,  $k_w$ , were determined as the exponential decay constant from an exponential fit of the time-dependent decrease in eBC mass (determined from optical absorption at  $\lambda=950 \text{ nm}$ ) with time. When eBC was below the instrumental detection limit (e.g., for experiments with vehicles equipped with retrofitted GPF), an average of the decay constants determined from based on the other experiments was applied ( $k_w=5.6 \times 10^{-5} \text{ s}^{-1}$ ). Diffusional losses of particles vary with particle size (McMurry and Grosjean, 1985). Our correction implicitly assumes assumed internally mixed OA/eBC particles, and does did not account separately for size-dependent effects.

Formatted: Indent: First line: 1.27 cm  
Field Code Changed  
Field Code Changed  
Field Code Changed

$$C_{\text{OA,wlc}}(t) = C_{\text{OA,suspended}}(t) + \int_0^t k_w * C_{\text{OA,suspended}}(t) * dt \quad (1)$$

Field Code Changed

A comparison of eBC mass before and after the up- and downstream the OFR OFR indicated no significant losses of particulates during UV on or UV off periods; the experimentally determined transmission was equal to 1, and consequently no further correction for particle losses was applied to OFR data. Additionally, particle wall losses in the OFR have been quantified previously by (Lambe et al., 2011), who reported above at least 80% transmission efficiency through the OFR for particles of mobility diameter ( $d_m$ )  $>150 \text{ nm}$  (Lambe et al., 2011). The particles measured behind downstream the OFR in the our current study had a median vacuum aerodynamic diameter ( $d_{va}$ ) of approximately between 200–400 nm based on HR-ToF-AMS (DeCarlo et al., 2006) measurements (HR-ToF-AMS-based size distributions are provided in Figure S109, Supporting Information). This corresponded to a  $d_m >150 \text{ nm}$  when assuming spherical

Field Code Changed  
Field Code Changed  
Field Code Changed

particles and an OA density of  $1.2 \text{ g cm}^{-3}$  (Turpin and Lim, 2001). ~~Particle size distributions in this range supported our experimentally determined transmission equal to 1. Therefore a transmission efficiency of at least 80% can be assumed.~~

### 2.2.5 Vapor losses in SC and OFR (on walls and through other non-OH processes)

5 Low-volatility vapors (especially semi-volatile (SVOC), and low volatility organic compounds (LVOC) are prone to losses on clean reactor walls and deposited OA particles, which compete with partitioning to suspended OA particles. Numerous publications discussed potential ~~SVOC and LVOC vapor~~ wall losses in ~~these SC systems recently~~ (e.g. ~~Krechmer et al., 2017~~; ~~Ye et al., 2016~~; ~~Zhang et al., 2014~~; ~~Hildebrandt et al., 2009~~); ~~Pagonis et al., 2017~~). ~~They~~ highlighted ~~that these losses may be important for result in~~ under-predictions ~~of~~ SOA yields ~~estimates~~. However, a robust strategy for their determination and correction remains challenging ~~(Krechmer et al., 2017)~~. In our previous work, we estimated that vapor wall losses may cause SOA yields to be underestimated for the ~~specific SC used herein~~ ~~(by a factor 1.5-2~~ (assessed based on gasoline vehicle exhaust SOA, see ~~Platt et al., 2017~~) ~~by roughly a factor 1.5-2 for our experimental conditions~~). ~~This is comparable to in line with suggestions by other systems~~ (e.g., a factor of 1.1-4.2 reported by ~~Zhang et al., 2014~~) and 1.1-6 reported by ~~La et al., 2016~~). ~~Hence, As such correction is not widely used, it is not applied herein to facilitate comparison with previously published data.~~ ~~data correction would increase our SC SOA yields on average by a factor 1.5-2.~~

10 ~~(Palm et al., 2016) recently estimated LVOC losses in the OFR, and described them as a result of losses to walls due to vapor wall losses, losses due to~~ insufficient residence time for partitioning to the particle phase (i.e., before vapors exit the OFR ~~before they condense~~), and ~~losses due to fragmentation due to upon~~ multiple OH reactions prior to vapor condensation on suspended OA. We tested the loss rate of vapors in our ~~OFR system based on this model during for~~ batch mode operation ~~of the OFR~~. Given the high SOA concentration and hence ~~seed high available particle surface~~  $(1-5) \times 10^9$  ~~4000-5000~~  $\text{nm}^2 \text{ cm}^{-3}$  based on the SMPS size distribution ~~of SOA~~, ~~less than 280%~~ of the formed LVOC was ~~ealculated-estimated to partition to the pre-existing OA mass be lost to the reactor walls using the Palm et al., 2016 model.~~ ~~Presented data are not corrected for this potential underestimation of SOA yields (Data correction would which would increase our OFR SOA yields them by a factor of 1.25 on average.)~~, ~~for comparison with previous data.~~

15 ~~Non-OH reaction processes in the OFR can be another pathway by which primary vapors SOA precursors (vapors) can be lost.~~ These processes have been ~~parameterized~~ parameterized by ~~(Peng et al., 2016)~~ as a function of residence time, photon-flux or  $\text{O}_3$  measurements, water vapor availability, and external OH reactivity ( $\text{OHR}_{\text{ext}}$ ), ~~which is~~ defined as the product of the available OH-reactive material and its respective OH rate constant. ~~In addition to OH, also p~~ Photons (185 nm, 254 nm), ~~and~~ oxygen allotropes (excited oxygen atoms ( $\text{O}(^1\text{D})$ ), ground state oxygen atoms ( $\text{O}(^3\text{P})$ ), ~~and~~ ozone ( $\text{O}_3$ )) were identified as relevant loss processes to precursor molecules, dependent on their chemical identity. To estimate ~~the influence of these parameters their contribution vs. OH-reactions~~, we applied the ~~model of~~ ~~(Peng et al., 2016) model.~~ ~~The results and implications of photon-induced effects on SOA formation or destruction to the current study as are~~ discussed in the ~~Supporting Information SI Section S4. In brief, F~~ for OFR-from-SC experiments, we predicted ~~an influence of~~ non-OH loss

Field Code Changed

Field Code Changed

Formatted: German (Switzerland)

Formatted: German (Switzerland)

Field Code Changed

Formatted: German (Switzerland)

Formatted: German (Switzerland)

Field Code Changed

Formatted: German (Switzerland)

Formatted: German (Switzerland)

Field Code Changed

Formatted: German (Switzerland)

Formatted: German (Switzerland)

Field Code Changed

Formatted: Not Highlight

Field Code Changed

Formatted: Indent: First line: 1.27 cm

Field Code Changed

Field Code Changed

processes of SOA precursors to yield (up to 25% UV loss for benzene and 10% for toluene, initiated by photons). For time-resolved OFR experiments, the model predicted more significant losses at low dilution ratios (1 ejector dilutor, which applies to experiments performed infrom 2014), but and smaller influences for experiments conducted with double dilution (2 ejector dilutors, which applies to experiments performed infrom 2015). This is due to the relatively higher [OH] at lower  $\text{OHR}_{\text{ex}}$ . Time-resolved OFR experiments from 2014 were also further impacted by OH suppression and relatively higher  $\text{NO}_x$  levels, for which For this reason they were we did not used them quantitatively within this publication (see discussion in SI and Section 3.3, SI Section S4).

Formatted: Subscript

### 2.2.6 SOA yields

Our SOA yields analysis is based on SC and OFR-from-SC experiments with GDI1-3 when tested over the full cycle or Ph1 only. An effective SOA yield ( $Y_e$ ), was calculated as the ratio of the formed SOA mass to the reacted SOA-forming mass species  $i$ :  $\Delta \text{NMOC}_{\text{reacted}}$  (in  $\Delta \mu\text{g m}^{-3}$ , Eq. (2)). The effective SOA yield provides the SOA mass formed via the We took into account all our identified SOA precursors ( $i$ ), i.e. the 8 dominant aromatic hydrocarbons presented in Figure 4d, neglecting non-reactive and non-SOA forming precursors. Thereby, we and assumed that all relevant SOA precursors were are measured. Identified SOA precursors  $i$  refers to the 8 dominant aromatic hydrocarbons presented in Figure 4d.

Formatted: Subscript

Formatted: Font: Italic

Field Code Changed

Field Code Changed

$$Y_e = \frac{\Delta \text{SOA}}{\sum_i \Delta \text{NMOC}_{\text{SOA-precursor } i, \text{reacted}}} \quad (2)$$

The SOA-forming precursor mass was determined by identifying and quantifying relevant SOA-precursor NMOCs by PTR-ToF-MS. SOA yields are presented as a function of the suspended (i.e. non particle wall loss corrected) organic aerosol mass (POA+SOA), for consistency with the wall loss correction method described above (i.e. neglecting vapor-wall interactions). In practice, this has little effect on the obtained SOA yield curves, as particle wall losses were limited due to the short SC experiment time (lasting 2 hours). As the The yield could an be calculated for each point in time since initiation of photochemistry, values in the SC or in the OFR sampling from the SC (OFR from SC). This results in a yield as a function of OH exposure, and also as a function of suspended OA were derived.

### 2.2.7 OH exposure estimation

The time-integrated OH exposure ( $\text{molec cm}^{-3} \text{ s}$ ), defined as the integrated OH concentration ( $[\text{OH}]$ ) over the reaction time ( $t$ ) was calculated from the decay of BuOH-D9 as described by (Barnet et al., 2012) for both the OFR and SC experiments. The obtained OH exposure can be was related to an approximate ambient aging time by assuming a mean atmospheric [OH] (e.g. of  $1 \times 10^6 \text{ molec cm}^{-3}$  for a global 24h daytime average, or applying a 12h average of  $2 \times 10^6 \text{ molec cm}^{-3}$ , taking into

Field Code Changed

account that OH radicals are predominantly available during daytime (average value taken from (Finlayson-Pitts and Pitts, 2000)). We also predicted OH concentration and exposure ~~are using the also predicted by OFR model (Peng et al., 2016) and OH exposure estimation from (Li et al., 2015) and Peng et al., 2016 as presented in the SI.~~ The tracer-based OH exposure was generally in good agreement with the model results, except at the highest OH exposures where the tracer method was on average a factor of 3 higher (SI Section S4). Tracer-based OH exposures were used throughout our analysis, as these measurements are specific to our experiments.

Field Code Changed

Field Code Changed

Field Code Changed

Field Code Changed

### 2.3. Mass spectrometric instrumentation and data processing

#### 2.3.1 Test bench instrumentation

Gaseous components were monitored with an exhaust gas measuring system Horiba MEXA 9400H, including measurements of CO and CO<sub>2</sub> by infrared analyzers (IR), hydrocarbons by flame ionization detector (FID) for total hydrocarbon (THC) and non-methane hydrocarbon (NMHC) measurements, NO/NO<sub>x</sub> with a chemo-luminescence analyzer (CLA) which was not heated and applicable only for diluted gas, and O<sub>2</sub> (Magnos). The dilution ratio in the CVS dilution tunnel is variable and was controlled by means of the CO<sub>2</sub> analysis. Non-legislated gaseous emission components were analyzed by FTIR (Fourier Transform Infrared Spectrometer, AVL SESAM) at the exhaust tailpipe, offering time-resolved measurement of approx. 30 emission components, including NO, NO<sub>2</sub>, NO<sub>x</sub>, NH<sub>3</sub>, N<sub>2</sub>O, HCN, HNCO, HCHO. Number concentration of non-volatile particles were measured with condensation particle counters (CPC) behind a thermo-conditioner heating the sample to 300°C.

#### 2.3.2 Non-regulatory equipment for photochemistry experiments

~~Along with a suite of basic gas-phase monitors for measurements of CO<sub>2</sub>, CO and CH<sub>4</sub> (CRDS, Picarro), THC, CH<sub>4</sub> and NMHC (FID, Horiba), NO, NO<sub>2</sub>, O<sub>2</sub> and particle phase instruments (CPC and SMPS for particle number and size measurements, and 7-wavelength aethalometers for eBC determination (Drinovec et al., 2015) (Aerosol d.o.o), high resolution time-of-flight mass spectrometers were applied to investigate the chemical composition of the fresh and aged exhaust (instruments are listed Table S2-S3, Supporting Information).~~

Field Code Changed

#### 2.3.3 PTR-ToF-MS

A ~~high-resolution~~ proton transfer reaction time-of-flight mass spectrometer ((Jordan et al., 2009); (Graus et al., 2010)) (PTR-ToF-MS), (PTR-TOF-8000, Ionicon Analytik Ges.m.b.H., Innsbruck, Austria), was used to study ~~the chemical composition of the~~ gaseous non-methane organic compounds (NMOC) in fresh and aged emissions. ~~The PTR-ToF-MS uses~~ We used hydronium ions (H<sub>3</sub>O<sup>+</sup>) as the primary reagent ~~to protonate gaseous organic molecules having a proton affinity higher than~~

Field Code Changed

Field Code Changed

that of water (691 kJ mol<sup>-1</sup>, (Gueneron et al., 2015)). Water clusters (H<sub>3</sub>O)(H<sub>2</sub>O)<sup>+</sup> were below 5% of the H<sub>3</sub>O<sup>+</sup> ion and were not considered for the calculations further. Detected compounds included most aromatic hydrocarbons of interest, alkanes (above >C<sub>10</sub>) and alkenes (above >C<sub>2</sub>), as well as oxygenated compounds (aldehydes, ketones and carboxylic acids) and thus includes many organic molecules expected in GDI vehicle exhaust ((Gueneron et al., 2015); (Schauer et al., 2002)). The sample was introduced into a drift tube and mixed with H<sub>3</sub>O<sup>+</sup> ions produced from water vapor in a hollow cathode ion source, leading to protonation of the analyte gas molecules, which were detected by time-of-flight mass spectrometry ((Jordan et al., 2009); (Graus et al., 2010)). For experimental set I (2014), the PTR-ToF-MS operated with at a drift voltage of 545 V, a chamber temperature of 90 °C, and a drift pressure of 2.2 mbar, and a resulting in a reduced electric field (*E/N*) of about 140 Td. In experimental set II (2015) and for single precursor experiments (2016), we used the drift voltage was 545 V, the drift tube temperature was 60 °C and the drift pressure was 2.1-2.2 mbar, respectively, resulting in an *E/N* of 130 Td. The mass resolution, as well as the mass accuracy and the relative transmission efficiency ((De Gouw and Warneke, 2007); (Müller et al., 2014)), were routinely verified using a 12-compound gas standard (Carbagas, protonated integer *m/z* 45 to 181, containing alcohols, carbonyls, alkenes, aromatic hydrocarbons (ArHC) and terpenes). Additionally further, we used an internal calibrant (diiodobenzene, C<sub>6</sub>H<sub>4</sub>I<sub>2</sub>) for mass calibration (protonated integer *m/z* 331), to support mass calibration at higher *m/z*.

Data were analyzed using the Tofware post-processing software (version 2.4.2, TOFWERK AG, Thun, Switzerland; PTR module as distributed by Ionicon Analytik GmbH, Innsbruck, Austria), running in the Igor Pro 6.3 environment (Wavemetrics Inc., Lake Oswego, OR, U.S.A.). In the absence of fragmentation (discussed below), ions are observed at the mass-to-charge (*m/z*) ratios corresponding to the neutral parent molecule shifted by the mass of one proton (denoted [NMOC+H]<sup>+</sup>). The exact mass was used to determine the elemental composition of an ion and was combined with previous reports of compounds identified in combustion emissions ((Schauer et al., 2002); (Schauer et al., 1999); (Gueneron et al., 2015); (Erickson et al., 2014)) to propose likely molecular structures. NMOC concentrations were derived from the H<sub>3</sub>O<sup>+</sup> normalized ion signal of [NMOC+H]<sup>+</sup>, the appropriate reaction rate constant towards H<sub>3</sub>O<sup>+</sup> (*k*<sub>H<sub>3</sub>O<sup>+</sup>) from (Cappellin et al., 2012), and (Cappellin et al., 2010), towards H<sub>3</sub>O<sup>+</sup> (*k*<sub>H<sub>3</sub>O<sup>+</sup>) and the residence time in the drift tube, following standard procedures. While ideally the molecular sum formula can be approximated by the exact mass of [NMOC+H]<sup>+</sup> (see discussion on fragmentation below), isomers, such as e.g. *o*-, *p*-, *m*-xylenes and ethylbenzene, cannot be resolved and the selection of *k*<sub>H<sub>3</sub>O<sup>+</sup> may thus be somewhat is uncertain. If available and applicable based on identification, we used when the exact reaction rate information reported in literature ((Cappellin et al., 2012); (Cappellin et al., 2010)), otherwise we assumed the was missing, we used the collisional rate constant of (2 × 10<sup>-9</sup> cm<sup>3</sup> s<sup>-1</sup>). Although protonation with H<sub>3</sub>O<sup>+</sup> is considered a soft ionization technique typically soft, fragmentation occurs for certain compounds including may occur for aldehydes, alcohols, alkanes, alkenes and substituted aromatics, with the non-oxygen-containing species being of particular importance for the current study herein ((Gueneron et al., 2015); (Erickson et al., 2014); (Buhr et al., 2002)). Fragments were observed here, but they constituted only a small fraction of the total signal in our analysis (see results) (see Figure 4), and therefore</sub></sub></sub>

Field Code Changed

Formatted: Indent: First line: 1.27 cm

Formatted: English (U.S.)

Field Code Changed

Formatted: English (U.S.)

Formatted: English (U.S.)

Field Code Changed

Formatted: English (U.S.)

Formatted: English (U.S.)

Field Code Changed

Formatted: English (U.S.)

Field Code Changed

Formatted: English (U.S.)

Formatted: English (U.S.)

Field Code Changed

Formatted: German (Switzerland)

Field Code Changed

~~n~~No corrections were applied. ~~Fragments that could not be attributed to an [NMOC+H]<sup>+</sup> parent are reported as “structurally unassigned”.~~

### 2.3.4 HR-ToF-AMS

5 Quantitative, size-resolved mass spectra of the non-refractory sub-micron particle composition were ~~provided by use of~~  
~~obtained using a~~ high resolution time-of-flight aerosol mass spectrometer (HR-ToF-AMS, Aerodyne, ~~(DeCarlo et al.,~~  
~~2006)~~, ~~(DeCarlo et al., 2006)~~, equipped with a ~~Particles are continuously sampled into the HR-ToF-AMS through a~~ PM<sub>1</sub>  
aerodynamic lens ~~and focused onto a heated porous tungsten vaporizer (T<sub>vap</sub> = 600 °C) in high vacuum (10<sup>-5</sup> Pa). The non-~~  
refractory particle components flash-vaporize and the resulting gas is ionized by electron ionization (EI, 70 eV), and then  
10 ~~classified by a time-of-flight mass spectrometer (ToF-MS). The particle beam is alternately blocked (“closed”) and~~  
~~unblocked (“open”), and, a~~All data presented herein are *open minus closed* signals derived from high resolution analysis  
fitting procedures (SQUIRREL1.51H, PIKA 1.10H), running in the Igor Pro 6.3 environment (Wavemetrics Inc., Lake  
Oswego, OR, U.S.A.). Following standard procedures ~~(Canagaratna et al., 2007)~~, the instrument ionization efficiency ~~(IE)~~  
and particle size measurement were calibrated using size-selected NH<sub>4</sub>NO<sub>3</sub> particles and polystyrene latex spheres ~~(PSLs)~~,  
15 respectively. A relative ionization efficiency ~~(RIE)~~ of 1.4 for organic material ~~and a collection efficiency (CE) of 1~~ was  
applied ~~to the data. We used a collection efficiency of 1, as upon photochemistry, significant amounts of NH<sub>4</sub>NO<sub>3</sub> were~~  
~~formed, and under our (NH<sub>4</sub>)<sub>2</sub>SO<sub>4</sub>-free conditions, our aerosol mixture is not expected to bounce significantly.~~ No  
corrections for lens transmission were performed; ~~pTOF distributions are provided in Figure S10.~~ HR-ToF-AMS data were  
corrected for background gas-phase CO<sub>2</sub> ~~in the emissions~~ by subtracting ~~the~~ CO<sub>2</sub>-signal measured in a particle-free sample.  
20 The interaction of inorganic salts with pre-deposited carbon on the tungsten vaporizer can lead to ~~the generation of a~~ CO<sub>2</sub><sup>+</sup>  
signal in the *open minus closed* HR-ToF-AMS mass spectra ~~(Pieber et al., 2016). Here p~~Photochemical aging ~~of the exhaust~~  
resulted in significant NH<sub>4</sub>NO<sub>3</sub> formation, reaching NO<sub>3</sub>/OA ratios of ~~roughly 5.~~ A CO<sub>2</sub><sup>+</sup> signal at 3.5% to NO<sub>3</sub> was  
determined by calibration ~~(see Figure S4S3, Supporting Information)~~ and corrected according to ~~(Pieber et al., 2016).~~

## 3 Results and discussion

### 3.1 Pollutant ~~emission factors (EFs)~~s as function of vehicle technology and driving cycle

25 ~~Figure 2~~Figure 2 summarizes emission factors (EFs) ~~of pollutants~~ across all vehicles and conditions tested. ~~We investigated~~  
NMHC, THC, primary PM (eBC, POA) and SOA. A detailed discussion on emissions of CO, NO<sub>x</sub>, particle number and  
~~genotoxic PAHs from cold- vs. hot-started cycle driven GDI vehicles in standard configuration is provided in Muñoz et al.,~~  
~~2018.~~ Investigation of THC, NMHC and gravimetric PM of time resolved emissions for cold and hot started WLTC and  
30 ~~EDC tests using GDH 3 demonstrated significant THC and NMHC emissions during cold engine tests.~~

Field Code Changed

### 3.1.1 NMHC and THC

No drastic test cycle-dependencies (WLTC vs. EDC) were observable in terms of NMHC or THC EFs for cold-start conditions (cW vs cE). The comparison for hot-started cycles (hW vs hE) was not conclusive, but indicated eventually lower EFs during hE for GDI1. ~~with emission factors~~ (Differences between cold- and hot-started tests were more dramatic: EFs of primary NMHC and THC were reduced by a factor of 90 for GDI1-3 during under hot-started cycles conditions compared to cold-started tests (Figure 2, panel a and c). Median NMHC EFs were  $1132 \text{ mg kg}_{\text{fuel}}^{-1}$  (cW) and  $12.9 \text{ mg kg}_{\text{fuel}}^{-1}$  (hW). EFs from cold-started WLTC (cW) for GDI1-3 were clearly dominated by Ph 1 (cW,  $4663 \text{ mg kg}_{\text{fuel}}^{-1}$ ), which exceeded all other test conditions phases of cold- and hot-started WLTC by 2 to 4 orders of magnitude (median, GDI1-3). For GDI4 ~~had we found~~ lower total emissions during cold-started cycles compared to other vehicles (~factor 3 lower than GDI1-3, median NMHC EF (cW):  $434 \text{ mg kg}_{\text{fuel}}^{-1}$ ) and a smaller difference between cold- and hot-started cycles. For GDI4, the cW NMHC EF was only 8 times higher than from hW, rather than 90 times as for GDI1-3; median NMHC EF for hW (GDI4):  $55.7 \text{ mg kg}_{\text{fuel}}^{-1}$ ). Instead, when looking at the total NMHC EF of hW, GDI4 exceeded those of GDI1-3 (the median for hW (GDI4) is  $55.7 \text{ mg kg}_{\text{fuel}}^{-1}$ ). This remained true for individual cycle phases of the driving cycle (e.g., comparing Ph 1 of cW and hW vs. Ph 2-3 or 4 of cW and hW) for different vehicle standards (GDI1-3 vs. GDI4), we find that while Ph 1 (cW) NMHC emissions for GDI4 are significantly lower compared to GDI1-3 (by a factor 3), revealed that, except for Ph 1 (cW), NMHC EF for GDI4 had higher EFs during all other phases appeared higher during all other phases than those of GDI1-3 (factor 2-30, with the biggest difference found for Ph 2-4 (hW)). The corresponding median data were 4663, 0.1, 23.8, 1.6 (for GDI1-3, Ph 1 (cW), Ph 1 (hW), Ph 2-4 (cW) and Ph 2-4 (hW) respectively), and 1507, 2.2, 56.8,  $41.1 \text{ mg kg}_{\text{fuel}}^{-1}$  (for GDI4). Lower cold start emissions of GDI4 compared to other vehicles may be explained by differences in the catalytic after-treatment system, the location of the catalyst as well as reduced cold start enrichment. In terms of NMHC and THC EFs, GDI4 can be considered in line with Euro 6 vehicles, for which regulation also focuses on the reduction of the cold-start HC emissions. No influence of GPF installation-retrofitting did not affect the NMHC or THC EFs was observed for either GDI1 or 4 under cold-started conditions (GDI2 and 3 were not tested), as as further discussed below (in Section 3.2).

### 3.1.2 Primary PM (gravimetric PM, eBC, POA)

Primary PM emissions are appeared less dramatically affected by the differences between cold- and hot-started cycles and among vehicles compared to above discussed NMHC and THC EFs (Figure 2, panel a). The largest difference was induced by the application of GPFs as discussed further below (Section 3.2). The total PM emitted by vehicles in standard configuration is dominated by eBC rather than POA (Figure 2b), and the low POA to eBC ratio is similar to diesel engines not equipped with DPFs, as also found by (Saliba et al., 2017). PM measured in the batch samples (sum of eBC and POA, Figure 2b) compares generally well with the gravimetric PM analysis of filters sampled from the CVS (Figure 2a). Selective sampling of phases of the cold-started cW into the SC (Figure 2, panel d) and time-resolved measurements (Figure 3, panel a)

Formatted: Not Highlight

Formatted: Heading 2

Field Code Changed

Formatted: Not Highlight

Formatted: Heading 2

Formatted: Not Highlight

Field Code Changed

3) indicated that significant eBC ~~wasis~~ emitted during cold-engine start-up (Ph 1 cW). ~~Equivalent BC~~ ~~Primary PM~~ emissions ~~are were~~, however, not as strongly reduced during hot-engine ~~conditions~~ (see Ph 2-4 from cold-started cycle) ~~emissions, and during hot started cycles~~ (as well as hW, in Figure 2 ~~Figure 2a~~ for total PM (CVS) ~~b/d~~ and Figure 3 ~~Figure 3~~ for eBC), as e.g. the NMHC EFs under hot engine conditions. (Muñoz et al., 2018) ~~The total PM emitted by vehicles in standard configuration was dominated by eBC rather than POA (Figure 2b), and the low POA-to-eBC ratio similar to diesel engines not equipped with DPFs, as also found by Saliba et al., 2017. PM measured in the batch samples (sum of eBC and POA) are compared with gravimetric PM analysis of filters sampled from the CVS in Figure S16, and chemical analysis of PM samples is further presented in Muñoz et al., 2018. Significant effects in the primary PM EFs were induced by the application of GPFs as discussed in Section 3.2.~~

### 3.1.3 Secondary Organic Aerosol (SOA)

Emissions of all cold-started vehicles, technologies and driving tests showed significant SOA formation upon photochemical oxidation (Figure 2 ~~Figure 2b~~), in line with ~~previous findings~~ other studies on GDI as well as port-fuel injection systems ((Platt et al., 2017); (Gordon et al., 2014); (Nordin et al., 2013); Saliba et al., 2017; (Zhao et al., 2018)). ~~This~~ ~~The findings~~ ~~we~~ ~~is~~ consistent with the above observation that NMHC and NMOC ~~aromatic hydrocarbon emissions~~ EFs (determined by the PTR-ToF-MS, see Figure 2 ~~Figure 2d~~) ~~are were~~ ~~greatly elevated~~ ~~significantly higher~~ during cold-started cycles compared to other conditions. Hot-engine emissions (Ph 2-4 sampling from cold-started WLTC, as presented in Figure 2d) also resulted in SOA formation, which was, however, 20-50 times lower in terms of EFs than SOA formed from Ph 1 sampling of a cold-started WLTC. This is likewise in agreement with the trends indicated by the phase-dependent NMHC EFs (Figure 2c). Also the SOA production factors for GDI4 (median: 12 mg kg<sup>-1</sup><sub>fuel</sub>) were around a factor 20 lower than the average SOA production of GDI1-3 (Figure 2b) (median: 222 mg kg<sup>-1</sup><sub>fuel</sub>). The observed SC SOA ~~production in~~ (on average 13-170 mg kg<sup>-1</sup><sub>fuel</sub>) ~~lies was within the range of previous~~ in line with previously aggregated data ((Jathar et al., 2014); (Platt et al., 2017)) (e.g. a median 60, range ~10-400 mg kg<sup>-1</sup><sub>fuel</sub> as reported in) (Jathar et al., 2014)) and with our previous findings for the SC experiments (range ~6-70 mg kg<sup>-1</sup><sub>fuel</sub>, Platt et al., 2017). ~~with vehicles in standard configuration (as well as equipped with GPF, discussed in Section 3.2). Similar to the observations for NMHC EFs, SOA production factors for GDI4 (median: 12 mg kg<sup>-1</sup><sub>fuel</sub>) are around a factor 20 lower compared to average SOA production factors for GDH-3 (Figure 2b) (median: 222 mg kg<sup>-1</sup><sub>fuel</sub>).~~ OFR experiments typically resulted in higher SOA ~~production values than the~~ compared to SC experiments (OFR SOA on average 11-500 mg kg<sup>-1</sup><sub>fuel</sub>); this was in parts due to ~~which can be explained by~~ the higher OH exposure ~~which, leading led to more~~ ~~to reaction of more~~ reacted precursor mass and ~~higher higher~~ OA loadings. High OA loadings induced and hence an influence of partitioning effects ((Pankow, 1994); (Donahue et al., 2006)), as discussed later (see SOA yield curve analysis, Figure 6), which needs to be considered when comparing OFR and SC data. This can be done by comparing SOA data as a function of OA, as presented in Section 3.6, Figure 6. Other differences which may affect the measured SOA mass within the two systems (including vapor losses, etc.) are discussed in Sections 2.2.5 and 3.6.

Field Code Changed

Formatted: Not Highlight

Field Code Changed

Formatted: Not Highlight

Field Code Changed

Photo-chemical aging of Ph 2-4, sampled into the SC and OFR from SC from a cold-started driving test, showed significantly lower SOA production factors (Figure 2d), in analogy to the lower NMHC and NMOC emission factors for hot engine conditions, which are discussed in detail later. While engineering measures to reduced cold-start emissions from GDI4 were effective to reduce SOA EFs, and the lower SOA EFs of hot-engine conditions indicated the relevance of a functional after-treatment system to reduce SOA, GPF-retrofitting appeared ineffective under cold-started conditions.

### 3.2 Effect of gasoline particle filters (GPF) on pollutants

Figure 2 provides emission factors (EFs) of GPF-retrofitting vehicles compared to standard configuration, as discussed in Section 3.1. We found that Gravimetric PM and eBC were greatly significantly reduced by the retrofitted GPFs (GPF tested on GDI1 and GDI4 (reduction was 98%, 96% and 84% for GDI1-GPF, GDI4-GPF and GDI4-catGPF during cW, respectively; corresponding hW reduction was 96%, 91%, and 73%). ; with GPF performance apparently compromised on GDI4, potentially due to aging of the filter; catGPF tested on GDI4 also performed poorly). While the retrofitted GPFs efficientlyThe significant primary PM reduction was linked to the removal of the non-volatile eBC fraction and thus significantly reduce total primary PM (Figure 2 panel a,b,d), which dominated the total primary PM and for which reduction values yielded >99%, 94% and 64% for GDI1-GPF, GDI4-GPF and GDI4-catGPF, respectively, during cW.

Retrofitted GPFs (including catGPF downstream the standard TWC) appeared also to reduce the POA fraction, but the effect was smaller (by 54 to 64% in 3 tests, but with a POA enhancement in a fourth test, which we cannot robustly interpret; all data correspond to cold-started cycles)he effect on POA is more complex. POA removal is more complex, given that POA has a wide range of volatilities and may thus encounter a particle filter in either vapor or particle phase. Thus GPFs can only efficiently remove theOnly the low volatility POA fraction may be efficiently removed by filtration, while more volatile POA-material passes through the filter as vapor and will condense when the exhaust is cooled in the ambient air. Within experimental uncertainty, retrofitted GPFs (including catGPF behind the standard TWC) did not affect the POA fraction. Further, GPFs did not affect FID-based NMHC (Figure 2a) and, PTR-ToF-MS-based NMOC aromatic hydrocarbon EFs (Figure 2d), or the PTR-ToF-MS-based NMOC composition as discussed later in Figure 4) during the cold-started cycles (discussed later in Figure 4). We have indications for GPF-induced hydrocarbon reduction during hot engine conditions (by 20-80% for the FID-based NMHC EFs measured from the CVS system) and believe this deserves further attention in follow up studies. The retrofitted GPFs did neither reduce the produced SOA mass-EFs under cold-started conditions (Figure 2, panel b,d, and Figure S14). SOA reduction requires hence additional after-treatments to remove NMHCs or selected NMOCs, such as reduced cold-start enrichment or engine-or-catalyst pre-heating, indicated by. Significantly lowered SOA formation-EFs of GDI4 and during Ph 2-4 SOA experiments are indicated by such engineering measures (when engine and after-treatment systems are already hot), compared to Ph 1 emissions (when engine/after-treatment systems are cold), as discussed above in (Section 3.1). No effects of the GPFs were observed on SOA yields or bulk chemical composition of cold-started tests, detailed later (Sections 3.6-3.7).

Formatted: Indent: First line: 1.27 cm  
Field Code Changed

Field Code Changed  
Formatted: Not Highlight  
Field Code Changed  
Formatted: Not Highlight  
Formatted: Not Highlight  
Formatted: Not Highlight  
Formatted: Not Highlight  
Formatted: Indent: First line: 1.27 cm  
Formatted: Font color: Auto, Not Highlight  
Formatted: Font color: Auto, Not Highlight  
Formatted: Font color: Auto, Not Highlight  
Formatted: Not Highlight  
Field Code Changed  
Field Code Changed  
Field Code Changed  
Formatted: Font color: Auto, Not Highlight  
Formatted: Not Highlight  
Formatted: Font color: Auto, Not Highlight  
Formatted: Not Highlight  
Formatted: Font color: Auto, Not Highlight  
Formatted: Not Highlight  
Formatted: Font color: Auto, Not Highlight  
Formatted: Not Highlight  
Formatted: Font color: Auto  
Field Code Changed

### 3.3 Time-resolved SOA formation ~~in the (OFR during dynamic test cycles)~~

Investigation of CVS and batch sampling of the individual ~~phases of~~ cold-started WLTC ~~phases indicates indicated~~ the highest emission of SOA precursors and SOA formation ~~from during~~ cold-started Ph 1 (cW), ~~consistent with theas detailed discussion~~ in Section 3.1.3/~~Figure 2d~~. This ~~was~~ confirmed by time-resolved SOA profiles from aging of the emissions in the OFR online during the driving cycles, ~~which we show in Figure 3. Figure 3 shows the time-resolved aged emissions for cold and hot-started WLTCcW and hW tests using GDI1 (sin standard configuration). The emissions are were exposed to OFR photochemistry in the OFR, with UV intensity at 100%. Particulate OA and nitrate (denoted NO<sub>3</sub>) are were monitored behind downstream the OFR by the HR-ToF-AMS; for the cold-started cycle, the POA signal measured during a separate experiment (with OFR UV off) is shown for reference. The large difference between the OA and POA traces indicates indicated that the observed OA is was predominantly SOA. During the cold-started cycle, we found significant SOA formation is observed by the HR-ToF-AMS during Ph 1 (i.e. start and low speed) and to a lesser extent during Ph 2-4 (simulated highway driving), which confirmed our observations from Section 3.1.3/~~Figure 2d~~. The peak at engine start is was observed during all cold-start vehicle tests, regardless of vehicle, driving cycle or presence/absence of GPFs-retrofit, while the small peak at the end of high-speed/extra urban driving is was finished appears-appeared inconsistently. The latter is related to a delay of the OFR signal by the residence time in the reactor, as also observed by (Zhao et al., 2018), and might potentially also be caused by a delay of SOA forming species which are retained on surfaces. (Pagonis et al., 2017). The cold-start SOA signal ~~correlates correlated~~ with ~~TH~~hydrocarbon measurements at the OFR inlet (Figure S6-S9)~~S-S8, Supporting Information~~, and is not evident during the hot-started cycle. These trends are consistent with the regulatory test bench measurements described above and EFs calculated from batch samples in the SC. The duration of the SOA peak observed at the engine start is was likely artificially increased by OFR residence/response timescales and reflects the first few seconds to minutes, prior to catalyst light-off, rather than representing consistently high emissions throughout Ph 1 (Figure S5-S8, Supporting Information). Supporting this explanation, the hot-started cycle (in which the catalyst operates operated efficiently from the beginning of the test) ~~does~~ not exhibit any significant emission of NMHC (Figure 2/~~Figure 2c~~), and ~~leads to resulted in relatively very~~ little SOA formation ~~also~~ when investigated online. Hence, ~~also during online measurements, the cold-start emissions appeared to dominate the total GDI SOA burden, and are selected below for investigation of relevant SOA precursors, SOA potential and yields in OFR from SC and SC photochemistry experiments.~~~~

Time-resolved SOA data from 2014 ~~are were~~ not used quantitatively herein, due to instabilities with the OH exposure throughout the driving cycle (lower OH exposure during high emissions period as well as ~~potential impacts~~ by photolysis and competing non-OH processes ~~(as discussed in i.e. high external OH reactivity, see SI Section S4, Eq. S2 and Figures S11-S12, (Peng et al., 2015); (Peng et al., 2016); (Li et al., 2015)). Further, those data were and potentially impacted by an of NO influence on the oxidation regime (high vs. low NO levels, NO<sub>3</sub> radical formation, see, discussed in SI Section S4 and (Peng and Jimenez, 2017)). This is was caused by the low dilution ratio we had applied (1 ejector dilutor, 1:8, and~~

Field Code Changed

Formatted: Indent: First line: 1.27 cm

Field Code Changed

Field Code Changed

Field Code Changed

Field Code Changed

~~additional 1:2 at OFR entrance~~) in 2014 (~~1 ejector dilutor, 1:8, and additional 1:2 at OFR entrance~~). For the experiments conducted in 2015, such experimental artefacts were reduced by ~~the use of using~~ a higher dilution ratio (2 ejector dilutors in series, each 1:8 and additional 1:2 at OFR entrance). Time-resolved data from 2015 collected with GDI4 were integrated to derived EFs labelled “Online, OFR100%” ~~in section 3.1, 3.2 and 3.4 (Figure 2Figure 2b, Figure 4Figure 4) and are comparable to agreed well data with data~~ derived from ~~GDI4-corresponding~~ SC experiments. While we ~~don't~~cannot rely on an absolute quantitative use of our 2014 data from time-resolved measurements, the relative profile (~~indicating that total SOA was dominated by the cold start-up as presented in Figure 3) holds remains~~ true regardless of those effects, and ~~is was~~ confirmed in the 2015 data set (Figure S144) ~~showing the same trends. Future work should investigate the quantitative use of online OFR data in further detail for additional quantification of cold- and hot-start contribution of SOA to the total SOA burden; a discussion of the associated technical issues (including also the condensational sink as well as the equilibration time inside the OFR reactor) has been recently published by (Zhao et al., 2018).~~

Field Code Changed

Field Code Changed

Field Code Changed

Field Code Changed

### 3.4 Primary NMOC composition investigated by PTR-ToF-MS

#### 3.4.1 Dependence on vehicle test conditions

~~Figure 4Figure 4a~~ shows the average NMOC mass spectrum ~~as~~ obtained by the PTR-ToF-MS ~~measurements~~ for exhaust from ~~vehicle~~ GDI1 over a ~~full~~ cold-started WLTC. The relative ~~NMOC~~ composition over all test conditions (driving cycles and phases, vehicle configuration ~~including GPF-retrofits~~) is given in ~~Figure 4Figure 4b~~. ~~Figure 4Figure 4c summarizes the ArHC aromatic hydrocarbon (ArHC) emission factors (EFs), and Figure 4Figure 4d gives provides the relative ArHC composition of the most dominant ArHC species; (A-a detailed description is provided later). In summary, while Gasoline as a fuel is mainly composed of aliphatic compounds and ArHC having withbetween 7 and to 10 carbons (making up roughly 35% of the fuel volume), the exhaust mass spectral composition from cold-started driving tests appears appeared to be instead dominated by surviving fuel additives (ArHC, and methyl-tert-butyl-ether (MTBE)), together with newly formed incomplete combustion products (-ArHC and short chain aliphatics, which which are incomplete combustion products). The composition depends was strongly dependent on the driving cycle phase, with ArHC dominating the emissions in Ph 1 (cW) and the full cycles (cW, cE) contributing on average 70% of the total signal of Ph 1 (cW) and the full cycles (cW, cE); while Instead, they constituting a smaller fraction on average only 14% of Ph 2-4 (cW). (Note that the NMOC concentrations for Ph 2-4 (cW) were close to our background measurements, i.e. the signal not significantly different from 3 standard deviations of the background measurement). As discussed above (Figure 2), NMHC ArHC EFs during Ph 1 (cW) are were far higher more than one order of magnitude higher than Ph 2-4 (cW) EFs, with the resulting effect that the emissions composition for the full WLTC closely resemble those of Ph 1, (i.e., dominated by ArHC) also from a chemical composition perspective. (Note that the NMOC concentrations for Ph 2-4 (cW) are close to our background measurements (signal not significantly different from 3 standard deviations of the background measurement)). As We showed above, that~~

Formatted: Not Highlight

Field Code Changed

~~GPF installation does~~GPF-retrofitting did not reduce NMHC ~~or ArHC~~ EFs (Figure 2~~Figure 2~~, Figure 4~~Figure 4c~~); ~~in addition, and likewise~~ it has~~d~~ no ~~obvious distinct~~ influence on the ~~overall gaseous~~-NMOC composition (Figure 4~~Figure 4b~~).

### 3.4.2 Speciation and carbon quantification

In the following we ~~speciate the chemical composition and establish a closure between FID-based and PTR-ToF-MS based measurements, in order to quantify our potential SOA-precursors for Sections 3.5-3.7. A small number of ArHC ions dominated~~ In detail, the mass spectrum and relative composition for full WLTC and Ph 1 (cW) experiments is dominated by a small number of ArHC ions; specifically: benzene ( $[C_6H_6+H]^+$ , integer  $m/z$  79, denoted BENZ), toluene ( $[C_7H_8+H]^+$ ,  $m/z$  93, ~~denoted TOL~~), *o*-/*m*-/*p*-xylene or ethylbenzene ( $[C_8H_{10}+H]^+$ ,  $m/z$  107, ~~denoted XYL/EBENZ~~) as well as  $C_3$ -benzenes ( $[C_9H_{12}+H]^+$ ,  $m/z$  121, ~~denoted C3BENZ~~). ~~Their Reaction rate constants of the above compounds are shown in Table 2~~ Table 2. The most important Relevant additional aromatic HC peaks in the spectra corresponded to  $C_4$ -benzenes ( $[C_{10}H_{14}+H]^+$ ,  $m/z$  135, ~~denoted C4BENZ~~), naphthalene ( $[C_{10}H_8+H]^+$ ,  $m/z$  129, ~~denoted NAPH~~), styrene ( $[C_8H_8+H]^+$ ,  $m/z$  105, ~~denoted STY~~) and methyl-styrene ( $[C_9H_{10}+H]^+$ ,  $m/z$  119, ~~denoted C1STY~~). While our primary ionization pathway was via  $H_3O^+$ , the ion source produced up to 5% unwanted  $O_2^+$ , which enabled further pathways (Amador Muñoz et al., 2016; Jordan et al., 2011; Knighton et al., 2009). Signals assigned to  $O_2^+$  pathways were excluded from our analysis (SI Section S5).

These ~~8 eight~~ above identified ArHC ions comprised  $96.7\pm 3.3\%$  of the total ArHC and  $69.5\pm 19.7\%$  of the total NMOC mass signal in  $\mu g m^{-3}$  and correspond to  $69.5\pm 19.7\%$  of the total NMOC signal for full cW, cE and Ph 1 (cW) experiments (Figure 4; Ph 2-4 (cW): fractions were  $65.2\pm 9.8\%$  and  $13.9\pm 12.1\%$ , respectively). Oxygenated ArHC, (such as phenolic compounds and benzaldehyde), ~~make made~~ up an additional  $1.2\pm 2.0\%$  ~~contribution~~ to the total ArHC fraction for cold-started conditions (cW, cE, Ph 1 (cW)). Their relative contribution ~~increased when under hot engine conditions are hot~~ (Ph 2-4 (cW):  $5.9\pm 1.2\%$ ). Also GDI4 ~~shows exhibited~~ enhanced contribution of oxygenated ArHC ~~to the total NMOC~~ compared to GDI1-3, ~~which is in line with relatively enhanced hot engine emissions. While the primary ionization pathway in the PTR ToF MS is proton transfer reaction by  $H_3O^+$  ions, the ion source produces up to 5% of unwanted  $O_2^+$ .  $O_2^+$  can lead to charge transfer or hydride abstraction reactions (Amador Muñoz et al., 2016); (Jordan et al., 2011); (Knighton et al., 2009)). Signals at  $[C_6H_6]^+$  ( $m/z$  78),  $[C_7H_8]^+$  ( $m/z$  92) and  $[C_8H_{10}]^+$  ( $m/z$  106) likely derive from  $O_2^+$  charged ions of ArHC, and are hence excluded from the analysis of the total mass (but support peak identification by correlation with their corresponding protonated ion at  $\sim 5\%$  of the protonated signal). Other ions deriving from  $O_2^+$  ionization are insignificant contributors to the total mass.~~

The carbon content of the quantified ArHC ~~corresponds corresponded~~ to  $48.8\pm 7.6\%$  of the FID-~~derived~~ NMHC signal (assuming equal response factors on the FID~~s~~) for full cW, cE and Ph 1 (cW). (Note, that the ratio of total NMOC mass in ( $\mu g C$ ) determined by the PTR-ToF-MS to NMHC measured by the FID (after subtraction ~~of ing~~  $CH_4$  as measured by the Picarro CRDS) is  $0.65\pm 0.15$  as average of cW, cE, Ph 1 (cW). ~~The NMHC/NMOC comparison for data for Ph2-4 are is~~ not presented due to interferences on FID ~~in~~ measurements of oxygen-containing hydrocarbons). ~~The high ArHC~~

Field Code Changed

Field Code Changed

Field Code Changed

Formatted: Not Highlight

Formatted: Not Highlight

Field Code Changed

Field Code Changed

Field Code Changed

Field Code Changed

Formatted: Subscript

Formatted: Superscript

Formatted: Indent: First line: 1.27 cm

Field Code Changed

Field Code Changed

Field Code Changed

Field Code Changed

~~contribution to the GDI emissions observed here are in line with reports by e.g. (Zimmerman et al., 2016a) and (Saliba et al., 2017). Figure 4c summarizes the ArHC emission factors, and Figure 4d gives the relative composition of the most dominant ArHC.~~

Of the non-aromatic peaks in ~~Figure 4~~ ~~Figure 4~~a, the largest signals ~~occurred~~ occurred at integer  $m/z$  57 ( $[C_4H_9]^+$ ), followed by 41 ( $[C_3H_5]^+$ ) and 43 ( $[C_3H_7]^+$ ), which taken together ~~make made~~ up  $7.9 \pm 4.8\%$  of the signal for the full cycle (cW, cE) ~~as well as for~~ Ph 1 (cW). A larger fraction ( $13.2 \pm 11.9\%$ ) ~~is was~~ observed ~~when investigating in~~ Ph 2-4 (cW), (i.e. hot engine conditions). These ions are often fragments of larger molecules and hence not straight-forward to assign. Thus, they are ~~included in the category of~~ ~~labelled as~~ structurally unassigned hydrocarbons ~~here in Figure 4. Often~~ ~~Frequently~~,  $[C_3H_5]^+$  and  $[C_3H_7]^+$  are considered fragments of oxygenated parent molecules. In our experiments, however, these ions ~~may~~ dominantly derived from propene ( $C_3H_6$ ), ~~based on ratios between those ions and  $[C_3H_6]^+$  (SI Section S5, Figure S15), for which protonation leads to  $[C_3H_6+H]^+$ , and a subsequent loss of  $H_2$  leads to  $[C_3H_5]^+$ . The observed ratio of  $[C_3H_5]^+$  and  $[C_3H_7]^+$  is consistent with the ratio seen for pure propene ( $C_3H_6$ ) injected into the instrument as reference (Figure S15). In analogy to  $O_2^+$  ionization of ArHC, we find  $[C_3H_6]^+$  in the spectra as insignificant signal (5% of  $[C_3H_6+H]^+$ ). It is likely related to an  $O_2^+$  charge transfer to propene ((Amador Muñoz et al., 2016); (Jordan et al.); (Knighton et al., 2009)), and supports the peak identification. The fuel ~~contains contained~~  $5\%_{vol}$  (2014) to  $8\%_{vol}$  (2015) of methyl-tert-butyl-ether (MTBE), as an anti-knocking agent ~~which, rather than butene, dominated the significant signal at  $m/z$  57 ( $[C_4H_9]^+$ ), which is elaborated in SI Section S5 further. Fragmentation by proton transfer reactions of MTBE can lead to a significant signal at  $m/z$  57 ( $[C_4H_9]^+$ ). Protonated butene would also yield  $[C_4H_9]^+$ , but analogous to the ArHC and propene, should also give a correlated signal at  $[C_4H_8]^+$  at approximately 5% of  $[C_4H_9]^+$ , which is not observed. The carbon content of unspecific fragments ( $[C_3H_5]^+$  ( $m/z$  41),  $[C_3H_7]^+$  ( $m/z$  43),  $[C_4H_9]^+$  ( $m/z$  57)) ~~accounted~~ for additional  $4.4 \pm 3.0\%$  of the FID NMHC signal (full cW, cE, and Ph 1 (cW)).~~~~

Based on the literature reports of e.g. ~~((Platt et al., 2013) and (Schauer et al., 2002))~~ we expect a significant contribution of ethene ( $C_2H_4$ ) to the exhaust hydrocarbons, ~~which~~ ~~This~~ however, cannot be quantified by proton transfer reaction ~~(Gueneron et al., 2015), and together with short-chain alkanes contributes contributes~~ in parts to the difference between the NMOC and FID-based NMHC signal (ratio of the two measurements:  $0.65 \pm 0.15$ ). ~~Further~~ ~~Other~~ possibilities for parents of ~~those above mentioned~~ potential fragments ~~may also contribute to the missing mass closure: e.g. (41, 43, 57, and further  $C_nH_{2n+1}^+$  may also derive from) are~~ alkyl-substituted monocyclic aromatics, alkenes with  $>C_4$ , or alkanes ( $>C_{10}$ , potentially  $>C_6$  if cyclic) ~~(Gueneron et al., 2015); (Erickson et al., 2014); (Buhr et al., 2002))~~. While ~~we detected~~ small intensities at the masses corresponding to  $C_nH_{2n+1}^+$  (e.g. 71, 85, 99) ~~are detected~~, we ~~did~~ not observe significant signals corresponding to aliphatic fragmentation patterns above  $m/z$  57. Signals indicating larger cycloalkanes or alkenes (e.g. most abundant fragments at  $m/z$  69 for substituted cyclohexane) ~~(Gueneron et al., 2015); (Erickson et al., 2014))~~ ~~are were~~ ~~neither also not~~ abundant in our spectra, although ~~their presence has been~~ reported by gas-chromatographic MS techniques in other experiments (e.g. ~~(Saliba et al., 2017); (Zhao et al., 2016))~~. We cannot ~~fully~~ exclude the presence of those compounds, ~~however~~, due to the limitations of our measurement principle ~~and they might contribute to the missing 35% carbon mass.~~

Formatted: Not Highlight

Formatted: Not Highlight

Field Code Changed

Formatted: Not Highlight

Formatted: Indent: First line: 1.27 cm

Field Code Changed

Formatted: English (U.S.)

Field Code Changed

Field Code Changed

Field Code Changed

Field Code Changed

5 ~~Their potential relevance for SOA is further discussed in Section 3.6. Further missing carbon mass fragmentation is further in the NMOC and NMHC measurements (may result from alkyl substituted mono aromatics which can also lead to fragments at  $m/z$  41, 43, 57, and further  $C_nH_{2n+1}^+$  as already mentioned above) discussed in SI Section S5. The fragmentation process would result into a significant mass loss, as the aromatic ring would remain predominantly neutral (especially for mono aromatics with long alkyl substituents (Gueneron et al., 2015)). For example, only 22% of the ion signal generated from n-pentylbenzene fragmentation retains the aromatic ring (19%  $M+H^+$ , 3% protonated benzene ring), and 88% is found at non-aromatic ions  $m/z$  41 or 43).~~

Field Code Changed

10 ~~We found Aa small contribution from oxygenated species (such as small acids and carbonyls) is found, while larger oxygenated molecules are were not detected in significant amounts except for traces of benzaldehyde ( $[C_7H_6O+H]^+$ ) and methyl-benzaldehyde ( $[C_8H_8O+H]^+$ ). Nitrogen is was found only in very few species, of which the dominant one is was assigned to acetonitrile ( $CH_3CN$ ). Due to challenges in its quantification without proper calibration of the PTR-ToF-MS, and its unknown source (including potential outgassing from Teflon sampling lines), it was excluded from our analysis. The carbon content of oxygenated compounds found in the NMOC fraction, which have a lower response in the FID, would make up only  $3.6 \pm 3.9\%$  of the FID signal assuming a response equal to pure HCs for cW, cE and Ph 1 (cW). Hence, even if oxygenated species have a limited response in FID measurements, they do not bias the total FID NMHC measurements substantially (assuming that the PTR-ToF-MS is able to detect and quantify all oxygenated species present).~~

15 ~~Summarizing, our above interpretation of the NMHC and NMOC closure holds for full cW and cE, and Ph 1 (cW) experiments, summing all these species and accounting for the uncertainties introduced by response factors and  $k_{H_2O_2}$  rates of fragments, as well as species that the PTR-ToF-MS is unable to detect.~~

### 20 3.5 SOA formation in OFR and SC: oxidation conditions and reacted SOA precursors

25 ~~Figure 5 Figure 5 shows a typical experiment during which collected primary emissions were sampled from the SC through the OFR (OFR-from-SC), and exposed to photochemistry at UV light settings of 100%, 70%, and 50% in the OFR, and characterized in dark conditions (Figure 5 Figure 5a). After investigating OFR from SC aging, typically Thereafter, photochemistry was initiated in the SC (Figure 5 Figure 5b). Reactive NMOC (displayed are the dominantly observed ArHC), decay upon exposure to OH radicals, and OA mass increases.~~

Field Code Changed

Field Code Changed

Field Code Changed

30 ~~The emissions of vehicle exhaust contained NO, which can influence the chemical pathways during atmospheric processing, given that the dominance of  $RO_2$ -NO or  $RO_2$ - $RO_2$  reactions is driven by NO levels. NO-to-NO<sub>y</sub> ratios are presented in the top panels of Figure 5. In the OFR, nitrogen monoxide (NO) is was converted rapidly to NO<sub>2</sub> (and further to HNO<sub>3</sub>) in the OFR, hence the OFR aging conditions when sampling from diluted exhaust (OFR from SC) can be considered "low NO conditions" (Lambe et al., 2017) and OFR aging conditions when sampling from diluted exhaust hence were considered "low NO"; (Peng and Jimenez, 2017)). Only at elevated NO levels (such as during online operation of the OFR during our 2014 measurements (as discussed also in Section 3.3 and S4 the SI), "high NO" conditions may have been reached in the OFR as defined by (Peng and Jimenez, 2017)). The dominance of the  $RO_2$ -NO or  $RO_2$ - $RO_2$  reactions is~~

Formatted: Indent: First line: 1.27 cm

Field Code Changed

Field Code Changed

Field Code Changed

Field Code Changed

driven by the NO levels. Based on (Platt et al., 2014), RO<sub>2</sub> radicals predominantly react with NO, when the concentration of NO is higher than only 1 ppb in the SC. Before starting the SC aging by injecting HONO and initiating photo-chemistry, we titrated NO present in the SC to NO<sub>2</sub> using O<sub>3</sub>. NO levels in the SC were typically below 5 ppb when photochemistry was initiated, and dropped to the detection limit (< 1 ppb) within few minutes of photochemistry. The total NO<sub>y</sub> signal increases with time of SC experiment, which we relate to the formation of nitric acid (HNO<sub>3</sub>) from primary NO<sub>x</sub> and continuous injection of nitrous acid (HONO) (see also particulate nitrate signal in Figure S10, Supporting Information), although the presence of NO<sub>2</sub> cannot be unambiguously quantified. We classified our SC experiments as “low NO” conditions: albeit initial NO concentrations can be higher than in the corresponding OFR experiments. Reduced SOA yields as a function of higher NO concentrations in gasoline exhaust have been recently discussed by (Zhao et al., 2017).

Upon photochemistry, reactive NMOCs decayed due to reactions with OH radicals (Figure 5a,b, middle panel), OA and secondary nitrate mass increased in turn (bottom panel). While in terms of abundance of potentially SOA-forming precursors toluene (TOL) and xylenes and ethylbenzene (XYL/EBENZ) dominate over benzene (BENZ) and the C3-benzenes (C3BENZ), their OH reaction rates (Table 2) have the opposite trend for these compounds (C3BENZ > XYL/EBENZ > TOL > BENZ). The reacted ArHC mass, which is the quantity relevant for SOA formation, at a given OH exposure was governed by the combination of their abundance and their reaction kinetics. Reacted ArHC (At the final OH exposure of  $(1.4-5.8) \times 10^{11}$  molec cm<sup>-3</sup> s<sup>-1</sup>) it was dominated by XYL/EBENZ (41±3%), which together with TOL (33±4%) comprises more than 70% of the reacted ArHC fraction. C3BENZ (13±2%) and BENZ (7±3%) provided smaller contributions, and in our eW, eE and Ph 1 (eW) experiments. C4BENZ, STY, C1STY and NAPH accounted for additional ~5% to the reacted ArHC fraction; other ArHC compounds were not considered. (fractions are provided in Time series of typical experiments are provided in Figure 5a,b (middle); averaged contributions of reacted ArHC as noted above in the text are displayed in Figure S54, Supporting Information, OH exposure data at the end point of SC experiments and for the OFR are provided in caption to Figure 6 and in Figure 7). NO<sub>x</sub>/OA as a surrogate to describe NH<sub>4</sub>NO<sub>3</sub> formation were 4.00±2.11 in the SC and comparatively lower in the OFR (0.43±0.26).

SOA mass was then predicted by accounting for the reacted mass of the dominant ArHC and their respective SOA potential using previously reported SOA yields (i.e.  $SOA_{predicted} = \sum_i (\Delta NMOC_{i,reacted}(t) * yield_{i,literature})$  assuming a constant yield as a function of OH exposure and suspended OA loading, yield data as reviewed in (Bruns et al., 2016)). As shown in the bottom panels of Figure 5 (a and b) this does not provide a closure between reacted precursor mass and SOA mass formed. Because SOA yields are a function of the suspended absorptive mass (partitioning theory (Pankow, 1994); (Donahue et al., 2006)), we further investigate the agreement between reacted SOA forming precursors and the formed SOA mass as SOA yield curves (discussed in the following Section 3.6).

Field Code Changed

Field Code Changed

Field Code Changed

Field Code Changed

Formatted: Superscript

Field Code Changed

Field Code Changed

Formatted: Subscript, Not Highlight

Formatted: Not Highlight

Field Code Changed

Formatted: Subscript, Not Highlight

Formatted: Not Highlight

Formatted: Subscript, Not Highlight

Formatted: Not Highlight

Field Code Changed

Field Code Changed

Field Code Changed

Formatted: English (U.S.)

Formatted: English (U.S.)

Field Code Changed

Formatted: English (U.S.)

Formatted: English (U.S.)

### 3.6 Effective SOA yields

Effective SOA yields ( $Y_e$ ) as a function of absorptive mass (Pankow, 1994; Donahue et al., 2006) are displayed in Figure 6, while Section 3.7 discusses differences in the chemical composition of for the SC and OFR experiments. In Figure 6 a we present For the GDI exhaust, our  $Y_e$  assumed BENZ, TOL, XYL/EBENZ, C3BENZ, C4BENZ, NAPH, STY, C1STY as sole SOA precursors and we focused on tests from cold-started GDH-3 (i.e. for full cW, cE; and Ph 1 (cW)), while GDH4 or hot engine conditions, i.e. Ph 2-4 (cW) were not included in our analysis. (This is, because the concentration levels were close to our background measurements. However, we would like to highlight that Zhao et al., 2018 recently reported higher effective SOA yields for hot-engine conditions compared to cold-engine conditions, which reflects also our observations.) yields for GDH-3 vehicle exhaust (SC and OFR from SC All yields (for exhaust as well as separate precursors) increased as function of the suspended OA, reaching 0.8-1 for OFR vehicle exhaust experiments with OA loadings above  $300 \mu\text{g m}^{-3}$ . In the atmospherically more relevant range of 10 to  $100 \mu\text{g m}^{-3}$ , yields spread from a few (<15%) to 20-50% together with single precursor yields (SC and OFR experiments reported in the literature and new data from our OFR). Note that for GDI exhaust,  $Y_e$  assumes solely BENZ, TOL, XYL/EBENZ, C3BENZ, C4BENZ, NAPH, STY, C1STY as SOA precursors. Data are presented as a function of suspended OA for all experimental conditions of cold-started GDH-3 (i.e. for full cW, cE; and Ph 1 (cW)), while GDH4 or hot engine conditions, i.e. Ph 2-4 (cW) are not included in the analysis (Zhao et al., 2018). Detailed discussions are provided later. In brief, For the GDI exhaust comparisons we find the following that

- SC- and OFR-derived GDI vehicle exhaust aged in the SC and the OFR result in similar effective yield curves for GDI exhaust agreed within our experimental variability the two systems, and had with a trend for lower higher yields obtained in the OFR in SC than the SC (experiment or, vice versa, lower yields for the SC than the OFR) (Figure 6c, see Section 3.6.1 for a detailed discussion). No distinct difference between Ph 1 (cW) SOA and the full cycle (cW, cE) SOA was observed, and neither an explicit effect of GPF-retrofitting.
- GDI vehicle exhaust effective SOA yields (SC and OFR) appeared relatively higher than our reference measurements conducted with the most relevant with specific SOA precursors, in the range of up to a factor of 2 for the OFR and lower discrepancies for the SC. (ArHC) present in the vehicle exhaust. Potential reasons for the discrepancy are discussed in detail further below (Figure 6a, see Section 3.6.2).
- OFR SOA yields of toluene, *o*-xylene and 1,2,4-TMB and their mixtures were in good agreement with those of other OFR studies (*m*-xylene, Ahlberg et al., 2017) and SC studies (benzene, toluene, *o*-xylene, from Li et al., 2016a and Li et al., 2016b, Figure 6b).

We performed separate OFR experiments with toluene, *o*-xylene and 1,2,4-TMB as appropriate surrogates. Their effective SOA yields obtained by our OFR measurements are in agreement with previously published SOA yield curves for ArHC

Formatted: Subscript

Formatted: English (U.S.)

Field Code Changed

Formatted: English (U.S.)

Field Code Changed

Formatted: English (U.S.)

Formatted: English (U.S.)

Field Code Changed

Formatted: Not Highlight

Field Code Changed

Formatted: Indent: Left: 0.63 cm, No bullets or numbering

photo-chemically aged in an analogous OFR (*m*-xylene, by (Ahlberg et al., 2017)) and in a SC (benzene, toluene, *o*-xylene, from (Li et al., 2016a) and (Li et al., 2016b), shown in Figure 6b). All yields (for vehicle exhaust as well as for single precursors) increase with the suspended OA concentration, and range up to 0.8-1 for OFR vehicle experiments above 300  $\mu\text{g m}^{-3}$ . In the atmospherically more relevant concentration range of 10 to 100  $\mu\text{g m}^{-3}$ , the effective yield spreads from a few percent (below 15%) up to 20-50% (at 100  $\mu\text{g m}^{-3}$ ).

### 3.6.1 SC vs. OFR yields of GDI vehicle exhaust (Figure 6c).

Aging of GDI vehicle exhaust in the SC and the OFR resulted in similar SOA yield curves within our experimental variability, in similar effective SOA yield curves. They exhibited, with a trend towards lower higher yields values for SC OFR experiments (or, vice versa, lower values for the SC) (Figure 6c). Yields determined in the SC experiments were, however, variable among themselves and investigations of agreement between SC- and OFR-derived yields consequently a function of the chosen reference point. We believe that experiments A2, A3 and B3 (as labelled in Figure 6 and Table S4) are reliable data points for comparison, while experiments A1, B1 and B2 are potentially associated with higher uncertainties (further discussed in the paragraph following the next).

The contribution of SOA precursors to the reacted ArHC fraction is comparable between the systems (Figure S4). Yields are expected to be underestimated by factors of 1.5-2 (SC) and 1.25 (OFR) (Platt et al., 2017; Palm et al., 2016) due to influences of vapor wall losses. Taking those correction factors into account reduces the discrepancy between the two systems. The relative contribution of species to the reacted ArHC fraction was not significantly different between the systems (Section 3.5, Figure S5). At average it agreed by a factor of  $1.0 \pm 0.3$ , and did not suggest inducing any differences in the SOA yields. However, other plausible explanations exist for the remaining gap in the yields. While OFR-derived effective yields for GDI vehicle exhaust appear higher than our SC-derived yields. One reason might be higher initial levels of NO in the SC experiments compared to the OFR, might suppressing the SC SOA yields formation, as recently discussed by (Zhao et al., 2017), the more likely scenario in our experiments is that the higher OH concentrations in the OFR ( $10^7$  molec  $\text{cm}^{-3}$  in the SC, vs.  $10^8$  to  $10^9$  in the OFR) led to more than one OH attack on the aromatic precursors (Molteni et al., 2018) and thereby enhanced the OFR yields. This is also supported by the tendency higher H:C found in OFR SOA (see discussion in Section 3.7).

As mentioned earlier, we also investigated on the variability among SC yields. However, as discussed in the Methods Section, we expect both SC and OFR yields to be underestimated, by factors of approximately 1.5-2 (SC) and 1.25 (OFR) (Platt et al., 2017; Zhang et al., 2014; Palm et al., 2016) due to vapor wall losses. Corrections would reduce the discrepancy between the two systems, which indicated a correlation of higher SOA yields with higher initial SC NO levels, such as e.g. for experiments A1, B1 and B2 (Figure 6, Table S4). This is contradictory to common knowledge and recent

Field Code Changed ... [20]

Formatted ... [21]

Formatted ... [22]

Formatted ... [23]

Field Code Changed

Field Code Changed

Formatted: Heading 3

Field Code Changed

Formatted ... [24]

Field Code Changed

Formatted ... [25]

Formatted: Indent: First line: 1.27 cm

Field Code Changed ... [26]

Formatted ... [27]

Field Code Changed

Formatted ... [28]

Formatted: Not Highlight

Field Code Changed ... [29]

Formatted ... [30]

Field Code Changed

Formatted ... [31]

work by Zhao et al., 2017. The higher initial NO levels, however, also correlated with higher concentrations of secondary  $\text{NH}_4\text{NO}_3$  in the SC (Table S4, using the  $\text{NO}_3$  as a surrogate).

Our SC derived yields themselves are variable (Figure 6e). While effective yields are presented vs. OA as assumed absorptive mass here, we find significant formation of  $\text{NH}_4\text{NO}_3$  during SC experiments (Figure S10b, Table S4;  $\text{NO}_3$  is used as a surrogate for  $\text{NH}_4\text{NO}_3$ ;  $\text{NO}_3/\text{OA}$  ratios are significantly higher in the SC ( $4.00 \pm 2.11$ ) compared to the OFR ( $0.43 \pm 0.26$ )). Presenting SC yields as a function of the sum of  $\text{OA} + \text{NO}_3 + \text{NH}_4$  in Figure S13 appears appeared to bring them into better agreement decrease variability among SC yields, and indicates indicating a relationship between the yields and  $\text{NH}_4\text{NO}_3$  dependencies for those three experiments (A1, B1, B2). Given that (and a correlated trend of higher yields at higher initial  $\text{NO}_3$  levels, which is contradicted by (Zhao et al., 2017)). The high concentrations of  $\text{NH}_4\text{NO}_3$  concentration formed in in 3 of these experiments (several hundreds of  $\mu\text{g m}^{-3}$ ) is was outside our  $\text{CO}_2^+$ -AMS interference calibration and, data of these datae three experiments may still be associated with a positive mass bias even after correction ((Pieber et al., 2016)). Neglecting a potential additional  $\text{CO}_2^+$ -AMS interference, the data experimental artifacts would allow for a speculation on the contribution of indicate that inorganic nitrate (as well as and the associated water) may contribute to, as the absorptive mass (Stirnweis et al., 2017), and the (unwanted) influence of  $\text{NO}_3$ -radicals at relatively higher concentrations of initial NO (Schwantes et al., 2017), (Schwantes et al., 2016)), however, a detailed analysis is, however, beyond the scope of our study.

### 3.6.2 SOA yield of GDI vehicle exhaust SOA yields in comparison to vs. single specific precursors (Figure 6 Figure 6a).

GDI vehicle exhaust effective SOA yields from (SC and OFR), appeared higher than our reference measurements conducted with the most relevant with specific SOA precursors, again from SC and OFR (ArHC) present in the vehicle exhaust. However, we can could match the yields at explain a significant fraction ( $\rightarrow$  at least 0.550% in OFR experiments and up to 100% in the SC, ) of our obtained vehicle exhaust effective yields with the mix of reacted o xylene and toluene (OXYL/TOL, 3:1) as presented in Figure 6 Figure 6a). For the remaining This generally indicates that we are able to identify the most relevant SOA precursors in the vehicle exhaust. The discrepane discrepancy of up to a factor 2 for the OFR y between the effective SOA yields for GDI and the measured yields of major precursors may result from various reasons we focus on the following two hypotheses:

#### 1) Unaccounted,

#### Missing pprecursors ((unidentified/undetected in NMOC analysis, see also see Section 3.4).

Our calculated effective SOA yields assumes that all our relevant SOA precursors found in the exhaust are were identified and their decay quantified, as defined in Eq. (2). We are were able to explain only 65%±15% of the total non-methane hydrocarbon signal with the carbon found in the PTR-ToF-MS measured NMOCs, and used the aromatic fraction (49±8%) as SOA precursors. This approach covers a significant fraction of likely SOA-precursors. While both, the aromatic

Formatted ... [32]

Field Code Changed

Formatted ... [33]

Field Code Changed

Formatted ... [34]

Field Code Changed

Formatted ... [35]

Field Code Changed

Formatted ... [36]

Field Code Changed

Formatted: Not Highlight

Field Code Changed

Formatted ... [37]

Formatted: Heading 3

Field Code Changed

Formatted ... [38]

Field Code Changed

Formatted ... [39]

Formatted: Font: Bold

Formatted: Indent: First line: 1.27 cm

Formatted: Font: Bold

Formatted: Normal, Indent: First line: 1.27 cm, No bullets or numbering

Formatted ... [40]

Formatted: Indent: Left: 0 cm, First line: 1.27 cm

Formatted ... [41]

(Odum et al., 1997; Ng et al., 2007b; Hildebrandt et al., 2009; Loza et al., 2012; Platt et al., 2014) and the aliphatic (especially alkanes) (Lim and Ziemann, 2005; Loza et al., 2014) species are known exhaust constituents and may form SOA. Aliphatic species are relevant only if their carbon chain is sufficiently long and does not substantially fragment during reaction. Short-chain alkanes (<C<sub>8</sub>) exhibit only low SOA yields at typical ambient OA levels (Jordan et al., 2008). ArHC, starting from the simplest with C<sub>6</sub>, instead produce highly oxygenated multifunctional organics with only few OH attacks (Molteni et al., 2018; Schwantes et al., 2017), and are therefore efficient SOA precursors exhibiting high yields. Oxygenated ArHC (phenolic, benzaldehyde) did not appear significant enough (<1% of the total NMOCs) to induce yield-enhancements and were neglected in our analysis. Further relevant compounds were not included as relevant SOA precursors, although (Section 3.4). This leaves on average about up to 35% additional carbon was available to be attributed undetected to other molecules (assuming the PTR-ToF-MS to FID comparison is a valid approach). Parts of those 35% are certainly not significant for SOA formation, such as e.g. ethene and other above-mentioned short-chain aliphatic compounds. While those might contribute significantly to the unidentified carbon fraction, they do not contribute significant SOA mass. Other undetected molecules instead might also form SOA, and leaving them unaccounted, artificially increases our calculated effective SOA yields.

Prominent candidates are alkyl-substituted monocyclic aromatic and long chain aliphatic compounds, as elaborated on in the following. While both aromatic ((Odum et al., 1997); (Ng et al., 2007b); (Hildebrandt et al., 2009); (Loza et al., 2012); (Platt et al., 2014)) and aliphatic (especially alkanes) ((Lim and Ziemann, 2005); (Loza et al., 2014)) species are found in vehicle exhaust and may form SOA, aliphatic species do so only if their carbon chain is sufficiently long and does not substantially fragment during reaction. Short-chain alkanes (<C<sub>8</sub>) are expected to have only low SOA yields at typical ambient OA levels (Jordan et al., 2008). ArHC (starting from the simplest with C<sub>6</sub>) instead have been shown to produce highly oxygenated multifunctional organics with only few OH attacks ((Molteni et al., 2016); (Schwantes et al., 2016)), making them efficient SOA precursors with high SOA yields, especially under "low NO" conditions (Ng et al., 2007b). As discussed above, identified ArHC dominate the total gas phase organic compounds as determined by the PTR-ToF-MS, were classified as VOCs based on their saturation concentration (C\*) at or above 10<sup>6</sup> µg m<sup>-3</sup> (VOCs) with a small contribution from aromatics (such as naphthalene) in the IVOC range (C\*=10<sup>2</sup>-10<sup>6</sup> µg m<sup>-3</sup>) (Pandis et al., 2013). While the larger contribution of VOCs than IVOCs to gasoline vehicle exhaust SOA is consistent with Zhao et al., 2016, they also suggest additional substituted monocyclic aromatic IVOCs, which we did not identify. Likewise, Nordin et al., 2013, postulated alkyl-substituted monocyclic aromatics previously as relevant precursors. Given that they fragment in the PTR-ToF-MS predominantly by losing the aromatic ring, those compounds could indeed be significant contributors to the 35% missing carbon mass and would also contribute to SOA. Long-chain aliphatic compounds are likewise plausible, although we found no significant indication in our mass spectra. Further investigations of those species using PTR-ToF-MS could be performed by inducing other ionization pathways such as by use of O<sub>2</sub><sup>+</sup> as the primary ion source (e.g., Amador Muñoz et al., 2016).

Field Code Changed ... [42]

Formatted ... [43]

Formatted ... [44]

Field Code Changed

Field Code Changed

Formatted: Not Highlight

Formatted ... [45]

Field Code Changed

Formatted ... [46]

Field Code Changed ... [47]

Formatted ... [48]

Field Code Changed

Formatted: Not Highlight

~~Finally, Also MTBE was present in significant amounts in the exhaust. It has currently not been considered as a significant SOA precursor, due to its small carbon number and high volatility, but We believe it should be investigated in future work considering it may contribute to SOA when contained in a complex mixture.~~

The identified ArHC have saturation vapor pressures ( $C^*$ ) at or above  $10^6 \mu\text{g m}^{-3}$  (VOCs) with a small contribution from aromatics (such as naphthalene) in the IVOC range ( $C^*=10^3-10^6 \mu\text{g m}^{-3}$ ), rather than SVOC ( $C^*=10^1-10^3 \mu\text{g m}^{-3}$ ) or lower volatility ( $C^* < 10^1 \mu\text{g m}^{-3}$ ) compounds (Pandis et al., 2013). The larger contribution of VOCs than IVOCs to SOA is consistent with the results by (Zhao et al., 2016), who found a ratio of  $\sim 10$  in the VOC to IVOC ratio for gasoline exhaust. The other detected or postulated organic compounds in our exhaust samples (e.g. short-chain alkanes, small oxygenated molecules) are not expected to contribute significantly to the SOA mass.

In sum, missing SOA precursors might thus comprise

○ 1) additional ArHC (e.g. (Nordin et al., 2013)) which are a) unidentified or b) present only in small quantities and hence not taken into account in the effective yield analysis (such as the oxygenated ArHC because they are present at only roughly 1% of our total NMOC).

○ 2) short-chain alkanes/alkenes which contribute a significant fraction to the total carbon in the gas phase, but have low SOA yields and

○ 3) long-chain alkanes and alkyl-substituted mono-aromatics which are not well detected by the PTR-ToF-MS technique due to low protonation affinity or substantial fragmentation.

~~Also MTBE is present in significant amounts in the exhaust. It has currently not been considered as a significant SOA precursor, due to its small carbon number and high volatility, but should be investigated in future work.~~

2)

~~Reference SOA yields aren't chosen correctly do not accurately represent the complex exhaust emissions;~~

○ Aromatic isomers show a distribution of yields based on carbon number, number of aromatic rings, and degree and location of substitution, which are not fully covered by the reference compounds selected for testing. Isomers present in the exhaust may enhance the effective SOA yield relative to the reference measurements.

Benzene contributes less than 10% to the reacted NMOCs (Section 3.5 and Figure S4) and was therefore not tested separately in our OFR. However, its SOA yield has been reported to exceed that of alkylated analogous compounds, such as xylenes or higher alkylated benzenes ((Li et al., 2017); (Bruns et al., 2016)). Benzene may hence contribute to the enhanced effective SOA yield relative to the reference measurements. The same is true for oxygenated ArHC which were not considered in our analysis due to their relatively low contribution to the NMOC composition. Complex mixtures of hydrocarbons and matrix effects might exhibit SOA yields which differ from single molecules or relatively simple mixtures. The influence of NO on SOA yields has been previously addressed in the literature for biogenic and anthropogenic sources (e.g. Ng et al., 2007a; Ng et al., 2007b), and generally indicates that at higher NO conditions, lower

Formatted: Not Highlight

Formatted: Indent: Left: 0 cm, First line: 1.27 cm, Bulleted + Level: 1 + Aligned at: 0.63 cm + Indent at: 1.27 cm

Formatted: Not Highlight

Formatted: Not Highlight

Formatted: Not Highlight

Formatted: Not Highlight

Formatted: Font color: Auto

Formatted: Indent: Left: 0 cm, First line: 1.27 cm

Formatted: Indent: First line: 0.63 cm

Field Code Changed

Field Code Changed

Formatted: Indent: Left: 0.63 cm, No bullets or numbering

Field Code Changed

Formatted: Font: Bold

Formatted: Normal, Indent: Left: 0 cm, First line: 1.27 cm

Formatted: Normal, Indent: First line: 1.27 cm, No bullets or numbering

Formatted: Font: Bold

Field Code Changed

Field Code Changed

Formatted: Not Highlight

Formatted: Not Highlight

Field Code Changed

Field Code Changed

SOA yields are observed. Zhao et al., 2017 confirmed this for gasoline exhaust, and we choose NO-free conditions as comparison points for our yields based on the discussion in Section 3.5. Choosing a high-NO reference would enhance discrepancies. Instead, ~~the influence of other exhaust constituents which are absent in our reference measurements, such as eBC acting as a seed, NH<sub>3</sub> and the formed NH<sub>4</sub>NO<sub>3</sub>, the presence of NO<sub>2</sub>, and/or chemical processing by unwanted formation of NO<sub>2</sub>-radicals ((Schwantes et al., 2017)) on SOA yields, are insufficiently addressed in the literature to discuss in detail for a final conclusions, but a potential influence cannot be excluded in our work. Matrix processes, along with potential non-linear effects of SOA-formation from mixed precursors, should be addressed in future studies. Further, aromatic isomers show a distribution of yields based on carbon number, number of aromatic rings, and degree and location of substitution, which are not fully covered by the reference compounds selected for testing. Isomers present in the exhaust may enhance the effective SOA yield relative to the reference measurements. Last, benzene contributed less than 10% to the reacted NMOCs (Section 3.5 and Figure S5) and was therefore not tested separately in our OFR. However, its SOA yield has been reported to exceed that of alkylated analogous compounds, such as xylenes or higher alkylated benzenes (Li et al., 2017; Bruns et al., 2016). Benzene may hence contribute to the enhanced effective SOA yield relative to the reference measurements.~~

• **Differences in the experimental conditions of single/mixed aromatics vs. the more complex vehicle exhaust:**

○ The influence of NO on SOA yields has been previously addressed in the literature for biogenic and anthropogenic sources (e.g. (Ng et al., 2007b); (Ng et al., 2007a)), and generally indicates that at higher NO conditions, lower SOA yields are observed. (Zhao et al., 2017) showed this recently also for gasoline exhaust. We choose NO free conditions as comparison points for our yields (based on the discussion in Section 3.5). Hence our SOA reference yields for comparison are an upper estimate in this regard, and choosing a high-NO reference would make the discrepancy to the vehicle exhaust even bigger).

○ The influence of other exhaust constituents which are absent in our reference measurements, such as eBC acting as a seed, NH<sub>3</sub> and the formed NH<sub>4</sub>NO<sub>3</sub>, the presence of NO<sub>2</sub> or chemical processing by unwanted formation of NO<sub>2</sub>-radicals ((Schwantes et al., 2016)) on SOA yields is insufficiently addressed in the literature to discuss in detail, but a potential influence cannot be excluded in our work.

**3.7 SOA elemental composition (of SC and OFR)**

The bulk OA elemental oxygen-to-carbon and hydrogen-to-carbon ratios (O:C and H:C) ratios for GDI exhaust SOA formed from GDI vehicle exhaust for the in SC and OFR-from-SC experiments at varied OH exposure (OFR UV intensity) are shown in Figure 7. In all cases, the SOA composition shifts shifted towards higher O:C and lower H:C ratios as a function of OH exposure in both systems. However, the OFR yields higher H:C values, with decreasing divergences at

Field Code Changed

Formatted: Font: (Default) +Headings (Times New Roman)

Formatted: Font: (Default) +Headings (Times New Roman)

Formatted: Not Highlight

Formatted: Font: (Default) +Headings (Times New Roman)

Formatted: Not Highlight

Formatted: Font: (Default) +Headings (Times New Roman)

Formatted: Not Highlight

Formatted: Font: (Default) +Headings (Times New Roman)

Formatted: Font: (Default) +Headings (Times New Roman)

Formatted: Not Highlight

Formatted: Font: (Default) +Headings (Times New Roman)

Formatted: Font color: Auto, Not Highlight

Formatted: Not Highlight

Formatted: Font color: Auto, Not Highlight

Formatted: Font color: Auto

Field Code Changed

Field Code Changed

Formatted: Normal, No bullets or numbering

Field Code Changed

higher OH exposures. The end point of the SC experiments in terms of max. OH exposure corresponds to the 70% UV setting in the OFR on average. Concerning the ~~While we found O:C ratio we find~~ agreement for the O:C between SC and with OFR-from-SC at similar OH exposure for three SC experiments (labelled A2, A3, B3 in Figure 7a,c), ~~while~~ the other three experiments ~~yield exhibited~~ relatively higher O:C ratios at the same equivalent OH exposure (labelled A1, B1, B2 in Figure 7b,c). The ~~three SC experiments with higher O:C latter ratios~~ also had higher SOA yields than the other experiments (see Figure S13 for detailed yields Section 3.6.1) and Figure S16 for the differences in the O:C ratios of these experiments). Those three experiments ~~and are were~~ characterized by a higher absolute as well as relative  $\text{NH}_4\text{NO}_3$  concentrations, which, ~~as noted above is were~~ outside our  $\text{CO}_2^+$ -AMS interference calibration and. We believe data may still be associated with a positive bias towards higher O:C even after correction ((Pieber et al., 2016)). Hence ~~we focused on A2, A3 and B3 and we~~ consider our O:C data in general agreement between OFR-SOA and SC-SOA, when represented with regards to the O:C ratio as a function of OH exposure in OFR and SC. This agreement ~~does did~~ not apply for the H:C ratio, however, for which the OFR yielded higher values than the SC. ~~Initially higher NO<sub>x</sub> levels in the SC and overall higher OH concentration in the OFR (leading to more than one OH addition to the aromatic ring) as discussed in Section 3.6 could explain the observed trends. Further, we speculate that reaction termination with HO<sub>2</sub> rather than RO<sub>2</sub> would also increase the H:C in the OFR relative to the SC. Possible reasons for differences in the products between OFR and SC in terms of the bulk elemental composition ratio include differences in the aging conditions (oxidant concentrations, ratios of OH/O<sub>3</sub>, presence/absence/amount of NO<sub>x</sub>, ratios of NO/NO<sub>2</sub>, (unwanted) presence of NO<sub>3</sub> radicals, presence of secondary NH<sub>4</sub>NO<sub>3</sub> and associated water acting as additional absorptive mass and leading to chemical differences of the products) and other experimental uncertainties (loss of secondary vapors to the walls or loss by UV interaction at different rates between SC and OFR, please refer also to the discussion in section 3.6).~~ Further investigation of those aspects requires information on a molecular level and should be the focus of future comparison studies ~~between the two systems. GPF-retrofitting did not distinctly affect SOA bulk elemental composition, in line with no clear effects on NMOC composition, SOA EFs or SOA yields.~~

#### 4 4- Conclusions

We studied exhaust from ~~modern Euro 4 and Euro 5~~ GDI vehicles as a function of driving cycles, individual phases thereof and engine temperature (cold-started, hot-started), and evaluated the effect of ~~retrofitted, retrofitted prototype~~ GPFs on the primary ~~and emissions and SOA secondary emissions~~. We presented a detailed analysis of primary NMOC composition from PTR-ToF-MS measurements, ~~identified relevant SOA precursors and the associated assessed SOA formation potential evaluated by SC and OFR experiments, and provide a quantitative link between the NMOC fraction and the observed SOA.~~ Here, We also provide OFR-obtained ArHC SOA yield curves for toluene, o-xylene and 1,2,4-TMB. we summarize the major conclusions.

Field Code Changed

Field Code Changed

Field Code Changed

Formatted: Font color: Auto, Not Highlight

Formatted: Font color: Auto, Not Highlight

Formatted: Not Highlight

Formatted: Font color: Auto, Subscript, Not Highlight

Formatted: Font color: Auto, Not Highlight

Formatted: Font color: Auto, Subscript, Not Highlight

Formatted: Font color: Auto, Not Highlight

Formatted: Font color: Auto, Not Highlight

Formatted: Not Highlight

Formatted: Numbered + Level: 1 + Numbering Style: 1, 2, 3, ... + Start at: 4 + Alignment: Left + Aligned at: 0.63 cm + Indent at: 1.27 cm

Formatted: Font color: Auto

For all GDI vehicles, the dominant fraction of ~~NMOC hydrocarbon~~ emissions ~~is was~~ released during ~~the starting~~ ~~phase of~~ cold-started vehicle tests, before after-treatment systems are ~~hot at operational temperature~~. ~~No drastic test cycle dependencies between WLTC and EDC were observable from our tests during cold-started cycles~~. Instead, EFs of primary NMHC and THC were reduced by up to a factor of 90 under hot-started conditions compared to cold-starts, and total emissions were dominated by the pollution during the first few minutes of the driving cycle. ~~NMOC~~ Chemically, the emissions of cold-started vehicles ~~are were~~ dominated by aromatic hydrocarbons, especially ~~by~~ toluene, xylenes/ethylbenzenes, ~~and C-3-alkyl~~ benzenes and benzene. SOA formation ~~was is~~ likewise governed by the cold-start emissions, and SOA formation under hot-engine conditions 20-50 times lower than under cold-engine conditions. These results ~~are were~~ independent of ~~the~~ testing protocol, demonstrating that ~~vehicle engineering and~~ the performance of after-treatment systems ~~and rather than~~ the driving behavior ~~governs governed~~ these emissions. Overall, the SOA potential (in terms of an emission factor) ~~agreed with recent literature reports from both, GDI and port fuel injection systems~~. It ~~appears appeared~~ that GDI4, which ~~is was~~ in line with Euro 6 regulations regarding its NMHC emissions, ~~has had~~ a reduced overall and cold-start NMHC EF, ~~and that but instead~~ its emissions during hot-engine conditions contributed a bigger relative fraction to the total ~~compared to GDI-3~~. Additionally, by trend, oxygenated ArHCs ~~have had~~ a slightly enhanced fraction in GDI4 compared to GDI-3 exhaust. ~~SOA formation of GDI4 was lower compared to GDI-3, in line with NMHC reduction induced by reduced cold-start enrichment or improved catalytic after-treatment system~~. Considering that GDI4 NMHC EFs follow those of Euro 6 vehicles, the determined SOA EFs may be representative of a newer generation of vehicles.

GPF ~~retrofitting application~~ efficiently ~~removes removed~~ eBC, which ~~is was~~ the dominant component of primary PM. ~~It but also showed has small effects on the minor POA fraction. The volatile POA fraction passes through the filter in the vapor phase and later condenses when the exhaust is emitted and cooled; hence POA emission factors are not, which was, however, not as significantly reduced as the refractory PM. Instead, NMOC emissions and SOA formation are unaffected by the tested GPFs, both GPF retrofitting did not alter NMHC EF, the chemical gas-phase composition, and neither did it reduce SOA formation in our cold-started tests. This result holds likely generally true when GPFs are~~ catalytically inactive, and at cold-started driving cycles also for catalytically active GPFs (i.e. when emissions pass through the TWC and the catGPF before light-off temperatures are reached). ~~and with catalytically active coating. This means It implies that, while~~ retrofitting GDI vehicles with GPFs will likely result in an important reduction of the total primary PM ~~emitted. emissions through (removal of refractory material), but it will not (or under conditions similar to our experiments) only to a small extent) reduce NMHC (or NMOC) hydrocarbon emissions including ArHC, and thereby and will not directly lead to a reduction of the SOA SOA reduction formation. Future work should assess GPF and catGPF effects under hot-engine conditions in more detail. Likewise, on tests on so-called "4-way catalysts", i.e. a TWC-GPF combination a TWC catalyst directly applied onto a GPF and installed at the location of the current TWC for simultaneous filtration of particulates and catalytic conversion of NMHC (or NMOC) gaseous pollutants should be conducted will be beneficial to~~

Formatted: Indent: First line: 1.25 cm

Formatted: Not Highlight

Formatted: Not Highlight

Formatted: Not Highlight

Formatted: Not Highlight

Formatted: Font color: Auto

Formatted: Font color: Auto, Not Highlight

Formatted: Font color: Auto

Formatted: Font color: Auto

Formatted: Font color: Auto

~~understand whether to understand whether~~ reductions of SOA precursors, SOA ~~production and and~~ semi-volatile primary PM can be achieved with further optimized systems.

Formatted: Font color: Auto

Formatted: Font color: Auto

Formatted: Indent: First line: 1.27 cm

Effective SOA yields ~~from GDI exhaust, while in general agreement considering our experimental variability, as a function of suspended OA mass concentration~~ appeared by tendency rather higher for the OFR than the SC (or, vice versa, lower in the SC than the OFR), and were not explicitly influenced by GPF-retrofitting. We believe that the differences are in parts due to unaccounted experimental losses, as well as a potential influence of NO<sub>x</sub> chemistry in our SC experiments. Trends in the ~~atomic elemental~~ O:C of the bulk SOA were related to different OH exposure levels in the two systems. Trends in ~~in and the~~ H:C ratios of the bulk OA mass suggest that differences in SC and OFR aging or operational conditions affect the chemical composition of the formed SOA. These divergences cannot be unambiguously attributed to a specific ~~indicated~~ instead differences in OFR and SC processing, which ~~call for~~ further investigation of those aspects requires information on a molecular level and should be the focus of future comparison studies between the two systems.

Based on gas phase compositional analysis, SOA precursors ~~formation from from~~ GDI vehicles exhaust are ~~appeared likely~~ dominated by a few aromatic hydrocarbons ~~ArHC~~ and was not affected by GPF-retrofitting. While a large significant fraction ( $\approx 0.5$ ) of the SOA ~~formed can could~~ be attributed to the identified aromatic precursors (especially in the SC experiments), ~~divergences in the effective SOA yields determined for GDI vehicle exhaust appear relatively higher than the sum of~~ remained up to a factor of 2 in the OFR when comparing to the yields of the major aromatic specific precursors identified (toluene, o-xylene, 1,2,4-TMB) under comparable OA loadings. This may have diverse reasons including the presence of other aromatic isomers, unaccounted for precursors (which cannot be detected by PTR-ToF-MS measurements), ~~and the influence of the complex exhaust gas matrix matrix effects (NO<sub>x</sub>, secondary NH<sub>4</sub>, NO<sub>2</sub>, eBC<sub>2</sub>, other constituents)~~ compared to single precursor testing, or experimental uncertainties which deserve further attention in follow up studies.

Formatted: Not Highlight

## Supporting Information

Provided as noted in the main text.

## Acknowledgements

This work was funded by the CCEM project GASasOMeEP (<http://www.ccem.ch/gasomep>). Many thanks to our collaborators within the GasOMeP project for their input during scientific meetings. SMP acknowledges support from the We also acknowledge support by the Swiss National Science Foundation (SNF Project 140590). JGS acknowledges support from the ~~and~~ SNF starting grant BSSG10\_155846). We would like to thank René Richter for his invaluable technical support as well as the staff of the Laboratories for IC-Engines and Exhaust Emission Control of the Berne University of Applied Sciences in Biel, who conducted the vehicle testing.

Field Code Changed

## References

- Ahlberg, E., Falk, J., Eriksson, A., Holst, T., Brune, W. H., Kristensson, A., Roldin, P., and Svenningsson, B.: Secondary organic aerosol from VOC mixtures in an oxidation flow reactor, *Atmos. Environ.*, 161, 210-220, 10.1016/j.atmosenv.2017.05.005, 2017.
- Aiken, A. C., DeCarlo, P. F., and Jimenez, J. L.: Elemental analysis of organic species with electron ionization high-resolution mass spectrometry, *Anal. Chem.*, 79, 8350-8358, 10.1021/ac071150w, 2007.
- Aiken, A. C., Decarlo, P. F., Kroll, J. H., Worsnop, D. R., Huffman, J. A., Docherty, K. S., Ulbrich, I. M., Mohr, C., Kimmel, J. R., Sueper, D., Sun, Y., Zhang, Q., Trimborn, A., Northway, M., Ziemann, P. J., Canagaratna, M. R., Onasch, T. B., Alfarra, M. R., Prevot, A. S. H., Dommen, J., Duplissy, J., Metzger, A., Baltensperger, U., and Jimenez, J. L.: O/C and OM/OC ratios of primary, secondary, and ambient organic aerosols with high-resolution time-of-flight aerosol mass spectrometry, *Environ. Sci. Technol.*, 42, 4478-4485, 10.1021/es703009q, 2008.
- Amador Muñoz, O., Miszta, P. K., Weber, R., Worton, D. R., Zhang, H., Drozd, G., and Goldstein, A. H.: Sensitive detection of n-alkanes using a mixed ionization mode Proton-Transfer-Reaction-Mass Spectrometer, *Atmospheric Measurement Techniques Discussions*, 1-21, 10.5194/amt-2016-64, 2016.
- Atkinson, R., and Arey, J.: Atmospheric degradation of volatile organic compounds, *Chem Rev*, 103, 4605-4638, 10.1021/cr0206420, 2003.
- Bahreini, R., Middlebrook, A. M., de Gouw, J. A., Warneke, C., Trainer, M., Brock, C. A., Stark, H., Brown, S. S., Dube, W. P., Gilman, J. B., Hall, K., Holloway, J. S., Kuster, W. C., Perring, A. E., Prevot, A. S. H., Schwarz, J. P., Spackman, J. R., Szidat, S., Wagner, N. L., Weber, R. J., Zotter, P., and Parrish, D. D.: Gasoline emissions dominate over diesel in formation of secondary organic aerosol mass, *Geophys. Res. Lett.*, 39, n/a-n/a, 10.1029/2011gl050718, 2012.
- Barnet, P., Dommen, J., DeCarlo, P. F., Tritscher, T., Praplan, A. P., Platt, S. M., Prévôt, A. S. H., Donahue, N. M., and Baltensperger, U.: OH clock determination by proton transfer reaction mass spectrometry at an environmental chamber, *Atmos. Meas. Tech.*, 5, 647-656, 10.5194/amt-5-647-2012, 2012.
- Barrett, S. R. H., Speth, R. L., Eastham, S. D., Dedoussi, I. C., Ashok, A., Malina, R., and Keith, D. W.: Impact of the Volkswagen emissions control defeat device on US public health, *Environmental Research Letters*, 10, 114005, 10.1088/1748-9326/10/11/114005, 2015.
- Bond, T. C., Streets, D. G., Yarber, K. F., Nelson, S. M., Woo, J. H., and Klimont, Z.: A technology-based global inventory of black and organic carbon emissions from combustion, *Journal of Geophysical Research*, 109, D14203, 2004.
- Borbon, A., Gilman, J. B., Kuster, W. C., Grand, N., Chevaillier, S., Colomb, A., Dolgorouky, C., Gros, V., Lopez, M., Sarda-Esteve, R., Holloway, J., Stutz, J., Petetin, H., McKeen, S., Beekmann, M., Warneke, C., Parrish, D. D., and de Gouw, J. A.: Emission ratios of anthropogenic volatile organic compounds in northern mid-latitude megacities: Observations versus emission inventories in Los Angeles and Paris, *J. Geophys. Res. D Atmos.*, 118, 2041-2057, 10.1002/jgrd.50059, 2013.
- Bruns, E. A., El Haddad, I., Keller, A., Klein, F., Kumar, N. K., Pieber, S. M., Corbin, J. C., Slowik, J. G., Brune, W. H., Baltensperger, U., and Prévôt, A. S. H.: Inter-comparison of laboratory smog chamber and flow reactor systems on organic aerosol yield and composition, *Atmos. Meas. Tech.*, 8, 2315-2332, 10.5194/amt-8-2315-2015, 2015.
- Bruns, E. A., El Haddad, I., Slowik, J. G., Kilic, D., Klein, F., Baltensperger, U., and Prévôt, A. S. H.: Identification of significant precursor gases of secondary organic aerosols from residential wood combustion, *Sci Rep*, 6, 27881, 10.1038/srep27881, 2016.
- Buhr, K., van Ruth, S., and Delahunty, C.: Analysis of volatile flavour compounds by Proton Transfer Reaction-Mass Spectrometry: fragmentation patterns and discrimination between isobaric and isomeric compounds, *Int. J. Mass Spectrom.*, 221, 1-7, Doi 10.1016/S1387-3806(02)00896-5, 2002.
- Calderon-Garciduenas, L., and Villarreal-Rios, R.: Living close to heavy traffic roads, air pollution, and dementia, *Lancet*, 389, 675-677, 10.1016/S0140-6736(16)32596-X, 2017.
- Canagaratna, M. R., Jayne, J. T., Jimenez, J. L., Allan, J. D., Alfarra, M. R., Zhang, Q., Onasch, T. B., Drewnick, F., Coe, H., and Middlebrook, A.: Chemical and microphysical characterization of ambient aerosols with the Aerodyne aerosol mass spectrometer, *Mass Spectrom Rev*, 26, 185-222, 2007.
- Cappellin, L., Probst, M., Limtrakul, J., Biasioli, F., Schuhfried, E., Soukoulis, C., Märk, T. D., and Gasperi, F.: Proton transfer reaction rate coefficients between H<sub>3</sub>O<sup>+</sup> and some sulphur compounds, *Int. J. Mass Spectrom.*, 295, 43-48, 10.1016/j.ijms.2010.06.023, 2010.
- Cappellin, L., Karl, T., Probst, M., Ismailova, O., Winkler, P. M., Soukoulis, C., Aprea, E., Märk, T. D., Gasperi, F., and Biasioli, F.: On quantitative determination of volatile organic compound concentrations using proton transfer reaction time-of-flight mass spectrometry, *Environ. Sci. Technol.*, 46, 2283-2290, 10.1021/es203985t, 2012.
- Chan, T. W., Meloche, E., Kubsh, J., and Brezny, R.: Black carbon emissions in gasoline exhaust and a reduction alternative with a gasoline particulate filter, *Environ Sci Technol*, 48, 6027-6034, 10.1021/es501791b, 2014.
- Czerwinski, J., Comte, P., Heeb, N., Mayer, A., and Hensel, V.: Nanoparticle Emissions of DI Gasoline Cars with/without GPF, SAE Technical Paper 2017-01-1004, 10.1021/acs.est.7b05045, 2017.

Formatted: Font: 9 pt

- De Gouw, J., and Warneke, C.: Measurements of volatile organic compounds in the earth's atmosphere using proton-transfer-reaction mass spectrometry, *Mass Spectrom Rev*, 26, 223-257, 10.1002/mas.20119, 2007.
- 5 de Gouw, J. A., Goldan, P. D., Warneke, C., Kuster, W. C., Roberts, J. M., Marchewka, M., Bertman, S. B., Pszenny, A. A. P., and Keene, W. C.: Validation of proton transfer reaction-mass spectrometry (PTR-MS) measurements of gas-phase organic compounds in the atmosphere during the New England Air Quality Study (NEAQS) in 2002, *J. Geophys. Res. D Atmos.*, 108, 10.1029/2003jd003863, 2003.
- DeCarlo, P. F., Kimmel, J. R., Trimborn, A., Northway, M. J., Jayne, J. T., Aiken, A. C., Gonin, M., Fuhrer, K., Horvath, T., Docherty, K. S., Worsnop, D. R., and Jimenez, J. L.: Field-deployable, high-resolution, time-of-flight aerosol mass spectrometer, *Anal. Chem.*, 78, 8281-8289, 10.1021/ac061249n, 2006.
- 10 Demuyck, J. F., C.; Bosteels, D.; Hamje, H.; Anderson, J. : Real-World Emissions Measurements of a Gasoline Direct Injection Vehicle without and with a Gasoline Particulate Filter, SAE Technical Paper 2017-01-0985, doi:10.4271/2017-01-0985., 2017.
- di Rattalma, M. F., and Perotti, G.: *The Dieselgate: A Legal Perspective.*, Springer International Publishing AG, 179-218 pp., 2017.
- Donahue, N. M., Robinson, A. L., Stanier, C. O., and Pandis, S. N.: Coupled partitioning, dilution, and chemical aging of semivolatile organics, *Environ Sci Technol*, 40, 2635-2643, 2006.
- 15 Drinovec, L., Močnik, G., Zotter, P., Prévôt, A. S. H., Ruckstuhl, C., Coz, E., Rupakheti, M., Sciare, J., Müller, T., Wiedensohler, A., and Hansen, A. D. A.: The "dual-spot" Aethalometer: an improved measurement of aerosol black carbon with real-time loading compensation, *Atmos. Meas. Tech.*, 8, 1965-1979, 10.5194/amt-8-1965-2015, 2015.
- Erickson, M. H., Gueneron, M., and Jobson, B. T.: Measuring long chain alkanes in diesel engine exhaust by thermal desorption PTR-MS, *Atmos. Meas. Tech.*, 7, 225-239, 10.5194/amt-7-225-2014, 2014.
- 20 Finlayson-Pitts, B. J., and Pitts, J. N.: *Chemistry of the Upper and Lower Atmosphere. Theory, Experiments, and Applications.*, Academic Press, 969 pp., 2000.
- Gentner, D. R., Jathar, S. H., Gordon, T. D., Bahreini, R., Day, D. A., El Haddad, I., Hayes, P. L., Pieber, S. M., Platt, S. M., de Gouw, J., Goldstein, A. H., Harley, R. A., Jimenez, J. L., Prevot, A. S., and Robinson, A. L.: Review of Urban Secondary Organic Aerosol Formation from Gasoline and Diesel Motor Vehicle Emissions, *Environ Sci Technol*, 10.1021/acs.est.6b04509, 2017.
- 25 Gordon, T. D., Presto, A. A., Nguyen, N. T., Robertson, W. H., Na, K., Sahay, K. N., Zhang, M., Maddox, C., Rieger, P., Chattopadhyay, S., Maldonado, H., M. Maricq, M. M., and Robinson, A. L.: Secondary organic aerosol production from diesel vehicle exhaust: impact of aftertreatment, fuel chemistry and driving cycle, *Atmospheric Chemistry and Physics Discussions*, 13, 24223-24262, 2013a.
- Gordon, T. D., Tkacik, D. S., Presto, A. A., Zhang, M., Jathar, S., Nguyen, N., Massetti, J., Truong, T., Cicero-Fernandez, P., Maddox, C., Rieger, P., Chattopadhyay, S., Maldonado, H., M. M., M., and Robinson, A. L.: Primary gas-and particle-phase emissions and secondary organic aerosol production from gasoline and diesel off-road engines, *Environ. Sci. Technol.*, 47(24), 1413-14146, 2013b.
- Gordon, T. D., Presto, A. A., May, A. A., Nguyen, N. T., Lipsky, E. M., Donahue, N. M., Gutierrez, A., Zhang, M., Maddox, C., Rieger, P., Chattopadhyay, S., Maldonado, H., Maricq, M. M., and Robinson, A. L.: Secondary organic aerosol formation exceeds primary particulate matter emissions for light-duty gasoline vehicles, *Atmos. Chem. Phys.*, 14, 4661-4678, 10.5194/acp-14-4661-2014, 2014.
- 35 Graus, M., Muller, M., and Hansel, A.: High resolution PTR-TOF: Quantification and formula confirmation of VOC in real time, *Journal of the American Society for Mass Spectrometry*, 21, 1037--1044, 2010.
- Gueneron, M., Erickson, M. H., Vanderschelden, G. S., and Jobson, B. T.: PTR-MS fragmentation patterns of gasoline hydrocarbons, *Int. J. Mass Spectrom.*, 379, 97-109, 10.1016/j.ijms.2015.01.001, 2015.
- 40 Hallquist, M., Wenger, J. C., Baltensperger, U., Rudich, Y., Simpson, D., Claeys, M., Dommen, J., Donahue, N. M., George, C., Goldstein, A. H., Hamilton, J. F., Herrmann, H., Hoffmann, T., Iinuma, Y., Jang, M., Jenkin, M. E., Jimenez, J. L., Kiendler-Scharr, A., Maenhaut, W., McFiggans, G., Mentel, T. F., Monod, A., Prévôt, A. S. H., Seinfeld, J. H., Surratt, J. D., Szmigielski, R., and Wildt, J.: The formation, properties and impact of secondary organic aerosol: current and emerging issues, *Atmos. Chem. Phys.*, 9, 5155-5236, 10.5194/acp-9-5155-2009, 2009.
- 45 Heeb, N. V., Forss, A. M., Brühlmann, S., Lüscher, R., Saxer, C. J., and Hug, P.: Three-way catalyst-induced formation of ammonia-velocity- and acceleration-dependent emission factors, *Atmos. Environ.*, 40, 5986-5997, 10.1016/j.atmosenv.2005.12.035, 2006.
- Hildebrandt, L., Donahue, N. M., and Pandis, S. N.: High formation of secondary organic aerosol from the photo-oxidation of toluene, *Atmos. Chem. Phys.*, 9, 2973-2986, 10.5194/acp-9-2973-2009, 2009.
- 50 Jathar, S. H., Gordona, T. D., Hennigan, C. J., Pye, H. O. T., Pouliot, G., Adams, P. J., Donahue, N. M., and Robinson, A. L.: Unspeciated organic emissions from combustion sources and their influence on the secondary organic aerosol budget in the United States, *Proc. Natl. Acad. Sci. U. S. A.*, 111, 10473-10478, 10.1073/pnas.1323740111, 2014.
- Jordan, A., Haidacher, S., Hanel, G., Hartungen, E., Märk, L., Seehauser, H., Schottkowsky, R., Sulzer, P., and Märk, T. D.: A high resolution and high sensitivity proton-transfer-reaction time-of-flight mass spectrometer (PTR-TOF-MS), *Int. J. Mass Spectrom.*, 286, 122-128, <http://dx.doi.org/10.1016/j.ijms.2009.07.005>, 2009.
- 55

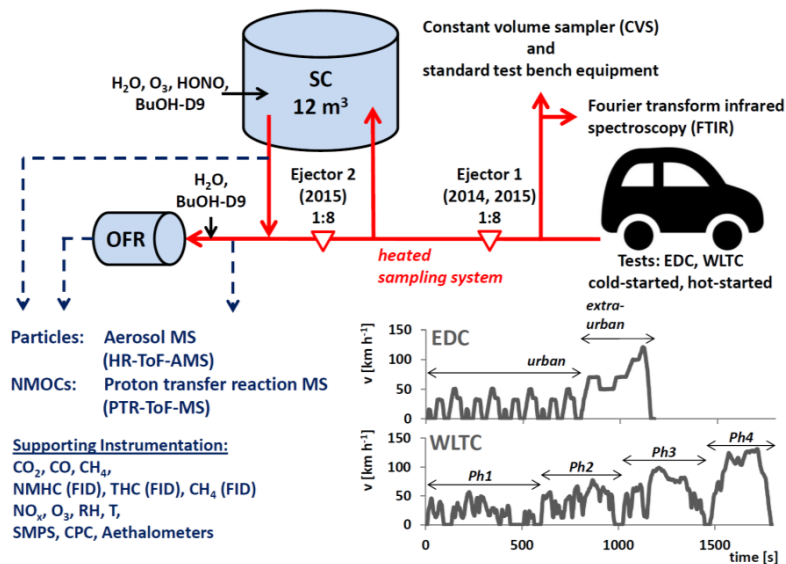
- Jordan, A., Jaksch, S., Jürschik, S., Edtbauer, A., Agarwal, B., Hanel, G., Hartungen, E., Seehauser, H., Märk, L., Sulzer, P., and Märk, T. D.:  $\text{H}_3\text{O}^+$ ,  $\text{NO}^+$  and  $\text{O}_2^+$  as precursor ions in PTR-MS: isomeric VOC compounds and reactions with different chemical groups, 5th International Conference on Proton Transfer Reaction Mass Spectrometry and its Applications, 2011.
- Jordan, C. E., Ziemann, P. J., Griffin, R. J., Lim, Y. B., Atkinson, R., and Arey, J.: Modeling SOA formation from OH reactions with C8–C17 n-alkanes, *Atmos. Environ.*, 42, 8015–8026, 10.1016/j.atmosenv.2008.06.017, 2008.
- Kang, E., Root, M. J., Toohey, D. W., and Brune, W. H.: Introducing the concept of Potential Aerosol Mass (PAM), *Atmos. Chem. Phys.*, 7, 5727–5744, 10.5194/acp-7-5727-2007, 2007.
- Karjalainen, P., Pirjola, L., Heikkilä, J., Lähde, T., Tzankiozis, T., Ntziachristos, L., Keskinen, J., and Rönkkö, T.: Exhaust particles of modern gasoline vehicles: A laboratory and an on-road study, *Atmos. Environ.*, 97, 262–270, 10.1016/j.atmosenv.2014.08.025, 2014.
- Karjalainen, P., Timonen, H., Saukko, E., Kuuluvainen, H., Saarikoski, S., Aakko-Saksa, P., Murtonen, T., Dal Maso, M., Ahlberg, E., Svenningsson, B., Brune, W. H., Hillamo, R., Keskinen, J., and Rönkkö, T.: Time-resolved characterization of primary and secondary particle emissions of a modern gasoline passenger car, *Atmos. Chem. Phys. Discuss.*, 2015, 33253–33282, 10.5194/acpd-15-33253-2015, 2015.
- Knighton, W. B., Fortner, E. C., Midey, A. J., Viggiano, A. A., Herndon, S. C., Wood, E. C., and Kolb, C. E.: HCN detection with a proton transfer reaction mass spectrometer, *Int. J. Mass Spectrom.*, 283, 112–121, 10.1016/j.ijms.2009.02.013, 2009.
- Krechmer, J. E., Day, D. A., Ziemann, P. J., and Jimenez, J. L.: Direct Measurements of Gas/Particle Partitioning and Mass Accommodation Coefficients in Environmental Chambers, *Environ Sci Technol*, 10.1021/acs.est.7b02144, 2017.
- Kunzi, L., Krapf, M., Daher, N., Dommen, J., Jeannot, N., Schneider, S., Platt, S., Slowik, J. G., Baumlin, N., Salathe, M., Prévôt, A. S. H., Kalberer, M., Strahl, C., Dumbgen, L., Sioutas, C., Baltensperger, U., and Geiser, M.: Toxicity of aged gasoline exhaust particles to normal and diseased airway epithelia, *Sci Rep*, 5, 11801, 10.1038/srep11801, 2015.
- La, Y. S., Camredon, M., Ziemann, P. J., Valorso, R., Matsunaga, A., Lannuque, V., Lee-Taylor, J., Hodzic, A., Madronich, S., and Aumont, B.: Impact of chamber wall loss of gaseous organic compounds on secondary organic aerosol formation: explicit modeling of SOA formation from alkane and alkene oxidation, *Atmos. Chem. Phys.*, 16, 1417–1431, 10.5194/acp-16-1417-2016, 2016.
- Lambe, A., Massoli, P., Zhang, X., Canagaratna, M., Nowak, J., Daube, C., Yan, C., Nie, W., Onasch, T., Jayne, J., Kolb, C., Davidovits, P., Worsnop, D., and Brune, W.: Controlled nitric oxide production via  $\text{O}(^1\text{D})+\text{N}_2\text{O}$  reactions for use in oxidation flow reactor studies, *Atmos. Meas. Tech.*, 10, 2283–2298, 10.5194/amt-10-2283-2017, 2017.
- Lambe, A. T., Ahern, A. T., Williams, L. R., Slowik, J. G., Wong, J. P. S., Abbatt, J. P. D., Brune, W. H., Ng, N. L., Wright, J. P., Croasdale, D. R., Worsnop, D. R., Davidovits, P., and Onasch, T. B.: Characterization of aerosol photooxidation flow reactors: heterogeneous oxidation, secondary organic aerosol formation and cloud condensation nuclei activity measurements, *Atmos. Meas. Tech.*, 4, 445–461, 10.5194/amt-4-445-2011, 2011.
- Lambe, A. T., Chhabra, P. S., Onasch, T. B., Brune, W. H., Hunter, J. F., Kroll, J. H., Cummings, M. J., Brogan, J. F., Parmar, Y., Worsnop, D. R., Kolb, C. E., and Davidovits, P.: Effect of oxidant concentration, exposure time, and seed particles on secondary organic aerosol chemical composition and yield, *Atmos. Chem. Phys.*, 15, 3063–3075, 10.5194/acp-15-3063-2015, 2015.
- Li, L., Tang, P., Nakao, S., Chen, C. L., and Cocker Iii, D. R.: Role of methyl group number on SOA formation from monocyclic aromatic hydrocarbons photooxidation under low- $\text{NO}_x$  conditions, *Atmos. Chem. Phys.*, 16, 2255–2272, 10.5194/acp-16-2255-2016, 2016a.
- Li, L., Tang, P., Nakao, S., and Cocker Iii, D. R.: Impact of molecular structure on secondary organic aerosol formation from aromatic hydrocarbon photooxidation under low- $\text{NO}_x$  conditions, *Atmos. Chem. Phys.*, 16, 10793–10808, 10.5194/acp-16-10793-2016, 2016b.
- Li, L., Qi, L., and Cocker, D. R.: Contribution of methyl group to secondary organic aerosol formation from aromatic hydrocarbon photooxidation, *Atmos. Environ.*, 151, 133–139, 10.1016/j.atmosenv.2016.11.064, 2017.
- Li, R., Palm, B. B., Ortega, A. M., Hlywiak, J., Hu, W., Peng, Z., Day, D. A., Knote, C., Brune, W. H., de Gouw, J. A., and Jimenez, J. L.: Modeling the radical chemistry in an oxidation flow reactor: radical formation and recycling, sensitivities, and the OH exposure estimation equation, *J Phys Chem A*, 119, 4418–4432, 10.1021/jp509534k, 2015.
- Lim, Y. B., and Ziemann, P. J.: Products and mechanism of secondary organic aerosol formation from reactions of n-alkanes with OH radicals in the presence of  $\text{NO}_x$ , *Environmental Science & Technology*, 39, 9229–9236, 10.1021/es051447g, 2005.
- Lindinger, W., and Jordan, A.: Proton-transfer-reaction mass spectrometry (PTR-MS): on-line monitoring of volatile organic compounds at pptv levels, *Chemical Society Reviews*, 27, 347–375, 10.1039/A827347Z, 1998.
- Loza, C. L., Chhabra, P. S., Yee, L. D., Craven, J. S., Flagan, R. C., and Seinfeld, J. H.: Chemical aging of m-xylene secondary organic aerosol: laboratory chamber study, *Atmos. Chem. Phys.*, 12, 151–167, 10.5194/acp-12-151-2012, 2012.
- Loza, C. L., Craven, J. S., Yee, L. D., Coggon, M. M., Schwantes, R. H., Shiraiwa, M., Zhang, X., Schilling, K. A., Ng, N. L., Canagaratna, M. R., Ziemann, P. J., Flagan, R. C., and Seinfeld, J. H.: Secondary organic aerosol yields of 12-carbon alkanes, *Atmos. Chem. Phys.*, 14, 1423–1439, 10.5194/acp-14-1423-2014, 2014.
- May, A. A., Nguyen, N. T., Presto, A. A., Gordon, T. D., Lipsky, E. M., Karve, M., Gutierrez, A., Robertson, W. H., Zhang, M., Brandow, C., Chang, O., Chen, S., Cicero-Fernandez, P., Dinkins, L., Fuentes, M., Huang, S. M., Ling, R., Long, J., Maddox, C., Massetti,

- J., McCauley, E., Miguel, A., Na, K., Ong, R., Pang, Y., Rieger, P., Sax, T., Truong, T., Vo, T., Chattopadhyay, S., Maldonado, H., Maricq, M. M., and Robinson, A. L.: Gas- and particle-phase primary emissions from in-use, on-road gasoline and diesel vehicles, *Atmos. Environ.*, 88, 247-260, 10.1016/j.atmosenv.2014.01.046, 2014.
- 5 McMurry, P. H., and Grosjean, D.: Gas and aerosol wall losses in Teflon film smog chambers, *Environ Sci Technol*, 19, 1176-1182, 10.1021/es00142a006, 1985.
- Molteni, U., Bianchi, F., Klein, F., El Haddad, I., Frege, C., Rossi, M. J., Dommen, J., and Baltensperger, U.: Formation of highly oxygenated organic molecules from aromatic compounds, *Atmos. Chem. Phys.*, 18, 1909-1921, 10.5194/acp-18-1909-2018, 2018. [Atmospheric Chemistry and Physics Discussions](#), 1-39, 10.5194/acp-2016-1126, 2016.
- 10 Müller, M., Mikoviny, T., and Wisthaler, A.: Detector aging induced mass discrimination and non-linearity effects in PTR-ToF-MS, *Int. J. Mass Spectrom.*, 365-366, 93-97, 10.1016/j.ijms.2013.12.008, 2014.
- Muñoz, M., Haag, R., Honegger, P., Zeyer, K., Mohn, J., Comte, P., Czerwinski, J., and Heeb, N. V.: Co-formation and co-release of genotoxic PAHs, alkyl-PAHs and soot nanoparticles from gasoline direct injection vehicles, *Atmos. Environ.*, 178, 242-254, 10.1016/j.atmosenv.2018.01.050, 2018.
- 15 Ng, N. L., Chhabra, P. S., Chan, A. W. H., Surratt, J. D., Kroll, J. H., Kwan, A. J., McCabe, D. C., Wennberg, P. O., Sorooshian, A., Murphy, S. M., Dalleska, N. F., Flagan, R. C., and Seinfeld, J. H.: Effect of NO<sub>x</sub> level on secondary organic aerosol (SOA) formation from the photooxidation of terpenes, *Atmos. Chem. Phys.*, 7, 5159-5174, 10.5194/acp-7-5159-2007, 2007a.
- Ng, N. L., Kroll, J. H., Chan, A. W. H., Chhabra, P. S., Flagan, R. C., and Seinfeld, J. H.: Secondary organic aerosol formation from *m*-xylene, toluene, and benzene, *Atmos. Chem. Phys.*, 7, 3909-3922, 2007b.
- 20 Ng, N. L., Canagaratna, M. R., Jimenez, J. L., Chhabra, P. S., Seinfeld, J. H., and Worsnop, D. R.: Changes in organic aerosol composition with aging inferred from aerosol mass spectra, *Atmos. Chem. Phys.*, 11, 6465-6474, 10.5194/acp-11-6465-2011, 2011.
- Nordin, E. Z., Eriksson, A. C., Roldin, P., Nilsson, P. T., Carlsson, J. E., Kajos, M. K., Hellén, H., Wittbom, C., Rissler, J., Löndahl, J., Swietlicki, E., Svenningsson, B., Bohgard, M., Kulmala, M., Hallquist, M., and Pagels, J. H.: Secondary organic aerosol formation from idling gasoline passenger vehicle emissions investigated in a smog chamber, *Atmos. Chem. Phys.*, 13, 6101-6116, 10.5194/acp-13-6101-2013, 2013.
- 25 Odum, J. R., Jungkamp, T. P. W., Griffin, R. J., Forstner, H. J. L., Flagan, R. C., and Seinfeld, J. H.: Aromatics, reformulated gasoline, and atmospheric organic aerosol formation, *Environ. Sci. Technol.*, 31, 1890-1897, 1997.
- Ortega, A. M., Day, D. A., Cubison, M. J., Brune, W. H., Bon, D., de Gouw, J. A., and Jimenez, J. L.: Secondary organic aerosol formation and primary organic aerosol oxidation from biomass-burning smoke in a flow reactor during FLAME-3, *Atmos. Chem. Phys.*, 13, 11551-11571, 10.5194/acp-13-11551-2013, 2013.
- 30 Pagonis, D., Krechmer, J. E., de Gouw, J., Jimenez, J. L., and Ziemann, P. J.: Effects of Gas-Wall Partitioning in Teflon Tubing and Instrumentation on Time-Resolved Measurements of Gas-Phase Organic Compounds, *Atmospheric Measurement Techniques Discussions*, 1-19, 10.5194/amt-2017-279, 2017.
- Palm, B. B., Campuzano-Jost, P., Ortega, A. M., Day, D. A., Kaser, L., Jud, W., Karl, T., Hansel, A., Hunter, J. F., Cross, E. S., Kroll, J. H., Peng, Z., Brune, W. H., and Jimenez, J. L.: In situ secondary organic aerosol formation from ambient pine forest air using an oxidation flow reactor, *Atmos. Chem. Phys.*, 16, 2943-2970, 10.5194/acp-16-2943-2016, 2016.
- 35 Pandis, S. N., Donahue, N. M., Murphy, B. N., Riipinen, I., Fountoukis, C., Karnezis, E., Patoulias, D., and Skyllakou, K.: Introductory lecture: atmospheric organic aerosols: insights from the combination of measurements and chemical transport models, *Faraday Discuss*, 165, 9-24, 10.1039/C3FD00108C, 2013.
- Pankow, J. F.: An Absorption-Model of Gas-Particle Partitioning of Organic-Compounds in the Atmosphere, *Atmos. Environ.*, 28, 185-188, Doi 10.1016/1352-2310(94)90093-0, 1994.
- 40 Peng, Z., Day, D. A., Stark, H., Li, R., Lee-Taylor, J., Palm, B. B., Brune, W. H., and Jimenez, J. L.: HO<sub>x</sub> radical chemistry in oxidation flow reactors with low-pressure mercury lamps systematically examined by modeling, *Atmos. Meas. Tech.*, 8, 4863-4890, 10.5194/amt-8-4863-2015, 2015.
- Peng, Z., Day, D. A., Ortega, A. M., Palm, B. B., Hu, W., Stark, H., Li, R., Tsigaridis, K., Brune, W. H., and Jimenez, J. L.: Non-OH chemistry in oxidation flow reactors for the study of atmospheric chemistry systematically examined by modeling, *Atmos. Chem. Phys.*, 16, 4283-4305, 10.5194/acp-16-4283-2016, 2016.
- 45 Peng, Z., and Jimenez, J. L.: Modeling of the chemistry in oxidation flow reactors with high initial NO, *Atmospheric Chemistry and Physics Discussions*, 1-37, 10.5194/acp-2017-266, 2017.
- Pieber, S. M., El Haddad, I., Slowik, J. G., Canagaratna, M. R., Jayne, J. T., Platt, S. M., Bozzetti, C., Daellenbach, K. R., Frohlich, R., Vlachou, A., Klein, F., Dommen, J., Miljevic, B., Jimenez, J. L., Worsnop, D. R., Baltensperger, U., and Prévôt, A. S. H.: Inorganic Salt Interference on CO<sub>2</sub><sup>+</sup> in Aerodyne AMS and ACSM Organic Aerosol Composition Studies, *Environ Sci Technol*, 50, 10494-10503, 10.1021/acs.est.6b01035, 2016.
- 50 Platt, S. M., El Haddad, I., Zardini, A. A., Clairotte, M., Astorga, C., Wolf, R., Slowik, J. G., Temime-Roussel, B., Marchand, N., Ježek, I., Drinovec, L., Močnik, G., Möhler, O., Richter, R., Barmet, P., Bianchi, F., Baltensperger, U., and Prévôt, A. S. H.: Secondary organic aerosol formation from gasoline vehicle emissions in a new mobile environmental reaction chamber, *Atmos. Chem. Phys.*, 13, 9141-9158, 10.5194/acp-13-9141-2013, 2013.
- 55

- Platt, S. M., El Haddad, I., Pieber, S. M., Huang, R. J., Zardini, A. A., Clairotte, M., Suarez-Bertoa, R., Barmet, P., Pfaffenberger, L., Wolf, R., Slowik, J. G., Fuller, S. J., Kalberer, M., Chirico, R., Dommen, J., Astorga, C., Zimmermann, R., Marchand, N., Hellebust, S., Temime-Roussel, B., Baltensperger, U., and Prevot, A. S.: Two-stroke scooters are a dominant source of air pollution in many cities, *Nat Commun*, 5, 3749, 10.1038/ncomms4749, 2014.
- 5 Platt, S. M., El Haddad, I., Pieber, S. M., Zardini, A. A., Suarez-Bertoa, R., Clairotte, M., Daellenbach, K. R., Huang, R. J., Slowik, J. G., Hellebust, S., Temime-Roussel, B., Marchand, N., de Gouw, J., Jimenez, J. L., Hayes, P. L., Robinson, A. L., Baltensperger, U., Astorga, C., and Prévôt, A. S. H.: Gasoline cars produce more carbonaceous particulate matter than modern filter-equipped diesel cars, *Sci Rep*, 7, 4926, 10.1038/s41598-017-03714-9, 2017.
- 10 Saliba, G., Saleh, R., Zhao, Y., Presto, A. A., Lambe, A. T., Frodin, B., Sardar, S., Maldonado, H., Maddox, C., May, A. A., Drozd, G. T., Goldstein, A. H., Russell, L. M., Hagen, F. P., and Robinson, A. L.: A comparison of gasoline direct injection (GDI) and port fuel injection (PFI) vehicle emissions: emission certification standards, cold start, secondary organic aerosol formation potential, and potential climate impacts, *Environ Sci Technol*, 10.1021/acs.est.6b06509, 2017.
- Schauer, J. J., Kleeman, M. J., Cass, G. R., and Simoneit, B. R. T.: Measurement of emissions from air pollution sources. 2. C1 through C30 organic compounds from medium duty diesel trucks, *Environ. Sci. Technol.*, 33, 1578-1587, 1999.
- 15 Schauer, J. J., Kleeman, M. J., Cass, G. R., and Simoneit, B. R. T.: Measurement of emissions from air pollution sources. 5. C1-C32 organic compounds from gasoline-powered motor vehicles, *Environ. Sci. Technol.*, 36, 1169-1180, 2002.
- Schwantes, R. H., Schilling, K. A., McVay, R. C., Lignell, H., Coggon, M. M., Zhang, X., Wennberg, P. O., and Seinfeld, J. H.: Formation of highly oxygenated low-volatility products from cresol oxidation, *Atmos. Chem. Phys.*, 17, 3453-3474, 10.5194/acp-17-3453-2017, 2017.
- 20 Stirmweis, L., Marcolli, C., Dommen, J., Barmet, P., Frege, C., Platt, S. M., Bruns, E. A., Krapf, M., Slowik, J. G., Wolf, R., Prévôt, A. S. H., Baltensperger, U., and El-Haddad, I.: Assessing the influence of NO<sub>x</sub> concentrations and relative humidity on secondary organic aerosol yields from  $\alpha$ -pinene photo-oxidation through smog chamber experiments and modelling calculations, *Atmos. Chem. Phys.*, 17, 5035-5061, 10.5194/acp-17-5035-2017, 2017.
- 25 Suarez-Bertoa, R., Zardini, A. A., and Astorga, C.: Ammonia exhaust emissions from spark ignition vehicles over the New European Driving Cycle, *Atmos. Environ.*, 97, 43-53, 10.1016/j.atmosenv.2014.07.050, 2014.
- Taira, M., and Kanda, Y.: Continuous generation system for low-concentration gaseous nitrous acid, *Anal. Chem.*, 62, 630-633, 1990.
- Tkacik, D. S., Lambe, A. T., Jathar, S., Li, X., Presto, A. A., Zhao, Y., Blake, D., Meinardi, S., Jayne, J. T., Croteau, P. L., and Robinson, A. L.: Secondary organic aerosol formation from in-use motor vehicle emissions using a potential aerosol mass reactor, *Environ. Sci. Technol.*, 48, 11235-11242, 10.1021/es502239v, 2014.
- 30 Turpin, B. J., and Lim, H.-J.: Species Contributions to PM<sub>2.5</sub> Mass Concentrations: Revisiting Common Assumptions for Estimating Organic Mass, *Aerosol Sci. Technol.*, 35, 602-610, 10.1080/02786820119445, 2001.
- Wang, T., Jerrett, M., Sinsheimer, P., and Zhu, Y.: Estimating PM<sub>2.5</sub>-associated mortality increase in California due to the Volkswagen emission control defeat device, *Atmos. Environ.*, 144, 168-174, 10.1016/j.atmosenv.2016.08.074, 2016.
- 35 Weitkamp, E. A., Sage, A. M., Pierce, J. R., Donahue, N. M., and Robinson, A. L.: Organic aerosol formation from photochemical oxidation of diesel exhaust in a smog chamber, *Environ. Sci. Technol.*, 41, 6969-6975, 10.1021/es070193r, 2007.
- Worton, D. R., Isaacman, G., Gentner, D. R., Dallmann, T. R., Chan, A. W., Ruehl, C., Kirchstetter, T. W., Wilson, K. R., Harley, R. A., and Goldstein, A. H.: Lubricating oil dominates primary organic aerosol emissions from motor vehicles, *Environ Sci Technol*, 48, 3698-3706, 10.1021/es405375j, 2014.
- 40 Ye, P., Ding, X., Hakala, J., Hofbauer, V., Robinson, E. S., and Donahue, N. M.: Vapor wall loss of semi-volatile organic compounds in a Teflon chamber, *Aerosol Sci. Technol.*, 50, 822-834, 10.1080/02786826.2016.1195905, 2016.
- Zhang, X., Cappa, C. D., Jathar, S. H., McVay, R. C., Ensberg, J. J., Kleeman, M. J., and Seinfeld, J. H.: Influence of vapor wall loss in laboratory chambers on yields of secondary organic aerosol, *Proc Natl Acad Sci U S A*, 111, 5802-5807, 10.1073/pnas.1404727111, 2014.
- 45 Zhao, Y., Nguyen, N. T., Presto, A. A., Hennigan, C. J., May, A. A., and Robinson, A. L.: Intermediate Volatility Organic Compound Emissions from On-Road Gasoline Vehicles and Small Off-Road Gasoline Engines, *Environ Sci Technol*, 50, 4554-4563, 10.1021/acs.est.5b06247, 2016.
- Zhao, Y., Saleh, R., Saliba, G., Presto, A. A., Gordon, T. D., Drozd, G. T., Goldstein, A. H., Donahue, N. M., and Robinson, A. L.: Reducing secondary organic aerosol formation from gasoline vehicle exhaust, *Proc Natl Acad Sci U S A*, 114, 6984-6989, 10.1073/pnas.1620911114, 2017.
- 50 Zhao, Y., Lambe, A. T., Saleh, R., Saliba, G., and Robinson, A. L.: Secondary Organic Aerosol Production from Gasoline Vehicle Exhaust: Effects of Engine Technology, Cold Start, and Emission Certification Standard, *Environ Sci Technol*, 52, 1253-1261, 10.1021/acs.est.7b05045, 2018.
- 55 Zhu, R., Hu, J., Bao, X., He, L., Lai, Y., Zu, L., Li, Y., and Su, S.: Tailpipe emissions from gasoline direct injection (GDI) and port fuel injection (PFI) vehicles at both low and high ambient temperatures, *Environ Pollut*, 216, 223-234, 10.1016/j.envpol.2016.05.066, 2016.

5

- Zimmerman, N., Wang, J. M., Jeong, C. H., Ramos, M., Hilker, N., Healy, R. M., Sabaliauskas, K., Wallace, J. S., and Evans, G. J.: Field Measurements of Gasoline Direct Injection Emission Factors: Spatial and Seasonal Variability, *Environ Sci Technol*, 50, 2035-2043, 10.1021/acs.est.5b04444, 2016a.
- Zimmerman, N., Wang, J. M., Jeong, C. H., Wallace, J. S., and Evans, G. J.: Assessing the Climate Trade-Offs of Gasoline Direct Injection Engines, *Environ Sci Technol*, 50, 8385-8392, 10.1021/acs.est.6b01800, 2016b.
- Zotter, P., El Haddad, I., Zhang, Y., Hayes, P. L., Zhang, X., Lin, Y.-H., Wacker, L., Schnelle-Kreis, J., Abbaszade, G., Zimmermann, R., Surratt, J. D., Weber, R., Jimenez, J. L., Szidat, S., Baltensperger, U., and Prévôt, A. S. H.: Diurnal cycle of fossil and nonfossil carbon using radiocarbon analyses during CalNex, *J. Geophys. Res. D Atmos.*, 119, 6818-6835, 10.1002/2013jd021114, 2014.



Formatted: Indent: Left: 0 cm, Hanging: 1 cm, Page break before

**Figure 1. Schematic (not to scale) of the experimental set-up.** Vehicles were driven over regulatory driving cycles (EDC and WLTC, for which speed profiles are shown in the figure) on a chassis dynamometer test bench. Emissions were sampled through a heated dilution and sampling system using 1 or 2 ejector dilutors into the PSI mobile SC (Platt et al., 2013) and the potential aerosol mass (PAM) oxidation flow reactor (OFR) (Bruns et al., 2015). Instrumentation for characterization of fresh and photo-chemically aged emissions is listed. The raw exhaust was also sampled at the tailpipe using standard test bench equipment to monitor regulatory species (diluted in a constant volume sampler, CVS) and unregulated emissions (with Fourier-Transformed Infrared Spectroscopy, FTIR).

Field Code Changed

Field Code Changed

Field Code Changed

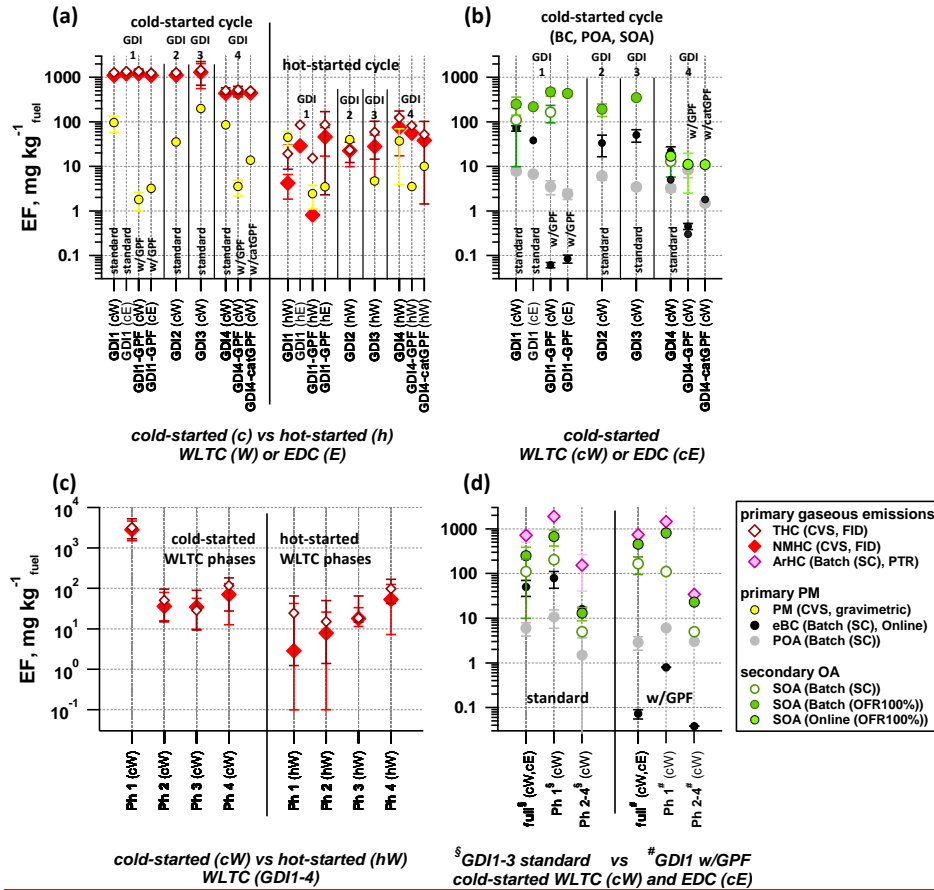


**Figure 2.** Emission factors (EF) of pollutants from cold-started (“c”) and hot-started (“h”) test cycles (WLTC (“W”) and EDC (“E”)). Individual cW and hW phases are indicated as “Ph” 1-4. (a) EFs of total and non-methane hydrocarbons (THC, NMHC) and primary gravimetric particulate matter (PM) from CVS measurements over entire test cycles for different vehicle configuration and test conditions (average±1SD). (b) EFs of primary PM (equivalent black carbon (eBC) and primary organic aerosol (POA)), and secondary organic aerosol (SOA) formed during photochemical aging in from SC, and OFR-from-SC experiments, and during from online operation of the OFR/OFR operation (OFR at 100% UV intensity) per vehicle configuration for cold-started test cycles (average±1SD). (note that POA EFs for GDI4-catGPF (cW) are not available). (c) EFs of the same THC and NMHC of cW and hW experiments presented in from (a) separated into individual cycle phases (median, and P25-P75 range are shown). (d) EFs of primary gravimetric PM, POA, eBC, and eBC, NMHC and aromatic hydrocarbons (ArHC) and SOA over the full cW and cE, compared to individual phases of cW from SC batch experiments and OFR-from-SC (average±1SD). Note that the EF for eBC for Ph 2-4 (cW) is 17 mg kg<sup>-1</sup> fuel and that the data point is hidden behind the SOA data points in the graphical presentation. (a-d) EF calculation is detailed provided in the SI Section S1. The time-resolved SOA profile from online OFR measurements conducted on GDI4 in 2015 (standard and catGPF) is available in the provided in Supporting Information Figure S14.

Field Code Changed



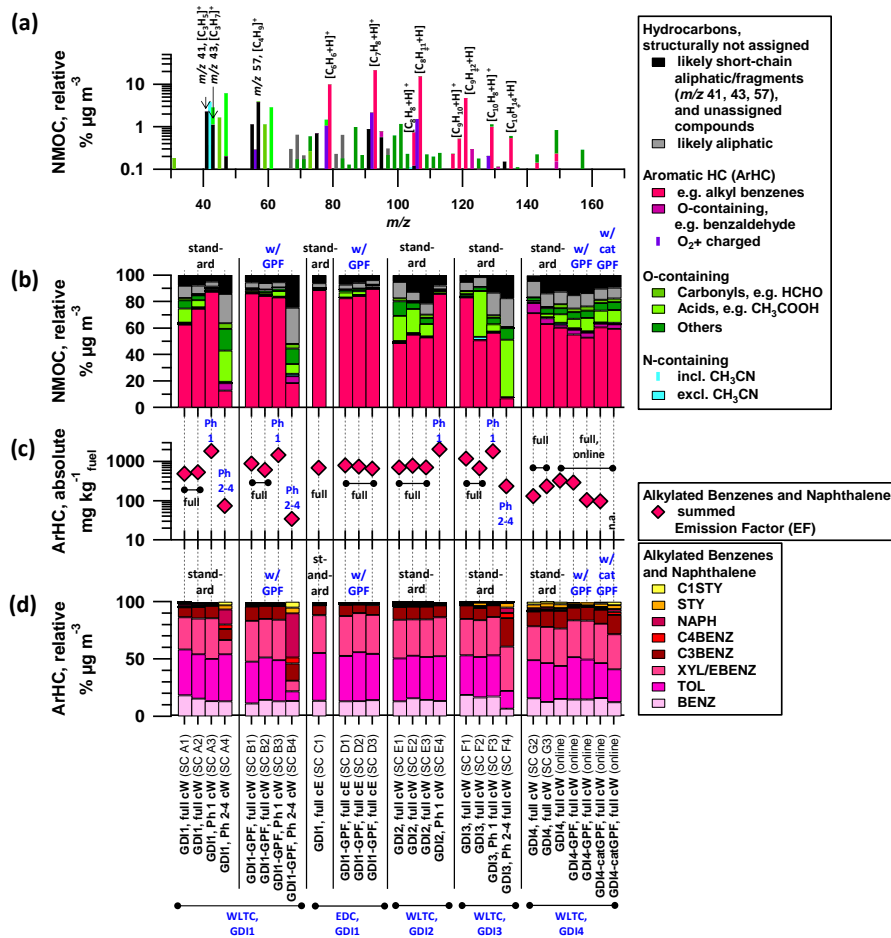


**Figure 4.** PTR-ToF-MS derived NMOC composition (cold-started cycles). Data are collected by batch sampling (“SC”) or during online measurements (“online”). (a) PTR-ToF-MS  $m/z$  mass spectrum of emissions from GDI1 emissions (in standard configuration) sampled into the SC during a cold-started WLTC (cW). (b) Relative composition of the PTR-ToF-MS derived NMOC fraction (which makes up  $65\% \pm 15$  of the FID-based NMHC signal on a carbon-basis for cW, cE, Ph 1(cW)), (c) total ArHC EFs (which make up  $49 \pm 8\%$  of the FID-based NMHC signal on a carbon-basis for cW, cE, Ph 1(cW)), and (d) relative contribution of the 8 dominant ArHC, which correspond to  $96.7 \pm 3.3\%$  of the total ArHC signal for cW, cE, Ph 1(cW)). (b-c) Data correspond to vehicle exhaust for GDI1 (expt. A-D), GDI2 (expt. E), GDI3 (expt. F) and GDI4 (expt. G) sampled into the SC during full cW and cE driving tests, or individual phases of cW, or measured “online”. The identifier in parenthesis specifies individual SC experiments (see described in also Supporting Information; Tables S4-S7, for SC experimental conditions). Note that the total NMOC levels for Ph 2-4 (cW) are were about 1/10 of full cW and Ph 1 (cW) concentrations only and measurements are close to the background measurements (i.e., signal not significantly different from 3 standard deviations SD of the background measurement).

Formatted: Indent: First line: 1.25 cm, Page break before

Field Code Changed

Formatted: Font: Not Bold

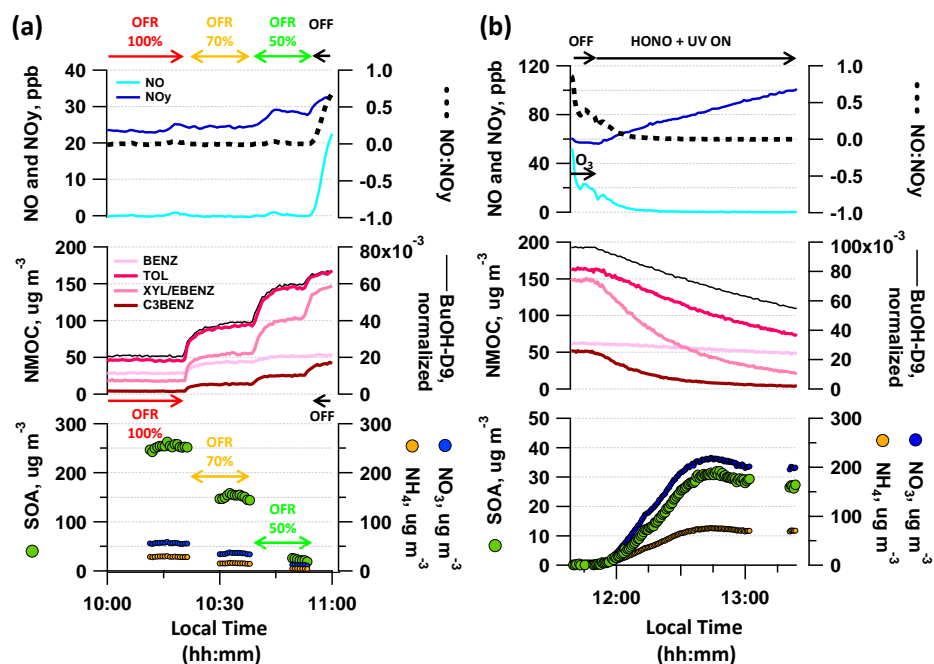


**Figure 5. SOA precursor behavior in Typical OFR-from-SC and SC during photo-chemistry experiment.** Example of decay of organic vapors (dominant SOA precursors) (selected aromatic NMOCs: benzene (BENZ), toluene (TOL), *o*-*m*-*p*-xylene (XYL) or ethylbenzene (EBENZ), C3-benzenes (C3BENZ)) upon photochemistry and associated SOA formation in (a) OFR (sampling from SC batch at different UV intensities, displayed is expt D3) and (b) aging in SC (displayed is expt B1A2). (a-b) UV on/off (and UV intensities for OFR) status, and  $O_3$  and HONO injection (for SC) are indicated along with the  $NO:NO_y$  ratio during the experiments, as well as the decay of the OH tracer BuOH-D9. “Predicted” refers to predicted SOA mass (purple color) from the reacted NMOC vapors and a constant literature based SOA yield applied to it (as reviewed in (Bruns et al., 2016) (BENZ: 0.32, TOL: 0.27, XYL/EBENZ: 0.20, C3-BENZ: 0.32). Note: ammonium nitrate ( $NH_4NO_3$ ) is also formed upon photo-oxidation due to the presence of  $NO_x$  and  $NH_3$ , but is not displayed here, see Supporting Information, Figure S10 instead. Reacted ArHC fractions upon OH exposure in the SC and OFR are provided in the Supporting Information, Figure S5 per experiment. Local time is given in intervals of (a) 30 min and (b) 15 min.

Field Code Changed

Formatted: Not Highlight

Field Code Changed

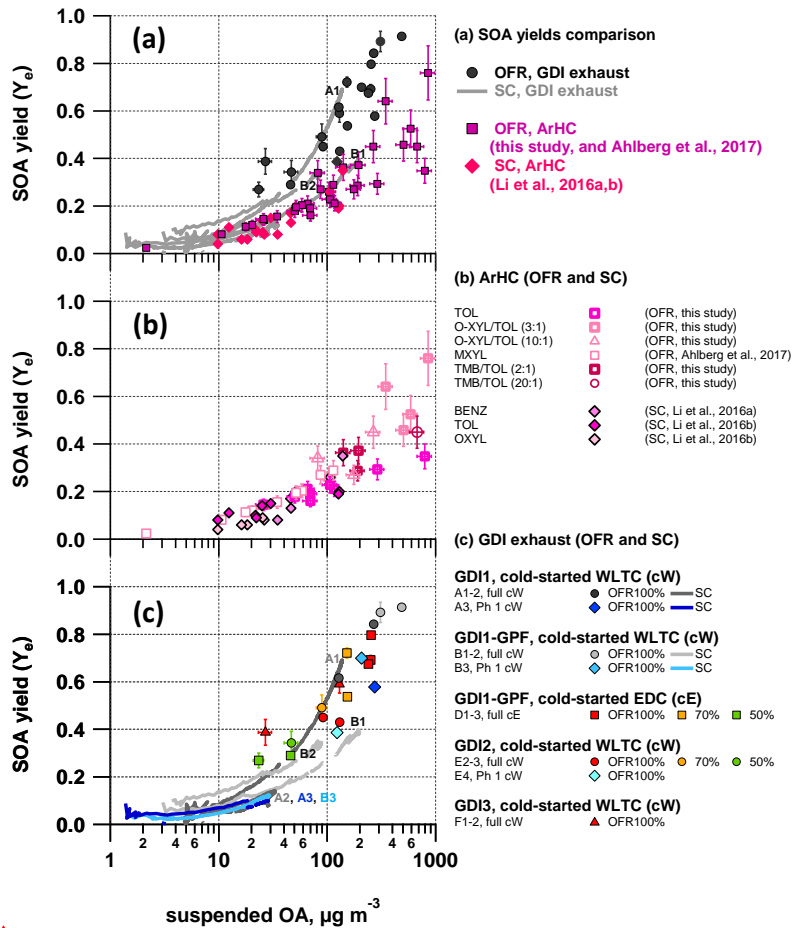


**Figure 6. Effective SOA yields.** Vehicle exhaust from GDI1-3 (full cW, full cE, Ph1 (cW)) photo-chemically aged in the SC and OFR-from-SC compared to effective SOA yields from selected ArHC (toluene, *o*-xylene, 1,2,4-TMB) photo-chemically aged in our OFR (this study, w/o NO; additional *m*-xylene data from (Ahlberg et al., 2017)) and in a SC (data from literature: benzene, toluene, *o*-xylene from (Li et al., 2016a) and (Li et al., 2016b), w/o NO). (a) all data combined, (b) OFR (average±15% measurement variability) and SC yields of single ArHC or mixtures, (c) vehicle exhaust photo-chemically aged in SC and OFR-from-SC (average±1SD of AMS OA measurement during stable conditions). **Note that e**Error bars on data from OFR represent the variability of the measurement **rather than the total uncertainty of the data**. SC yield curves **per experiment** are presented in **more detail in** Figure S13 **and potential factors enhancing yields in experiments A1, B1, B2 (Table S4) are discussed in Section 3.6.1.** (a-c) OH data are given in the legend of Figure 7 and summarized here: OH exposures (Barnet et al., 2012) range up to  $1.4 \times 10^{11}$  molec cm<sup>-3</sup> s, **in-after** ~2 hours of SC photochemistry experiments (average [OH]= $2 \times 10^7$  molec cm<sup>-3</sup>). OFR100%: [OH]= $(2.7-5.2) \times 10^9$  molec cm<sup>-3</sup>; [OH]<sub>exp</sub>= $(3.0-5.8) \times 10^{11}$  molec cm<sup>-3</sup> s (at ~8 ppm O<sub>3</sub>). OFR70%: [OH]= $(1.4-2.2) \times 10^9$  molec cm<sup>-3</sup>; [OH]<sub>exp</sub>= $(1.6-2.5) \times 10^{11}$  molec cm<sup>-3</sup> s (at ~3 ppm O<sub>3</sub>). OFR50%: [OH]= $(0.28-0.44) \times 10^9$  molec cm<sup>-3</sup>; [OH]<sub>exp</sub>= $(0.31-0.49) \times 10^{11}$  molec cm<sup>-3</sup> s (at ~0.7 ppm O<sub>3</sub>). The max. OH exposure in the SC experiments corresponds to the range of green to orange colored OFR data points in panel (c)-, see Figure 7.

Formatted: English (U.S.)

Field Code Changed

Formatted: Italian (Italy)

Formatted: Italian (Italy)

Formatted: Italian (Italy)

Field Code Changed

Formatted: Italian (Italy)

Formatted: Italian (Italy)

Formatted: Italian (Italy)

Field Code Changed

Formatted: Italian (Italy)

Formatted: Italian (Italy)

Field Code Changed

Formatted: Font: Not Bold

Field Code Changed

Field Code Changed

Formatted: Font: Not Bold

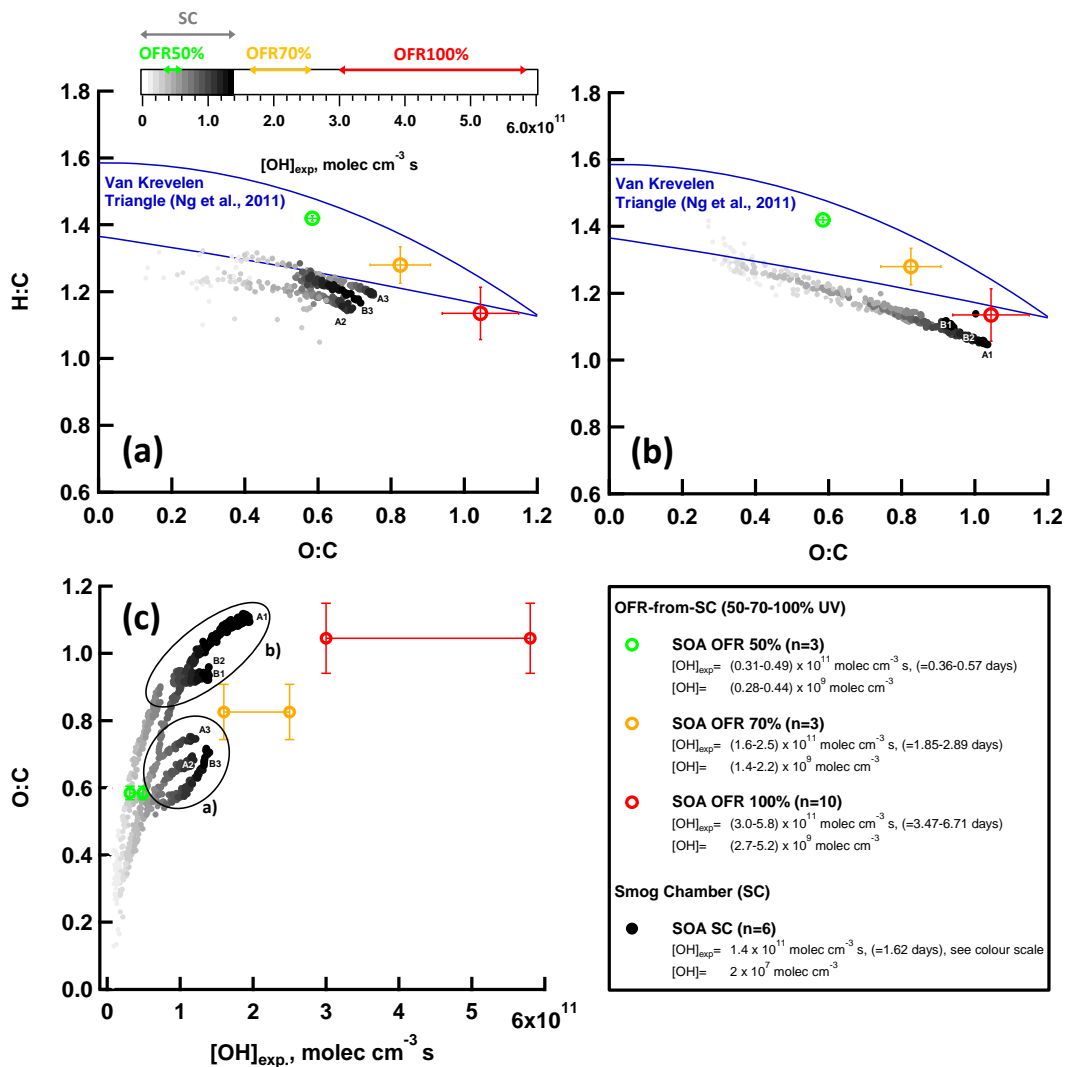


Figure 7. Bulk OA composition of SC and OFR SOA. a-b) Van-Krevelen plot (O:C vs. H:C-ratio) for SOA formed during SC expts (n=6, GDI1 standard and w/GPF, cW and Ph 1 (cW)) and OFR-from-SC data points (n=10, GDI1 standard and w/GPF, full cW, full cE, Ph 1 (cW)) at different OFR UV settings (100%, 70%, 50%). a) shows SC Expt (A2, A3, B3; Table S4) and b) SC Expt (A1, B1, B2; Table S4), experiments with NH<sub>4</sub>NO<sub>3</sub> levels outside our CO<sub>2</sub>-AMS interference calibration range (Pieber et al., 2016). The POA contribution was subtracted from the total OA bulk composition; SOA/POA ratios were far above a factor of > 10. OH and O<sub>3</sub> information is provided in Figure 6. The Aiken parameterization (Aiken et al., 2007; Aiken et al., 2008) has been applied to HR fitted data in order to allow for a better comparison with previously published data. Lines indicate the Van-Krevelen (VK) space

Field Code Changed

Field Code Changed

Field Code Changed

5

typical for ambient AMS measurements ~~as presented by (Ng et al., 2011)~~. Error bars represent one standard deviation ~~corresponding to the average for several experiments presented and reflect~~ of measurement variability ~~rather than total uncertainties~~. ~~[OH]<sub>exp</sub> in days refers to an assumed average ambient [OH] of 10<sup>6</sup> molec cm<sup>-3</sup>. Figure S16 provides details on single SC experiments.~~ (c) O:C of a) and b) as a function of [OH] exposure. [OH]<sub>exp</sub> in days refers to an assumed average ambient [OH] of 10<sup>6</sup> molec cm<sup>-3</sup>.

Field Code Changed

Formatted: Caption

**Table 1. Vehicles** (details in Table S1, [Supporting Information](#)) and tests ( $n$  gives the number of driving tests conducted; EDC tests were only conducted with GD11 and GD11 w/GPF).

Vehicle Code	Vehicle Type	Expt. Set	cold-	hot-	cold-	hot-
			started	started	started	started
			WLTC	WLTC	EDC	EDC
GD11	Opel Insignia; Euro 5, standard configuration	2014 (I)	$n=4$	$n=4$	$n=1$	$n=1$
GD11 w/GPF	Opel Insignia; Euro 5, with retrofitted GPF (underfloor)	2014 (I)	$n=4$	$n=4$	$n=3$	$n=3$
GD12	Opel Zafira Tourer, Euro 5	2015 (II)	$n=4$	$n=4$	--	--
GD13	VW Golf Plus, Euro 4	2015 (II)	$n=4$	$n=4$	--	--
GD14 (2014)	Volvo V60, Euro 5, standard configuration	2014 (I)	$n=4$	$n=4$	--	--
GD14 (2015)	Volvo V60, Euro 5, standard configuration	2015 (II)	$n=3$	$n=1$	--	--
GD14 w/GPF	Volvo V60, Euro 5, with retrofitted GPF (underfloor)	2015 (II)	$n=4$	$n=2$	--	--
GD14 w/catGPF	Volvo V60, Euro 5, with retrofitted catGPF (underfloor)	2015 (II)	$n=4$	$n=2$	--	--

**Table 2. NMOC information** (list of dominant peaks).

Ion $m/z$	Chem. Formula	Assignment	Denotation	$k_{H_3O^+}^a)$ $cm^3 s^{-1}$	$k_{OH}^b)$ $cm^3 molec^{-1} s^{-1}$
79	$[C_6H_6+H]^+$	benzene	BENZ	$1.93 \times 10^9$	$1.22 \times 10^{12}$
93	$[C_7H_8+H]^+$	toluene	TOL	$2.08 \times 10^9$	$5.63 \times 10^{12}$
107	$[C_8H_{10}+H]^+$	<i>o</i> -/ <i>m</i> -/ <i>p</i> -xylene, ethylbenzene	XYL/E-BENZ	$2.26 \times 10^9$	$(7-23) \times 10^{12}$
121	$[C_9H_{12}+H]^+$	$C_3$ -alkyl-benzenes	C3BENZ	$2.39 \times 10^9$	$(6-57) \times 10^{12}$
135	$[C_{10}H_{14}+H]^+$	$C_4$ -alkyl-benzenes	C4BENZ	$2.50 \times 10^9$	$(5-15) \times 10^{12}$
129	$[C_{10}H_8+H]^+$	naphthalene	NAPH	$2.45 \times 10^9$	$23 \times 10^{12}$
105	$[C_8H_8+H]^+$	styrene	STY	$2.27 \times 10^9$	$28 \times 10^{12}$
119	$[C_9H_{10}+H]^+$	methyl-styrene	CISTY	$2.00 \times 10^9$	$(51-57) \times 10^{12}$
41	$[C_3H_3]^+$	HC fragment	-	$2.00 \times 10^9$	n.a.
43	$[C_3H_2]^+$	HC fragment	-	$2.00 \times 10^9$	n.a.
57	$[C_4H_4]^+$	HC fragment	-	$2.00 \times 10^9$	n.a.

Ions are referred to with their integer mass-to-charge ( $m/z$ ) ratio for simplicity, but are identified based on the HR derived exact  $m/z$  instead. n.a.=not applicable. <sup>a)</sup> $k_{H_3O^+}$  from (Cappellin et al., 2012), <sup>b)</sup> $k_{OH}$  from (Atkinson and Arey, 2003), range in (brackets) corresponds to isomers.

Formatted: Page break before

Field Code Changed

Formatted: Italian (Italy)

Formatted: Italian (Italy)

Formatted: Italian (Italy)

Field Code Changed

Field Code Changed

Field Code Changed

<b>Page 5: [1] Change</b>	<b>Unknown</b>
---------------------------	----------------

Field Code Changed

<b>Page 5: [1] Change</b>	<b>Unknown</b>
---------------------------	----------------

Field Code Changed

<b>Page 5: [1] Change</b>	<b>Unknown</b>
---------------------------	----------------

Field Code Changed

<b>Page 5: [1] Change</b>	<b>Unknown</b>
---------------------------	----------------

Field Code Changed

<b>Page 5: [1] Change</b>	<b>Unknown</b>
---------------------------	----------------

Field Code Changed

<b>Page 5: [2] Formatted</b>	<b>Pieber Simone Maria</b>	<b>08.05.2018 16:58:00</b>
------------------------------	----------------------------	----------------------------

English (U.S.)

<b>Page 5: [2] Formatted</b>	<b>Pieber Simone Maria</b>	<b>08.05.2018 16:58:00</b>
------------------------------	----------------------------	----------------------------

English (U.S.)

<b>Page 5: [3] Change</b>	<b>Unknown</b>
---------------------------	----------------

Field Code Changed

<b>Page 5: [3] Change</b>	<b>Unknown</b>
---------------------------	----------------

Field Code Changed

<b>Page 5: [3] Change</b>	<b>Unknown</b>
---------------------------	----------------

Field Code Changed

<b>Page 5: [3] Change</b>	<b>Unknown</b>
---------------------------	----------------

Field Code Changed

<b>Page 5: [3] Change</b>	<b>Unknown</b>
---------------------------	----------------

Field Code Changed

<b>Page 5: [4] Change</b>	<b>Unknown</b>
---------------------------	----------------

Field Code Changed

<b>Page 5: [4] Change</b>	<b>Unknown</b>
---------------------------	----------------

Field Code Changed

<b>Page 5: [4] Change</b>	<b>Unknown</b>
---------------------------	----------------

Field Code Changed

<b>Page 5: [4] Change</b>	<b>Unknown</b>
---------------------------	----------------

Field Code Changed

<b>Page 5: [4] Change</b>	<b>Unknown</b>
---------------------------	----------------

Field Code Changed

<b>Page 5: [4] Change</b>	<b>Unknown</b>
---------------------------	----------------

Field Code Changed

Page 5: [4] Change	Unknown	
Field Code Changed		
Page 5: [4] Change	Unknown	
Field Code Changed		
Page 5: [5] Formatted	Pieber Simone Maria	08.05.2018 16:58:00
Italian (Italy)		
Page 5: [5] Formatted	Pieber Simone Maria	08.05.2018 16:58:00
Italian (Italy)		
Page 5: [6] Formatted	Pieber Simone Maria	08.05.2018 16:58:00
Italian (Italy)		
Page 5: [6] Formatted	Pieber Simone Maria	08.05.2018 16:58:00
Italian (Italy)		
Page 5: [7] Change	Unknown	
Field Code Changed		
Page 5: [7] Change	Unknown	
Field Code Changed		
Page 5: [8] Change	Unknown	
Field Code Changed		
Page 5: [8] Change	Unknown	
Field Code Changed		
Page 5: [9] Change	Unknown	
Field Code Changed		
Page 5: [9] Change	Unknown	
Field Code Changed		
Page 5: [9] Change	Unknown	
Field Code Changed		
Page 5: [9] Change	Unknown	
Field Code Changed		
Page 5: [10] Formatted	Pieber Simone Maria	08.05.2018 16:58:00
Not Highlight		
Page 5: [10] Formatted	Pieber Simone Maria	08.05.2018 16:58:00
Not Highlight		
Page 5: [11] Formatted	Pieber Simone Maria	08.05.2018 16:58:00
Italian (Italy)		
Page 5: [11] Formatted	Pieber Simone Maria	08.05.2018 16:58:00
Italian (Italy)		

Page 5: [12] Formatted	Pieber Simone Maria	08.05.2018 16:58:00
------------------------	---------------------	---------------------

Italian (Italy)

Page 5: [12] Formatted	Pieber Simone Maria	08.05.2018 16:58:00
------------------------	---------------------	---------------------

Italian (Italy)

Page 5: [13] Formatted	Pieber Simone Maria	08.05.2018 16:58:00
------------------------	---------------------	---------------------

Italian (Italy)

Page 5: [13] Formatted	Pieber Simone Maria	08.05.2018 16:58:00
------------------------	---------------------	---------------------

Italian (Italy)

Page 5: [14] Formatted	Pieber Simone Maria	08.05.2018 16:58:00
------------------------	---------------------	---------------------

Italian (Italy)

Page 5: [14] Formatted	Pieber Simone Maria	08.05.2018 16:58:00
------------------------	---------------------	---------------------

Italian (Italy)

Page 5: [15] Formatted	Pieber Simone Maria	08.05.2018 16:58:00
------------------------	---------------------	---------------------

Italian (Italy)

Page 5: [15] Formatted	Pieber Simone Maria	08.05.2018 16:58:00
------------------------	---------------------	---------------------

Italian (Italy)

Page 5: [16] Formatted	Pieber Simone Maria	08.05.2018 16:58:00
------------------------	---------------------	---------------------

Italian (Italy)

Page 5: [16] Formatted	Pieber Simone Maria	08.05.2018 16:58:00
------------------------	---------------------	---------------------

Italian (Italy)

Page 5: [17] Formatted	Pieber Simone Maria	08.05.2018 16:58:00
------------------------	---------------------	---------------------

Italian (Italy)

Page 5: [17] Formatted	Pieber Simone Maria	08.05.2018 16:58:00
------------------------	---------------------	---------------------

Italian (Italy)

Page 5: [18] Change	Unknown	
---------------------	---------	--

Field Code Changed

Page 5: [18] Change	Unknown	
---------------------	---------	--

Field Code Changed

Page 5: [18] Change	Unknown	
---------------------	---------	--

Field Code Changed

Page 5: [18] Change	Unknown	
---------------------	---------	--

Field Code Changed

Page 5: [18] Change	Unknown	
---------------------	---------	--

Field Code Changed

Page 5: [18] Change	Unknown	
---------------------	---------	--

Field Code Changed

<b>Page 5: [19] Formatted</b>	<b>Pieber Simone Maria</b>	<b>08.05.2018 16:58:00</b>
-------------------------------	----------------------------	----------------------------

English (U.S.)

<b>Page 5: [19] Formatted</b>	<b>Pieber Simone Maria</b>	<b>08.05.2018 16:58:00</b>
-------------------------------	----------------------------	----------------------------

English (U.S.)

<b>Page 5: [19] Formatted</b>	<b>Pieber Simone Maria</b>	<b>08.05.2018 16:58:00</b>
-------------------------------	----------------------------	----------------------------

English (U.S.)

<b>Page 28: [20] Change</b>	<b>Unknown</b>	
-----------------------------	----------------	--

Field Code Changed

<b>Page 28: [20] Change</b>	<b>Unknown</b>	
-----------------------------	----------------	--

Field Code Changed

<b>Page 28: [21] Formatted</b>	<b>Pieber Simone Maria</b>	<b>08.05.2018 16:58:00</b>
--------------------------------	----------------------------	----------------------------

Italian (Italy)

<b>Page 28: [21] Formatted</b>	<b>Pieber Simone Maria</b>	<b>08.05.2018 16:58:00</b>
--------------------------------	----------------------------	----------------------------

Italian (Italy)

<b>Page 28: [22] Formatted</b>	<b>Pieber Simone Maria</b>	<b>08.05.2018 16:58:00</b>
--------------------------------	----------------------------	----------------------------

Italian (Italy)

<b>Page 28: [22] Formatted</b>	<b>Pieber Simone Maria</b>	<b>08.05.2018 16:58:00</b>
--------------------------------	----------------------------	----------------------------

Italian (Italy)

<b>Page 28: [23] Formatted</b>	<b>Pieber Simone Maria</b>	<b>08.05.2018 16:58:00</b>
--------------------------------	----------------------------	----------------------------

Italian (Italy)

<b>Page 28: [23] Formatted</b>	<b>Pieber Simone Maria</b>	<b>08.05.2018 16:58:00</b>
--------------------------------	----------------------------	----------------------------

Italian (Italy)

<b>Page 28: [24] Formatted</b>	<b>Pieber Simone Maria</b>	<b>08.05.2018 16:58:00</b>
--------------------------------	----------------------------	----------------------------

Font color: Auto

<b>Page 28: [24] Formatted</b>	<b>Pieber Simone Maria</b>	<b>08.05.2018 16:58:00</b>
--------------------------------	----------------------------	----------------------------

Font color: Auto

<b>Page 28: [24] Formatted</b>	<b>Pieber Simone Maria</b>	<b>08.05.2018 16:58:00</b>
--------------------------------	----------------------------	----------------------------

Font color: Auto

<b>Page 28: [24] Formatted</b>	<b>Pieber Simone Maria</b>	<b>08.05.2018 16:58:00</b>
--------------------------------	----------------------------	----------------------------

Font color: Auto

<b>Page 28: [24] Formatted</b>	<b>Pieber Simone Maria</b>	<b>08.05.2018 16:58:00</b>
--------------------------------	----------------------------	----------------------------

Font color: Auto

<b>Page 28: [24] Formatted</b>	<b>Pieber Simone Maria</b>	<b>08.05.2018 16:58:00</b>
--------------------------------	----------------------------	----------------------------

Font color: Auto

<b>Page 28: [24] Formatted</b>	<b>Pieber Simone Maria</b>	<b>08.05.2018 16:58:00</b>
--------------------------------	----------------------------	----------------------------

Font color: Auto

<b>Page 28: [24] Formatted</b>	<b>Pieber Simone Maria</b>	<b>08.05.2018 16:58:00</b>
--------------------------------	----------------------------	----------------------------

Font color: Auto

<b>Page 28: [24] Formatted</b>	<b>Pieber Simone Maria</b>	<b>08.05.2018 16:58:00</b>
--------------------------------	----------------------------	----------------------------

Font color: Auto

<b>Page 28: [24] Formatted</b>	<b>Pieber Simone Maria</b>	<b>08.05.2018 16:58:00</b>
--------------------------------	----------------------------	----------------------------

Font color: Auto

<b>Page 28: [24] Formatted</b>	<b>Pieber Simone Maria</b>	<b>08.05.2018 16:58:00</b>
--------------------------------	----------------------------	----------------------------

Font color: Auto

<b>Page 28: [25] Formatted</b>	<b>Pieber Simone Maria</b>	<b>08.05.2018 16:58:00</b>
--------------------------------	----------------------------	----------------------------

Not Highlight

<b>Page 28: [25] Formatted</b>	<b>Pieber Simone Maria</b>	<b>08.05.2018 16:58:00</b>
--------------------------------	----------------------------	----------------------------

Not Highlight

<b>Page 28: [25] Formatted</b>	<b>Pieber Simone Maria</b>	<b>08.05.2018 16:58:00</b>
--------------------------------	----------------------------	----------------------------

Not Highlight

<b>Page 28: [25] Formatted</b>	<b>Pieber Simone Maria</b>	<b>08.05.2018 16:58:00</b>
--------------------------------	----------------------------	----------------------------

Not Highlight

<b>Page 28: [26] Change</b>	<b>Unknown</b>	
-----------------------------	----------------	--

Field Code Changed

<b>Page 28: [26] Change</b>	<b>Unknown</b>	
-----------------------------	----------------	--

Field Code Changed

<b>Page 28: [26] Change</b>	<b>Unknown</b>	
-----------------------------	----------------	--

Field Code Changed

<b>Page 28: [27] Formatted</b>	<b>Pieber Simone Maria</b>	<b>08.05.2018 16:58:00</b>
--------------------------------	----------------------------	----------------------------

Font color: Auto, Not Highlight

<b>Page 28: [27] Formatted</b>	<b>Pieber Simone Maria</b>	<b>08.05.2018 16:58:00</b>
--------------------------------	----------------------------	----------------------------

Font color: Auto, Not Highlight

<b>Page 28: [27] Formatted</b>	<b>Pieber Simone Maria</b>	<b>08.05.2018 16:58:00</b>
--------------------------------	----------------------------	----------------------------

Font color: Auto, Not Highlight

<b>Page 28: [27] Formatted</b>	<b>Pieber Simone Maria</b>	<b>08.05.2018 16:58:00</b>
--------------------------------	----------------------------	----------------------------

Font color: Auto, Not Highlight

<b>Page 28: [27] Formatted</b>	<b>Pieber Simone Maria</b>	<b>08.05.2018 16:58:00</b>
--------------------------------	----------------------------	----------------------------

Font color: Auto, Not Highlight

<b>Page 28: [27] Formatted</b>	<b>Pieber Simone Maria</b>	<b>08.05.2018 16:58:00</b>
--------------------------------	----------------------------	----------------------------

Font color: Auto, Not Highlight

<b>Page 28: [27] Formatted</b>	<b>Pieber Simone Maria</b>	<b>08.05.2018 16:58:00</b>
--------------------------------	----------------------------	----------------------------

Font color: Auto, Not Highlight



<b>Page 28: [29] Change</b>	<b>Unknown</b>
-----------------------------	----------------

Field Code Changed

<b>Page 28: [29] Change</b>	<b>Unknown</b>
-----------------------------	----------------

Field Code Changed

<b>Page 28: [29] Change</b>	<b>Unknown</b>
-----------------------------	----------------

Field Code Changed

<b>Page 28: [30] Formatted</b>	<b>Pieber Simone Maria</b>	<b>08.05.2018 16:58:00</b>
--------------------------------	----------------------------	----------------------------

Not Highlight

<b>Page 28: [30] Formatted</b>	<b>Pieber Simone Maria</b>	<b>08.05.2018 16:58:00</b>
--------------------------------	----------------------------	----------------------------

Not Highlight

<b>Page 28: [30] Formatted</b>	<b>Pieber Simone Maria</b>	<b>08.05.2018 16:58:00</b>
--------------------------------	----------------------------	----------------------------

Not Highlight

<b>Page 28: [31] Formatted</b>	<b>Pieber Simone Maria</b>	<b>08.05.2018 16:58:00</b>
--------------------------------	----------------------------	----------------------------

Not Highlight

<b>Page 28: [31] Formatted</b>	<b>Pieber Simone Maria</b>	<b>08.05.2018 16:58:00</b>
--------------------------------	----------------------------	----------------------------

Not Highlight

<b>Page 29: [32] Formatted</b>	<b>Pieber Simone Maria</b>	<b>08.05.2018 16:58:00</b>
--------------------------------	----------------------------	----------------------------

Not Highlight

<b>Page 29: [32] Formatted</b>	<b>Pieber Simone Maria</b>	<b>08.05.2018 16:58:00</b>
--------------------------------	----------------------------	----------------------------

Not Highlight

<b>Page 29: [32] Formatted</b>	<b>Pieber Simone Maria</b>	<b>08.05.2018 16:58:00</b>
--------------------------------	----------------------------	----------------------------

Not Highlight

<b>Page 29: [32] Formatted</b>	<b>Pieber Simone Maria</b>	<b>08.05.2018 16:58:00</b>
--------------------------------	----------------------------	----------------------------

Not Highlight

<b>Page 29: [32] Formatted</b>	<b>Pieber Simone Maria</b>	<b>08.05.2018 16:58:00</b>
--------------------------------	----------------------------	----------------------------

Not Highlight

<b>Page 29: [32] Formatted</b>	<b>Pieber Simone Maria</b>	<b>08.05.2018 16:58:00</b>
--------------------------------	----------------------------	----------------------------

Not Highlight

<b>Page 29: [32] Formatted</b>	<b>Pieber Simone Maria</b>	<b>08.05.2018 16:58:00</b>
--------------------------------	----------------------------	----------------------------

Not Highlight

<b>Page 29: [33] Formatted</b>	<b>Pieber Simone Maria</b>	<b>08.05.2018 16:58:00</b>
--------------------------------	----------------------------	----------------------------

Not Highlight

<b>Page 29: [33] Formatted</b>	<b>Pieber Simone Maria</b>	<b>08.05.2018 16:58:00</b>
--------------------------------	----------------------------	----------------------------

Not Highlight

<b>Page 29: [33] Formatted</b>	<b>Pieber Simone Maria</b>	<b>08.05.2018 16:58:00</b>
--------------------------------	----------------------------	----------------------------

Not Highlight

Page 29: [33] Formatted	Pieber Simone Maria	08.05.2018 16:58:00
-------------------------	---------------------	---------------------

Not Highlight

Page 29: [33] Formatted	Pieber Simone Maria	08.05.2018 16:58:00
-------------------------	---------------------	---------------------

Not Highlight

Page 29: [34] Formatted	Pieber Simone Maria	08.05.2018 16:58:00
-------------------------	---------------------	---------------------

Not Highlight

Page 29: [34] Formatted	Pieber Simone Maria	08.05.2018 16:58:00
-------------------------	---------------------	---------------------

Not Highlight

Page 29: [34] Formatted	Pieber Simone Maria	08.05.2018 16:58:00
-------------------------	---------------------	---------------------

Not Highlight

Page 29: [35] Formatted	Pieber Simone Maria	08.05.2018 16:58:00
-------------------------	---------------------	---------------------

Not Highlight

Page 29: [35] Formatted	Pieber Simone Maria	08.05.2018 16:58:00
-------------------------	---------------------	---------------------

Not Highlight

Page 29: [35] Formatted	Pieber Simone Maria	08.05.2018 16:58:00
-------------------------	---------------------	---------------------

Not Highlight

Page 29: [35] Formatted	Pieber Simone Maria	08.05.2018 16:58:00
-------------------------	---------------------	---------------------

Not Highlight

Page 29: [35] Formatted	Pieber Simone Maria	08.05.2018 16:58:00
-------------------------	---------------------	---------------------

Not Highlight

Page 29: [36] Formatted	Pieber Simone Maria	08.05.2018 16:58:00
-------------------------	---------------------	---------------------

Font color: Auto

Page 29: [36] Formatted	Pieber Simone Maria	08.05.2018 16:58:00
-------------------------	---------------------	---------------------

Font color: Auto

Page 29: [37] Formatted	Pieber Simone Maria	08.05.2018 16:58:00
-------------------------	---------------------	---------------------

Font color: Auto, Not Highlight

Page 29: [37] Formatted	Pieber Simone Maria	08.05.2018 16:58:00
-------------------------	---------------------	---------------------

Font color: Auto, Not Highlight

Page 29: [38] Formatted	Pieber Simone Maria	08.05.2018 16:58:00
-------------------------	---------------------	---------------------

Not Highlight

Page 29: [38] Formatted	Pieber Simone Maria	08.05.2018 16:58:00
-------------------------	---------------------	---------------------

Not Highlight

Page 29: [39] Formatted	Pieber Simone Maria	08.05.2018 16:58:00
-------------------------	---------------------	---------------------

Not Highlight

Page 29: [39] Formatted	Pieber Simone Maria	08.05.2018 16:58:00
-------------------------	---------------------	---------------------

Not Highlight

<b>Page 29: [39] Formatted</b>	<b>Pieber Simone Maria</b>	<b>08.05.2018 16:58:00</b>
--------------------------------	----------------------------	----------------------------

Not Highlight

<b>Page 29: [40] Formatted</b>	<b>Pieber Simone Maria</b>	<b>08.05.2018 16:58:00</b>
--------------------------------	----------------------------	----------------------------

Font: Bold

<b>Page 29: [40] Formatted</b>	<b>Pieber Simone Maria</b>	<b>08.05.2018 16:58:00</b>
--------------------------------	----------------------------	----------------------------

Font: Bold

<b>Page 29: [40] Formatted</b>	<b>Pieber Simone Maria</b>	<b>08.05.2018 16:58:00</b>
--------------------------------	----------------------------	----------------------------

Font: Bold

<b>Page 29: [40] Formatted</b>	<b>Pieber Simone Maria</b>	<b>08.05.2018 16:58:00</b>
--------------------------------	----------------------------	----------------------------

Font: Bold

<b>Page 29: [40] Formatted</b>	<b>Pieber Simone Maria</b>	<b>08.05.2018 16:58:00</b>
--------------------------------	----------------------------	----------------------------

Font: Bold

<b>Page 29: [41] Formatted</b>	<b>Pieber Simone Maria</b>	<b>08.05.2018 16:58:00</b>
--------------------------------	----------------------------	----------------------------

Font color: Auto

<b>Page 29: [41] Formatted</b>	<b>Pieber Simone Maria</b>	<b>08.05.2018 16:58:00</b>
--------------------------------	----------------------------	----------------------------

Font color: Auto

<b>Page 29: [41] Formatted</b>	<b>Pieber Simone Maria</b>	<b>08.05.2018 16:58:00</b>
--------------------------------	----------------------------	----------------------------

Font color: Auto

<b>Page 29: [41] Formatted</b>	<b>Pieber Simone Maria</b>	<b>08.05.2018 16:58:00</b>
--------------------------------	----------------------------	----------------------------

Font color: Auto

<b>Page 30: [42] Change</b>	<b>Unknown</b>
-----------------------------	----------------

Field Code Changed

<b>Page 30: [42] Change</b>	<b>Unknown</b>
-----------------------------	----------------

Field Code Changed

<b>Page 30: [42] Change</b>	<b>Unknown</b>
-----------------------------	----------------

Field Code Changed

<b>Page 30: [42] Change</b>	<b>Unknown</b>
-----------------------------	----------------

Field Code Changed

<b>Page 30: [42] Change</b>	<b>Unknown</b>
-----------------------------	----------------

Field Code Changed

<b>Page 30: [42] Change</b>	<b>Unknown</b>
-----------------------------	----------------

Field Code Changed

<b>Page 30: [42] Change</b>	<b>Unknown</b>
-----------------------------	----------------

Field Code Changed

<b>Page 30: [43] Formatted</b>	<b>Pieber Simone Maria</b>	<b>08.05.2018 16:58:00</b>
--------------------------------	----------------------------	----------------------------

Font color: Auto

<b>Page 30: [43] Formatted</b>	<b>Pieber Simone Maria</b>	<b>08.05.2018 16:58:00</b>
--------------------------------	----------------------------	----------------------------

Font color: Auto

<b>Page 30: [44] Formatted</b>	<b>Pieber Simone Maria</b>	<b>08.05.2018 16:58:00</b>
--------------------------------	----------------------------	----------------------------

Not Highlight

<b>Page 30: [44] Formatted</b>	<b>Pieber Simone Maria</b>	<b>08.05.2018 16:58:00</b>
--------------------------------	----------------------------	----------------------------

Not Highlight

<b>Page 30: [45] Formatted</b>	<b>Pieber Simone Maria</b>	<b>08.05.2018 16:58:00</b>
--------------------------------	----------------------------	----------------------------

Not Highlight

<b>Page 30: [45] Formatted</b>	<b>Pieber Simone Maria</b>	<b>08.05.2018 16:58:00</b>
--------------------------------	----------------------------	----------------------------

Not Highlight

<b>Page 30: [45] Formatted</b>	<b>Pieber Simone Maria</b>	<b>08.05.2018 16:58:00</b>
--------------------------------	----------------------------	----------------------------

Not Highlight

<b>Page 30: [45] Formatted</b>	<b>Pieber Simone Maria</b>	<b>08.05.2018 16:58:00</b>
--------------------------------	----------------------------	----------------------------

Not Highlight

<b>Page 30: [45] Formatted</b>	<b>Pieber Simone Maria</b>	<b>08.05.2018 16:58:00</b>
--------------------------------	----------------------------	----------------------------

Not Highlight

<b>Page 30: [45] Formatted</b>	<b>Pieber Simone Maria</b>	<b>08.05.2018 16:58:00</b>
--------------------------------	----------------------------	----------------------------

Not Highlight

<b>Page 30: [45] Formatted</b>	<b>Pieber Simone Maria</b>	<b>08.05.2018 16:58:00</b>
--------------------------------	----------------------------	----------------------------

Not Highlight

<b>Page 30: [45] Formatted</b>	<b>Pieber Simone Maria</b>	<b>08.05.2018 16:58:00</b>
--------------------------------	----------------------------	----------------------------

Not Highlight

<b>Page 30: [45] Formatted</b>	<b>Pieber Simone Maria</b>	<b>08.05.2018 16:58:00</b>
--------------------------------	----------------------------	----------------------------

Not Highlight

<b>Page 30: [45] Formatted</b>	<b>Pieber Simone Maria</b>	<b>08.05.2018 16:58:00</b>
--------------------------------	----------------------------	----------------------------

Not Highlight

<b>Page 30: [45] Formatted</b>	<b>Pieber Simone Maria</b>	<b>08.05.2018 16:58:00</b>
--------------------------------	----------------------------	----------------------------

Not Highlight

<b>Page 30: [45] Formatted</b>	<b>Pieber Simone Maria</b>	<b>08.05.2018 16:58:00</b>
--------------------------------	----------------------------	----------------------------

Not Highlight

<b>Page 30: [45] Formatted</b>	<b>Pieber Simone Maria</b>	<b>08.05.2018 16:58:00</b>
--------------------------------	----------------------------	----------------------------

Not Highlight

<b>Page 30: [45] Formatted</b>	<b>Pieber Simone Maria</b>	<b>08.05.2018 16:58:00</b>
--------------------------------	----------------------------	----------------------------

Not Highlight

<b>Page 30: [45] Formatted</b>	<b>Pieber Simone Maria</b>	<b>08.05.2018 16:58:00</b>
--------------------------------	----------------------------	----------------------------

Not Highlight

Page 30: [45] Formatted	Pieber Simone Maria	08.05.2018 16:58:00
-------------------------	---------------------	---------------------

Not Highlight

Page 30: [45] Formatted	Pieber Simone Maria	08.05.2018 16:58:00
-------------------------	---------------------	---------------------

Not Highlight

Page 30: [45] Formatted	Pieber Simone Maria	08.05.2018 16:58:00
-------------------------	---------------------	---------------------

Not Highlight

Page 30: [45] Formatted	Pieber Simone Maria	08.05.2018 16:58:00
-------------------------	---------------------	---------------------

Not Highlight

Page 30: [45] Formatted	Pieber Simone Maria	08.05.2018 16:58:00
-------------------------	---------------------	---------------------

Not Highlight

Page 30: [45] Formatted	Pieber Simone Maria	08.05.2018 16:58:00
-------------------------	---------------------	---------------------

Not Highlight

Page 30: [45] Formatted	Pieber Simone Maria	08.05.2018 16:58:00
-------------------------	---------------------	---------------------

Not Highlight

Page 30: [45] Formatted	Pieber Simone Maria	08.05.2018 16:58:00
-------------------------	---------------------	---------------------

Not Highlight

Page 30: [45] Formatted	Pieber Simone Maria	08.05.2018 16:58:00
-------------------------	---------------------	---------------------

Not Highlight

Page 30: [45] Formatted	Pieber Simone Maria	08.05.2018 16:58:00
-------------------------	---------------------	---------------------

Not Highlight

Page 30: [46] Formatted	Pieber Simone Maria	08.05.2018 16:58:00
-------------------------	---------------------	---------------------

Font color: Auto

Page 30: [46] Formatted	Pieber Simone Maria	08.05.2018 16:58:00
-------------------------	---------------------	---------------------

Font color: Auto

Page 30: [46] Formatted	Pieber Simone Maria	08.05.2018 16:58:00
-------------------------	---------------------	---------------------

Font color: Auto

Page 30: [46] Formatted	Pieber Simone Maria	08.05.2018 16:58:00
-------------------------	---------------------	---------------------

Font color: Auto

Page 30: [46] Formatted	Pieber Simone Maria	08.05.2018 16:58:00
-------------------------	---------------------	---------------------

Font color: Auto

Page 30: [46] Formatted	Pieber Simone Maria	08.05.2018 16:58:00
-------------------------	---------------------	---------------------

Font color: Auto

Page 30: [47] Change	Unknown	
----------------------	---------	--

Field Code Changed

Page 30: [47] Change	Unknown	
----------------------	---------	--

Field Code Changed

<b>Page 30: [47] Change</b>	<b>Unknown</b>
-----------------------------	----------------

Field Code Changed

<b>Page 30: [47] Change</b>	<b>Unknown</b>
-----------------------------	----------------

Field Code Changed

<b>Page 30: [47] Change</b>	<b>Unknown</b>
-----------------------------	----------------

Field Code Changed

<b>Page 30: [47] Change</b>	<b>Unknown</b>
-----------------------------	----------------

Field Code Changed

<b>Page 30: [47] Change</b>	<b>Unknown</b>
-----------------------------	----------------

Field Code Changed

<b>Page 30: [47] Change</b>	<b>Unknown</b>
-----------------------------	----------------

Field Code Changed

<b>Page 30: [47] Change</b>	<b>Unknown</b>
-----------------------------	----------------

Field Code Changed

<b>Page 30: [47] Change</b>	<b>Unknown</b>
-----------------------------	----------------

Field Code Changed

<b>Page 30: [47] Change</b>	<b>Unknown</b>
-----------------------------	----------------

Field Code Changed

<b>Page 30: [48] Formatted</b>	<b>Pieber Simone Maria</b>	<b>08.05.2018 16:58:00</b>
--------------------------------	----------------------------	----------------------------

Not Highlight

<b>Page 30: [48] Formatted</b>	<b>Pieber Simone Maria</b>	<b>08.05.2018 16:58:00</b>
--------------------------------	----------------------------	----------------------------

Not Highlight

<b>Page 30: [48] Formatted</b>	<b>Pieber Simone Maria</b>	<b>08.05.2018 16:58:00</b>
--------------------------------	----------------------------	----------------------------

Not Highlight

<b>Page 30: [48] Formatted</b>	<b>Pieber Simone Maria</b>	<b>08.05.2018 16:58:00</b>
--------------------------------	----------------------------	----------------------------

Not Highlight

<b>Page 30: [48] Formatted</b>	<b>Pieber Simone Maria</b>	<b>08.05.2018 16:58:00</b>
--------------------------------	----------------------------	----------------------------

Not Highlight

<b>Page 30: [48] Formatted</b>	<b>Pieber Simone Maria</b>	<b>08.05.2018 16:58:00</b>
--------------------------------	----------------------------	----------------------------

Not Highlight

<b>Page 30: [48] Formatted</b>	<b>Pieber Simone Maria</b>	<b>08.05.2018 16:58:00</b>
--------------------------------	----------------------------	----------------------------

Not Highlight

<b>Page 30: [48] Formatted</b>	<b>Pieber Simone Maria</b>	<b>08.05.2018 16:58:00</b>
--------------------------------	----------------------------	----------------------------

Not Highlight

<b>Page 30: [48] Formatted</b>	<b>Pieber Simone Maria</b>	<b>08.05.2018 16:58:00</b>
--------------------------------	----------------------------	----------------------------

Not Highlight

Page 30: [48] Formatted	Pieber Simone Maria	08.05.2018 16:58:00
-------------------------	---------------------	---------------------

Not Highlight

Page 30: [48] Formatted	Pieber Simone Maria	08.05.2018 16:58:00
-------------------------	---------------------	---------------------

Not Highlight

Page 30: [48] Formatted	Pieber Simone Maria	08.05.2018 16:58:00
-------------------------	---------------------	---------------------

Not Highlight

Page 30: [48] Formatted	Pieber Simone Maria	08.05.2018 16:58:00
-------------------------	---------------------	---------------------

Not Highlight

Page 30: [48] Formatted	Pieber Simone Maria	08.05.2018 16:58:00
-------------------------	---------------------	---------------------

Not Highlight

Page 30: [48] Formatted	Pieber Simone Maria	08.05.2018 16:58:00
-------------------------	---------------------	---------------------

Not Highlight

Page 30: [48] Formatted	Pieber Simone Maria	08.05.2018 16:58:00
-------------------------	---------------------	---------------------

Not Highlight

Page 30: [48] Formatted	Pieber Simone Maria	08.05.2018 16:58:00
-------------------------	---------------------	---------------------

Not Highlight

Page 30: [48] Formatted	Pieber Simone Maria	08.05.2018 16:58:00
-------------------------	---------------------	---------------------

Not Highlight

Page 30: [48] Formatted	Pieber Simone Maria	08.05.2018 16:58:00
-------------------------	---------------------	---------------------

Not Highlight

Page 30: [48] Formatted	Pieber Simone Maria	08.05.2018 16:58:00
-------------------------	---------------------	---------------------

Not Highlight

Page 30: [48] Formatted	Pieber Simone Maria	08.05.2018 16:58:00
-------------------------	---------------------	---------------------

Not Highlight

Page 30: [48] Formatted	Pieber Simone Maria	08.05.2018 16:58:00
-------------------------	---------------------	---------------------

Not Highlight

Page 30: [48] Formatted	Pieber Simone Maria	08.05.2018 16:58:00
-------------------------	---------------------	---------------------

Not Highlight

Page 30: [48] Formatted	Pieber Simone Maria	08.05.2018 16:58:00
-------------------------	---------------------	---------------------

Not Highlight

Page 30: [48] Formatted	Pieber Simone Maria	08.05.2018 16:58:00
-------------------------	---------------------	---------------------

Not Highlight

Page 30: [48] Formatted	Pieber Simone Maria	08.05.2018 16:58:00
-------------------------	---------------------	---------------------

Not Highlight

Page 30: [48] Formatted	Pieber Simone Maria	08.05.2018 16:58:00
-------------------------	---------------------	---------------------

Not Highlight

<b>Page 30: [48] Formatted</b>	<b>Pieber Simone Maria</b>	<b>08.05.2018 16:58:00</b>
--------------------------------	----------------------------	----------------------------

Not Highlight

<b>Page 30: [48] Formatted</b>	<b>Pieber Simone Maria</b>	<b>08.05.2018 16:58:00</b>
--------------------------------	----------------------------	----------------------------

Not Highlight

<b>Page 30: [48] Formatted</b>	<b>Pieber Simone Maria</b>	<b>08.05.2018 16:58:00</b>
--------------------------------	----------------------------	----------------------------

Not Highlight

<b>Page 30: [48] Formatted</b>	<b>Pieber Simone Maria</b>	<b>08.05.2018 16:58:00</b>
--------------------------------	----------------------------	----------------------------

Not Highlight

<b>Page 30: [48] Formatted</b>	<b>Pieber Simone Maria</b>	<b>08.05.2018 16:58:00</b>
--------------------------------	----------------------------	----------------------------

Not Highlight

<b>Page 30: [48] Formatted</b>	<b>Pieber Simone Maria</b>	<b>08.05.2018 16:58:00</b>
--------------------------------	----------------------------	----------------------------

Not Highlight

<b>Page 30: [48] Formatted</b>	<b>Pieber Simone Maria</b>	<b>08.05.2018 16:58:00</b>
--------------------------------	----------------------------	----------------------------

Not Highlight

<b>Page 30: [48] Formatted</b>	<b>Pieber Simone Maria</b>	<b>08.05.2018 16:58:00</b>
--------------------------------	----------------------------	----------------------------

Not Highlight

<b>Page 30: [48] Formatted</b>	<b>Pieber Simone Maria</b>	<b>08.05.2018 16:58:00</b>
--------------------------------	----------------------------	----------------------------

Not Highlight

<b>Page 30: [48] Formatted</b>	<b>Pieber Simone Maria</b>	<b>08.05.2018 16:58:00</b>
--------------------------------	----------------------------	----------------------------

Not Highlight

<b>Page 30: [48] Formatted</b>	<b>Pieber Simone Maria</b>	<b>08.05.2018 16:58:00</b>
--------------------------------	----------------------------	----------------------------

Not Highlight

<b>Page 30: [48] Formatted</b>	<b>Pieber Simone Maria</b>	<b>08.05.2018 16:58:00</b>
--------------------------------	----------------------------	----------------------------

Not Highlight

<b>Page 30: [48] Formatted</b>	<b>Pieber Simone Maria</b>	<b>08.05.2018 16:58:00</b>
--------------------------------	----------------------------	----------------------------

Not Highlight

<b>Page 30: [48] Formatted</b>	<b>Pieber Simone Maria</b>	<b>08.05.2018 16:58:00</b>
--------------------------------	----------------------------	----------------------------

Not Highlight

**Supporting Information:**

**Gas phase composition and secondary organic aerosol formation from standard and particle filter-retrofitted gasoline direct injection vehicles investigated in a batch and flow reactor**

**Gas phase composition and secondary organic aerosol formation from gasoline direct injection vehicles investigated in batch and flow reactors: effects of prototype gasoline particle filters.**

Simone M. Pieber<sup>1,\*</sup>, Nivedita K. Kumar<sup>1</sup>, Felix Klein<sup>1</sup>, Pierre Comte<sup>2</sup>, Deepika Bhattu<sup>1</sup>, Josef Dommen<sup>1</sup>, Emily A. Bruns<sup>1</sup>, Dogushan Kilic<sup>1,†</sup>, Imad El Haddad<sup>1</sup>, Alejandro Keller<sup>3</sup>, Jan Czerwinski<sup>2</sup>, Norbert Heeb<sup>4</sup>, Urs Baltensperger<sup>1</sup>, Jay G. Slowik<sup>1</sup> and André S. H. Prévôt<sup>1,\*</sup>

<sup>1</sup>Paul Scherrer Institute, ~~Laboratory of Atmospheric Chemistry~~, CH-5232 Villigen, Switzerland

<sup>2</sup>Bern University of Applied Sciences, CH-2560 Nidau, Switzerland

<sup>3</sup>Empa Material Science and Technology, CH-8600 Dübendorf, Switzerland

<sup>4</sup>University of Applied Sciences Northwestern Switzerland, CH-5210 Windisch, Switzerland

<sup>†</sup>Now at Istanbul Technical University, Eurasian Institute of Earth Sciences, 34467 Sariyer, Turkey

\*Correspondence to: [simone.pieber@psi.ch](mailto:simone.pieber@psi.ch), [andre.prevot@psi.ch](mailto:andre.prevot@psi.ch)

Supporting information contains Sections S1-S5, Figures S1-S16, and Tables S1-S4.

Formatted: German (Switzerland)

Formatted: Centered

### **S1. Emission Factors (EFs)**

Emission factors from batch experiments ~~are-were~~ calculated based on a carbon mass balance as described in (Platt et al., 2013); ~~and~~ (Platt et al., 2017) (Eq. (S1)), where  $P$  is the species of interest,  $\omega_C$  the carbon fraction (0.85) of the fuel and  $\text{CO}_2$  and CO, NMOC and eBC ~~are~~ in units of carbon mass.

$$EF = \frac{\Delta P}{\Delta \text{CO}_2 + \Delta \text{CO} + \Delta \text{NMOC} + \Delta \text{eBC}} * \omega_C \quad (\text{S1})$$

Regulatory emission factors from the test bench were provided in accordance with the ECE Regulation No. 83, ~~and use the a~~ fuel consumption of the vehicle in accordance with the ECE Regulation No. 101 and ~~the-an~~ effective fuel density (~~of~~ 0.75 kg L<sup>-1</sup>).

### **S2. Test bench instrumentation (extended)**

~~Gaseous components were monitored with an exhaust gas measuring system Horiba MEXA-9400H, including measurements of CO and CO<sub>2</sub> by infrared analyzers (IR), hydrocarbons by flame ionization detector (FID) for total hydrocarbon (THC) and non-methane hydrocarbon (NMHC) measurements, NO/NO<sub>x</sub> with a chemoluminescence analyzer (CLA) which was not heated and applicable only for diluted gas, and O<sub>2</sub> (Magnos). The dilution ratio in the CVS-dilution tunnel was variable and controlled by means of the CO<sub>2</sub>-analysis as described in the main text. Non-legislated gaseous emission components were analyzed by FTIR (Fourier Transform Infrared Spectrometer, AVL SESAM) at the exhaust tailpipe, offering time-resolved measurement of approx. 30 emission components, including NO, NO<sub>2</sub>, NO<sub>x</sub>, NH<sub>3</sub>, N<sub>2</sub>O, HCN, HNCO, HCHO. Number concentration of non-volatile particles was measured with condensation particle counters (CPC) behind a thermo-conditioner heating the sample to 300°C (following the requirements of the PMP- Particle Measurement Program of the ECE GRPE Group).~~

### **S3. Sampling materials and length**

- ~~• Tubing to sample direct emissions from the vehicle tailpipe for injection into the SC or online-OFR, or direct gas-phase measurements were made of SilcoTek®-coated steel (12 mm diameter), temperature controlled at 140°C and operated under high flows (30 L min<sup>-1</sup>) to avoid substantial losses over the sampling length of roughly 8 m. Ejector dilutor 1 was placed in a temperature controlled housing (200°C), and ejector dilutor 1 operated at 80°C.~~

Formatted: Page break before

Formatted: Not Highlight

Formatted: Centered

- Instruments sampling either from the SC, behind the OFR, or directly from the dilution system were connected via specific tubing for gas-phase and particle phase. Particle-phase tubing was made of stainless steel (6 mm diameter), and up to 2 m length. Support pumps were used at the instrument inlets, to minimize sampling residence time by increasing the flow rate. Total tubing length to reach all of the gas-phase instrument inlets, which were likewise equipped with support pumps was up to 2 m. Tubing was made of Teflon or SilcoTek®-coated steel. The sampling line of the PTR-ToF-MS instrument and FID was temperature controlled at 60°C.
- SilcoTek®-coating and Teflon are suitable for sampling of species known to be easily retained on surfaces, such as formaldehyde, acetic acid, acetaldehyde, for which otherwise, in addition to the uncertainties of PTR-ToF-MS analysis, also tubing losses could induce a shift in our gas-composition analysis.
- The sampling system between the SC and OFR (for OFR-from-SC experiments) was made of a combination of SilcoTek® coated steel and conductive Teflon tubing, suitable for simultaneous gas- and particle phase sampling. The total length between SC and OFR inlet was roughly 35 cm (6 mm diameter, ca. 8 L min<sup>-1</sup> flow). Additionally, all measurements from the dark SC batch sample were performed for at least 10 minutes, to reach a stable signal.

Formatted: Not Highlight

Formatted: Not Highlight

#### **S4. OFR data quality (OH exposure, non-OH losses and NO<sub>x</sub> influence)**

Several recent studies (Li et al., 2015);(Peng et al., 2016;Peng et al., 2015)) have estimated the contribution of alternative reaction processes in the OFR other than OH radical-induced ones in the OFRs across a range of operating conditions (residence time, water vapor availability, and external OH reactivity (OHR<sub>ext</sub>), which is the available OH-reactive material). These non-OH processes include reaction with photons (185 nm, 254 nm), and reactions with oxygen allotropes (excited oxygen atoms (O(<sup>1</sup>D)), ground state oxygen atoms (O(<sup>3</sup>P)), ozone (O<sub>3</sub>)) were identified as relevant loss processes to precursor molecules. Under certain operating conditions, also suppression of OH formation is critical. We applied a previously published model ((Peng et al., 2016;Peng et al., 2015)(Li et al., 2015);(Peng et al., 2016;Peng et al., 2015))) to estimate competing reaction with OH and loss of precursor molecules by non-OH sources, and estimated the influence of NO<sub>x</sub> based on (Peng and Jimenez, 2017)). Details on model input parameters are presented in the following:

Formatted: Subscript

(a) **OFR-from-SC** (see results in Figure S11~~Figure S11~~). As input to the model we used OHR<sub>ext</sub>=100 s<sup>-1</sup>, [O<sub>3</sub>]=1.97x10<sup>14</sup> molec cm<sup>-3</sup> (corresponding to 8 ppm at 100% UV intensity), a water mixing ratio=0.01 (1% absolute humidity, corresponding to 50% RH at 25°C) and a residence time=100 sec. O<sub>3</sub> measured at our reactor output for 70% UV intensity was 0.74x10<sup>14</sup> molec cm<sup>-3</sup> (3 ppm), and at 50% UV intensity 0.17x10<sup>14</sup> molec cm<sup>-3</sup> (0.7 ppm). OHR<sub>ext</sub> was calculated following Eq. (S2).

Formatted: Centered

$$OHR_{ext} = \sum_i (c_{NMOC,i} * k_{OH,NMOC,i});$$

$i=BENZ, TOL, XYL/EBENZ, C3-BENZ, CO, BuOH-D9$  (S2)

where  $k_{OH}$  of benzene (BENZ), toluene (TOL), xylene/ethylbenzene (XYL/EBENZ), C3-benzene (C3-BENZ) are given in Table 2 (main text); here we applied  $k_{OH,BENZ}=1.22 \times 10^{-12}$ ,  $k_{OH,TOL}=5.63 \times 10^{-12}$ ,  $k_{OH,XYL/EBENZ}=(7-23) \times 10^{-12}$ ,  $k_{OH,C3-BENZ}=(6-57) \times 10^{-12}$ ,  $k_{OH,CO}=1.5 \times 10^{-13}$  (from IUPAC, 2005),  $k_{OH,BuOH-D9}=3.4 \times 10^{-12}$  (from Barmet et al., 2012); all in  $\text{cm}^3 \text{ molec}^{-1} \text{ s}^{-1}$  and used a concentration average of expt A1 of  $c_{BENZ}=4 \times 10^{11}$ ,  $c_{TOL}=1 \times 10^{12}$ ,  $c_{XYL/EBENZ}=8 \times 10^{11}$ ,  $c_{C3-BENZ}=2 \times 10^{11}$ ,  $c_{CO}=(3-7) \times 10^{14}$ ,  $c_{BuOH-D9}=(3.7-7.4) \times 10^{11}$ ; all in  $\text{molec cm}^{-3}$  as input. This results in an  $OHR_{ext}$  of  $\sim 70-100 \text{ s}^{-1}$ . Based on these input parameters, the model from (Li et al., 2015) and (Peng et al., 2016; Peng et al., 2015) (Peng et al., 2016) predicted an  $[OH]_{\text{exposure}}$  (OH concentration integrated over time, see discussion in main text "OH exposure estimation", in  $\text{molec cm}^{-3} \text{ s}$ ) in the OFR as follows:

UV100%:  $[OH]_{\text{exposure}}=(10-13) \times 10^{11}$   
 UV70%:  $[OH]_{\text{exposure}}=(2.4-3.1) \times 10^{11}$   
 UV50%:  $[OH]_{\text{exposure}}=(0.35-0.48) \times 10^{11}$ .

The estimated  $[OH]_{\text{exposure}}$  (in  $\text{molec cm}^{-3} \text{ s}$ ) and OH concentration (in  $\text{molec cm}^{-3}$ ),  $[OH]$ , based on the experimental measurements of the decay of BuOH-D9 correspond instead to

UV100%:  $[OH]_{\text{exposure}}=(3.0-5.8) \times 10^{11}$ , i.e.  $[OH]=(2.7-5.2) \times 10^9$   
 UV70%:  $[OH]_{\text{exposure}}=(1.6-2.5) \times 10^{11}$ , i.e.  $[OH]=(1.4-2.2) \times 10^9$   
 UV50%:  $[OH]_{\text{exposure}}=(0.31-0.49) \times 10^{11}$ , i.e.  $[OH]=(0.28-0.44) \times 10^9$

The ratio of OH (measured) to  $O_3$  (measured) remained relatively constant at our test points ( $OH/O_3$  at 100%:  $(1.4-2.6) \times 10^{-5}$ ,  $(1.9-3.0) \times 10^{-5}$  at 70%,  $(1.7-2.6) \times 10^{-5}$  at 50%). The corresponding OH information derived from measurements in the SC was an  $[OH]_{\text{exposure}}$  of  $1.4 \times 10^{11} \text{ molec cm}^{-3} \text{ s}$  at the maximum aging time (after around 2 hours), at a constant  $[OH]=2 \times 10^7 \text{ molec cm}^{-3}$ .

Non-OH loss analysis (Figure S11) predicts predicted losses of aromatic hydrocarbons as SOA precursors to up to between 10-15 and 25% by UV185 nm and UV254 nm, but no impact of  $O_3$ , (neither  $O(^1D)$  or  $O(^3P)$ ) for the OFR-from-SC conditions. This only refers to the reactive interaction of OH vs. the excitation by UV, and does not allow conclusions on the formation of SOA. Also chemistry initiated by UV185 or UV254 may lead to the formation of SOA, and likewise

Formatted: Not Highlight

Field Code Changed

Formatted: Not Highlight

Field Code Changed

Formatted: Not Highlight

Formatted: Centered

photons may also destruct OH-formed SOA; both processes deserve attention in future research. Additionally, it does not suggest any conclusions allow conclusions about the interaction of O<sub>3</sub> with double bonds made available by first ring-opening reactions, and. However, as our results suggest that yields and O:C ratios between OFR and SC compare well, we believe that the additional impact of photolysis and O<sub>3</sub> on the initial SOA precursors in the OFR is negligible in our OFR from SC experiments. Potential effects of O<sub>3</sub> on first generation products potential effects are not taken into account. Under those our diluted conditions (initial NO < 100 ppb), we regard the experiments in OFR as low NO conditions as defined by (Peng and Jimenez, 2017). The dominant SOA precursors found in the exhaust are not reactive towards NO<sub>3</sub> radicals that can be formed in the OFR; potential effects on first generation products are were not taken into account, however. A full discussion of this issue is was presented by in (Peng and Jimenez, 2017), who state that under conditions with several hundreds of ppb of NO, an NO<sub>3</sub>exposure-to-OH<sub>exposure</sub> of 0.1-1 may be reached, with potential impacts under which on first generation oxidation products (such as phenolic compounds) might be impacted.

(b) **Time-Resolved OFR** (see results in Figure S12 Figure S12). As input to the model we used OHR<sub>ext</sub>=1000 s<sup>-1</sup> (for experiments conducted with 1 dilution step, 2014) and OHR<sub>ext</sub>=100 s<sup>-1</sup> for experiments with 2 dilution steps (2015), [O<sub>3</sub>]=1.97x10<sup>14</sup> molec cm<sup>-3</sup>, a water mixing ratio=0.005 (0.5% absolute humidity, corresponding to ~20% RH at 25°C) and a residence time=100 s. Based on these parameters, the model (Peng et al., 2016) predicts predicted an [OH]<sub>exposure</sub>=(5.9)x10<sup>10</sup> molec cm<sup>-3</sup> s. For the 2015 experiments (OHR<sub>ext</sub>=100 s<sup>-1</sup>); results the conditions discussed in from (a) applied apply (Figure S11 Figure S11). Due to the lower dilution ratio in the time-resolved OFR experiments in 2014, however, a significant fraction of the emissions (up to 50-60% of the ArHC) are might be lost with UV185 and UV254 nm radicals instead of OH, as a high OHR<sub>ext</sub> leads to OH suppression in the reactor, making non-OH processes relatively more important. Also O(<sup>1</sup>D) and O(<sup>3</sup>P) reduce ArHC by ca 10-20% under these conditions (Figure S12 Figure S12). Potential effects of O<sub>3</sub> on first generation products are not taken into account analogously to (a). As detailed in (Peng and Jimenez, 2017), the NO<sub>x</sub>/VOC ratio is a function of the driving cycle. Under conditions with insufficient dilution during time-resolved measurements conducted in 2014, we additionally cannot exclude the influence of NO and NO<sub>3</sub> during simulated photochemical aging, as NO levels had reached “a few ppm levels” during the initial phases of the test cycles. During time-resolved measurements conducted in 2015 (double dilution), NO levels were on the order of a few hundreds of ppb and based on this we estimate no significant impact on our 2015 time-resolved SOA profiles, as well as or the integrated SOA mass on first generation products. Again, for a full discussion of this issue please refer to (Peng and Jimenez, 2017), who state that under conditions with several hundreds of ppb of NO, an NO<sub>3</sub>exposure-to-OH<sub>exposure</sub> of 0.1-1 may be reached, with potential impacts on first generation oxidation products (such as phenolic compounds).

**Quantitative use of OFR data (OFR-from-SC and time-resolved OFR).** ~~The~~ SOA yields analysis in the main text is based on SC and OFR-from-SC experiments only. SOA emission factors (EF) are calculated ~~based on SC and mainly from~~ OFR-from-SC experiments, ~~and~~. ~~Additionally,~~ time-resolved data from 2015 collected with GDI4 were integrated to derived EFs labelled “Online, OFR100%” ~~in the main text~~ (Sections 3.1, 3.2 and 3.4, ~~and main text~~ Figures 2b, Figure 4) and ~~are were~~ comparable to data derived from GDI4 SC experiments. Time-resolved SOA data from 2014 ~~instead were are~~ not used quantitatively herein, due to instabilities with the OH exposure throughout the driving cycle (lower OH exposure during high emissions period as well as ~~potential~~ impacts by photolysis and competing non-OH processes (i.e. high external OH reactivity ( $\text{OHR}_{\text{ext}}$ , see Figure S12, ~~as well as~~ ((Peng et al., 2015); (Peng et al., 2016); (Li et al., 2015)) ~~and, and potential~~ changing  $\text{NO}_x$  levels in the emissions as a function of driving cycle with potential impacts on the oxidation regime (high vs. low  $\text{NO}_x$  levels, ~~see~~ (Peng and Jimenez, 2017)) ~~as discussed above~~). While these processes limited the use of time-resolved data collected in 2014 due to the low dilution ratio that was applied (only one-fold dilution, i.e. 1 ejector dilutor, 1:8, and additional 1:2 at OFR entrance) and the resulting high  $\text{OHR}_{\text{ext}}$  ( $>1000 \text{ s}^{-1}$ , see Eq. S2, and  $\text{NO}_x$  levels), data from 2015 ~~are were~~ not significantly impacted. ~~For data from 2015~~ (an example is given in Figure S14 for GDI4 in standard configuration and w/catGPF), ~~as~~ such experimental artefacts were reduced by use of a higher dilution ratio (2 ejector dilutors in series, 2x 1:8 and additional 1:2 at OFR entrance,  $\text{OHR}_{\text{ext}}$  on the order of  $100 \text{ s}^{-1}$ ). ~~We would like to add that~~ ~~W~~while we don't rely on an absolute quantitative use of our time-resolved data from 2014, the relative ~~time-resolved profile~~ ~~(dominated by cold start)~~ holds true regardless of these effects and ~~is was also~~ confirmed in the 2015 data set (Figure S14) ~~showing the same trends~~ ~~(largest SOA formation observed at cold engine start)~~. ~~Future work should investigate the quantitative use of online OFR data in further detail for additional quantification of cold- and hot-start contribution of SOA to the total SOA burden; a discussion of the associated technical issues (i.e. changes in OH-exposure and condensational sink as well as the equilibration time inside the OFR reactor) has been recently published by~~ (Zhao et al., 2018).

Field Code Changed

Formatted: Font color: Auto, Not Highlight

Field Code Changed

### **S5. $\text{O}_2^+$ charging and fragmentation in the PTR-ToF-MS**

~~While the primary ionization pathway in the PTR-ToF-MS is proton transfer reaction by  $\text{H}_3\text{O}^+$  ions, the ion source produced~~ up to 5% of unwanted  $\text{O}_2^+$ .  $\text{O}_2^+$  can lead to charge transfer or hydride abstraction reactions (Amador Muñoz et al., 2016; Jordan et al., 2011; Knighton et al., 2009). Signals at  $[\text{C}_6\text{H}_6]^+$  ( $m/z$  78),  $[\text{C}_7\text{H}_8]^+$  ( $m/z$  92) and  $[\text{C}_8\text{H}_{10}]^+$  ( $m/z$  106) likely derive from  $\text{O}_2^+$  charged ions of aromatic hydrocarbons (ArHC), and were hence excluded from the analysis of the total mass. However, they supported peak identification by correlation with their corresponding protonated ion at ~5% of the protonated signal. Other ions derived from  $\text{O}_2^+$  ionization were insignificant contributors to the total mass.

Formatted: Indent: First line: 0 cm

Frequently,  $[\text{C}_3\text{H}_5]^+$  and  $[\text{C}_3\text{H}_7]^+$  are considered fragments of oxygenated parent molecules. In our experiments, however, these ions may dominantly derive from propene ( $\text{C}_3\text{H}_6$ ), for which protonation led to  $[\text{C}_3\text{H}_6+\text{H}]^+$ , and a subsequent loss of  $\text{H}_2$  led to  $[\text{C}_3\text{H}_5]^+$ . The observed ratio of  $[\text{C}_3\text{H}_5]^+$  and  $[\text{C}_3\text{H}_7]^+$  was consistent with the ratio seen for pure propene ( $\text{C}_3\text{H}_6$ ) injected into the instrument as reference (Figure S15). In analogy to  $\text{O}_2^+$  ionization of ArHC, we found  $[\text{C}_3\text{H}_6]^+$  in the

Formatted: Centered

5 spectra as insignificant signal (5% of  $[C_3H_6+H]^+$ ). It is likely related to an  $O_2^+$  charge transfer to propene (Amador Muñoz et al., 2016; Jordan et al., 2011; Knighton et al., 2009), and supported the peak identification. The fuel contained 5%<sub>vol.</sub> (2014) to 8%<sub>vol.</sub> (2015) of methyl-tert-butyl-ether (MTBE), as an anti-knocking agent. Fragmentation by proton transfer reactions of MTBE can lead to a significant signal at  $m/z$  57 ( $[C_4H_9]^+$ ). Protonated butene would also yield  $[C_4H_9]^+$ , but analogous to the ArHC and propene, should also give a correlated signal at  $[C_4H_8]^+$  at approximately 5% of  $[C_4H_9]^+$ , which we did not observe.

10 The fragmentation process of alkyl-substituted mono-aromatics would result into a significant mass loss, as the aromatic ring would remain predominantly neutral (especially for mono-aromatics with long alkyl-substituents following Gueneron et al., 2015). For example, only 22% of the ion signal generated from n-pentylbenzene fragmentation retains the aromatic ring (19%  $M+H^+$ , 3% protonated benzene ring), and 88% is found at non-aromatic ions  $m/z$  41 or 43). Alkyl-substituted monocyclic aromatics might hence (together with long-chain aliphatic compounds which might also substantially fragment) be significant contributors to the missing carbon mass (on average 35%), based on a comparison of FID-based and PTR-ToF-MS based measurements.

SI Figures (Supporting Information)



Figure S12. Pictures of a) original “muffler” and GPF in comparison, b) retrofitted GPF, installed underfloor in replacement to “muffler”.

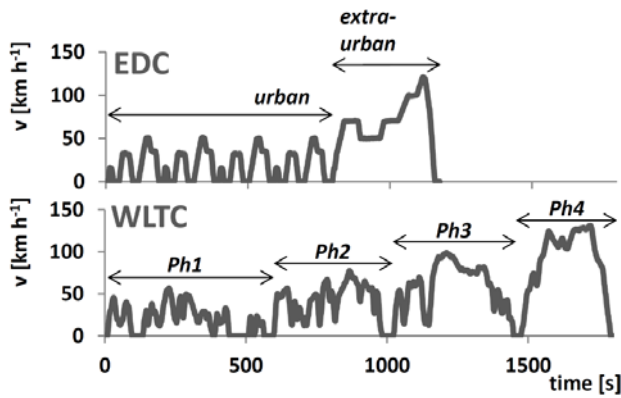


Figure S2. Speed profile of regulatory driving tests. Speed profile ( $v$ , in  $\text{km h}^{-1}$ ) versus test time (in seconds) of EDC (new European driving cycle, top) and WLTC (world-wide light duty test cycle, class-3, bottom). While the EDC is characterized by two phase (an urban, and an extra-urban phase of highly repetitive characteristics) and lasts 20 min, the WLTC (class-3) is characterized by four phases at different speed levels (referred to as Phase (Ph) 1-4, or low, medium, high, and extra-high speed, respectively); it contains patterns of disruptive acceleration and deceleration, and lasts 30 min. The WLTC is believed to represent typical driving conditions around the world and was developed based on combination of collected in-use data and suitable weighting factors by an expert group from China, EU, India, Japan, South Korea, Switzerland and the USA.

Formatted: No page break before

Formatted: Centered, No page break before

Formatted: Font: Not Bold

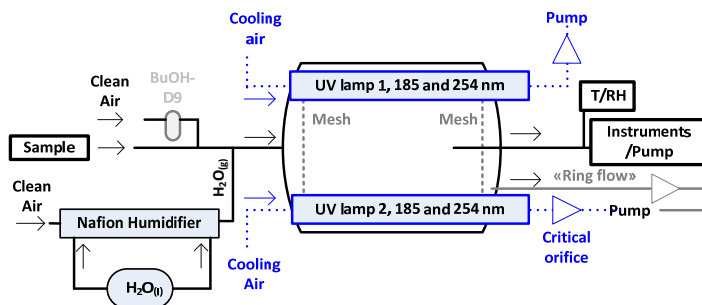
Formatted: Caption

Field Code Changed

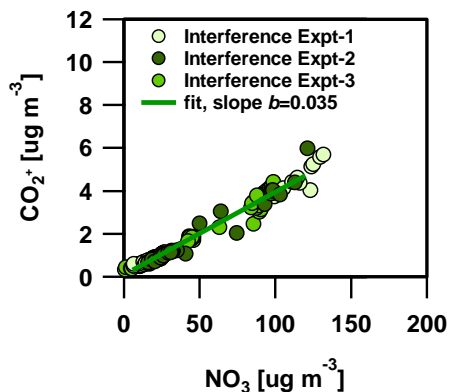
Formatted: Font: Not Bold

Formatted: Font: Not Bold

Formatted: Centered



5 **Figure S31. OFR schematic (not to scale).** The OFR version deployed here was previously described in (Bruns et al., 2015). The reactor is a 0.015 m<sup>3</sup>, cylindrical glass chamber (0.46 m L, 0.22 m diameter) flanked by two UV lamps on the upper part of the reactor, each with discrete emission lines at 185 and 254 nm (BHK Inc.). The lamps are cooled by a constant flow of air, or N<sub>2</sub>. The incoming reactant flow is radially dispersed in the OFR by passing through a perforated mesh screen at the inlet flange. The flow through the OFR is determined by the flow pulled by instruments and pumps behind the reactor. The reactor is equipped with an injection system for water vapor (H<sub>2</sub>O) and NMOs (notably BuOH-D9, and selected precursor for single molecule testing). Water vapor is provided via a Nafion humidifier. Air is passing on one side of the Nafion membrane, collecting water vapor from the liquid on the other side of the membrane. In addition, other chemicals, such as BuOH-D9 (used as an OH tracer) can be injected by passing a small stream of clean air through a vial containing the liquid NMO.



15 **Figure S43. Ammonium nitrate (NH<sub>4</sub>NO<sub>3</sub>) interference on CO<sub>2</sub><sup>+</sup>** (Pieber et al., 2016). The CO<sub>2</sub><sup>+</sup> signal (RIE=1) vs the NO<sub>3</sub> signal (RIE=1) from pure ammonium nitrate (NH<sub>4</sub>NO<sub>3</sub>) aerosol with d<sub>m</sub>=400 nm from 3 calibration experiments. An orthogonal distance least squares fit yields a slope of b=0.035. Corrections were applied via the fragmentation table as noted in the main text.

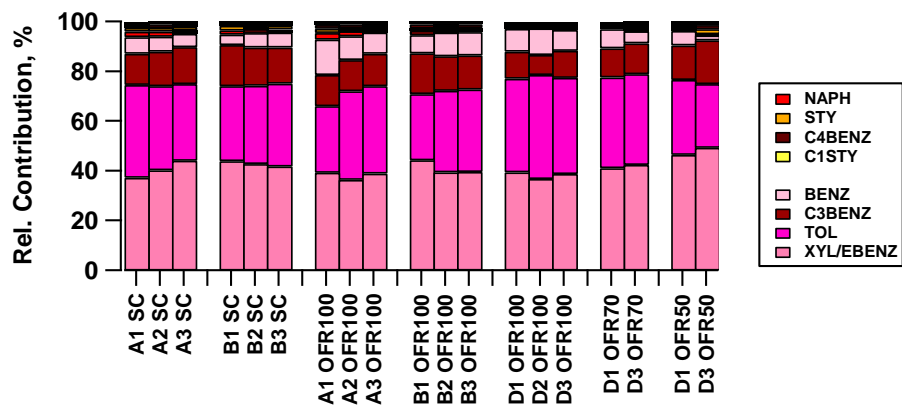
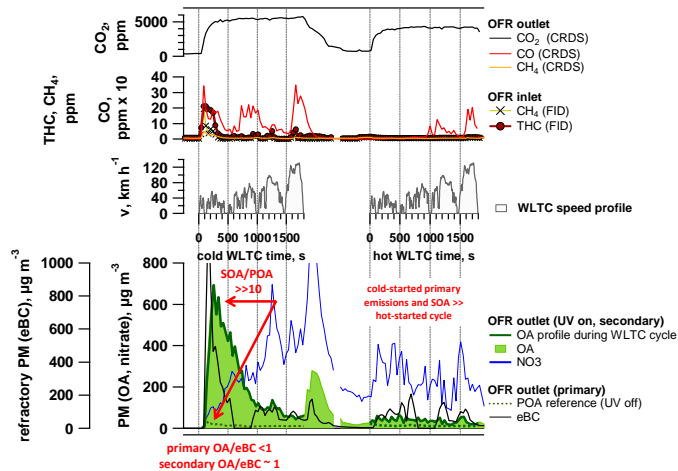


Figure S54. Reacted NMOC fraction in the SC (at t=2h after UV on), and the OFR at 100, 70 and 50% UV intensity (8 dominant ArHC). A-D identifiers refer to individual experiments (GDI 1 only). The max-final OH exposure in the SC compares to an OH exposure of the OFR at 50-70% UV setting.

5

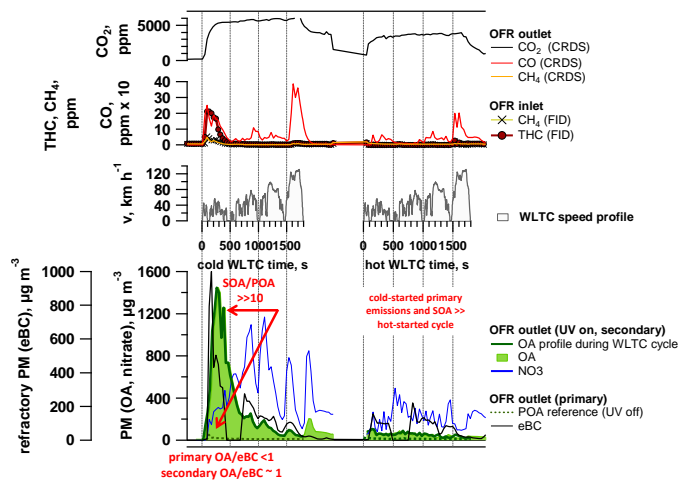
Formatted: Page break before

Formatted: Centered



5 **Figure S65.** Time-resolved aging of emissions (WLTC) (GD11, standard configuration, Expt A1). Cold and hot started WLTC of vehicle GD11 (standard configuration). CO<sub>2</sub>, CO, CH<sub>4</sub> (as measured by CRDS), THC and CH<sub>4</sub> (as measured by FID, note that the THC signal reaches its range limit at 20 ppm) are presented, together with organic aerosol (primary (denoted POA) and total (POA+SOA), denoted as OA. "OA profile during WLTC" highlights the measurement during the driving cycle, whereas OA shows the extended signal taking into account a delay due to the OFR residence time. Secondary nitrate aerosol (inorganic, ammonium nitrate, displayed is only NO<sub>3</sub>), and primary equivalent black carbon (eBC). Note: data in these graphs are not normalized to CO<sub>2</sub>, and have slightly different dilution ratios between cold- and hot-started cycle, as indicated by the CO<sub>2</sub> time-trace. Data reflect measured concentrations; no dilution corrections are applied. CRDS was diluted by a factor of 10 compared to FID and particle phase measurements.

10



5 **Figure S76.** Time-resolved aging of emissions (WLTC) (GD11, standard configuration, Expt A2, extended version of main text Figure 3). Cold and hot started WLTC of vehicle GDH (standard configuration). CO<sub>2</sub>, CO, CH<sub>4</sub> (as measured by CRDS), THC and CH<sub>4</sub>

5

(as measured by FID, note that the THC signal reaches its range limit at 20 ppm) are presented, together with organic aerosol (primary (denoted POA) and total (POA+SOA), denoted as OA. "OA profile during WLTC cycle" highlights the measurement during the driving cycle, whereas OA shows the extended signal taking into account a delay due to the OFR residence time. Secondary nitrate aerosol (inorganic, ammonium nitrate, displayed is only NO<sub>3</sub>), and primary equivalent black carbon (eBC). Note: data in these graphs are not normalized to CO<sub>2</sub>, and have slightly different dilution ratios between cold and hot started cycle, as indicated by the CO<sub>2</sub> time trace. Data reflect measured concentrations; no dilution corrections are applied. CRDS was diluted by a factor of 10 compared to FID and particle phase measurements. See Figure S6 caption for further details.

Formatted: Font: Not Bold

Field Code Changed

Formatted: Centered

Formatted: Page break before

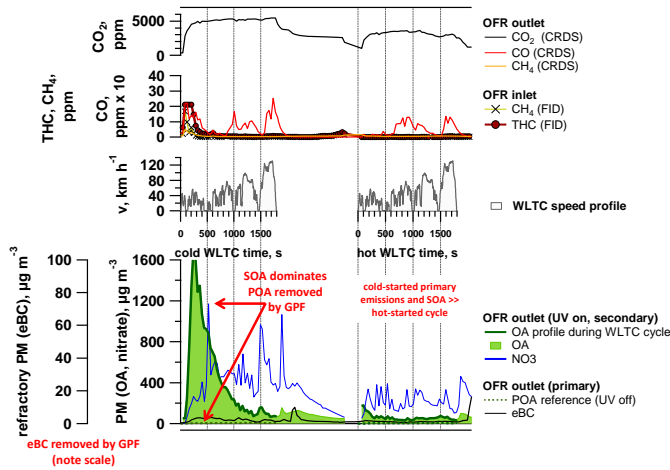
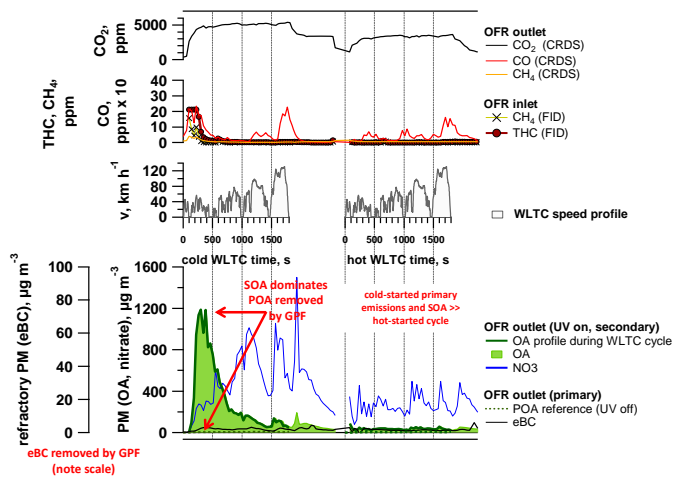


**Figure S87.** Time-resolved aging of emissions (WLTC) (GDI1 w/ GPF, Expt B1). Cold and hot started WLTC of vehicle GDI1 (w/GPF). CO<sub>2</sub>, CO, CH<sub>4</sub> (as measured by CRDS), THC and CH<sub>4</sub> (as measured by FID, note that the THC signal reaches its range limit at 20 ppm) are presented, together with organic aerosol (primary (denoted POA) and total (POA+SOA), denoted as OA. "OA profile during WLTC cycle" highlights the measurement during the driving cycle, whereas OA shows the extended signal taking into account a delay due to the OFR residence time. Secondary nitrate aerosol (inorganic, ammonium nitrate, displayed is only NO<sub>3</sub>), and primary equivalent black carbon (eBC). Note: data in these graphs are not normalized to CO<sub>2</sub>, and have slightly different dilution ratios between cold and hot started cycle, as indicated by the CO<sub>2</sub> time trace. Data reflect measured concentrations; no dilution corrections are applied. CRDS was diluted by a factor of 10 compared to FID and particle phase measurements. See Figure S6 caption for further details.

Formatted: Font: Not Bold



Formatted: Centered

5

**Figure S98. Time-resolved aging of emissions (WLTC) (GDI1 w/ GPF, Expt B2).** Cold and hot started WLTC of vehicle-GDI1 (w/GPF). CO<sub>2</sub>, CO, CH<sub>4</sub> (as measured by CRDS), THC and CH<sub>4</sub> (as measured by FID, note that the THC signal reaches its range limit at 20 ppm) are presented, together with organic aerosol (primary (denoted POA) and total (POA+SOA), denoted as OA. "OA profile during WLTC cycle" highlights the measurement during the driving cycle, whereas OA shows the extended signal taking into account a delay due to the OFR residence time. Secondary nitrate aerosol (inorganic, ammonium nitrate, displayed is only NO<sub>3</sub>), and primary equivalent black carbon (eBC). Note: data in these graphs are not normalized to CO<sub>2</sub>, and have slightly different dilution ratios between cold and hot started cycle, as indicated by the CO<sub>2</sub> time-trace. Data reflect measured concentrations; no dilution corrections are applied. CRDS was diluted by a factor of 10 compared to FID and particle phase measurements. See Figure S6 caption for further details.

Formatted: Font: Not Bold

Formatted: Centered

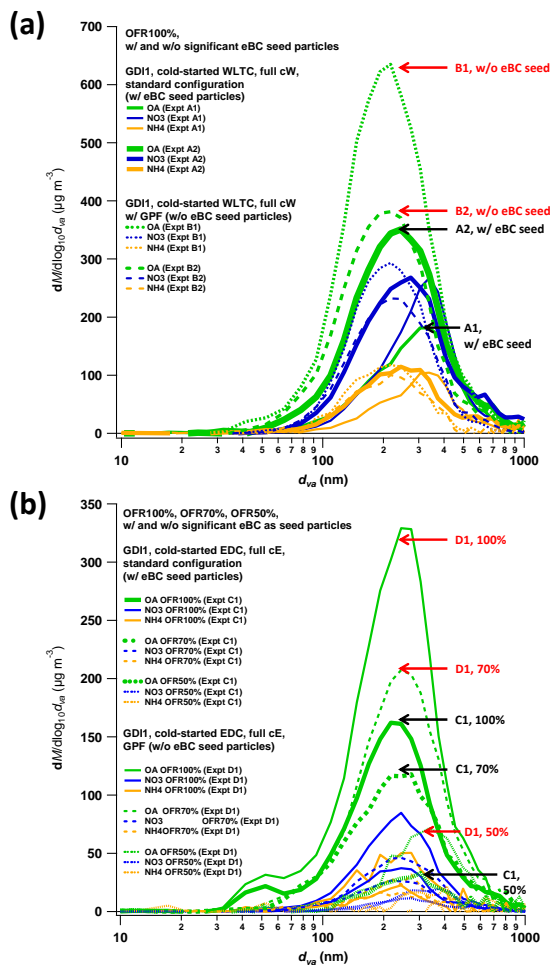


**Figure S109.** Particle size distributions for experiments from (a) WLTC and (b) EDC, measured behind the OFR-from-SC. All expts are OFR-from-SC tests leading to typically  $200 \mu\text{g m}^{-3}$  ( $\sim 100\text{-}500 \mu\text{g m}^{-3}$ ) SOA formed at 100%, down to  $\sim 50 \mu\text{g m}^{-3}$  for 50% UV conditions. Expt A-D are identifiers for experiments referring to [Table S4](#), [Table S4](#).

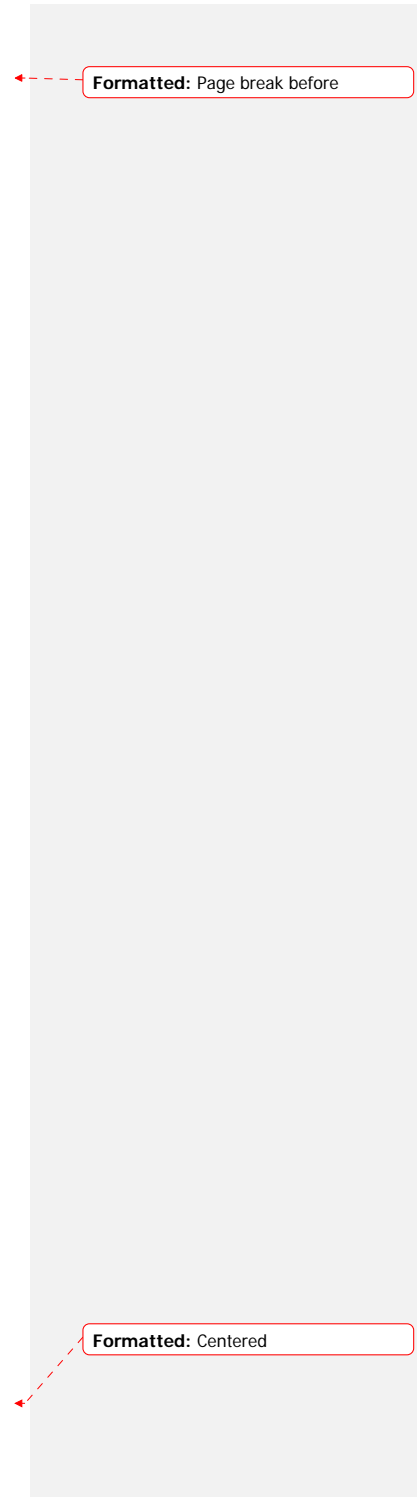
Formatted: Page break before

Formatted: Font: Not Bold, English (U.S.)

Formatted: No page break before

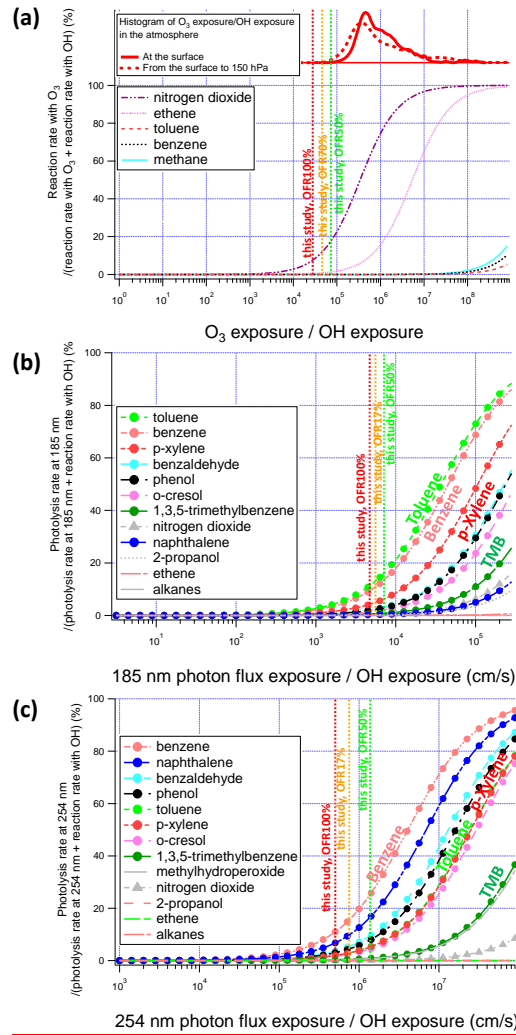
Formatted: Centered

|



**Formatted:** Page break before

**Formatted:** Centered



Formatted: Centered

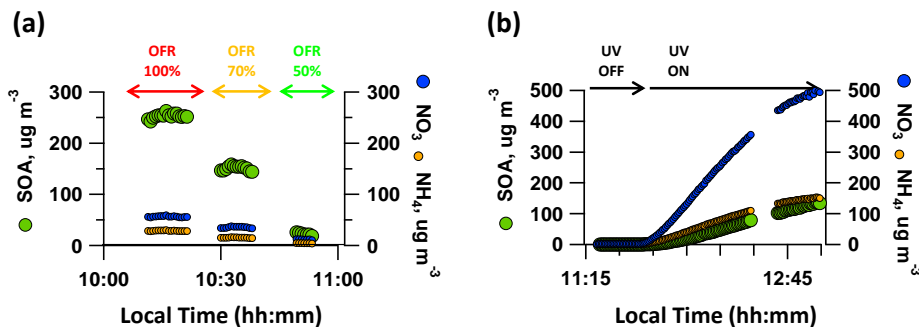


**Figure S10. Bulk aerosol composition: OA, nitrate (denoted NO<sub>3</sub>) and ammonium (denoted NH<sub>4</sub>).** Example of experiments in (a) OFR from-SC at varied UV intensities (Expt A1), local time in 30-min intervals, (b) SC (Expt B1), local time in 15-min intervals.

5 **Figure S114. OFR-from-SC and Online OFR 2015: non-OH loss estimation (Peng et al. OFR model by (Peng et al., 2016); settings: "OFR185 Option 2").** Results are presented for OFR-from-SC Expts at 100% UV intensity, i.e. [OH]= 2.7-5.2 10<sup>9</sup> molec cm<sup>-3</sup>. (a) O<sub>3</sub>, (b) 185 nm, (c) 254 nm; please refer to Peng et al. for the legend. (Peng et al., 2016). Input parameters to "2016-10-12\_OFRExposures\_Estimator\_v2.3": OHR<sub>ext</sub>=100 s<sup>-1</sup>, [O<sub>3</sub>]=1.97 x 10<sup>14</sup> molec cm<sup>-3</sup> (at 100%), [O<sub>3</sub>]=0.74 x 10<sup>14</sup> molec cm<sup>-3</sup> (at 70%), [O<sub>3</sub>]=0.17 x 10<sup>14</sup> molec cm<sup>-3</sup> (at 50%), water mixing ratio = 0.01 (1% absolute humidity), residence time=100 sec.

Formatted: Indent: Left: 0 cm

Formatted: Not Highlight

Formatted: Not Highlight

Formatted: Centered

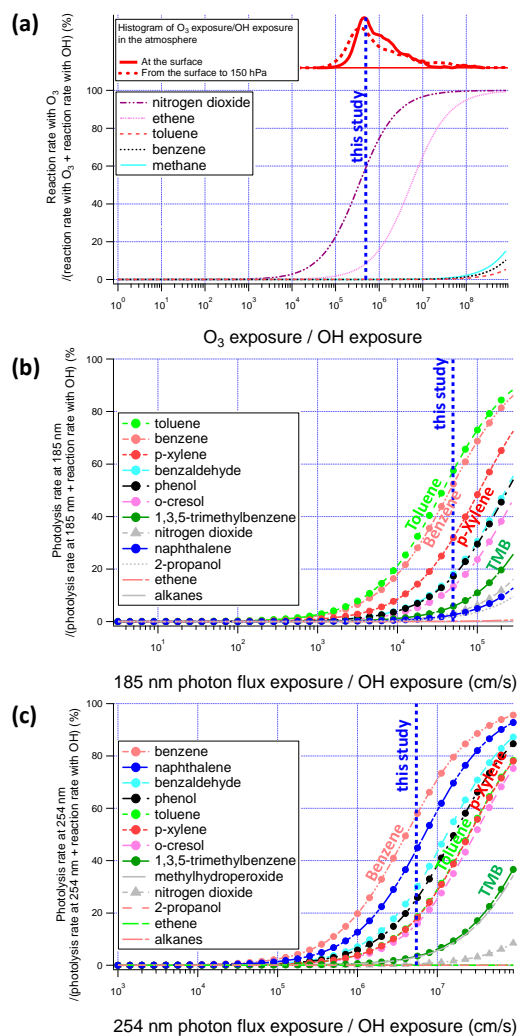
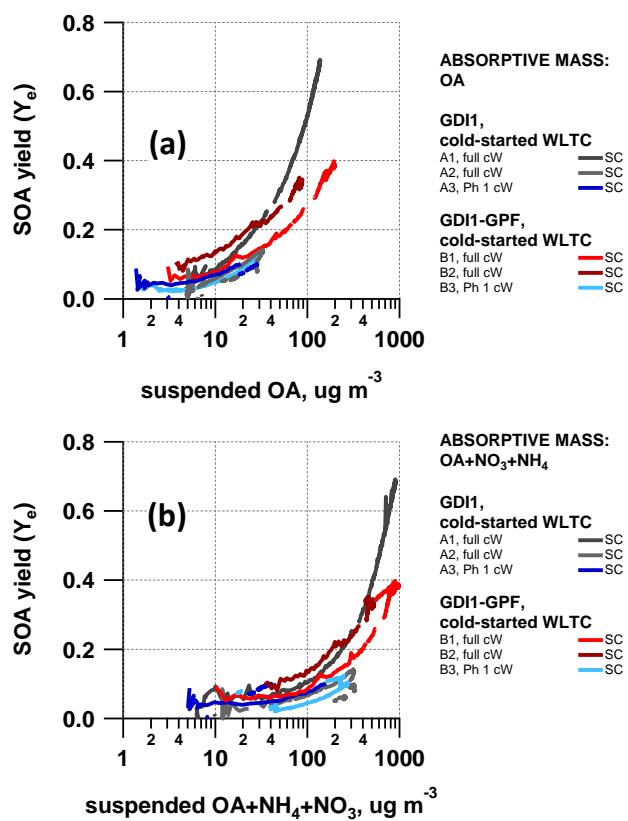


Figure S124. Online OFR 2014: Non-OH loss estimation (OFR model by (Peng et al., 2016); settings: "OFR185 Option 2")(Peng et al. OFR model (Peng et al., 2016)). Time-resolved OFR Expts at 100% UV intensity (GD11, 1 ejector dilution). (a)  $O_3$ , (b) 185 nm, (c) 254 nm; please refer to Peng et al. for the legend (Peng et al., 2016). Input parameters to "2016-10-12\_OFRe\_Exposures\_Estimator\_v2.3": OH<sub>ext</sub>=1000 s<sup>-1</sup>, [O<sub>3</sub>]=1.97x10<sup>14</sup> molec cm<sup>-3</sup>, water mixing ratio=0.005 (0.5% absolute humidity), residence time=100 s; model-predicted OH-exposure=(5.9)x10<sup>10</sup> molec cm<sup>-3</sup> s.



5  
10  
**Figure S1313.** Effective SOA yields from SC experiments with different assumptions of absorptive mass. (a) Yields as a function of suspended OA concentration, and (b) as a function of the sum of OA, HR-ToF-AMS derived ammonia (NH<sub>4</sub>) and nitrate (NO<sub>3</sub>), assuming that NH<sub>4</sub>NO<sub>3</sub> acts as additional absorptive mass. Identifiers (A1-A3, B1-B3) allow retrieving the SC experimental conditions for each experiment from Table S4-S7.

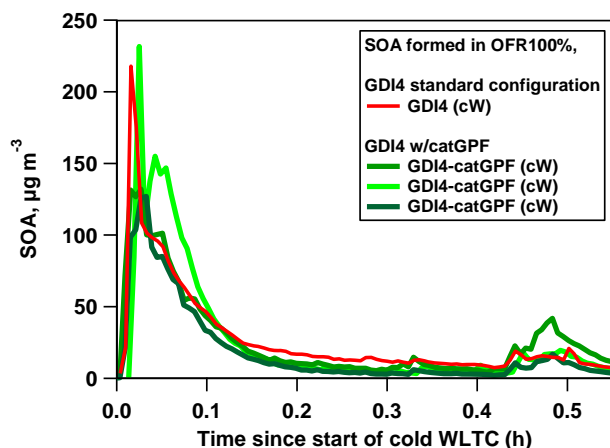


Figure S144. Time-resolved SOA from GDI4 in standard configuration and equipped with a prototype, catalytically active GPF. SOA was generated by exposure of emissions to photochemistry in the OFR during cold-started WLTC test bench experiments.

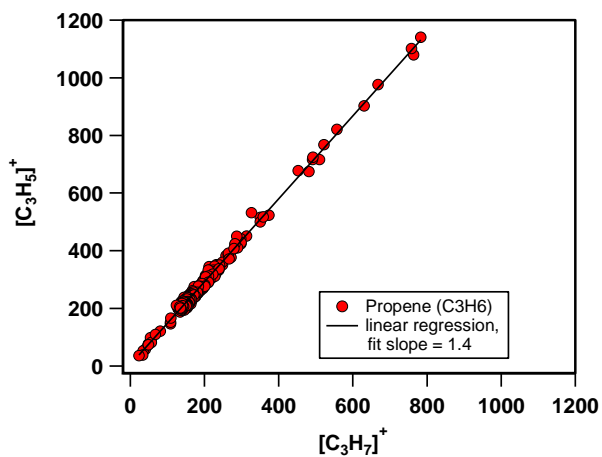
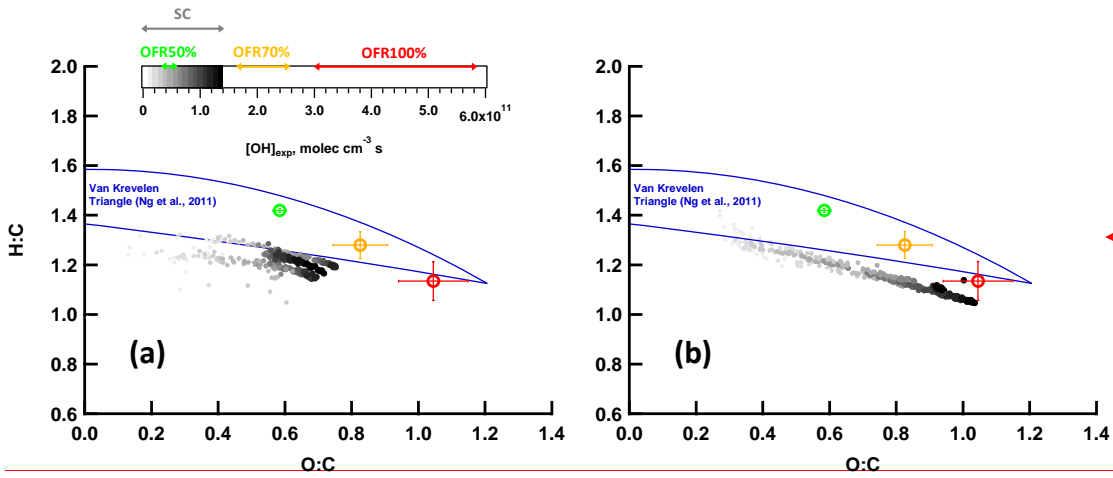


Figure S145. Propene fragmentation ratio in the PTR-ToF-MS. Measurements were conducted at a concentration of around 0-150 ppbv propene ( $C_3H_6$ ), as measured by the FID instrument.

Formatted: Page break before

Formatted: Font: Not Bold

Formatted: Centered



Formatted: Page break before

Formatted: Centered

**Figure S16. Bulk OA composition of SC and OFR SOA as presented in the main text (Figure 7), here split into (a) SC Expt (2014-05-21, -23, -28, i.e. A2, A3, B3, n=3) and (b) SC Expt (2014-05-20, -26, -27, i.e. A1, B1, B2, n=3).** Please refer to the figure legend and the caption in the main text, as well as see also Supporting Information, Table S4-S7, for SC experimental conditions.

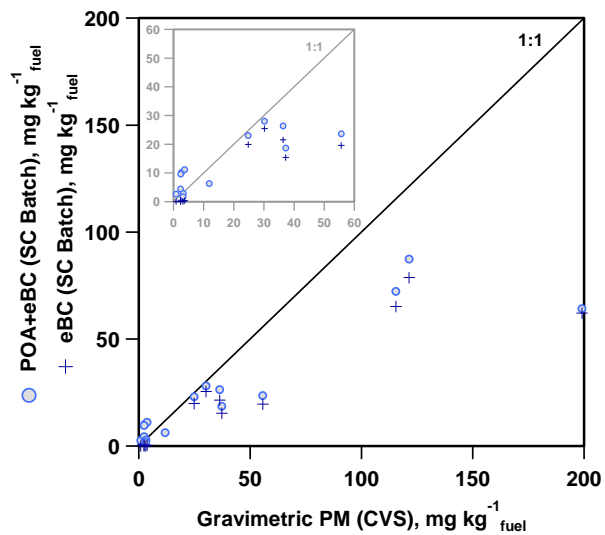


Figure S1616. POA and eBC measurements in the SC batch sample compared to gravimetric PM measurements from the CVS (a zoomed-in version is embedded in the figure).

Formatted: Font: Not Bold

Formatted: Centered

### 3 Tables (SI Tables Supporting Information)

Table S1. Vehicle specifications.

Parameters	GDI1	GDI2	GDI3	GDI4
Vehicle Type	Opel Insignia 1.6 EcoFlex	Opel Zafira Tourer	VW Golf Plus	Volvo V60 T4F
Engine code	A16XHT	A16XHT	CAV	B4164T2
Cylinder (number/ arrangement)	4 / in line	4 / in line	4 / in line	4 / in line
Displacement, cm <sup>3</sup>	1598	1598	1390	1596
Power, kW	125 @ 6000 rpm	125 @ 6000 rpm	118 @ 5800 rpm	132 @ 5700 rpm
Torque, Nm	260 @ 1650-3200 rpm	260 @ 1650 - 3200 rpm	240 @ 1500 rpm	240 @ 1600 rpm
Injection type	DI	DI	DI	DI
Curb weight, kg	1701	1678	1348 - 1362	1554
Gross vehicle weight, kg	2120	2360	1960 - 1980	2110
Drive wheel	Front-wheel drive	Front-wheel drive	Front-wheel drive	Front-wheel drive
Gearbox	m6	m6	m6	a6
First registration	2014	22.07.2014	01.02.2010	27.01.2012
Exhaust	EURO 5b+	EURO 5b+	EURO 4	EURO 5a
VIN	YV1FW075BC1043598	WOLPD9E20E2096446	WVWZZZ1KZ9W844855	YV1FW075BC1043598

Formatted Table

Table S2. Gas-phase instrumentation.

Gas phase Instruments	Measured Parameter	Manufacturer	Lower limit (or Range)
Picarro Cavity Ring-Down Spectrometer G2401	CO <sub>2</sub> + CO + CH <sub>4</sub> + H <sub>2</sub> O	Picarro	0-1000 ppmC (CO <sub>2</sub> ) 0-5 ppmC (CO) 0-20 ppmC (CH <sub>4</sub> ) 0-7% (H <sub>2</sub> O)
THC Monitor APHA-370	Total Hydrocarbon (THC), Non-methane hydrocarbon (NMHC)	Horiba	0.02-100 ppmC
High Resolution-Proton-Transfer-Reaction-Time-of-Flight-Mass Spectrometer (HR-PTR-ToF-MS8000)	Trace volatile organic compounds (VOCs)	Ionicon Analytik	10 ppt-1 ppm

Formatted Table

Table S3. Particle-phase instrumentation.

Particle Phase Instruments	Measured Parameter	Manufacturer	Lower limit (or Range)
High Resolution-Aerosol-Time-of-Flight-Mass Spectrometer (HR-ToF-AMS)	Size resolved non-refractory particulate matter	Aerodyne	<1 μg m <sup>-3</sup> , d <sub>p</sub> 0.1-1 μm
Scanning Mobility Particle Sizer (SMPS)	Number-weighted aerosol size distribution	Home built, with TSI DMA, and 3022 CPC	0.01 particles cm <sup>-3</sup> , d <sub>p</sub> 15-850 nm
Aethalometer AE33	Equivalent Black Carbon (eBC)	Aerosol d.o.o	30 ng m <sup>-3</sup> , 10 ng m <sup>-3</sup> -100 ng m <sup>-3</sup>
Condensation particle counter CPC 3776	Particle number	TSI	4 nm, 0.01-10 <sup>7</sup> particles cm <sup>-3</sup> , d <sub>p</sub> >4 nm

Formatted Table

Formatted: Font color: Auto, Not Highlight

Formatted: Font color: Auto, Not Highlight

Formatted: Not Highlight

Formatted: Centered

**Formatted:** Centered

**Table S4. Average concentration after sampling into the SC, formed in the SC or OFR-from-SC (GDI1, cold-started WLTC and EDC).**

Expt	Veh.	Test cycle <sup>#</sup>	Ph	NMHC	CO	CO <sub>2</sub>	NO <sub>x</sub>	NMHC/NO <sub>x</sub>	NMOC	NMOC	ArHC	eBC	POA	SOA*	Nitrate*
				(FID) ppbC	ppm	ppm	ppb	ppbC ppb <sup>1</sup>	µg m <sup>-3</sup>	µgC m <sup>-3</sup>	µg m <sup>-3</sup>				
A1	GDI1	cW	full	1610	47	1717	72	22	586	462	358	58	6.4	134	606
A2	GDI1	cW	cW	1700	36	1909	62	27	575	180	428	53	5.7	(128")	(134")
A3	GDI1	cW	full	2280	17	700	25	91	762	670	669	33	2.8	32	217
A4	GDI1	cW	cW	2280	17	700	25	91	762	670	669	33	2.8	(266")	(185")
A4	GDI1	cW	Ph 1	274	24	1328	33	8	146	93	26	9.7	1.9	61	29.9
A4	GDI1	cW	Ph 2-4	274	24	1328	33	8	146	93	26	9.7	1.9	(275")	(99")
B1	GDI1-GPF	cW	full	2400	41	2123	58	41	891	776	759	0.05	2.4	2.8	198
B2	GDI1-GPF	cW	cW	1800	29	1766	56	32	558	481	458	0.05	3.3	2.8	198
B3	GDI1-GPF	cW	full	1540	15	592	23	66	433	370	361	0.2	1.4	2.8	189
B4	GDI1-GPF	cW	cW	1540	15	592	23	66	433	370	361	0.2	1.4	(206")	(99")
B4	GDI1-GPF	cW	Ph 2-4	182	21	1240	47	4	16	12	4	0.2	1.6	2.5	64
C1	GDI1	cE	full	1870	12	1304	41	46	440	390	391	21	3.7	(12")	(144")
C1	GDI1	cE	cE	1870	12	1304	41	46	440	390	391	21	3.7	120 <sup>a</sup>	19 <sup>a</sup>
D1	GDI1-GPF	cE	full	1830	12	1235	32	58	479	413	397	0.05	1.4	239 <sup>a</sup>	43 <sup>a</sup>
D2	GDI1-GPF	cE	cE	1770	12	1250	34	52	457	396	388	n.a.	1.5	255 <sup>a</sup>	86 <sup>a</sup>
D3	GDI1-GPF	cE	full	2020	14	1650	38	53	497	439	447	0.05	1.2	255 <sup>a</sup>	57 <sup>a</sup>
D3	GDI1-GPF	cE	cE	2020	14	1650	38	53	497	439	447	0.05	1.2	255 <sup>a</sup>	57 <sup>a</sup>

5 <sup>#</sup>cW refers to cold-started WLTC, cE refers to cold-started EDC cycle; the driving tests were conducted over the full cycle, Ph 1, Ph 2-4 and "full" indications refer to selective sampling of driving cycle phases into the SC and hence presents average exhaust gas concentrations as input to SC (A1-B4) and OFR-from-SC (A1-D3) photochemical experiments. Online time-resolved tests were monitored and emissions were photochemically aged in the OFR over the full driving cycle for each driving test (integrated data are, however, not presented herein except for GDI4 in 2015). \*secondary aerosol mass formed upon simulated photochemistry (SC experiments, "OFR-from-SC experiments UV100, not wlc). n.a.=data not available.

10

Formatted: Centered

**Table S5. Average concentration after sampling into the SC, formed in OFR-from-SC (GDI2, cold-started WLTC).**

Expt	Veh.	Test cycle <sup>#</sup>	Ph	NMHC (FID) ppbC	CO ppm	CO <sub>2</sub> ppm	NO <sub>x</sub> ppb	NMHC/NO <sub>x</sub> ppbC ppb <sup>-1</sup>	NMOC (PTR) μg m <sup>-3</sup>	NMOC (PTR) μgC m <sup>-3</sup>	ArHC (PTR) μg m <sup>-3</sup>	eBC μg m <sup>-3</sup>	POA μg m <sup>-3</sup>	SOA* μg m <sup>-3</sup>	Nitrate* μg m <sup>-3</sup>
E1	GDI2	cW	full cW	996	8.05	1334	n.a.	n.a.	634	460	315	n.a.	3.5	70 <sup>“</sup>	10 <sup>“</sup>
E2	GDI2	cW	full cW	1430	12.7	1303	n.a.	n.a.	771	575	412	25.1	3.9	129 <sup>“</sup>	24.6 <sup>“</sup>
E3	GDI2	cW	full cW	n.a.	8.4	1003	n.a.	n.a.	504	400	265	9.07	2.1	94 <sup>“</sup>	33.1 <sup>“</sup>
E4	GDI2	cW	Ph 1	n.a.	7.6	398	n.a.	n.a.	378	332	326	7.64	1.1	118 <sup>“</sup>	29.5 <sup>“</sup>

<sup>#</sup>cW refers to cold-started WLTC, cE refers to cold-started EDC cycle; the driving tests were conducted over the full cycle, Ph 1, Ph 2-4 and “full” indications refer to selective sampling of driving cycle phases into the SC and hence presents average exhaust gas concentrations as input to OFR-from-SC photochemical experiments. Online time-resolved tests were monitored and emissions were photochemically aged in the OFR over the full driving cycle for each driving test (integrated data are, however, not presented herein except for GDI4 in 2015). \*secondary aerosol mass formed upon simulated photochemistry (“OFR-from-SC experiments UV100). n.a.=data not available.

**Table S6. Average concentration after sampling into the SC, formed OFR-from-SC (GDI3, cold-started WLTC).**

Expt	Veh.	Test cycle <sup>#</sup>	Ph	NMHC (FID) ppbC	CO ppm	CO <sub>2</sub> ppm	NO <sub>x</sub> ppb	NMHC/NO <sub>x</sub> ppbC ppb <sup>-1</sup>	NMOC (PTR) μg m <sup>-3</sup>	NMOC (PTR) μgC m <sup>-3</sup>	ArHC (PTR) μg m <sup>-3</sup>	eBC μg m <sup>-3</sup>	POA μg m <sup>-3</sup>	SOA* μg m <sup>-3</sup>	Nitrate* μg m <sup>-3</sup>
F1	GDI3	cW	full cW	1198	10.0	525	n.a.	n.a.	447	380	264	13.9	0.48	123 <sup>“</sup>	267 <sup>“</sup>
F2	GDI3	cW	full cW	n.a.	2.07	485	n.a.	n.a.	229	147	137	8.03	0.96	31.2 <sup>“</sup>	42.4 <sup>“</sup>
F3	GDI3	cW	Ph 1	n.a.	1.47	158	n.a.	n.a.	202	154	121	5.45	1.06	26.4 <sup>“</sup>	52.2 <sup>“</sup>
F4	GDI3	cW	Ph 2-4	n.a.	0.49	339	n.a.	n.a.	191	101	33	2.16	0.05	2.3 <sup>“</sup>	65.1 <sup>“</sup>

<sup>#</sup>cW refers to cold-started WLTC, cE refers to cold-started EDC cycle; the driving tests were conducted over the full cycle, Ph 1, Ph 2-4 and “full” indications refer to selective sampling of driving cycle phases into the SC and hence presents average exhaust gas concentrations as input to OFR-from-SC photochemical experiments. Online time-resolved tests were monitored and emissions were photochemically aged in the OFR over the full driving cycle for each driving test (integrated data are, however, not presented herein except for GDI4 in 2015). \*secondary aerosol mass formed upon simulated photochemistry (“OFR-from-SC experiments UV100). n.a.=data not available.

**Table S7. Average concentration after sampling into the SC, formed in SC (GDI4, cold-started WLTC).**

Expt	Veh.	Test cycle <sup>#</sup>	Ph	NMHC (FID) ppbC	CO ppm	CO <sub>2</sub> ppm	NO <sub>x</sub> ppb	NMHC/NO <sub>x</sub> ppbC ppb <sup>-1</sup>	NMOC (PTR) μg m <sup>-3</sup>	NMOC (PTR) μgC m <sup>-3</sup>	ArHC (PTR) μg m <sup>-3</sup>	eBC μg m <sup>-3</sup>	POA μg m <sup>-3</sup>	SOA* μg m <sup>-3</sup>	Nitrate* μg m <sup>-3</sup>
G1	GDI4	cW	full cW	438	6.01	1218	n.a.	n.a.	429	180	169	9.99	n.a.	10.1	9.1
G2	GDI4	cW	full cW	486	7.03	1555	57	8.5	415	136	177	10.1	2.11	5.1	8.8
G3	GDI4	cW	full cW	750	10.1	1830	112	6.7	508	288	251	14.9	3.05	4.5	27.5
G4	GDI4	cW	full cW	688	n.a.	n.a.	118	5.8	356	215	185	20.1	n.a.	n.a.	n.a.

<sup>#</sup>cW refers to cold-started WLTC, cE refers to cold-started EDC cycle; the driving tests were conducted over the full cycle. Online time-resolved tests were monitored and emissions were photochemically aged in the OFR over the full driving cycle for each driving test (integrated data are, however, not presented herein except for GDI4 in 2015, which are labelled “online OFR” in the corresponding figures in the main text). \*secondary aerosol mass formed upon simulated photochemistry (SC experiments, not wlc). n.a.=data not available.

Formatted: Centered

## References (Supporting Information)

- Amador Muñoz, O., Misztal, P. K., Weber, R., Worton, D. R., Zhang, H., Drozd, G., and Goldstein, A. H.: Sensitive detection of n-alkanes using a mixed ionization mode Proton-Transfer-Reaction-Mass Spectrometer, *Atmospheric Measurement Techniques Discussions*, 1-21, 10.5194/amt-2016-64, 2016.
- 5 Barmet, P., Dommen, J., DeCarlo, P. F., Tritscher, T., Praplan, A. P., Platt, S. M., Prévôt, A. S. H., Donahue, N. M., and Baltensperger, U.: OH clock determination by proton transfer reaction mass spectrometry at an environmental chamber, *Atmos. Meas. Tech.*, 5, 647-656, 10.5194/amt-5-647-2012, 2012.
- Bruns, E. A., El Haddad, I., Keller, A., Klein, F., Kumar, N. K., Pieber, S. M., Corbin, J. C., Slowik, J. G., Brune, W. H., Baltensperger, U., and Prévôt, A. S. H.: Inter-comparison of laboratory smog chamber and flow reactor systems on organic aerosol yield and composition, *Atmos. Meas. Tech.*, 8, 2315-2332, 10.5194/amt-8-2315-2015, 2015.
- 10 Gueneron, M., Erickson, M. H., Vanderschelden, G. S., and Jobson, B. T.: PTR-MS fragmentation patterns of gasoline hydrocarbons, *Int. J. Mass Spectrom.*, 379, 97-109, 10.1016/j.ijms.2015.01.001, 2015.
- IUPAC Task Group on Atmospheric Chemical Kinetic Data Evaluation – Data Sheet HO<sub>x</sub> VOC10 (last updated January 12, 2005). <http://iupac.pole-ether.fr/> (accessed February 12, 2017). International Union of Pure and Applied Chemistry, 2005.
- 15 Jordan, A., Jaksch, S., Jürschik, S., Edtbauer, A., Agarwal, B., Hanel, G., Hartungen, E., Seehauser, H., Märk, L., Sulzer, P., and Märk, T. D.: H<sub>3</sub>O<sup>+</sup>, NO<sup>+</sup> and O<sub>2</sub><sup>+</sup> as precursor ions in PTR-MS: isomeric VOC compounds and reactions with different chemical groups, 5th International Conference on Proton Transfer Reaction Mass Spectrometry and its Applications, 2011.
- 20 Knighton, W. B., Fortner, E. C., Midey, A. J., Viggiano, A. A., Herndon, S. C., Wood, E. C., and Kolb, C. E.: HCN detection with a proton transfer reaction mass spectrometer, *Int. J. Mass Spectrom.*, 283, 112-121, 10.1016/j.ijms.2009.02.013, 2009.
- Li, R., Palm, B. B., Ortega, A. M., Hlywiak, J., Hu, W., Peng, Z., Day, D. A., Knote, C., Brune, W. H., de Gouw, J. A., and Jimenez, J. L.: Modeling the radical chemistry in an oxidation flow reactor: radical formation and recycling, sensitivities, and the OH exposure estimation equation, *J Phys Chem A*, 119, 4418-4432, 10.1021/jp509534k, 2015.
- 25 Peng, Z., Day, D. A., Stark, H., Li, R., Lee-Taylor, J., Palm, B. B., Brune, W. H., and Jimenez, J. L.: HO<sub>x</sub> radical chemistry in oxidation flow reactors with low-pressure mercury lamps systematically examined by modeling, *Atmos. Meas. Tech.*, 8, 4863-4890, 10.5194/amt-8-4863-2015, 2015.
- Peng, Z., Day, D. A., Ortega, A. M., Palm, B. B., Hu, W., Stark, H., Li, R., Tsigaridis, K., Brune, W. H., and Jimenez, J. L.: Non-OH chemistry in oxidation flow reactors for the study of atmospheric chemistry systematically examined by modeling, *Atmos. Chem. Phys.*, 16, 4283-4305, 10.5194/acp-16-4283-2016, 2016.
- Peng, Z., and Jimenez, J. L.: Modeling of the chemistry in oxidation flow reactors with high initial NO, *Atmospheric Chemistry and Physics Discussions*, 1-37, 10.5194/acp-2017-266, 2017.
- 30 Pieber, S. M., El Haddad, I., Slowik, J. G., Canagaratna, M. R., Jayne, J. T., Platt, S. M., Bozzetti, C., Daellenbach, K. R., Frohlich, R., Vlachou, A., Klein, F., Dommen, J., Miljevic, B., Jimenez, J. L., Worsnop, D. R., Baltensperger, U., and Prévôt, A. S. H.: Inorganic Salt Interference on CO<sub>2</sub><sup>+</sup> in Aerodyne AMS and ACSM Organic Aerosol Composition Studies, *Environ Sci Technol*, 50, 10494-10503, 10.1021/acs.est.6b01035, 2016.
- Platt, S. M., El Haddad, I., Zardini, A. A., Clairotte, M., Astorga, C., Wolf, R., Slowik, J. G., Temime-Roussel, B., Marchand, N., Ježek, I., Drinovec, L., Močnik, G., Möhler, O., Richter, R., Barmet, P., Bianchi, F., Baltensperger, U., and Prévôt, A. S. H.: Secondary organic aerosol formation from gasoline vehicle emissions in a new mobile environmental reaction chamber, *Atmos. Chem. Phys.*, 13, 9141-9158, 10.5194/acp-13-9141-2013, 2013.
- 40 Platt, S. M., El Haddad, I., Pieber, S. M., Zardini, A. A., Suarez-Bertoa, R., Clairotte, M., Daellenbach, K. R., Huang, R. J., Slowik, J. G., Hellebust, S., Temime-Roussel, B., Marchand, N., de Gouw, J., Jimenez, J. L., Hayes, P. L., Robinson, A. L., Baltensperger, U., Astorga, C., and Prévôt, A. S. H.: Gasoline cars produce more carbonaceous particulate matter than modern filter-equipped diesel cars, *Sci Rep*, 7, 4926, 10.1038/s41598-017-03714-9, 2017.
- 45 Schwantes, R. H., Schilling, K. A., McVay, R. C., Lignell, H., Coggon, M. M., Zhang, X., Wennberg, P. O., and Seinfeld, J. H.: Formation of highly oxygenated low-volatility products from cresol oxidation, *Atmos. Chem. Phys.*, 17, 3453-3474, 10.5194/acp-17-3453-2017, 2017.

Formatted: English (U.S.)

Field Code Changed

Field Code Changed

Formatted: English (U.S.)

Formatted: English (U.S.)

Formatted: Centered

- 5 Stirnweis, L., Marcolli, C., Dommen, J., Barmet, P., Frege, C., Platt, S. M., Bruns, E. A., Krapf, M., Slowik, J. G., Wolf, R., Prévôt, A. S. H., Baltensperger, U., and El-Haddad, I.: Assessing the influence of NO<sub>x</sub> concentrations and relative humidity on secondary organic aerosol yields from  $\alpha$ -pinene photo-oxidation through smog chamber experiments and modelling calculations, *Atmos. Chem. Phys.*, 17, 5035-5061, 10.5194/acp-17-5035-2017, 2017.
- 10 Zhao, Y., Saleh, R., Saliba, G., Presto, A. A., Gordon, T. D., Drozd, G. T., Goldstein, A. H., Donahue, N. M., and Robinson, A. L.: Reducing secondary organic aerosol formation from gasoline vehicle exhaust, *Proc Natl Acad Sci U S A*, 114, 6984-6989, 10.1073/pnas.1620911114, 2017.
- Zhao, Y., Lambe, A. T., Saleh, R., Saliba, G., and Robinson, A. L.: Secondary Organic Aerosol Production from Gasoline Vehicle Exhaust: Effects of Engine Technology, Cold Start, and Emission Certification Standard, *Environ Sci Technol*, 52, 1253-1261, 10.1021/acs.est.7b05045, 2018.

Formatted: English (U.S.)

Formatted: Centered